AN ABSTRACT OF THE DISSERTATION OF

Donovon Alexandar Adpressa for the degree of Doctor of Philosophy in Chemistry presented on June 1, 2018.

Title: Gene Activation Strategies in Filamentous Fungi for Natural Products Discovery

Abstract approved:

_____

Sandra Loesgen

Fungi have long been a prolific source of clinically approved drugs. The antibiotic penicillin, the cholesterol lowering statins, and the immunosuppressant cyclosporine have changed the treatment of human diseases in the last century. Recently, genome analysis of filamentous fungi has revealed that the biosynthetic potential for natural product expression is far greater than what is traditionally observed in laboratory culture. To this end, strategies to induce the expression of these otherwise transcriptionally silent natural product gene clusters are key to the continued discovery of chemical diversity. The research presented includes four manuscripts on gene activation strategies in fungi, with foci including ecological, chemical, and genetic approaches. Knockout of an epigenetic regulator in *Fusarium graminearum* resulted in the identification of two novel terpenes (tricinolonoic acid and tricinolone) and one novel polyketide (protofusarin). Furthermore, bioinformatics analysis allowed for the identification of the gene clusters responsible for the production of tricin terpenes and gibepyrones. In *Chalara* sp. 6661, treatment with the HDAC inhibitor vorinostat resulted in the production of four novel xanthones (chalanilines A-B and two xanthone-adenosine derivatives). Synthesis of isotopically labeled vorinostat and consequent feeding studies confirmed that chalanilines A and B were biotransformation products of vorinostat. A nutrient manipulation study in *Aspergillius terreus* showed selective production of metabolites via LCMS based metabolomics and enabled the discovery of new compounds including 7-desmethyl citreoviridin. Co-cultivation of two developmental forms of *Aspergillius alliaceus* resulted in the expression of novel,

cytotoxic, bianthrone polyketides (allianthrones A-C). In each instance presented, application of a gene activation technique elicited the production of previously undescribed natural products.

Gene Activation Strategies in Filamentous Fungi for Natural Products Discovery

by

Donovon Alexandar Adpressa

A DISSERTATION

submitted to

Oregon State University

in partial fulfillment of

the requirements for the

degree of

Doctor of Philosophy

Presented June 1, 2018

Commencement June 2018

Doctor of Philosophy dissertation of Donovon Alexandar Adpressa

presented on June 1, 2018

APPROVED:

_____

Major Professor, representing Chemistry

_____

Head of the Department of Chemistry

_____

Dean of the Graduate School

I understand that my dissertation will become part of the permanent collection of Oregon State University libraries. My signature below authorizes release of my dissertation to any reader upon request.

_____

Donovon Alexandar Adpressa, Author

ACKNOWLEDGEMENTS

First and foremost, I would like to thank Prof. Sandra Loesgen for her unrelenting support throughout this incredible adventure. I would not be the scientist I have become without the mentoring she has provided these years.

I would like to thank Prof. Michael Freitag for incredible support throughout my studies and providing a challenging and interesting project as fodder for my development. Steven Huhn has provided invaluable mentoring in NMR and I am forever grateful.

I would like to thank my committee for their support and guidance through the years. Thank you Prof. BJ Philmus for pushing me to be better in my early years at OSU. Thank you Prof. Phil Proteau for the great discussions throughout my time here and for serving on my committee with very little consultation or notice. Prof. Paul Blakemore, thank you for the wonderful courses. My notebooks from those courses remain some of my favorite.

Thank you to Prof. Paul Cheong for years of support and confidence. You've been a great ally. I would like to also thank Kerry McPhail for being a great mentor though the years of shared group meetings.

Finally, I would like to thank my incredible wife Katie. I wouldn't be here today without the support you've given me throughout this journey. Thank you for pushing me to chase my dreams and putting up with so much along the way.

CONTRIBUTION OF AUTHORS

Prof. Sandra Loesgen was the major advisor on all projects and assisted with the design and writing of all chapters contained herein. Prof. Michael Freitag assisted with the design and writing of Chapter Two, provided fungal genetic mutants of *Fusarium graminearum*, and provided resources and expertise in fungal genomics. Lanelle Connolly provided the fungal transformants, and performed transcriptomics analysis of these transformants, which are the basis of the work described in Chapter Two. Zachary Konkel assisted in the isolation of zearalenone related metabolites from *Fusarium graminearum* described in Chapter Two. Dr. Christina Smith provided transcriptomics analysis of the fungal transformants described in Chapter Two. Brett Pierce and Xiao Chang assisted in the preparation of fungal transformants used in Chapter Two. Kayla Stalheim assisted in the isolation and bioassay testing of secondary metabolites described in Chapter Three. Prof. Philip J. Proteau assisted with the interpretation of data and writing of Chapter Three. Paige Mandelare performed much of the LCMS analysis of *A. alliaceus* extracts, as well as much of the NMR analysis in Chapter Five and contributed to the writing of the chapter. Dr. Lev Zakharov performed the X-ray crystallography of allianthrone A in Chapter Five. Elizabeth Kaweesa performed cytotoxicity testing of all compounds in Chapter Five.

TABLE OF CONTENTS

TABLE OF CONTENTS (Continued)

LIST OF FIGURES

LIST OF TABLES

LIST OF APPENDIX FIGURES

LIST OF APPENDIX FIGURES (Continued)

LIST OF APPENDIX FIGURES (Continued)

LIST OF APPENDIX FIGURES (Continued)

Chapter 1 – General Introduction

Donovon A. Adpressa

1.1 Natural products

Natural products, compounds isolated from natural sources such as plants or microbes, have served to ameliorate the perils of the human condition for millennia. Natural preparations for use as medicine have been recorded as early as 1550 BC within the pages of the Ebers Papyrus, where over 700 medical preparations from plants are described.[1] In the modern era, over fifty percent of FDA approved drugs since 1981 have been sourced from or inspired by natural products.[2,3] Natural products are not just useful as medicine, however, and have found widespread usage in a variety of other applications. Compounds such as strobilurin, azadirachtin, and rotenone have had positive impacts on the stability of agriculture the world over.[4] Recently, the inherent bioactivity of natural products and a movement towards green chemistry principles has inspired the pursuit of natural products as antifouling agents for marine vehicles, seeking to displace broadly toxic and accumulating agents such as tributyltin or lead currently in use.[5,6] Furthermore, natural products chemistry has proven indispensable to our understanding of the natural world, providing invaluable understanding of the chemical language of the organisms cohabitating the world around us (Figure 1.1).[7-9]
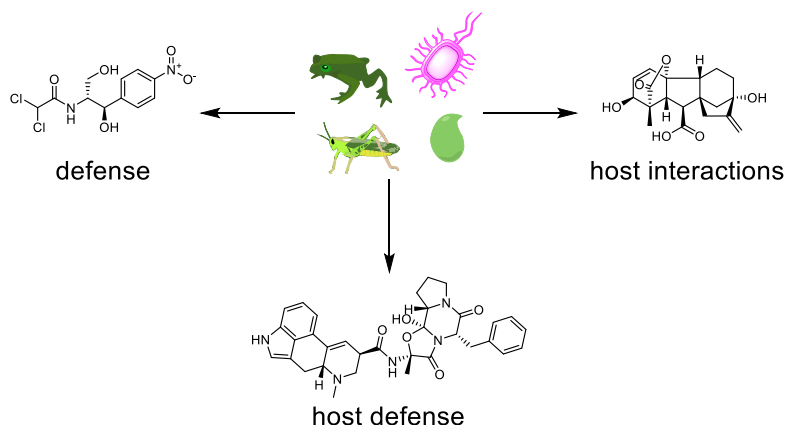
Figure 1.1: Natural products can serve various functions in nature, for example as chemical signals between organisms (gibberellic acid, right), as host defense mechanisms conferring a selection mechanism for survival (ergotamine, middle), or may provide defense mechanisms for the organism themselves (chloramphenicol, left).

1.2 Fungal natural products

Among the various sources of natural products, fungi have proven an incredible source of chemical leads in the fight against human disease. The discovery of penicillin in 1929 ushered in the era of microbial antibiotics, saving millions of lives and affecting the course of World War II.[10,11] Intensive surveying of the fungal world for new medicines would result in the discovery of extraordinary bioactive metabolites, yielding important immunosuppressant drugs such as cyclosporin and mizoribine, the first in class HMG-CoA reductase inhibitors lovastatin and simvastatin, and potent antifungal agents such as griseofulvin and caspofungin.[12-14] Fungi continue to be a promising source of bioactive natural products due to their incredible biodiversity. To date, approximately 100,000 fungal species have been investigated, but there are estimates that over one million species of

fungi may inhabit our planet.[15] Despite the incredible efforts put forth in the discovery of natural products from fungi, recent analyses of fungal genomes indicate that we have only just begun to elucidate the potential of genetically encoded small molecules from fungi. The well of compounds encoded by these incredible microorganisms is much deeper than originally anticipated (Figure 1.2).[16-18] The combination of biodiversity and the abundance of cryptic secondary metabolites make fungi a promising source for continued natural product discovery efforts.
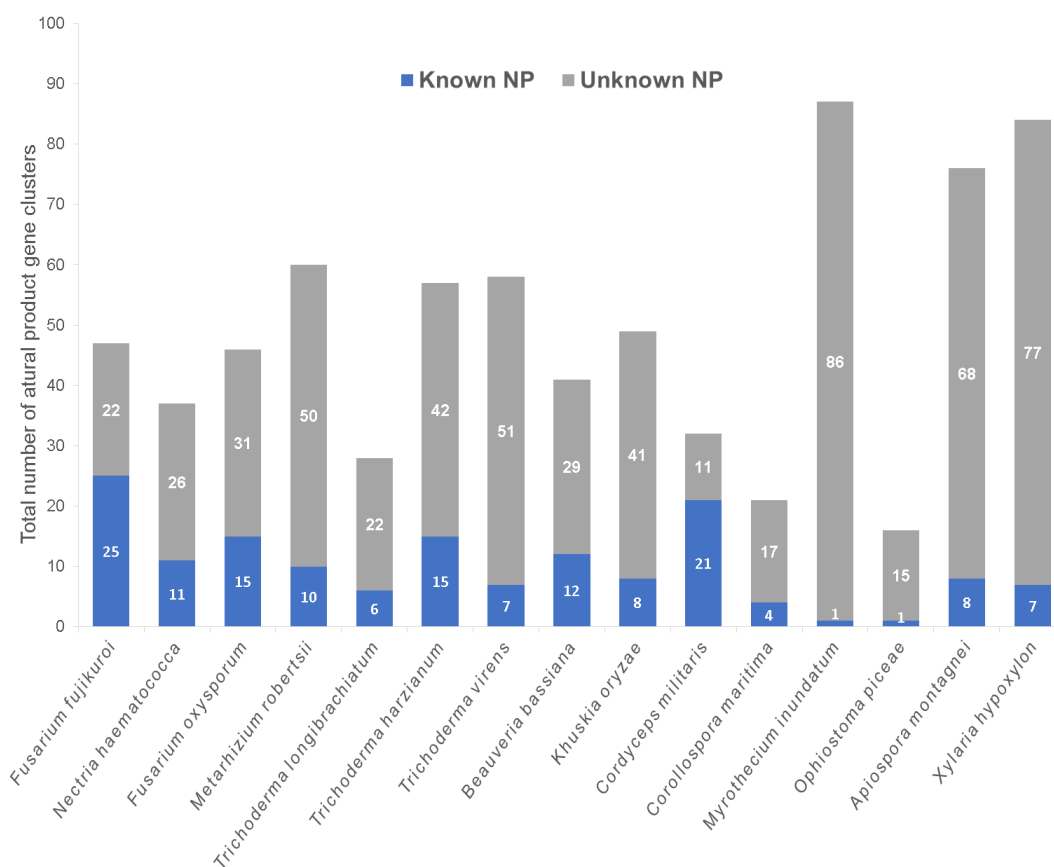
Figure 1.2: A recent survey of sequenced fungal genomes showing the total number of predicted secondary metabolite gene clusters (total bar height) with the known number of

natural product classes for each fungus indicated (blue bar). (Adpressa et al., unpublished results).

1.3 Gene activation strategies in fungi

Despite the incredible genetic potential encoded within their genomes, discovery efforts from fungal sources remain hampered by re-isolation of previously described compounds.[19-21] Dereplication strategies relying on LCMS, MS/MS, UV, and NMR spectroscopic libraries have hastened the isolation of novel leads by avoiding re-isolation of previously identified natural products early in the course of discovery.[22-25] Genomics-driven approaches have enabled accelerated discovery of novel scaffolds as well as allowing for rapid connection of the newly discovered compounds to their biosynthetic origins.[26-30] A number of gene activation techniques, ranging from nutrient manipulation to genetic knockout have been employed to elicit the expression of new natural products.[31-34]

One of the earliest activation techniques used to elicit production of novel compounds in fungi was alteration of nutrient conditions away from standard laboratory growth media. The OSMAC concept (One Strain, MAny Compounds) has been employed extensively to induce the expression of novel compounds from filamentous fungi.[35-39] In addition to manipulation of nutrient content and availability, pH, temperature, osmotic pressure, oxygen content, and agitation conditions have all been shown to produce effects on the secondary metabolite profile of fungi.[40-42] A great deal of effort has been put forth to mimic the ecological conditions fungi face in nature. To this end, cocultivation of fungi with other

fungal species or with bacteria has also been shown to elicit the production of novel classes of compounds.[43-49]

Recently, extensive attention has been paid to the role of epigenetic regulation in fungi and their effects on fungal differentiation and development.[50-54] Among these, many studies have chronicled the effects epigenetics exert on the derepression of otherwise silent natural products genes in fungi.[55-57] Importantly, many studies have shown that knockout of histone modifying enzymes in fungi can elicit the production of bioactive metabolites.[58-61]

1.4 Metabolomics approaches in natural product discovery

As the techniques available to induce expression of silent natural products gene clusters have increased, so too has the need for rapid detection of metabolic changes. Multivariate analyses of mass spectrometric data, first utilized and improved for primary metabolomics, have accelerated the detection and dereplication of secondary metabolites in recent years.[62] These statistical techniques offer not only tools for the detection changes in metabolic profile across treatment conditions, but also offer robust analyses of the significance of the induced effects to help prioritize isolation efforts. Though promising advances are reported each year, untargeted NMR metabolomics of natural product extracts is still in many ways underdeveloped, with limitations on the throughput and rapid determination of chemical structure hindering the widespread implementation of this technique.[63,64] Conversely, LCMS based metabolomics have enjoyed a great deal of success profiling changes in microbial metabolic output for the detection of newly expressed secondary metabolites (Figure 1.3). OSMAC perturbations have been successfully profiled by LCMS-based

multivariate techniques such as molecular networking or relative abundances analysis.[65-67] LCMS-based metabolomics techniques have further been applied to detect the effects of both chemical and gene knockout-based epigenetic effects in fungi.[68-70] Another promising application of metabolomics in natural products discovery is the coupling of bioassay data to LCMS-based abundance analysis to rapidly identify compounds likely to be responsible for bioactivity.[71-73] In all, hyphenation of multiple data sources through statistical techniques holds great promise for future discovery efforts.[74,75]

Culture and extraction of fungi

LCMS analysis and peak list generation

Metabolomics guided isolation
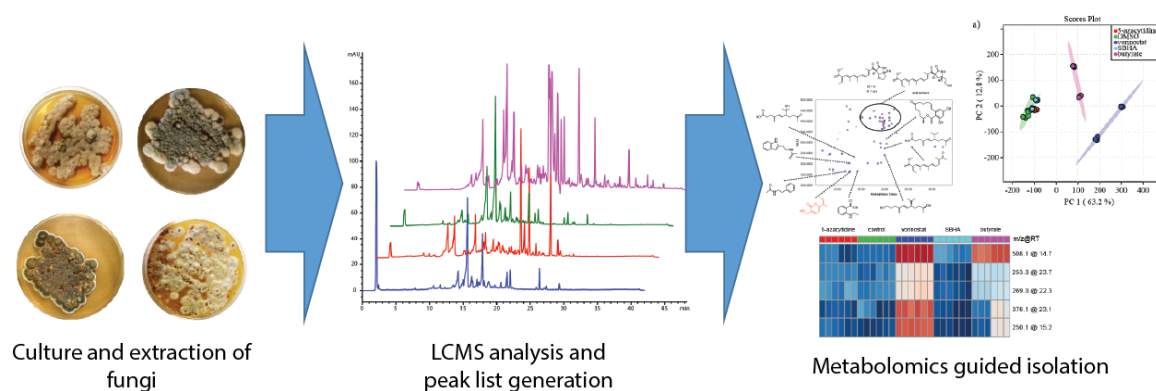
Figure 1.3: A typical fungal natural products metabolomics guided discovery workflow involving culture of fungi under a variety of conditions, followed by extraction and LCMS analysis of the organic extracts. Finally, metabolomics outputs such as PCA, log ratio, or relative expression analysis aid in prioritization of culture conditions and isolation efforts.

1.5 Chapter overview

Chapter Two details the metabolomics guided isolation of new and known secondary metabolites from *Fusarium graminearum* strain *Δkmt6*, possessing a knockout mutation of histone 3 lysine 27 methyltransferase (*kmt6*). This mutant exhibits significant

morphological changes from the wildtype strain, and transcriptomics data indicate overexpression of genes related to secondary metabolism. LCMS-based log ratio analysis compared to wildtype *F. graminearum* guided the isolation and elucidation of thirteen known and three novel natural products from the *Δkmt6* mutant. Furthermore, bioinformatics analysis coupled with gene knockout experiments identified the gene clusters responsible for the production of the tricin-terpene and gibepyrone class of compounds in *F. graminearum* for the first time. This chapter is adapted from the manuscript in preparation Adpressa, D.A.; Connolly, L.R.; Konkel, Z.M.; Chang, X.L.; Pierce, B.R.; Smith, K.M.; Freitag, M.; Loesgen, S. "Overexpression and Discovery of New Secondary Metabolites *Fusarium graminearum* Strains Lacking the Histone H3 Lysine27 Methyltransferase KMT6".

Chapter Three recounts the treatment of *Chalara* sp. 6661 with epigenetic modifying drugs and the joint investigation of culture extracts by LCMS-based relative abundance analysis. Relative abundance analysis guided the isolation of three novel modified xanthones from cultures treated with the HDAC inhibitor vorinostat. Further antimicrobial activity guided isolation resulted in the identification of another novel modified xanthone structure, chalaniline B, with Gram-positive antibacterial activity. Synthesis of isotopically labeled vorinostat and subsequent feeding studies revealed that chalanilines are biotransformation products of vorinostat. This chapter is adapted from the published article Adpressa, D.A.; Stalheim, K.; Proteau, P.J.; Loesgen, S. "Unexpected Biotransformation of the HDAC Inhibitor Vorinostat Yields Aniline-Containing Fungal Metabolites" *ACS Chemical Biology* **2017**, *12* (7), pp 1842–1847 (DOI: 10.1021/acschembio.7b00268).

Chapter Four presents the chemical bioprospecting of *Aspergillus terreus* treated under the OSMAC premise. The fungus was cultured under eleven nutrient conditions and the resulting metabolic changes profiled by LCMS-based principle component and log ratio analyses. The structures of sixteen known compounds and one novel compound were elucidated by one and two dimensional NMR and subjected to antimicrobial and cytotoxicity screening. The coupling of log ratio analysis to cytotoxicity data revealed terrein as the cytotoxic metabolite produced in potato dextrose broth cultures. This chapter is adapted from the published article Adpressa, D.A.; Loesgen, S. "Bioprospecting Chemical Diversity and Bioactivity in a Marine Derived *Aspergillus terreus" Chemistry & Biodiversity* **2016,** 13 (2), pp 253-259 (DOI: 10.1002/cbdv.201500310).

Chapter Five describes the expression of novel, cytotoxic bianthrone polyketides by coculture of two distinct developmental stages of *Aspergillus alliaceus*. Separate chemical profiling of two morphs of *A. alliaceus* revealed ochratoxin A as the major metabolite of the sclerotia forming phenotype, while the anthraquinones naligolaxin and nalgiovensin were observed to be the major metabolites present in the extracts of the conidia forming phenotype. Co-cultivation of the two morphologies resulted in the production of allianthrones A-C, whose structures and absolute configurations were elucidated through a combination of crystallography, two dimensional NMR, and circular dichroism paired with computation of chiroptical properties. This chapter is adapted from the published article Mandelare, P.E.; Adpressa, D.A.; Kaweesa, E.N.; Zakharov, L.N.; Loesgen, S. "Coculture of Two Developmental Stages of a Marine-Derived *Aspergillus alliaceus* Results in the Production of the Cytotoxic Bianthrone Allianthrone A" *Journal of Natural Products* **2018,**

81 (4), pp 1014-1022 (DOI: 10.1021/acs.jnatprod.8b00024). The dissertation author is the second author of this manuscript and assisted in the writing of the article, culture and extraction of the fungus, acquisition and interpretation of the NMR spectra, and computation of ECD spectra.

The final chapter presents a conclusion for the works presented, summarizing the methods employed to induce and detect the novel metabolites presented throughout each chapter, and offers a brief perspective on the future of fungal natural products discovery.

1.6 References

1. Daniel A. Dias, S. U., and Ute Roessner *Metabolites* **2012**, *2*, 303336.
2. Newman, D. J.; Cragg, G. M. *J. Nat. Prod.* **2016**, *79*, 629.
3. Newman, D. J.; Cragg, G. M. *J. Nat. Prod.* **2012**, *75*, 311.
4. Dayan, F. E.; Cantrell, C. L.; Duke, S. O. *Biorg. Med. Chem.* **2009**, *17*, 4022.
5. Wang, K.-L.; Wu, Z.-H.; Wang, Y.; Wang, C.-Y.; Xu, Y. *Mar. Drugs* **2017**, *15*, 266.
6. Qian, P. Y.; Xu, Y.; Fusetani, N. *Biofouling* **2010**, *26*, 223.
7. Dean, L. J.; Prinsep, M. R. *Nat. Prod. Rep.* **2017**, *34*, 1359.
8. Spiteller, P. *Nat. Prod. Rep.* **2015**, *32*, 971.
9. Eisner, T. *Proc. Natl. Acad. Sci. U.S.A.* **2003**, *100*, 14517.
10. Alharbi, S. A.; Wainwright, M.; Alahmadi, T. A.; Salleeh, H. B.; Faden, A. A.; Chinnathambi, A. *Saudi J. Biol. Sci.* **2014**, *21*, 289.
11. Kardos, N.; Demain, A. L. *Appl. Microbiol. Biotechnol.* **2011**, *92*, 677.
12. Endo, A. *Prc. Jpn. Acad. Ser. B Phys. Biol. Sci.* **2010**, *86*, 484.
13. Allison, A. C. *Immunopharmacology* **2000**, *47*, 63.
14. Roemer, T.; Krysan, D. J. *Cold Spring Harb. Perspect. Med.* **2014**, *4*, a019703.
15. Schueffler, A.; Anke, T. *Nat. Prod. Rep.* **2014**, *31*, 1425.
16. Grigoriev, I.V.; Hadrias, S.; Kuo, A.; Ohm, R.; Otillar, R.; Riley, R.; Salamov, A.; Zhao, X.; Korzeniewski, R.; Smirnova, T.; Nordberg, H.; Dubchak, I.; Shabalov, I. *Nucleic Acids Res.* **2014**, *42*, D699.
17. Brakhage, A. A. *Nat. Rev. Microbiol.* **2013**, *11*, 21.
18. Wiemann, P.; Keller, N. P. *J. Ind. Microbiol. Biotechnol.* **2014**, *41*, 301.
19. Tulp, M.; Bohlin, L. *Biorg. Med. Chem.* **2005**, *13*, 5274.
20. Amirkia, V.; Heinrich, M. *Front. Pharmacol.* **2015**, *6*, 237.
21. Roemer, T.; Xu, D.; Singh, Sheo B.; Parish, Craig A.; Harris, G.; Wang, H.; Davies, Julian E.; Bills, Gerald F. *Chem. Biol.* **2011**, *18*, 148.
22. Abdelmohsen, U.; Cheng, C.; Viegelmann, C.; Zhang, T.; Grkovic, T.; Ahmed, S.; Quinn, R.; Hentschel, U.; Edrada-Ebel, R. *Mar. Drugs* **2014**, *12*, 1220.
23. Chervin, J.; Stierhof, M.; Tong, M. H.; Peace, D.; Hansen, K. Ø.; Urgast, D. S.; Andersen, J. H.; Yu, Y.; Ebel, R.; Kyeremeh, K.; Paget, V.; Cimpan, G.; Wyk, A. V.; Deng, H.; Jaspars, M.; Tabudravu, J. N. *J. Nat. Prod.* **2017**, *80*, 1370.
24. Gaudencio, S. P.; Pereira, F. *Nat. Prod. Rep.* **2015**, *32*, 779.
25. Nielsen, K. F.; Månsson, M.; Rank, C.; Frisvad, J. C.; Larsen, T. O. *J. Nat. Prod.* **2011**, *74*, 2338.
26. Zhang, M. M.; Qiao, Y.; Ang, E. L.; Zhao, H. *Expert Opin. Drug Discov.* **2017**, *12*, 475.
27. Ikeda, H. *Biosci. Biotechnol. Biochem.* **2017**, *81*, 13.
28. Harvey, A. L.; Edrada-Ebel, R.; Quinn, R. J. *Nat. Rev. Drug Discov.* **2015**, *14*, 111.
29. Harvey, C. J. B.; Tang, M.; Schlecht, U.; Horecka, J.; Fischer, C. R.; Lin, H.-C.; Li, J.; Naughton, B.; Cherry, J.; Miranda, M.; Li, Y. F.; Chu, A. M.; Hennessy, J. R.; Vandova, G. A.; Inglis, D.; Aiyar, R. S.; Steinmetz, L. M.; Davis, R. W.; Medema, M. H.; Sattely, E.; Khosla, C.; St. Onge, R. P.; Tang, Y.; Hillenmeyer, M. E. *Sci. Adv.* **2018**, *4*.

30. Wiemann, P.; Soukup, A. A.; Folz, J. S.; Wang, P.-M.; Noack, A.; Keller, N. P. *Fungal Biol. Biotechnol.* **2018**, *5*, 6.

31. Rutledge, P. J.; Challis, G. L. *Nat. Rev. Microbiol.* **2015**, *13*, 509.

32. Ochi, K.; Hosaka, T. *Appl. Microbiol. Biotechnol.* **2013**, *97*, 87.

33. Brakhage, A. A.; Schroeckh, V. *Fungal Genet. Biol.* **2011**, *48*, 15.

34. Scherlach, K.; Hertweck, C. *Org. Biomol. Chem.* **2009**, *7*, 1753.

35. Bode, H. B.; Bethe, B.; Hofs, R.; Zeeck, A. *ChemBioChem* **2002**, *3*, 619.

36. Hemphill, C. F. P.; Sureechatchaiyan, P.; Kassack, M. U.; Orfali, R. S.; Lin, W.; Daletos, G.; Proksch, P. *J. Antibiot.* **2017**, *70*, 726.

37. Gubiani, J. R.; Habeck, T. R.; Chapla, V. M.; Silva, G. H.; Bolzani, V. S.; Araujo, A. R. *Quim. Nova* **2016**, *39*, 1221.

38. Hewage, R. T.; Aree, T.; Mahidol, C.; Ruchirawat, S.; Kittakoop, P. *Phytochemistry* **2014**, *108*, 87.

39. Wei, H.; Lin, Z.; Li, D.; Gu, Q.; Zhu, T. *Wei Sheng Wu Xue Bao* **2010**, *50*, 701.

40. Overy, D.; Correa, H.; Roullier, C.; Chi, W.-C.; Pang, K.-L.; Rateb, M.; Ebel, R.; Shang, Z.; Capon, R.; Bills, G.; Kerr, R. *Mar. Drugs* **2017**, *15*, 254.

41. Lösgen, S.; Magull, J.; Schulz, B.; Draeger, S.; Zeeck, A. *Eur. J. Org. Chem.* **2008**, *2008*, 698.

42. Afshari, M.; Shahidi, F.; Mortazavi, S. A.; Tabatabai, F.; Es'haghi, Z. *Nat. Prod. Res.* **2015**, *29*, 1300.

43. Sterierle, A.A.; Decato, D.; Priestly, N.D.; Alverson, J.P.; Hoody, J.; McGrath, K.; Klepacki, D. *J. Nat. Prod.* **2017**, *80*, 1150.

44. Shang, Z.; Capon, R.J. *J. Nat. Prod.* **2017**, *80*, 1167.

45. Meng, L.; Li, X.; Xu, G.; Ji, N.; Wang, B. *J. Nat. Prod.* **2015**, *78*, 2301.

46. Oh, D.; Kauffman, C.A, Fenical, W. *Biorg. Med. Chem.* **2005**, *13*, 5267.

47. Oh, D.; Jensen, P.R.; Fenical, W. *J. Nat. Prod.* **2007**, *70*, 515.

48. Cueto, M.; Kauffman, C.A, Fenical, W.; Lobkovsky, E.; Clardy, J. *J. Nat. Prod.* **2001**, *64*, 1444.

49. Shuai Liu, H. D.; Heering, C.; Janiak, C.; Lin, W.; Liu, Z.; Proksch, P. *Tetrahedron Lett.* **2017**, *58*, 257.

50. Calvo, A. M.; Wilson, R. A.; Bok, J. W.; Keller, N. P. *Microbiol. Mol. Biol. Rev.* **2002**, *66*, 447.

51. Bok, J. W.; Keller, N. P. *Eukaryot. Cell* **2004**, *3*, 527.

52. Fox, E. M.; Howlett, B. J. *Curr. Opin. Microbiol.* **2008**, *11*, 481.

53. Connolly, L. R.; Smith, K. M.; Freitag, M. *PLoS Genet.* **2013**, *9*, e1003916.

54. Jeon, J.; Choi, J.; Lee, G.-W.; Park, S.-Y.; Huh, A.; Dean, R. A.; Lee, Y.-H. *Sci. Rep.* **2015**, *5*, 8567.

55. Cherblanc, F. L.; Davidson, R. W. M.; Di Fruscia, P.; Srimongkolpithak, N.; Fuchter, M. J. *Nat. Prod. Rep.* **2013**, *30*, 605.

56. Williams, R. B.; Henrikson, J. C.; Hoover, A. R.; Lee, A. E.; Cichewicz, R. H. *Org. Biomol. Chem.* **2008**, *6*, 1895.

57. Aghcheh, R. K.; Kubicek, C. P. *Appl. Microbiol. Biotechnol.* **2015**, *99*, 6167.

58. Niehaus, E.-M.; Kleigrewe, K.; Wiemann, P.; Studt, L.; Sieber, Christian M. K.; Connolly, Lanelle R.; Freitag, M.; Güldener, U.; Tudzynski, B.; Humpf, H.-U. *Chem. Biol.* **2013**, *20*, 1055.
59. Smith, K. M.; Kothe, G. O.; Matsen, C. B.; Khlafallah, T. K.; Adhvaryu, K. K.; Hemphill, M.; Freitag, M.; Motamedi, M. R.; Selker, E. U. *Epigenetics Chromatin* **2008**, *1*, 5.
60. Jamieson, K.; Rountree, M. R.; Lewis, Z. A.; Stajich, J. E.; Selker, E. U. *Proc. Natl. Acad. Sci. U. S. A.* **2013**, *110*, 6027.
61. Sarikaya-Bayram, Ö.; Bayram, Ö.; Feussner, K.; Kim, J.-H.; Kim, H.-S.; Kaever, A.; Feussner, I.; Chae, K.-S.; Han, D.-M.; Han, K.-H.; Braus, Gerhard H. *Dev. Cell* **2014**, *29*, 406.
62. Hautbergue, T.; Jamin, E. L.; Debrauwer, L.; Puel, O.; Oswald, I. P. *Nat. Prod. Rep.* **2018**, *35*, 147.
63. Markley, J. L.; Brüschweiler, R.; Edison, A. S.; Eghbalnia, H. R.; Powers, R.; Raftery, D.; Wishart, D. S. *Curr. Opin. Biotechnol.* **2017**, *43*, 34.
64. Robinette, S. L.; Brüschweiler, R.; Schroeder, F. C.; Edison, A. S. *Acc. Chem. Res.* **2012**, *45*, 288.
65. Macintyre, L.; Zhang, T.; Viegelmann, C.; Martinez, I. J.; Cheng, C.; Dowdells, C.; Abdelmohsen, U. R.; Gernert, C.; Hentschel, U.; Edrada-Ebel, R. *Mar. Drugs* **2014**, *12*, 3416.
66. Roullier, C.; Bertrand, S.; Blanchet, E.; Peigné, M.; Robiou du Pont, T.; Guitton, Y.; Pouchus, Y. F.; Grovel, O. *Mar. Drugs* **2016**, *14*, 103.
67. Adpressa, D. A.; Loesgen, S. *Chem. Biodivers.* **2016**, *13*, 253.
68. Henke, M. T.; Soukup, A. A.; Goering, A. W.; McClure, R. A.; Thomson, R. J.; Keller, N. P.; Kelleher, N. L. *ACS Chem. Biol.* **2016**, *11*, 2117.
69. Albright, J. C.; Henke, M. T.; Soukup, A. A.; McClure, R. A.; Thomson, R. J.; Keller, N. P.; Kelleher, N. L. *ACS Chem. Biol.* **2015**, *10*, 1535.
70. Adpressa, D. A.; Stalheim, K. J.; Proteau, P. J.; Loesgen, S. *ACS Chem. Biol.* **2017**.
71. Kellogg, J. J.; Todd, D. A.; Egan, J. M.; Raja, H. A.; Oberlies, N. H.; Kvalheim, O. M.; Cech, N. B. *J. Nat. Prod.* **2016**, *79*, 376.
72. Tawfike, A. F.; Tate, R.; Abbott, G.; Young, L.; Viegelmann, C.; Schumacher, M.; Diederich, M.; Edrada-Ebel, R. *Chem. Biodivers.* **2017**, *14*, e1700040.
73. Covington, B. C.; McLean, J. A.; Bachmann, B. O. *Nat. Prod. Rep.* **2017**, *34*, 6.
74. Barkal, L. J.; Theberge, A. B.; Guo, C. J.; Spraker, J.; Rappert, L.; Berthier, J.; Brakke, K. A.; Wang, C. C.; Beebe, D. J.; Keller, N. P.; Berthier, E. *Nat. Commun.* **2016**, *7*, 10610.
75. Hou, Y.; Braun, D. R.; Michel, C. R.; Klassen, J. L.; Adnani, N.; Wyche, T. P.; Bugni, T. S. *Anal. Chem.* **2012**, *84*, 4277.

Chapter 2 – adapted from the manuscript to be submitted

"Overexpression and Discovery of New Secondary Metabolites from

***Fusarium graminearum* Strains Lacking the Histone H3 Lysine27**

Methyltransferase KMT6"

Donovon A. Adpressa, Lanelle R. Connolly, Zachary M. Konkel, Xiao L. Chang,

Brett R. Pierce, Kristina M. Smith, Michael Freitag, Sandra Loesgen

2.1 Abstract

Biosynthetic gene clusters (BGCs) that produce secondary metabolites are often repressed during standard laboratory growth conditions, one persistent problem complicating the search for novel bioactive compounds. Chemical or genetic manipulation of fungi has become popular to relieve this transcriptional repression. Regions encoding for secondary metabolites in the genus *Fusarium* are enriched for trimethylated histone 3 lysine 27 (H3K27me3), a histone modification correlated with transcriptional gene silencing. Removal of all H3K27me3 by deletion of the gene for the H3K27 histone methyltransferase, *kmt6*, resulted in over-expression of ~20% of the genome. Here we show that deletion of this global repressor allows the identification of new compounds. We applied multivariate analysis of liquid chromatography–mass spectrometry (LCMS) data from organic culture extracts derived from both wild type and *kmt6* to guide isolation efforts. We uncovered drastic differences in the metabolic profiles. Our approach allows rapid visualization of the genetically induced changes in metabolite expression, analysis of overexpressed metabolites, and discovery of new molecules. Several low molecular weight, amino acid-derived metabolites were identified by relative abundance analysis. *N*-ethyl anthranillic acid (**1**) was isolated as a natural product for the first time alongside phenethylacetamide (**2**), and *N*-acetyltryptamine (**3**). Known compounds, such as zearalenone (**4**) and the fusarin class of compounds (**5-7**)**,** including biosynthetic intermediates and various derivatives, were highly enriched in *kmt6*. Relative abundance analysis guided the isolation and identification of a previously undescribed compound, protofusarin (**8**), validating our approach. We also isolated gibepyrone A and fusarpyrones

A and B (**9-11**) and demonstrated that these are made by the PKS5 gene cluster in *F. graminearum.* Additionally, we discovered tricinolone (**12**) and tricinolonoic acid (**13**), new metabolites belonging to the tricinonoic acid (**14**) class of compounds, which are generated by STC5, an orphan sesquiterpene biosynthesis cluster. Of the 16 fungal metabolites identified by detailed spectroscopic analyses in *kmt6*, 11 compounds had not been reported from *F. graminearum* before, and three metabolites are novel. In summary, we show that unleashing silent metabolic pathways can result in the discovery of new chemistry, and that this helps to connect new or known small molecules to the BGCs responsible for their production.
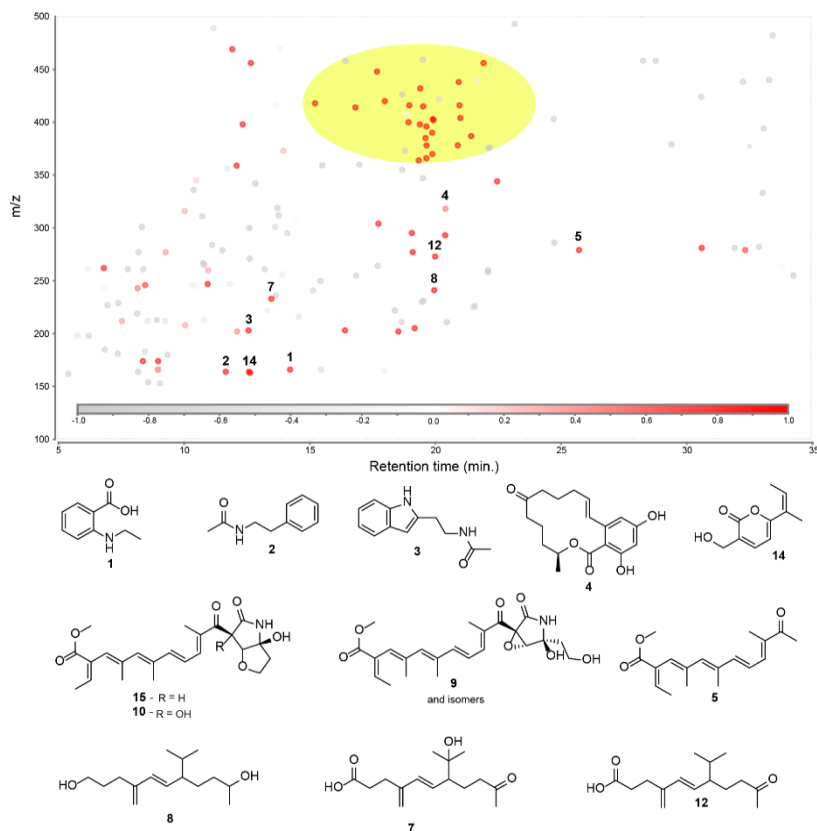
Figure 2.1. **Metabolomics guided approach for analysis and isolation of compounds overproduced upon deletion of kmt6 in *F. graminearum* by log-ratio analysis of LCMS data.** Results from log-ratio analysis of LCMS data from *kmt6* (light red to dark red dots) and wildtype (grey to light grey dots) strains highlights secondary metabolites overexpressed in the *kmt6* mutant. The yellow shaded region indicates fusarin isoforms and MS fragment ions. Compounds discussed in the main text are numbered in the figure and structures are shown below.

2.2 Introduction

For nearly a century, filamentous fungi have been exploited for their bioactive, industrially important, and agriculturally relevant secondary metabolites (SecMets). Recent genome mining efforts suggested that the capability of fungi to produce SecMets has been severely underestimated.[1] The majority of SecMet gene clusters remain silent under common laboratory culture conditions, prompting the demand for new methods to unlock and study these cryptic biosynthetic pathways. Chromatin structure, specifically histone post-translational modifications, can play essential roles in the regulation of fungal development, often by regulating the production of SecMets.[2-6] Thus, perturbing normal histone modification by chemical or genetic means has not only emerged as tool to explore the cryptic secondary metabolome but also aids our understanding of effects and functions SecMets may have in fugal development.[7-10]

Interfering with histone modifications or deleting the genes that encode the modifying enzymes has been shown to alter the production of bioactive metabolites when compared to wildtype strains.[3,5,8,11-16] Histone methylation, in particular, has been demonstrated to be a key regulator of secondary metabolism in several industrially important fungi. Early studies focused on perturbation of marks for active gene expression (e.g. H3K9 acetylation or H3K4 dimethylation) or a mark for constitutive gene silencing (e.g. H3K9 trimethylation).

The polycomb group of proteins (PcG) are responsible for histone H3 methylation at lysine 27 and are essential for the maintenance of cell identity and the regulation of development in animal and plants.[17,18] In the fungus *Fusarium graminearum*, the PcG

catalytic subunit (EZH2 in mammals) is encoded by the *kmt6* gene.[5,17] Lack of KMT6 or reduction in KMT6 levels results in de-repression of secondary metabolism in *F. graminearum*[5,13] and *F. fujikuroi*[19], respectively.

Here we demonstrate that deletion of the *F. graminearum kmt6* gene results in production of metabolites not found under normal lab growth conditions. To show this we applied our recently developed LCMS-based metabolomics approach, which can detect new metabolites arising after nutrient manipulation[20] or histone deacetylase inhibitor (HDACi) treatment.[21] We found metabolites or compounds previously not known from *F. graminearum*, including several amino acids derivatives, terpenes, and polyketides.

2.3 Results

2.3.1 RNA expression data. Previously we showed that deletion of *kmt6* resulted in upregulation of ~20% of all genes in the *F. graminearum* genome, many of which are predicted to be involved in secondary metabolite pathways.[5] To understand which metabolites are overproduced, we extended and updated the annotation of SecMet gene clusters that are affected by *kmt6* deletion (Table 2.1), supported by RNA-seq data from additional *kmt6* and WT strains, and following the nomenclature suggested.[33] Of the 67 predicted clusters, many of them recognizable by the presence of non-ribosomal peptide synthetase (NRPS), terpene synthase, or polyketide synthase (PKS) genes, 49 are enriched with H3K27me3 while 18 show no such enrichment and are located within typical gene-rich euchromatin. Cluster C11 is only partially covered by H3K27me3 and also does not appear to be co-regulated in some of our RNA-seq datasets. Therefore, we consider C11 as

two separate clusters. Of the 49 clusters enriched with H3K27me3, 44 are upregulated in the *kmt6* mutant, even in rich YPD medium. For four clusters (C1, C25, C32, C61), removal of the repressive H3K27me3 mark alone was insufficient to yield high expression levels (Table 2.1); products from these clusters are still unknown. Among the 18 clusters not enriched with H3K27me3, C6 was expressed in *kmt6* grown in nutrient poor medium, while C59 and C64 were expressed in *kmt6* in rich medium, but none of these clusters were expressed in WT. A total of 15 clusters showed no significant expression under any of our growth conditions in either WT or *kmt6* (Table 2.1). To harness the power of this genetic de-repression system, and to identify as many of the putatively new natural products, we turned to metabolomics-based screening.

Table 2.1. H3K27me3 enrichment and expression as measured by RNA-seq of 67 BGCs in *F. graminearum*

Cluster	Loci in cluster	# of loci	Length (kb)	Signature	Metabolite	K27me3	exp in WT	increased in kmt6
C01	FGSG_17598 - FGSG_00015	13	26.6			+	no	no
C02	FGSG_11653 - FGSG_00049	18	73.8	NPS8	apicidin-like (?)	+	no	yes
C03	FGSG_00067 - FGSG_00071	5	12.9		trichothecene (Tri1 and Tri16)	+	no	yes
C04	FGSG_15692 - FGSG_15693	3	7.5			+	no	yes
C05	FGSG_00448 - FGSG_00456	9	22.7	STC2	terpene (?)	-	no	no
C06	FGSG_01675 - FGSG_15676	13	38.9	NPS16; NPS19	leptomycin B; AM toxin (?)	-	no	L
C07	FGSG_01731 - FGSG_15133	17	52.6		terpenoid (?)	+	L	yes
C08	FGSG_15885 - FGSG_01795	15	37.0	PKS25	fumonisin	+	L	yes
C09	FGSG_02111 - FGSG_12068	12	22.7			+	no	yes
C10	FGSG_02136 - FGSG_02139	4	10.7			+	no	yes
C11	FGSG_02248 - FGSG_02251	4	10.1			-/+	no	
C12	FGSG_15962 - FGSG_15966	20	55.6			+	no	yes
C13	FGSG_02320 - FGSG_02330	11	27.4	PKS12, NPS4	aurofusarin	+	L	H
C14	FGSG_15969 - FGSG_02372	9	80.9			+	no	yes
C15	FGSG_02393 - FGSG_15983	9	36.7	NPS15, PKS22, PKS27	zearalenone	+	no	yes
C16	FGSG_04596 - FGSG_04588	10	23.0	PKS29		+	no	yes
C17	FGSG_16123 - FGSG_04333	6	21.5			-		no
C18	FGSG_03971 - FGSG_03956	18	55.7	PKS28	orcinol, orsellinic acid (?)	+	no	yes
C19	FGSG_03931 - FGSG_03912	21	45.1			+		yes
C20	FGSG_03862 - FGSG_03855	8	19.4			+		yes
C21	FGSG_03747 - FGSG_16212	5	17.3	NPS6	triacetylfusarinine	-	H	no
C22	FGSG_03737 - FGSG_03728	9	29.4			+		yes
C23	FGSG_03543 - FGSG_03529	15	34.4		trichothecene	+	yes	yes
C24	FGSG_03498 - FGSG_03489	12	20.3	STC4	acorenol	+		yes
C25	FGSG_03416 - FGSG_03412	5	16.2			+	H	no
C26	FGSG_03347 - FGSG_03340	8	28.5	PKS13		+	no	yes
C27	FGSG_03258 - FGSG_03254	5	8.8			+	no	yes
C28	FGSG_03067 - FGSG_03064	4	9.2	DTC1	carotenoids	+	H	yes
C29	FGSG_02874 - FGSG_16376	16	33.2			+		yes
C30	FGSG_02829 - FGSG_16391	6	11.9			+		yes
C31	FGSG_12582 - FGSG_04702	13	35.5	PKS1, PKS2		+	no	yes
C32	FGSG_12597 - FGSG_16406	6	12.8			+		no
C33	FGSG_16474 - FGSG_05374	9	43.3	NPS2	ferricrocin siderophore	+	L	yes
C34	FGSG_17677 - FGSG_05796	3	14.5	PKS5	gibepyrone	+	yes	yes
C35	FGSG_16594 - FGSG_06051	11	32.2			-		no
C36	FGSG_06442 - FGSG_06448	7	16.5		longiborneol (?)	+		yes
C37	FGSG_06449 - FGSG_06462	15	39.4			+		yes
C38	FGSG_06500 - FGSG_06511	14	41.4	NPS10		-	yes	no
C39	FGSG_16672 - FGSG_06542	8	18.6			-		no
C40	FGSG_07582 - FGSG_07596	17	39.8			+		yes
C41	FGSG_07672 - FGSG_07674	3	6.7	STC1	germacrene D (Ff)	+	H	yes
C42	FGSG_07795 - FGSG_16901	12	33.0	PKS10, PKS10	fusarin C	+	L	yes
C43	FGSG_08944 - FGSG_08941	4	6.3			-		no
C44	FGSG_08802 - FGSG_15512	13	45.1	PKS7		-	L	no
C45	FGSG_08414 - FGSG_08410	6	11.4			-		no
C46	FGSG_08321 - FGSG_17057	3	11.4			-		no
C47	FGSG_08209 - FGSG_17085	5	28.9	NPS7, PKS23	fusaristatin A	+	L	yes
C48	FGSG_17087 - FGSG_08175	19	41.6	STC5	tricinonoic acid	+	no	yes
C49	FGSG_08084 - FGSG_08077	8	17.9		butenolide	+		yes
C50	FGSG_08066 - FGSG_08061	6	10.2			+		yes
C51	FGSG_08028 - FGSG_08005	34	78.1			+		yes
C52	FGSG_09060 - FGSG_09086	29	69.1			+		yes
C53	FGSG_17168 - FGSG_09195	14	36.4	PKS3	fusarubin	+	no	yes
C54	FGSG_17177 - FGSG_09217	10	18.5			+		yes
C55	FGSG_09331 - FGSG_09339	13	35.8			+		yes
C56	FGSG_09378 - FGSG_09383	6	19.8			-		no
C57	FGSG_09593 - FGSG_09599	7	14.3			-		no
C58	FGSG_10094 - FGSG_10101	9	32.9			-		no
C59	FGSG_10384 - FGSG_10397	15	37.9	STC9	culmorin	-	no	yes
C60	FGSG_10458 - FGSG_10464	7	22.1	PKS24	fusarielin	+	L	yes
C61	FGSG_10542 - FGSG_17387	8	49.4	NPS18, PKS21		+	L	no
C62	FGSG_10608 - FGSG_10617	11	30.3		terpenoid	+	L	yes
C63	FGSG_11029 - FGSG_11026	4	24.3	NPS1	malonichrome	-	no	no
C64	FGSG_10995 - FGSG_17487	8	54.1	NPS5, NPS9	AM toxin related	-	no	yes
C65	FGSG_10938 - FGSG_17498	11	29.4			-		no
C66	FGSG_11397 - FGSG_11387	11	33.1	NPS14		+	no	yes
C67	FGSG_11557 - FGSG_16059	7	20.3			+		yes

2.3.2 Metabolomics-based chemical screening. We compared SecMet profiles of the *F. graminearum* wildtype to those in the *kmt6* deletion mutant. Previously, we demonstrated that comparative LCMS metabolomics provides a simple yet powerful tool for the analysis of chemical profiles of fungi that were challenged by environmental[20] or chemical stressors.[21] Here we applied similar techniques to identify changes in SecMet output induced by the absence of H3K27 trimethylation. LCMS-based log-ratio analysis was employed to identify metabolites which were overproduced in *kmt6* compared to WT.

Organic extracts of *kmt6* and WT were prepared in biological triplicate and subjected to LC/MS analysis in technical duplicate. LC/MS profiles for each replicate were imported into MZmine 2 for peak binning, followed by log-ratio analysis with the MZmine 2 integrated statistical software package,[24] and the relative expression plot was used to identify metabolites that exhibited high abundance in *kmt6* but not WT. The "log-ratio plot" (Fig. 2.1) shows metabolites associated with WT as grey to light grey dots and metabolites associated strongly with *kmt6* in red or pink, and aids identification of metabolites for isolation.[20]

2.3.3 Overexpression of primary metabolites. We identified a polar, fluorescent compound with an *m/z* value of 166.2 at 14.3 min retention time as *N*-ethyl anthranilic acid (**1**) by 2D NMR (Appendix A, Fig. A1-A5). Though anthranilates are common both as primary metabolites and building blocks in more complex natural products within the fungal kingdom, to the best of our knowledge, this is the first time *N*-ethyl anthranilic acid has been reported as a natural product. WT *Fusarium* does not produce **1**, confirmed by UV/retention time analysis and Extracted Ion Chromatography (EIC) at 166.1 *m/z*. Due to

the surprising *N*-ethyl functionality which is more common in industrial products than natural metabolites, media blanks as controls as well as the culture extracts of three other fungi (*Chalara* sp., *Aspergillus terreus, Phoma* sp.) from the Loesgen Fungal Culture Collection grown on YPD were analyzed by EIC for presence of **1**. No other culture extract was found to produce **1** or a compound of similar retention time and mass, confirming that this metabolite is solely found after deletion of the *kmt6* gene in *F. graminearum*.

Phenethylacetamide (**2**) was isolated with a retention time of 12.6 min, *m/z* value of 203.1, and its structure was elucidated by extensive 2D NMR spectroscopy (Appendix A, Fig. A6-A9). Notably, both **2** and *N*-acetyltryptamine (**3**) are detectable by UV, retention time, and EIC in WT cultures, but are overexpressed twenty- and two-fold, respectively, in the *kmt6* cultures. *N*-acetyltryptamine, exhibits fluorescence at 366 nm and the indole functionality was revealed via Ehrlich's reagent, staining **3** purple on thin layer chromatography (TLC) and possessing matching spectroscopic data (Appendix A, Fig. A10-A12) to *N*-acetyltryptamine from *Fusarium incarnatum*.[34]

2.3.4 Chromatin environment at the fusarin gene cluster. The fusarin C gene cluster (C42) lies on chromosome 4, which contains a total of 17 of the 67 BGCs in *F. graminearum* (Fig. 2.2A). In contrast to H3K27me3 distribution in plants, animals or *Neurospora* (Jamieson et al., 2013), this histone mark is localized in large blocks in *F. graminearum*. The middle 400 kb of the 8.1 Mb chromosome 4 shows dense enrichment with H3K4me3 but a dearth of H3K4me2, a histone modification associated with gene activity (Fig. 2.2B). RNA-seq showed that few genes in this region are expressed in WT, while many, including the three BGCs covered by H3K27me3 (C40, C41 STC1, C42

PKS10/fusarin C), are specifically upregulated in *kmt6* (Fig. 2.2B). Within the predicted fusarin C gene cluster, eight of the eleven proposed cluster genes show increased mRNA levels compared to WT (Fig. 2.2C), confirming our previous RNA-seq analyses that showed upregulation by ~60-fold.[5] The first three genes of the cluster as defined previously[33], however, show no difference in gene expression and should therefore no longer be considered as part of a co-regulated cluster C42.

2.3.5 Overexpression of fusarins in *F. graminearum kmt6*. When compared to WT, dozens of *m/z* peaks were identified as unique or overexpressed from *kmt6* cultures grown in standard yeast-peptone-dextrose (YPD) liquid nutrient medium by either HPLC-DAD, LCMS, or log-ratio analysis. HPLC-DAD analysis indicated that the majority of newly produced metabolites belonged to the same structural class, sharing a common UV chromophore and similar *m/z* profile (Fig. 2.1, yellow highlighted region). Isolation of the major peak produced in *kmt6* led to the identification of fusarin C (**5**) as the primarily overexpressed metabolite and was confirmed by ^{1}H NMR and HRMS (432.2001 [M+H]$^+$ $C_{23}H_{30}NO_7$, calc'd for 432.2020) and NMR (Appendix A, Fig. A13-A15). Our RNA-seq analyses support the ~600-fold higher abundance of total fusarin analogs based on ion count determined here. Two additional members of the fusarin class were identified as fusarin A (**6**) and fusarin D (**7**) by LRMS and NMR analysis (Appendix A, Fig. A16-A20). For each of the three identified metabolites of the proposed fusarin pathway, many double bond isomers have been reported, and isomerization in the presence of UV light has been widely observed.[26] Based on the similar *m/z* values and UV spectra, as well as the structural

confirmation of the isolated fusarins A, C, and D, the cluster of peaks identified in Figure

2.2 were all assigned as fusarin analogs and fragment ions.

A

Chromosome 4

H3K27me3

H3K4me3

BGCs
C36 C38 NPS10   C40   C42 PKS10   C57   C56 C54   C52
C37   C41 STC1   C55 C53 PKS3
C39

B

H3K4me3

H3K27me3

BGCs   C40   C41 STC1   C42 PKS10

Genes

mRNA WT

mRNA kmt6

C

BGCs   C42 PKS10 (fusarin C)

Genes   1 2   3   4 5 6 7 8 9 10 11

mRNA WT

mRNA kmt6

D

fus1::neo⁺ fus8::neo⁺   fus1::neo⁺ fus8::neo⁺
1   2   1   2   WT   1   2   1   2   WT

5 kb
3 kb
2 kb

E

acetyl-CoA
6x malonyl-CoA
4x AdoMet   Fus1   +   Fus 1

displacement

17

decarboxylation

18

methyl group oxidation
O-methyl transfer

8

methyl group oxidation
O-methyl transfer
epoxidation
hydroxylation

Figure 2.2. Chromatin marks on *F. graminearum* chromosome 4, location of biosynthetic gene clusters (BGCs), expression in wildtype and *kmt6* strains, structure of the fusarin C BGC (C42), and proposed biogenesis of fusarins. (A) Chromatin marks and BGCs on chromosome 4. Most BGCs are located in regions with H3K27me3 (orange) enrichment. Gene-rich regions are enriched with H3K4me2 (green). **(B)** Silent regions occur in large blocks, often extending hundreds of kilobases. This view shows that many, but not all genes (dark blue) enriched with H3K27me3 are upregulated after deletion of *kmt6*, suggesting that no additional positive regulators are required for their activation. mRNA levels in WT (blue) and *kmt6* (maroon) were determined by strand-specific RNA-seq. **(C)** Expression landscape around the fusarin C BGC (C42; genes are numbered: 1, FGSG_07796; 2, FGSG_07797; 3, FGSG_07798, fus1/pks10; 4, FGSG_13222, fus2; 5, FGSG_13223, fus3; 6, FGSG_07800, fus4; 7, FGSG_07801, fus5; 8, FGSG_07802, fus6; 9, FGSG_07803, fus7; 10, FGSG_07804, fus8 cytochrome P450; 11, FGSG_07805; Gene numbers in red indicate requirement for fusarin production in *F. fujikuroi* (Niehaus et al). The first, unlabelled gene in C42 (defined by Sieber et al.) is not differentially expressed and thus should not be part of this BGC. Similarly, genes 5 (*fus3*) and 7 (*fus5*) show only minor increase in expression in *kmt6*; neither gene is required for fusarin synthesis in *F. fujikuroi*. Genes 1 and 2 are not induced in *kmt6* or other growth conditions (varied nitrogen and carbon) we have tried. Potential functions for genes 6, 8, and 9 remain to be discovered. Two genes, *fus1/pks10* and *fus8*, were disrupted by integration of a *neo* gene, resulting in G418-resistant transformants (see supplemental data). **(D)** Proposed biogenesis of fusarins A, C and D, as well as the newly identified protofusarin (**8,** blue).

Because fusarins are a predominant class of compounds expressed in *kmt6*, we disrupted the signature gene, *fus1/pks10*, encoding for the FUS1 PKS, and the nearby *fus8* gene, encoding for a cytochrome P450 (Fig. 2.2D). Both genes are required for fusarin C production in *F. fujikuroi*.[13] As described below, this approach made it easier to observe and isolate sufficient quantities of novel compounds such as tricinolone (**9**) masked by the many fusarin isoforms. The cultures did not show overt phenotypes on YPD or minimal medium but we noticed that both *fus1::neo+* and *fus8::neo+* strains were unable to undergo a "selfing"; *F. graminearum* is a homothallic, or self-fertile, species and thus does not require a partner of opposite mating type, as heterothallic fungi do. In previous work, we found that *kmt6* is female sterile (i.e., crosses can only be carried out with *kmt6* spores as "male" or nucleus donor strain). In crosses with tester strains that lack mating type idiomorphs, both *fus1* and *fus8* mutants were sterile both as males and females. To make full use of the global *kmt6*-mediated gene derepression we observed and also reduce the background of fusarins, we thus disrupted the *fus1* and *fus8* genes in the *kmt6* strain.

2.3.6 Isolation of protofusarin. Protofusarin (**8**) was identified as a target for isolation based on its abundance in the log-ratio plot at 26 min with an *m/z* value of 289.2 (Fig. 2.2). Fraction one contained a peak with a matching retention time and *m/z* with an HRMS formula of $C_{18}H_{24}O_3$ (289.1784 *m/z* [M+H]$^+$ calculated for 289.180). The simple UV spectrum (λ_{max} = 347 nm) bore a striking similarity to the fusarin class of compounds. Despite the similar UV, no fusarin published thus far matched the molecular formula obtained by HRMS. The ^{1}H NMR spectrum contained a series of downfield resonances almost identical to fusarin C, yet lacked the resonances associated with the homoserine

moiety usually present in fusarins. A methylketone resonance at 199.9 ppm in the HMBC spectrum indicated truncation of the polyene moiety at the location of the NRPS-PKS connection point. Full 2D NMR assignment (Appendix A, Fig. A21-A25) of the structure revealed a shunt metabolite of the fusarin pathway, which we named protofusarin (**6**). The fusarin C biosynthetic pathway has been well-characterized in *F. fujikuroi*[13] and protofusarin is generated by the action of the PKS, Fus1 (Fig. 2.2).

2.3.7 Overexpression of zearalenones. In addition to the fusarin class of compounds, two gene clusters with PKS genes involved in the zearalenone biosynthetic pathway (*pks4* and *pks13*) have been identified as overexpressed by RNA-seq in *kmt6* YPD cultures (Table 2.1). The log-ratio plot indicates the presence of the parent zearalenone ion (Fig 2.1, **4**, 21 min retention time, *m/z* 319.1) in twofold greater abundance than in WT, which was confirmed by isolation and comparison with a zearalenone standard. Interestingly, *kmt6* cultures grown on barley-spelt medium produced even more zearalenone congeners, in total six known zearalenone isoforms were identified by techniques including NMR, MS, and UV (Appendix A, Fig. A26-A40).

2.3.8 Isolation of fusaristatin. During the metabolomics-guided isolation of new products from *kmt6*, we discovered and isolated a compound with a formula of $C_{36}H_{58}N_4O_7$ (659.4355 *m/z* [M+H]$^+$ calculated for 659.4380) as determined by HRMS. Extracted ion chromatograms indicated that the compound was only produced in *kmt6* cultures, and not in WT cultures, but that it poorly ionizes in positive electron-spray ionization mode and therefore was barely detectable in the log-ratio analysis (Fig. 2.1). Only 100 µg of the metabolite wsa isolated, limiting analysis to HRMS and ^{1}H NMR analysis (Appendix A,

Fig. A41). A review of the literature suggested fusaristatin A (**16**), a cyclic lipopeptide as the likely isolated compound.[27,28] Our RNA-seq data show that none of the genes required for fusaristatin A biosynthesis (in C47) are expressed in WT in YPD, while all C47 genes are overexpressed in *kmt6* (Figure 2.3A). The confirmation of the structure by HRMS and ^{1}H NMR affirmed the production of fusaristatin A in *kmt6*. Lastly, to prove that *pks6* was required for fusaristatin A biosynthesis in the *kmt6* genetic background, we generated a *pks6 kmt6* double mutant in which fusaristatin A synthesis was abolished (Figure 2.3B).
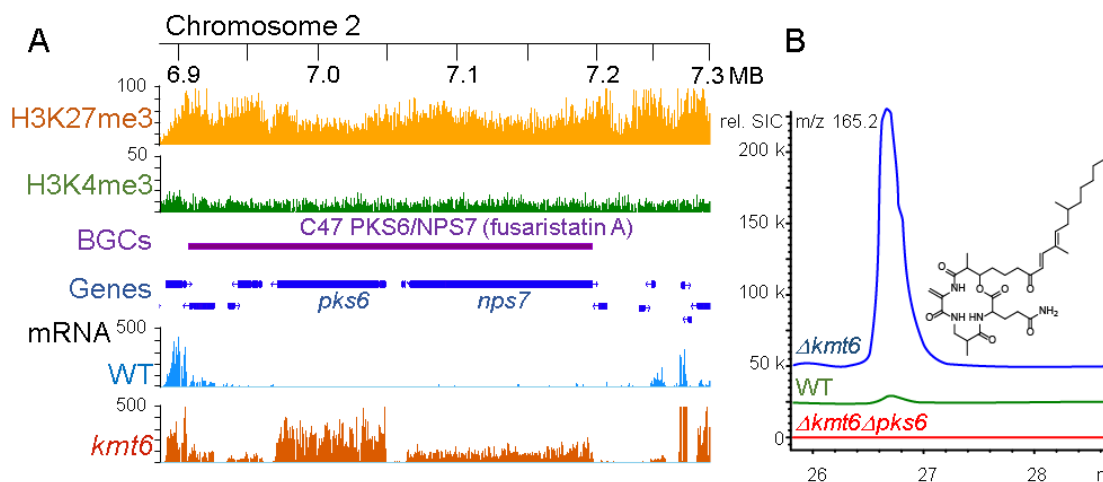
Figure 2.3. BGC C47, including *pks6* and *nrps7*, encodes the machinery to synthesize Fusaristatin A. (A) Chromatin environment, BGCs, genes, and RNAseq of WT and *kmt6*. **(B)** LCMS analysis of *Δkmt6* and *Δkmt6Δpks6* at SIM *m/z* 659.4 in positive mode indicating complete removal of fusaristatin A production in the double delete mutant.

2.3.9 Isolation of gibepyrone A (fusalanipyrone) and fusarpyrones A and B from *F. graminearum.* Further analysis of the log-ratio plot for newly and overproduced

compounds from *kmt6* focused on a peak at 12 min with an *m/z* value of 181.1. Subsequent isolation of the compound from fraction 6d resulted in assignment of the structure as fusarpyrone A (**10**). Subsequently, fusarpyrone B (**11**) and the parent metabolite, gibepyrone A (**9**, aka "fusalanipyrone," [35-37]) were isolated and fully elucidated by 2D NMR (Fig. S42-50).

Recently the biosynthetic origins of gibepyrone in *F. fujikuroi* were reported.[35] In their biosynthetic studies, Janevska et al. determined that gibepyrone F, bearing a similar ketone functionality as fusarpyrone B, is derived non-enzymatically from gibepyrone A. Fusarpyrone A/B production is not reported in *F. fujikuroi* and differs by a hydroxyl-methylene functionality. This oxidized methylene moiety is likely to arise from a P450 monooxygenase which may be cluster independent, as was the case for the oxidized prenyl moieties in gibepyrones B-D in *F. fujikuroi.*

Fusarpyrone B is poorly ionized under positive ionization mode and therefore did not readily appear in the log-ratio analysis. No traces of fusarpyrones A and B can be found in WT by EIC, however low titers of gibepyrone A are detectable. All three compounds have been previously reported from *F. solani*[38] or *F. fujikuroi*[35] but were not previously known from *F. graminearum*. These polyketide derived pyrones have not been associated with a specific BGC in *F. graminearum*, but the presence of these compounds in *F. solani*[37,38] suggests that these gene clusters may be conserved among the two species. Comparing the reference genomes of *F. solani*[39] and *F. graminearum*[40], we found that the PKS5 and PKS7 gene clusters were present in both species and also transcribed in *F. graminearum kmt6*. However, only the predicted PKS5 BGC contains an *S*-adenosylmethionine (SAM)-

dependent methyltransferase domain that is necessary for the biosynthesis of these methylated pyrones.[36] Our RNA-seq data for PKS5 match the production profile observed for gibepyrone A, with low constitutive expression in WT, but enhanced expression in *kmt6* (Fig. 2.4A). Deletion of *pks5* (Fig. 2.4B) in the *kmt6* genetic background abolished gibepyrone/fusarpyrone biosynthesis (Fig. 2.4C).
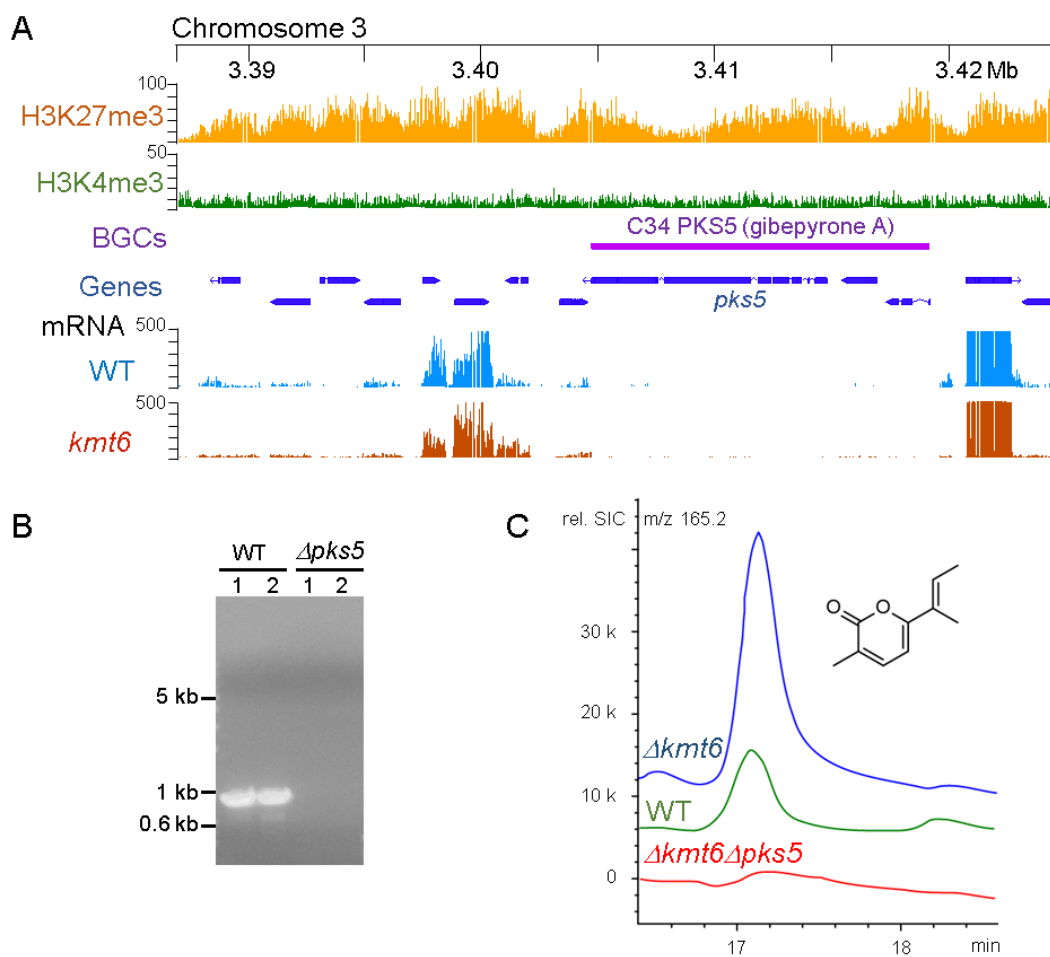
Figure 2.4. BGC C34, encodes and produces gibepyrone A. (A) Chromatin environment, BGCs, genes, and RNAseq of WT and *kmt6* for C34 **(B)** LCMS analysis of *Δkmt6* and *Δkmt6Δpks5* at SIM *m/z* 165.2 in positive mode indicating complete removal of fusaristatin A production in the double delete mutant.

2.3.10 Discovery of the new tricinolone and tricinolonoic acid sesquiterpenes. Log-ratio analysis provided several additional target compounds co-eluting with fusarin-type metabolites. Based on their *m/z* values, these metabolites did not appear to be fragments or

previously unidentified shunt metabolites associated with fusarin. Extensive normal and reversed phase chromatography efforts yielded two compounds with a single UV maximum at 238 nm and *m/z* values of 241.2 and 275.2, matching the log-ratio peaks identified around 20 min. Characterization by 2D NMR revealed tricindiol (**15**) and tricinonoic acid (**14**) (Table 2.2; Appendix A, Fig. A51-A58), originally reported from *F. trinctium.*[41]

Based on this information, we scanned the list of BGCs in *F. graminearum* to assign the most likely gene cluster responsible for production of these sesquiterpenes. The STC5 (C48) gene cluster was the most likely candidate BGC. This cluster as defined previously[33] was predicted to contain 19 genes. Our RNA-seq data revealed that not all 19 genes are co-regulated and that this cluster may need to be broken into subclusters (Fig. 2.5A). We focused on four genes that encode two putative transcription factors (5 and 8), a putative terpene synthase (7), and a putative NRPS (10). We used strains in which either transcription factor *zc117* (Δ1) or *zc116* (Δ2) were deleted and compared expression of these strains to expression in WT cells (Fig. 2.5B). While the histone H3 gene, *hH3*, was expressed in all strains, all four genes showed expression only in *kmt6* (Fig. 2.5B). Even in WT no expression was detected; we used PCR with genomic DNA as controls to indicate size of expected fragments (Fig. 2.5B). LCMS analyses of WT, *kmt6*, *zc117*, and *zc116* strains showed that WT produced low levels of tricinoic acid, which was increased in *kmt6* and abolished in both strains in which the putative transcription factors were deleted, *zc117* and *zc116* (Fig. 2.5D).
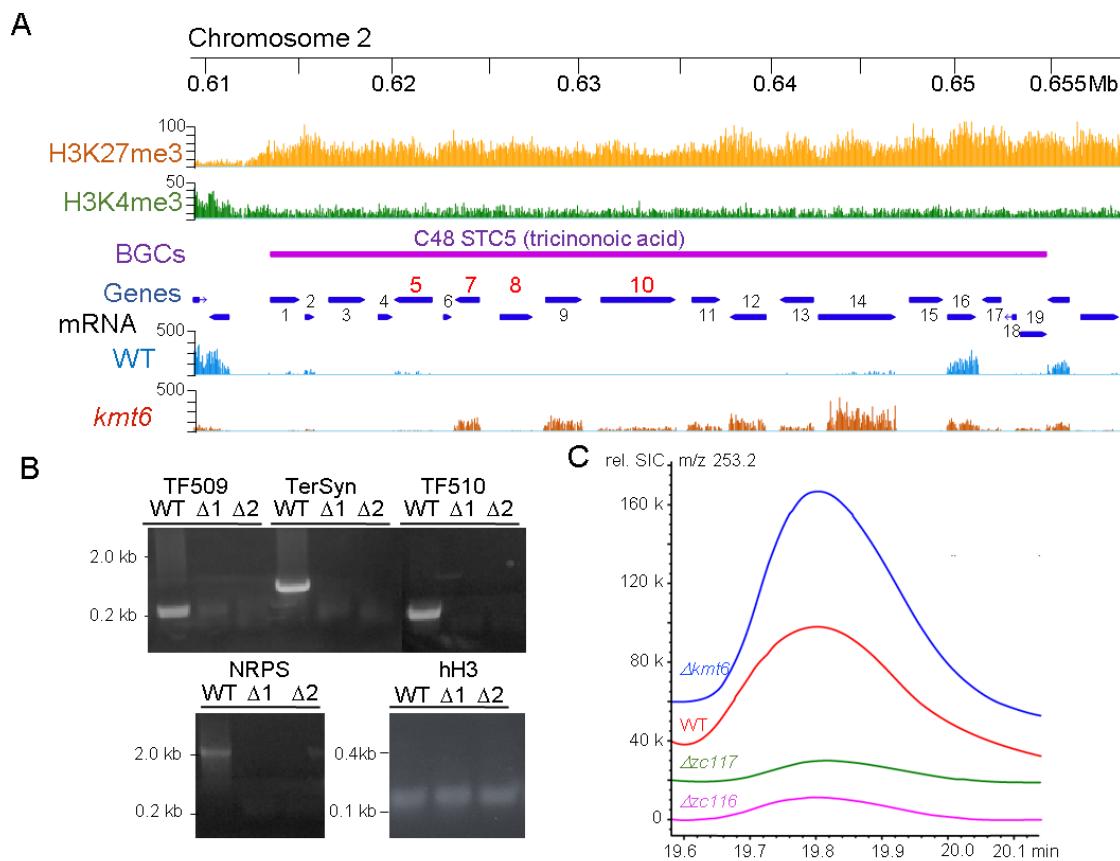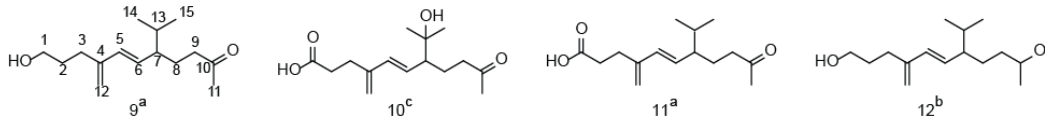
Figure 2.5: BGC C48 encodes a terpene cyclase of the STC5-type and produces tricinonoic acid. (A) Genes in the STC5 BGC: 1, FGSG08175, CHP; 2, FGSG08176, CHP; 3, FGSG08177, MFS sugar transporter; 4, FGSG08178, acetoacetate decarboxylase; 5, FGSG08179, TF510 (*zc117*); 6, FGSG08180, CHP; 7, FGSG08181, related to presilphiperfolan-8-beta-ol synthase (terpene synthase); 8, FGSG08182, TF509 (*zc116*); 9, FGSG08183, Cytochrome P450; 10, FGSG08184, related to nonribosomal peptide synthetase MxcG; 11, FGSG08185, related to spore wall maturation protein (DIT112) involved in pyoverdine or dityrosine biosynthesis, 12, FGSG08186, Cytochrome P450, trichodiene oxygenase; 13, FGSG08187, Cytochrome P450, ent-kaurene oxidase; 14, FGSG08188, copper-transporting ATPase 2, 15, FGSG13429, integral membrane protein,

16, FGSG13428, CHP, 17, FGSG08190, CHP, isoflavone reductase family; 18, FGSG_15467, related to trichodiene synthase; 19, FGSG08191, related to 7-alpha-hydroxycholest-4-en-3-one 12-alpha-hydroxylase. B. D1 938, D2, 939 Genes, histone marks, RNA for C48 **(B)** PCR evidence of deletion of TF genes **(C)** LCMS analysis of ph1 and *Δzc116* and *Δzc117* at SIM *m/z* 253.2 indicating significant reduction of tricinonoic acid production in the transcription factor delete mutants.

During the isolation of tricindiol and tricinonoic acid, another metabolite with 13.5 min retention time in the log-ratio plot and with an *m/z* value of 251.2 ([M-H2O+H]$^+$) caught our interest as it seemed related to tricinonoic acid with a UV profile maximum at 232 nm. HRMS analysis revealed the sodium adduct ion for the compound to be 291.1553, corresponding with a molecular formula of $C_{15}H_{24}O_4Na^+$ (calc'd for 291.1570). Comparison of the ^{1}H NMR spectrum of **13** with that of tricinonoic acid revealed a downfield shift in the methyl signals corresponding to the isopropyl side chain, as well as a loss of coupling between H-11/12 and H-10. Analysis of the HMBC spectrum revealed C-13 was shifted in the new compound to 72.6 ppm, indicating the position was possibly hydroxylated. With the remaining signals almost unchanged the structure was thusly assigned as newly described tricinolonoic acid (Table 2.2; Appendix A, Fig. A59-A61).

Table 2.2. Structures and NMR data for tricinolone, tricinolonoic acid, tricinonoic acid, and tricindiol, recorded in CDCl$_3$ at 500 MHz for proton[a], 800 MHz for tricinolonoic acid[b], and 700 MHz in d$_4$-methanol for tricindiol[c].

position	δH	δC	δH	δC‡	δH	δC	δH	δC‡
	9[a]		10[c]		11[a]		12[b]	
1	3.69 t (6.4)	62.8, CH$_2$		175.5, C$_q$		179.0, C$_q$	3.69 t (6.5)	62.8, CH$_2$
2	1.76 m	31.4, CH$_2$	2.56 br s	32.4, CH$_2$	2.54 br s	33.0, CH$_2$	1.72 m	32.3, CH$_2$
3	2.28 t (7.8)	28.6, CH$_2$	2.56 br s	26.6, CH$_2$	2.54 br s	27.1, CH$_2$	2.29 t (7.7)	28.6, CH$_2$
4		145.7, C$_q$		143.6, C$_q$		144.1, C$_q$		147.0, C$_q$
5	5.98 d (15.8)	133.6, CH	6.1 d (15.8)	135.3, CH	5.99 d (15.8)	133.2, CH	6.01 d (15.8)	134.2, CH
6	5.42 dd (15.8, 9.4)	132.0, CH	5.5 dd (15.8, 9.4)	129.6, CH	5.41 dd (15.8, 9.4)	132.1, CH	5.52 dd (15.8, 9.4)	133.6, CH
7	1.76 m	49.8, CH	1.96 m	54.9, CH	1.77 m	49.7, CH	1.79 m	51.4, CH
8	1.76 m, 1.51 m	26.4, CH$_2$	1.99 m, 1.48 m	23.1, CH$_2$	1.77 m, 1.50 m	26.4, CH$_2$	1.62 m, 1.26 m	29.4, CH$_2$
9	2.36 m	42.2, CH$_2$	2.41 m, 2.37 m	42.0, CH$_2$	2.36 m	42.2, CH$_2$	1.37 m	38.6, CH$_2$
10		209.5, C$_q$		209.9, C$_q$		209.6, C$_q$	3.68 sext. (6.2)	68.7, CH
11	2.10 s	30.3, CH$_3$	2.11 s	29.9, CH$_3$	2.11 s	30.3, CH$_3$	1.31 d (6.2)	23.3, CH$_3$
12	4.93 br s, 4.91 br s	114.0, CH$_2$	5.02 s, 4.98 s	115.0, CH$_2$	4.96 s, 4.91	114.4, CH$_2$	4.91‡, 4.89‡	114.0, CH$_2$
13	1.61 oct. (6.7)	32.5, CH		72.3, C$_q$	1.61 oct. (6.7)	32.5, CH	1.63 oct. (6.7)	33.3, CH
14	0.89 d (6.7)	20.9, CH$_3$	1.21 s	26.6, CH$_3$	0.89 d (6.7)	20.9, CH$_3$	0.91 d (6.7)	21.2, CH$_3$
15	0.84 d (6.7)	19.4, CH$_3$	1.18 s	27.3, CH$_3$	0.84 d (6.7)	19.4, CH$_3$	0.86 d (6.7)	19.4, CH$_3$

Further chemical screening revealed the presence of an additional congener with an *m/z* value of 239.2 and a simple UV spectrum with a maximum at 238 nm. Comparison of the ^{1}H and ^{13}C spectra revealed a nearly identical structure as tricinonoic acid and tricindiol (Table 2.2; Appendix A, Fig. A62-A66). Here, features of tricinonoic acid, a ketone carbonyl ^{13}C NMR shift at 209.4 ppm, and tricindiol, a hydroxy bearing carbon at 62.7 ppm, are combined in tricinolone (**12**), a possible biosynthetic intermediate of tricindiol and tricinolonic acid.

During the original isolation, the stereochemistry of tricindiol was assigned by a combination of Mosher-ester NMR analysis for the C-10 hydroxyl functionality, and *J*-based analysis for the isopropyl moiety at position C-7. We decided to utilize ECD analysis combined with computational prediction of the chiroptical properties of tricindiol, tricinonoic acid, and tricinolone to verify their absolute configuration. The computational

spectra indicated that tricinolone, similarly to tricinonoic acid, exhibits the *S* configuration at the C-7 position (Appendix A, Fig. A67-A68). However, comparison of ECD spectra for tricindiol suggests that the configuration is 7-*R*,10-*S* (Appendix A, Fig. A69) Furthermore, DP4+ analysis of computed and experimental NMR spectra further support the assignment of tricindiol as 7-*R*,10-*S* (Appendix A, Fig. A70). Insufficient material of **12** was available for ECD experiments. Due to the biosynthetic similarities in **12**, **13**, and **14**, we assume the same *S* configuration at the C-7 position. Additionally, fungal sesquiterpene cyclases reported to date appear to exhibit stereoselectivity in their products [42,43], suggesting that the epimerization at C-7 in tricindiol occurs at a step later in the biosynthesis, or is an artifact of culture or isolation conditions. Further synthetic efforts are underway to confirm the absolute configurations of these compounds.

2.4 Discussion

The single H3K27 methyltransferase in *F. graminearum*, KMT6, is an important, global repressor of secondary metabolism, and essential for development and cell differentiation.[5,19] In *F. fujikuroi* it is an essential protein.[19] Elucidating the changes in secondary metabolism in *F. graminearum* upon deletion of *kmt6* was the primary aim of this study. We used LCMS-metabolomics analysis to track changes in secondary metabolite profiles, and to aid isolation and identification natural products resulting from the removal of this regulatory enzyme. In total, sixteen metabolites were isolated, of them eleven were described from *F. graminearum* for the first time, while three metabolites are newly disclosed.

The compounds described here fall into different groups, both in terms of strategy applied to identify and isolate new compounds, and in terms of novelty. In some cases, the absence of KMT6 alone resulted in sufficient overexpression of metabolic pathways that allowed identification of new compounds, as was the case for the three primary metabolites described (*N*-ethyl anthranilic acid (**1**), phenethylacetamide (**2**), and *N*-acetyltryptamine (**3**), as well as zearalenones and fusaristatin A (**16**). *N*-phenethylacetamide (**2**) has not been reported as a metabolite from any *Fusarium* species, but has been isolated from *Protostropharia semiglobata*[44], *Tricladium* sp.[45], and other species[46], and *N*-acetyltryptamine (**3**) has been previously reported from *F. incarnatum* with matching spectroscopic data.[34] Previously, production of fusaristatin A, like that of many other secondary metabolites, required the testing of many different growth media and culture conditions to find situations in which this compound was overproduced. Sørensen and co-workers identified the biosynthetic gene cluster for fusaristatin A from *F. graminearum* in 2014 and found it selectively expressed only in yeast extract/sucrose medium[27,47], slightly different to the yeast peptone/glucose medium used in this study.

Removal of *kmt6* resulted in massive over-production of fusarins, but also identification of the newly described shunt intermediate, protofusarin. This finding exemplifies one general consequence of genetic or chemical perturbation to overproduce natural products by activation of gene clusters, namely that a relatively blunt tool may result in imbalances in precursor or intermediate metabolism that may affect relative abundance of intermediates or final products, or generation of new scaffolds. Protofusarin, with the characterized and well-conserved biosynthetic pathway for fusarin in *F. fujikuroi*

suggests that protofusarin is generated by the action of the PKS, Fus1.[13] Spontaneous decarboxylation of **17** would lead to **18,** which is further tailored by the P450 and O-methylation enzymes, encoded by *fus8* and *fus9*, respectively, to yield the protofusarin (**8**, Fig. 2.2). Interestingly, the tailoring enzymes appear promiscuous and process **18** the same way as fusarin analogues. Notably, the homoserine moiety does not seem to be required for oxidative processing. Though previous shunt metabolites of this pathway have been reported, this is the first time protofusarin has been described.

Like protofusarin, several additional compounds have been found for the first time in *F.graminearum*. For example, fusarpyrone A (**10**), fusarpyrone B (**11**) and gibepyrone A/fusalanipyrone (**9**) were fully elucidated by 2D NMR. While previously reported from *F. solani* and *F. fujikuroi*, we were able to assign BGCs to the production of these compounds in *F. graminearum* by deletion of the gene encoding the signature enzyme of the most likely BGCs.

2.5 Materials and Methods

2.5.1 Strains and culture conditions. A wildtype (WT) *F. graminearum* strain (PH-1) and the *kmt6* deletion strain (FMF361) have been described.[5] The same approach was used to disrupt *fus1* (aka *pks10*; FGSG_07798), *fus8* (FGSG_07804) and *pks5* (FGSG_17677) by insertion of the *neo* gene, which confers resistance to G418. Strains bearing deletions of transcription factor genes *zc116* (TF509, FMF938) and *zc117* (TF510; FMF939) were a kind gift from Yin-Won Lee and Hokyoung Son (Seoul National University, Korea) and were constructed as described.[22]

Unless specified elsewhere, strains were grown in liquid yeast extract-peptone-dextrose (YPD) to collect vegetative tissue. To generate macroconidia, a small amount of frozen conidia or tissue was inoculated into 50 ml flasks containing CMC medium (carboxymethylcellulose) and shaken at 150 rpm for 3–4 days at room temperature (RT, ~22 °C). Conidia were collected by filtration through cheesecloth and stored at −80 °C in 25% glycerol. Crosses were performed on carrot agar at RT, taking usually ~10 days. For metabolomics analysis, triplicate 50 ml cultures of PH1 and *kmt6* were grown for seven days in YPD broth in the dark. For secondary metabolite isolation, cultures of YPD broth were inoculated with conidia and grown for seven days at 200 rpm at 21 °C.

2.5.2 RNA-seq analysis. Total RNA was isolated from aliquots of the same tissue that was used for chromatin immunoprecipitation (ChIP) by a previously described method, and mRNA was isolated using a Poly(A)Purist MAG kit (Ambion). We removed DNA by treatment with RNase-free DNAase (Qiagen), followed by column clean-up according to manufacturer's instructions. cDNA was generated with Superscript III (Thermo) and either subjected to region-specific semi-quantitative PCR with gene-specific primers or used to make libraries for high-throughput sequencing. We used Illumina TruSeq RNA Sample Preparation kits to make RNA-seq libraries; cDNA was sequenced on Illumina HiSeq2000 or HiSeq3000 genome analyzers and analyzed as described previously[5]

2.5.3 General spectroscopic and chromatographic procedures. UV spectra were recorded on a BioRad SmartSpec3000. IR spectra were recorded on a Thermo Scientific Nicolet 6700 FT-IR spectrometer. NMR spectra were acquired on a Bruker Avance III 500 MHz or Bruker Avance III 700 MHz spectrometer, equipped with a 5 mm TXI probe or 5

mm BBO probe (500 MHz and 700 MHz) or TCI cryoprobe (700 MHz), with the residual solvent used as an internal standard (d_6-DMSO 2.50/39.52; CDCl$_3$: 7.26/77.16; d4-methanol: 3.31/49.00, d_5-pyridine: 8.74/150.35). Low-resolution ESI-MS and high-resolution TOF-MS (ESI+) mass spectra were recorded on Agilent 1100 series LC with MSD 1946 and Agilent 1260 series LC with 6230 TOF MS, respectively. A Teledyne Isco CombiFlash Companion system was used for adaptive gradient, automated flash chromatography. Analytical HPLC was performed using an Agilent 1100 HPLC system equipped with a photodiode array detector. The mobile phase consisted of ultra-pure water (A) and MeCN (B) with 0.05% formic acid in each solvent. A gradient method from 10% B to 100% B in 35 min at a flow rate of 0.8 ml/min was used. The column (Phenomenex Kinetex C18, 5 μm x 150 mm x 4.6 mm) was re-equilibrated before each injection, and the column compartment was maintained at 30 °C throughout each run. Semi-preparative HPLC (Phenomenex Kinetex C18, 5 μm x 150 mm x 10 mm column) utilized isocratic elution conditions or a gradient system with a flow rate of 4 ml/min on an Agilent 1100 HPLC system operating at room temperature equipped with a photodiode array detector. Preparative HPLC (Phenomenex Luna C18, 5 μm x 250 mm x 21mm column) was conducted at room temperature, using isocratic elution conditions or a gradient system with a flow rate of 20 ml/min utilizing an Agilent 1260 Infinity series HPLC equipped with a DAD detector. All samples were filtered through a 0.45 μm nylon filter before LCMS and HPLC analysis. Analytical thin layer chromatography (TLC) was performed on pre-coated silica gel 60 F254 plates (Eppendorf). TLC plates were visualized by UV (254 and 360

nm), and by spraying with p-anisaldehyde solution followed by heating at 80 °C. General solvents and reagents were from Sigma-Aldrich Corp. and VWR International.

2.5.4 Metabolomics analysis. Triplicate cultures of WT and *kmt6* grown in YPD medium were extracted with 50 ml EtOAc at 200 rpm and ambient temperatures for 48 h. The organic phase was separated and washed with a single 50 ml portion of distilled H_2O before drying *in vacuo.* Each extract was prepared to 10 mg/ml in 1:1 ACN:MeOH for LCMS analysis. Each sample was analyzed in duplicate on an Agilent 1100 series LC/MS platform. Positive mode ionization was found to detect most metabolites and used for all further analyses; similar results have been previously observed by other groups.[23] Data sets were exported from Agilent's Chemstation software as .netCDF files and imported into MZmine 2.21.[24] Peak picking was performed with established protocols[20,23,25] resulting in 202 marker ions. Mass detection was centroid with 1E2 minimum height. Chromatogram building was limited to peaks greater than 0.1 min with 0.1 *m/z* tolerance and 5E2 minimum height. Data smoothing was performed at a filter width of 13. Chromatogram deconvolution utilized local minimum search with 50% threshold, 5 min search range, 25% relative height, 1E4 minimum abs. height, 2 minimum ratio of top/edge, and peak duration from 0.2-3 minutes. All treatments were then aligned and duplicate peaks combined with a tolerance of 0.1 *m/z* and 0.2 minutes. Peak finder gap filling was performed with 75% shape tolerance and 0.1 *m/z* tolerance. Log-ratio analysis was carried out with MZmine's integrated statistical software.

2.5.5 Isolation and structure elucidation. For the preliminary metabolite isolation culture, 4 l of YPD broth was inoculated with *kmt6* conidia and grown in the light for 5

days at 200 rpm. The culture was extracted with 4 l EtOAc overnight. The organic layer was collected and dried *in vacuo* to yield 3.2 g. This extract was separated by semiautomated flash column chromatography with an ISCO Combiflash on a 40 g silica column (Grace Reveleris) utilizing a gradient from 100% hexane to 100% EtOAc to 100% MeOH with adaptive gradient pausing. Seven fractions were combined by analysis of UV chromatograms at 254 and 280 nm and labeled as fractions 1-7. Final compound isolations were performed utilizing HPLC-DAD. Fusarin C (**5**), A(**6**), and D (**7**) were isolated from fraction 2 and identified base on UV, LR-MS, and ^{1}H NMR compared to literature.[13,26] Fusaristatin A (**16**) was isolated from fraction 5 and its structure confirmed by HRMS and ^{1}H NMR.[27,28] Zearalenone (**4**) was identified by LRMS, HRMS, UV, and retention time as compared with a confirmed standard.[29] Protofusarin (**8**) and tricinolonoic acid (**13**) were isolated from fraction 1.

A second 18 l culture of YPD broth with 50 g of XAD-7 resin (Acros) per liter was inoculated with conidia of *kmt6* grown in the dark at 200 rpm for seven days. The XAD resin was filtered off and washed with 18 l of distilled H_2O. The resin was then stirred with 5 l acetone and methanol. The organic extracts were combined and dried *in vacuo* to yield 44 g product. The culture extract was loaded onto 88 g silica (SiliaFlash P60, Silicycle) and subjected to vacuum liquid chromatography with step gradients of 99:1, 50:1, 30:1, 15:1, 9:1, 3:1, 2:1, 1:1, and 0:1 DCM:MeOH and labeled as fractions 1-9. Fraction 6 (2.36 g) was further separated by semiautomated flash column chromatography with an ISCO Combiflash on a 12 g silica column (Grace Reveleris) utilizing a gradient from 100% hexane to 100% EtOAc to 100% MeOH with adaptive gradient pausing. Ten fractions were

separated by analysis of UV chromatograms at 254 and 280 nm and labeled as fractions 6a-6j. Tricindiol (**15**) was isolated from fraction 6d and tricinonoic acid (**14**) and tricinolone (**12**) from 6c. Gibepyrone A (**9**) was isolated from fraction 3. Related fusarpyrones A (**10**) and B (**11**) were isolated from fraction 6d. *N*-acetyltryptamine (**3**) was isolated from fraction 6g. Phenethylacetamide (**2**) and *N*-ethylanthranilic acid (**1**) were isolated from fraction 6c.

2.5.6 Computational details. Initial conformational analysis for tricinolone (**12**), tricindiol (**15**), and tricinonoic acid (**14**) was performed in Spartan '14 (Wavefunction) using MMFF94 with 100,000 maximum conformers generated. All conformers with a relative energy lower than 5 kcal/mol were carried forward for QM analysis. The conformers were saved as an .SDF file and a Python script was used to generate Gaussian 09[30] input files for each geometry for gas and solvated optimization and frequency calculations as well as TDDFT computations. Gas phase geometry optimization and frequency calculations were performed at the B3LYP/6-31G level and were analyzed for duplicate conformers and imaginary frequencies using a Python script.[31] Conformers with a relative energy lower than 5 kcal/mol were once again carried forward for more rigorous QM geometry optimization with IEFPCM in acetonitrile at the B3LYP/def2TZVP level. The Gaussian outfiles were analyzed as above, and conformers contributing to greater than 1% were carried forward in TDDFT calculations. The ECD spectra were calculated by the TDDFT methodology at the B3LYP/def2TZVP level utilizing integral equation formalism variant polarizable continuum model (IEFPCM) with 40 states in acetonitrile. UV and ECD spectra were generated and Boltzmann averaged utilizing a Python script developed by the

authors which is available upon request. The script relies significantly on the computational chemistry parsing utility cclib.[32] Tricinonoic acid and tricinolone were found to have 7-*S* configurations. Tricindiol was further analyzed by computation of NMR shielding tensors at the MPW1PW91/6-31+G* level and analyzed by DP4+. The combination of DP4+ and ECD computation support a configuration of 7-*R*, 10-*S* for tricindiol, however future synthetic studies are required to verify the absolute configuration of tricindiol.

2.5.7 Characterization of new secondary metabolites.

***N*-Ethylanthranillic acid.** 1.5 mg (**1**): colorless oil; UV (MeOH) λ_{max} (log ε) 216 (1.16), 254 (0.40) nm; HRESIMS: 164.0719 *m/z* [M-H]$^-$ (calcd for $C_9H_{10}NO_2^-$ 164.0720, Δppm: 1.2); ^{13}C NMR (176 MHz, d_4-methanol) 172.4 (C, C-1), 152.6 (C, C-7), 135.5 (CH, C-5), 133.2 (CH, C-3), 115.4 (CH, C-4), 112.2 (CH, C-6), 111.7 (C, C-2, HMBC), 38.3 (CH$_2$, C-8), 14.8 (CH$_3$, C-9); δ ^{1}H NMR (700 MHz, d_4-methanol) δ 7.89 (1H, dd, *J* = 7.9, 1.6 Hz, H-1), 7.33 (1H, ddd, *J* = 8.5, 7.1, 1.7, H-3), 6.71 (1H, d, *J* = 8.5 Hz, H-4), 6.54 (1H, ddd, *J* = 8.5, 7.9, 1.0 Hz, H-2), 3.22 (2H, q, *J* = 7.2 Hz, H-5), 1.29 (3H, t, *J* = 7.2 Hz, H-6).

Protofusarin. 1.5 mg (**8**): straw yellow oil; UV (MeOH) λ_{max} (log ε) 347 (0.37) nm; HRESIMS: 289.1784 *m/z* [M+H]$^+$ (calculated for $C_{18}H_{25}O_3$ 289.1800, Δppm = 4.9); ^{13}C NMR (176 MHz, CDCl$_3$, dept135/HMBC) 199.7 (C, C-11), 167.8 (C, C-1), 145.6 (CH, C-7), 140.0 (CH, C-14), 139.8 (CH, C-9), 138.9 (CH, C-5), 137.6 (C, C4), 135.8 (C, C-10), 135.0 (C, C-6), 130.5 (C, C-2), 125.4 (CH, C-3), 123.8 (CH, C-8), 51.9 (CH$_3$, C-13), 25.5 (CH$_3$, C-12), 18.8 (CH$_3$, C16), 16.0 (CH$_3$, C-15), 14.1 (CH$_3$, C-17), 11.6 (CH$_3$, C-18); δ[1]H NMR (700 MHz, CDCl$_3$) δ 7.13 (1H, d, *J* = 10.6, H-9), 6.99 (1H, qd, *J* = 7.3, 0.8 Hz, H-

14), 6.66 (1H, d, $J = 15.1$ Hz, H-3), 6.60 (1H, dd, $J = 15.1, 10.6$ Hz, H-4), 6.22 (1H, s, H-2), 6.05 (1H, s, H-1), 3.75 (3H, s, H-7), 2.37 (3H, s, H-6), 2.08 (3H, s, H-11), 1.94 (3H, s, H-12), 1.78 (3H, dd, $J = 7.2, 1.2$ Hz, H-9), 1.73 (3H, s, H-10).

Tricinolone. 6.1 mg (**12**): colorless oil; UV (MeOH) λ_{max} (log ε) 233 nm (1.37); HRESIMS: 273.1633 *m/z* [M+Cl]$^-$ (calculated for $C_{15}H_{26}O_2Cl^-$ 273.1630, Δppm: 2.3); *see table 2.2 for NMR data.*

Tricinolonoic acid. 150 μg (**13**): colorless oil; UV (MeOH) λ_{max} (log ε) 238 nm (1.31); HRESIMS: 291.1554 *m/z* [M+Na]$^+$ (calcd for $C_{15}H_{24}O_4Na^+$ 291.1570, Δppm: 2.34); *see table 2.2 for NMR data.*

2.6 Supplemental Material

Supplemental material for this article may be found in Appendix A of this dissertation.

2.7 Acknowledgements

2.8 References

1. Brakhage, A. A. *Nat. Rev. Microbiol.* **2013**, *11*, 21.
2. Calvo, A. M.; Wilson, R. A.; Bok, J. W.; Keller, N. P. *Microbiol. Mol. Biol. Rev.* **2002**, *66*, 447.
3. Bok, J. W.; Keller, N. P. *Eukaryot. Cell* **2004**, *3*, 527.
4. Fox, E. M.; Howlett, B. J. *Curr. Opin. Microbiol.* **2008**, *11*, 481.
5. Connolly, L. R.; Smith, K. M.; Freitag, M. *PLoS Genet.* **2013**, *9*, e1003916.
6. Jeon, J.; Choi, J.; Lee, G.-W.; Park, S.-Y.; Huh, A.; Dean, R. A.; Lee, Y.-H. *Sci. Rep.* **2015**, *5*, 8567.
7. Cherblanc, F. L.; Davidson, R. W. M.; Di Fruscia, P.; Srimongkolpithak, N.; Fuchter, M. J. *Nat. Prod. Rep.* **2013**, *30*, 605.
8. Williams, R. B.; Henrikson, J. C.; Hoover, A. R.; Lee, A. E.; Cichewicz, R. H. *Org. Biomol. Chem.* **2008**, *6*, 1895.
9. Brakhage, A. A.; Schroeckh, V. *Fungal Genet. Biol.* **2011**, *48*, 15.
10. Aghcheh, R. K.; Kubicek, C. P. *Appl. Microbiol. Biotechnol.* **2015**, *99*, 6167.
11. Albright, J. C.; Henke, M. T.; Soukup, A. A.; McClure, R. A.; Thomson, R. J.; Keller, N. P.; Kelleher, N. L. *ACS Chem. Bio.* **2015**, *10*, 1535.
12. Henke, M. T.; Soukup, A. A.; Goering, A. W.; McClure, R. A.; Thomson, R. J.; Keller, N. P.; Kelleher, N. L. *ACS Chem. Biol.* **2016**, *11*, 2117.
13. Niehaus, E.-M.; Kleigrewe, K.; Wiemann, P.; Studt, L.; Sieber, Christian M. K.; Connolly, Lanelle R.; Freitag, M.; Güldener, U.; Tudzynski, B.; Humpf, H.-U. *Chem. Biol.* **2013**, *20*, 1055.
14. Smith, K. M.; Kothe, G. O.; Matsen, C. B.; Khlafallah, T. K.; Adhvaryu, K. K.; Hemphill, M.; Freitag, M.; Motamedi, M. R.; Selker, E. U. *Epigenetics Chromatin.* **2008**, *1*, 5.
15. Jamieson, K.; Rountree, M. R.; Lewis, Z. A.; Stajich, J. E.; Selker, E. U. *Proc. Natl. Acad. Sci. USA* **2013**, *110*, 6027.
16. Sarikaya-Bayram, Ö.; Bayram, Ö.; Feussner, K.; Kim, J.-H.; Kim, H.-S.; Kaever, A.; Feussner, I.; Chae, K.-S.; Han, D.-M.; Han, K.-H.; Braus, Gerhard H. *Dev. Cell* **2014**, *29*, 406.
17. Shaver, S.; Casas-Mollano, J. A.; Cerny, R. L.; Cerutti, H. *Epigenetics* **2010**, *5*, 301.
18. Margueron, R.; Reinberg, D. *Nature* **2011**, *469*, 343.
19. Studt, L.; Rösler, S. M.; Burkhardt, I.; Arndt, B.; Freitag, M.; Humpf, H.-U.; Dickschat, J. S.; Tudzynski, B. *Appl. Environ. Microbiol* **2016**, *18*, 4037.
20. Adpressa, D. A.; Loesgen, S. *Chem. Biodivers.* **2016**, *13*, 253.
21. Adpressa, D. A.; Stalheim, K. J.; Proteau, P. J.; Loesgen, S. *ACS Chem. Biol.* **2017**.
22. Son, H.; Seo, Y. S.; Min, K.; Park, A. R.; Lee, J.; Jin, J. M.; Lin, Y.; Cao, P.; Hong, S. Y.; Kim, E. K.; Lee, S. H.; Cho, A.; Lee, S.; Kim, M. G.; Kim, Y.; Kim, J. E.; Kim, J. C.; Choi, G. J.; Yun, S. H.; Lim, J. Y.; Kim, M.; Lee, Y. H.; Choi, Y. D.; Lee, Y. W. *PLoS Pathog.* **2011**, *7*, e1002310.
23. Hou, Y.; Braun, D. R.; Michel, C. R.; Klassen, J. L.; Adnani, N.; Wyche, T. P.; Bugni, T. S. *Anal. Chem.* **2012**, *84*, 4277.

24. Pluskal, T.; Castillo, S.; Villar-Briones, A.; Oresic, M. *BMC Bioinformatics* **2010**, *11*, 395.

25. Abdelmohsen, U.; Cheng, C.; Viegelmann, C.; Zhang, T.; Grkovic, T.; Ahmed, S.; Quinn, R.; Hentschel, U.; Edrada-Ebel, R. *Mar.Drugs* **2014**, *12*, 1220.

26. Kleigrewe, K.; Aydin, F.; Hogrefe, K.; Piecuch, P.; Bergander, K.; Würthwein, E.-U.; Humpf, H.-U. *J. Agric. Food. Chem.* **2012**, *60*, 5497.

27. Sørensen, J. L.; Sondergaard, T. E.; Covarelli, L.; Fuertes, P. R.; Hansen, F. T.; Frandsen, R. J. N.; Saei, W.; Lukassen, M. B.; Wimmer, R.; Nielsen, K. F.; Gardiner, D. M.; Giese, H. *J. Nat. Prod.* **2014**, *77*, 2619.

28. Shiono, Y.; Tsuchinari, M.; Shimanuki, K.; Miyajima, T.; Murayama, T.; Koseki, T.; Laatsch, H.; Funakoshi, T.; Takanami, K.; Suzuki, K. *J Antibiot.* **2007**, *60*, 309.

29. Cordier, C.; Gruselle, M.; Jaouen, G.; Hughes, D. W.; McGlinchey, M. J. *Magn. Reson. Chem.* **1990**, *28*, 835.

30. Frisch, M. J.; Trucks, G. W.; Schlegel, H. B.; Scuseria, G. E.; Robb, M. A.; Cheeseman, J. R.; Scalmani, G.; Barone, V.; Mennucci, B.; Petersson, G. A.; Nakatsuji, H.; Caricato, M.; Li, X.; Hratchian, H. P.; Izmaylov, A. F.; Bloino, J.; Zheng, G.; Sonnenberg, J. L.; Hada, M.; Ehara, M.; Toyota, K.; Fukuda, R.; Hasegawa, J.; Ishida, M.; Nakajima, T.; Honda, Y.; Kitao, O.; Nakai, H.; Vreven, T.; Montgomery Jr., J. A.; Peralta, J. E.; Ogliaro, F.; Bearpark, M. J.; Heyd, J.; Brothers, E. N.; Kudin, K. N.; Staroverov, V. N.; Kobayashi, R.; Normand, J.; Raghavachari, K.; Rendell, A. P.; Burant, J. C.; Iyengar, S. S.; Tomasi, J.; Cossi, M.; Rega, N.; Millam, N. J.; Klene, M.; Knox, J. E.; Cross, J. B.; Bakken, V.; Adamo, C.; Jaramillo, J.; Gomperts, R.; Stratmann, R. E.; Yazyev, O.; Austin, A. J.; Cammi, R.; Pomelli, C.; Ochterski, J. W.; Martin, R. L.; Morokuma, K.; Zakrzewski, V. G.; Voth, G. A.; Salvador, P.; Dannenberg, J. J.; Dapprich, S.; Daniels, A. D.; Farkas, Ö.; Foresman, J. B.; Ortiz, J. V.; Cioslowski, J.; Fox, D. J.; Gaussian, Inc.: Wallingford, CT, USA, 2009.

31. Willoughby, P. H.; Jansma, M. J.; Hoye, T. R. *Nat. Protocols* **2014**, *9*, 643.

32. O'Boyle, N. M.; Tenderholt, A. L.; Langner, K. M. *J. Comput. Chem.* **2008**, *29*, 839.

33. Sieber, C. M. K.; Lee, W.; Wong, P.; Münsterkötter, M.; Mewes, H.-W.; Schmeitzl, C.; Varga, E.; Berthiller, F.; Adam, G.; Güldener, U. *PLOS ONE* **2014**, *9*, e110311.

34. Li, L. Y.; Ding, Y.; Groth, I.; Menzel, K. D.; Peschel, G.; Voigt, K.; Deng, Z. W.; Sattler, I.; Lin, W. H. *J. Asian Nat. Prod. Res.* **2008**, *10*, 775.

35. Janevska, S.; Arndt, B.; Niehaus, E.-M.; Burkhardt, I.; Rösler, S. M.; Brock, N. L.; Humpf, H.-U.; Dickschat, J. S.; Tudzynski, B. *J. Biol. Chem.* **2016**.

36. Abraham, W.-R.; Knoch, I.; Witte, L. *Phytochemistry* **1990**, *29*, 2877.

37. Abraham, W.-R.; Arfmann, H.-A. *Phytochemistry* **1988**, *27*, 3310.

38. Trisuwan, K.; Rukachaisirikul, V.; Borwornwiriyapan, K.; Phongpaichit, S.; Sakayaroj, J. *Phytochemistry Lett.* **2013**, *6*, 495.

39. Coleman, J. J.; Rounsley, S. D.; Rodriguez-Carres, M.; Kuo, A.; Wasmann, C. C.; Grimwood, J.; Schmutz, J.; Taga, M.; White, G. J.; Zhou, S.; Schwartz, D. C.; Freitag, M.; Ma, L.-j.; Danchin, E. G. J.; Henrissat, B.; Coutinho, P. M.; Nelson, D. R.; Straney, D.; Napoli, C. A.; Barker, B. M.; Gribskov, M.; Rep, M.; Kroken, S.; Molnár, I.; Rensing, C.; Kennell, J. C.; Zamora, J.; Farman, M. L.; Selker, E. U.; Salamov, A.;

Shapiro, H.; Pangilinan, J.; Lindquist, E.; Lamers, C.; Grigoriev, I. V.; Geiser, D. M.; Covert, S. F.; Temporini, E.; VanEtten, H. D. *PLOS Genet.* **2009**, *5*, e1000618.

40. Cuomo, C. A.; Güldener, U.; Xu, J.-R.; Trail, F.; Turgeon, B. G.; Di Pietro, A.; Walton, J. D.; Ma, L.-J.; Baker, S. E.; Rep, M.; Adam, G.; Antoniw, J.; Baldwin, T.; Calvo, S.; Chang, Y.-L.; DeCaprio, D.; Gale, L. R.; Gnerre, S.; Goswami, R. S.; Hammond-Kosack, K.; Harris, L. J.; Hilburn, K.; Kennell, J. C.; Kroken, S.; Magnuson, J. K.; Mannhaupt, G.; Mauceli, E.; Mewes, H.-W.; Mitterbauer, R.; Muehlbauer, G.; Münsterkötter, M.; Nelson, D.; O'Donnell, K.; Ouellet, T.; Qi, W.; Quesneville, H.; Roncero, M. I. G.; Seong, K.-Y.; Tetko, I. V.; Urban, M.; Waalwijk, C.; Ward, T. J.; Yao, J.; Birren, B. W.; Kistler, H. C. *Science* **2007**, *317*, 1400.

41. Bashyal, B. P.; Leslie Gunatilaka, A. A. *Nat. Prod. Res.* **2010**, *24*, 349.

42. Schmidt-Dannert, C. *Adv. Biochem. Eng. Biotechnol.* **2015**, *148*, 19.

43. Lopez-Gallego, F.; Wawrzyn, G. T.; Schmidt-Dannert, C. *Appl. Environ. Microbiol.* **2010**, *76*, 7723.

44. Reinoso, R.; Cajas-Madriaga, D.; Martínez, M.; San Martín, A.; Pérez, C.; Fajardo, V.; Becerra, J. *J. Chil. Chem. Soc.* **2013**, *58*, 2016.

45. Zou, X.; Liu, S.; Zheng, Z.; Zhang, H.; Chen, X.; Liu, X.; Li, E. *Chem. Biodivers.* **2011**, *8*, 1914.

46. Wu, H.-H.; Tian, L.; Chen, G.; Xu, N.; Wang, Y.-N.; Sun, S.; Pei, Y.-H. *J. Asian Nat. Prod. Res* **2009**, *11*, 748.

47. Hegge, A.; Lønborg, R.; Nielsen, D.; Sørensen, J. *Metabolites* **2015**, *5*, 184.

48. Smith, K. M.; Phatale, P. A.; Bredeweg, E. L.; Connolly, L. R.; Pomraning, K. R.; Freitag, M. In *Reviews in Cell Biology and Molecular Medicine*; Wiley-VCH Verlag GmbH & Co. KGaA: 2006.

Chapter 3 – adapted from the published article

"Unexpected biotransformation of the HDAC inhibitor vorinostat yields aniline-containing fungal metabolites"

Donovon A. Adpressa, Kayla J. Stalheim, Philip J. Proteau, and Sandra Loesgen

3.1 Abstract

The diversity of genetically encoded small molecules produced by filamentous fungi remains largely unexplored, which makes these fungi an attractive source for the discovery of new compounds. However, accessing their full chemical repertoire under common laboratory culture conditions is a challenge. Epigenetic manipulation of gene expression has become a well-established tool for overcoming this obstacle. Here we report that perturbation of the endophytic ascomycete *Chalara* sp. 6661, producer of the isofusidienol class of antibiotics, with the HDAC inhibitor vorinostat resulted in the production of four new modified xanthones. The structures of chalanilines A (**19**) and B (**20**) and adenosine-coupled xanthones A (**21**) and B (**22**) were determined by extensive NMR spectroscopic analyses, and the bioactivities of 19-22 were tested in antibiotic and cytotoxicity assays. Incorporation studies with deuterium-labeled vorinostat indicate that the aniline moiety in chalalanine A is derived from vorinostat itself. Our study shows that *Chalara* sp. is able to metabolize the HDAC inhibitor vorinostat to release aniline. This is a rare report of fungal biotransformation of the popular epigenetic modifier vorinostat into aniline-containing polyketides.

3.2 Introduction

Filamentous fungi have been successfully mined for natural product derived drug leads since the discovery of the first widely used modern antibiotic, penicillin, by Sir Alexander Fleming.[1] Apart from beta-lactam antibiotics, filamentous fungi have inspired and revolutionized modern medicine by providing the antilipidemic lovastatin, the immune

suppressive cyclosporine, the antifungal griseofulvin, and numerous alkaloids.[2] Nonetheless, with close to 1,000 genomes of diverse filamentous fungi sequenced, it has become evident that most fungal strains have far more biosynthetic gene clusters for secondary metabolites than the number of compounds usually identified in chemical studies.[3] This suggests that under standard laboratory conditions many of these gene clusters are transcriptionally suppressed and that there is a large untapped chemical potential that lies dormant in fungi. The discovery of various novel bioactive compounds from these organisms shows an untapped wealth of products is encoded in these newly annotated fungal secondary metabolite gene clusters.[4-6] Recent advances in chromatin-based genetic regulation, as well as chemical manipulation via epigenetic modification, could make the products of these cryptic or silent gene clusters accessible.[7, 8] Indeed, even exceedingly well-studied fungal model organisms (e.g., *Aspergillus nidulans*, *A. niger, Fusarium fujikuroi*) have been found to produce novel compounds upon genetic modifications.[9, 10]

In a previous study, we isolated chromone-3-oxepines from *Chalara* sp. 6661, an endophytic fungus isolated from the salt tolerant plant Artemisia vulgaris. When the fungus is cultured under a variety conditions, the so-called "One Strain Many Compounds" (OSMAC) concept,[11] it produces the isofusidienol family of anti-microbial polyketides. We found that this strain produces primarily isofusidienols A and B (**24,25**) when grown on malt agar plates, but produces the saturated congeners isofusidienols C and D (**26,27**) in static liquid cultures.[12] In addition to varied environmental conditions, chemical epigenetic perturbation agents, such as histone deacetylase (HDAC) inhibitors or DNA

methyltransferase inhibitors, have been successfully employed to induce transcriptional up-regulation of many polyketides and peptide encoding gene clusters. For example, the HDAC inhibitor suberoylanilide hydroxamic acid (**23**, vorinostat) has been widely used and induced the production of the meroterpenoid chaetophenol,[13] the chlorinated daldinone E,[14] and the cyclodepsipeptide EGM-556[15] in various fungi. In an effort to further explore the chemical potential of *Chalara*, we employed a chemical perturbation strategy to epigenetically induce the expression of a greater diversity of secondary metabolites. After establishing a tolerable concentration, we treated the fungus with three HDAC inhibitors: sodium butyrate, suberobishydroxamic acid (SBHA), and vorinostat (**23**), as well as the DNA methyltransferase inhibitor 5-azacytidine (Figure 3.1).[16]
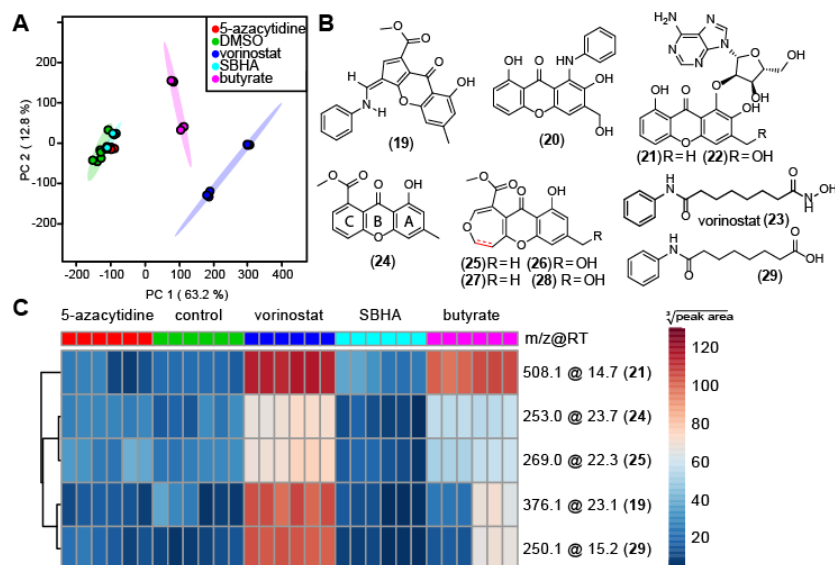
Figure 3.1. a) LCMS PCA analysis of culture extracts from *Chalara* sp. 6661 treated with 5-azacytidine, vorinostat (**23**), suberobishydroxamic acid (SBHA), sodium butyrate, or DMSO (0.1%). b) Metabolites isolated from *Chalara* sp. 6661 in this study (**19-22,24**) and previously (**25-28**). c) Relative expression analysis of compound TIC intensity based on LCMS data of culture treatments.

We recently disclosed a comparative metabolomics study of a marine alga-derived fungus, grown under various culture conditions which led to the discovery of 7-desmethyl citreoviridin and the media dependent production of the cytotoxin, terrein.[17] Multivariate analysis of LCMS data proved to be a simple yet powerful tool to analyze the differentiated chemical profile of environmental challenged or epigenetically modulated fungi versus unperturbed cultures.[18,19] Here we applied similar techniques to identify chemically induced changes in the secondary metabolite spectrum of *Chalara* sp. 6661 treated with

the epigenetic modifiers as evidenced by principal component analysis of LCMS data (Figure 3.1A). LCMS-based relative expression analysis in combination with evaluation of individual LCMS traces (survey of retention time, UV spectrum, and *m/z* value and pattern) identified the most abundant and unique metabolites in the vorinostat treatment (Figure 3.1B). This approach combined with traditional bioactivity assays guided isolation led to the discovery of two new aniline-modified xanthones (**19,20**), and two new adenosine-coupled xanthones (**21,22**). In total nine compounds were identified from this fungus. To our surprise, we found that the HDAC inhibitor vorinostat was biotransformed, providing an aniline precursor to the 'unnatural' natural products chalanilines A (**19**) and B (**20**).

3.3 Results and discussion

Detailed molecular and phylogenetic identification of fungus *Chalara* sp. 6661 based on sequencing of the complete internal transcribed spacer regions 1 and 2 and 5.8S nrDNA (ITS) and 28S rDNA region (LSU) can be found in the Supporting Information (see S4 and Appendix B, Figures B1-B4).[20] *Chalara* sp. 6661 will be submitted to the German Culture Collection (DSMZ).

Chalaniline A (**19**) is one of the most abundant targets within the vorinostat treated culture extract by relative expression analysis (*m/z* value 376.1 @ 23.1 min, Figure 3.1b). The supernatant of a 4 L culture of *Chalara* sp. 6661 treated with vorinostat (1 mM) yielded 13.5 mg of compound **19** as a yellow solid after initial separation by normal phase automated flash chromatography, followed by preparative scale HPLC. The HR-ESI-MS analysis supports the low-resolution data (*m/z* 376.1178, [M+H]$^+$) and assigns a molecular

formula of $C_{22}H_{17}NO_5$, indicative of 15 degrees of unsaturation. The xanthone backbone was mainly established from NMR data based on characteristic chemical shifts, COSY, and ^3J-based HMBC correlations (Figure 3.2a).[21-23] However, unusual chemical shifts in the A ring and analysis of homodecoupled 1,1 ADEQUATE and HMBC correlations (Appendix B, Figures B5-B6) provided unequivocal evidence for the presence of a fulvene ring connected to an aniline moiety (Figure 3.2b). The unusually large coupling constant (14.7 Hz) observed between the bridging methine (H-11) and the aniline NH prompted us to search the literature for synthetic anilino-fulvene containing compounds. We found an example of a 12 Hz coupling constant for the ^3J coupling at an analogous exocyclic amine position.[24] Fulvenes are known to exhibit zwitterionic character depending on their substitution pattern.[25] Indeed, the extent of the iminium character in **19** is confirmed by quantum mechanical (QM) calculations to determine the ground state conformation of **19**.[26] NMR QM calculations further upheld the *Z*-iminium character of **19** with a calculated coupling constant between H-11 and NH of 14.8 Hz, almost identical to the experimentally observed coupling (Appendix B, Table B1).
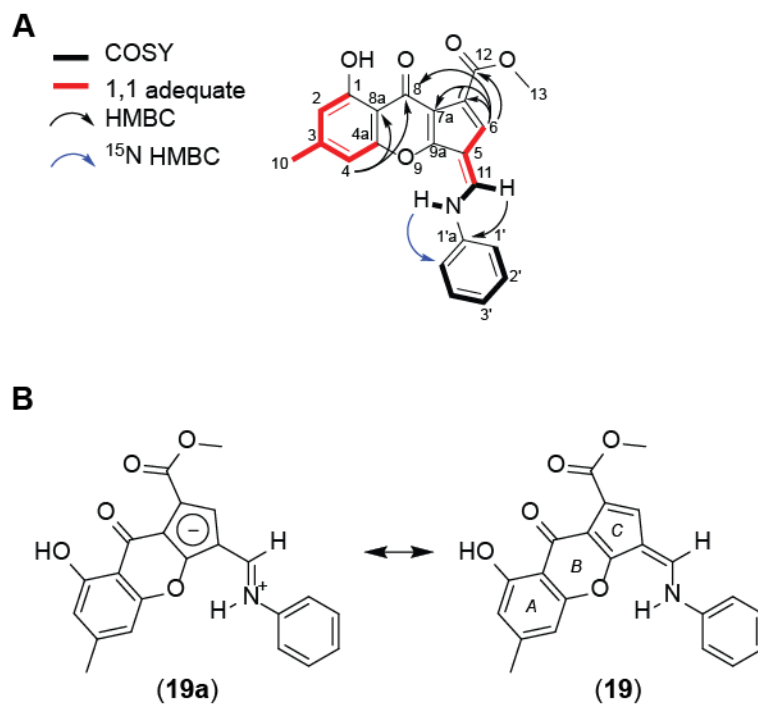
Figure 3.2. a) Selected NMR correlations and b) resonance structures of (**1**). DFT calculation of NMR coupling constants for H-11 indicates that **19a** is the favored resonance structure.

Compound **20**, named chalaniline B, was isolated via antimicrobial-bioassay guided isolation from the vorinostat treated culture, using HPLC fractionation and single point microbroth dilution assays against *Staphylococcus aureus* and *Enterococcus faecium*. HR-ESI-MS analysis revealed a molecular formula of $C_{20}H_{15}NO_5$, indicative of 14 degrees of unsaturation. The ^1H NMR spectrum of **19** exhibits three exchangeable protons (δ_H 12.38, 9.15, 5.58), eight aromatic signals, and a deshielded methylene group (δ_H 4.84). The ^{13}C

NMR spectrum displays carbonyl resonances similar to known xanthones but shows additional aromatic signals (δ_C 141.2, 128.4, 121.2, 116.8). Two-dimensional NMR spectroscopy confirmed a xanthone backbone with an anilino moiety at position 1 on the A ring (Figure 3.3a). Single dose diffusion disk assays were performed due to the limited amount of **20** (0.7 mg) revealing moderate antimicrobial activity against *S. aureus* and multidrug-resistant *S. aureus* (ATCC# BAA-44) at doses as low as 50 µg/disk (Figure 3.3b).
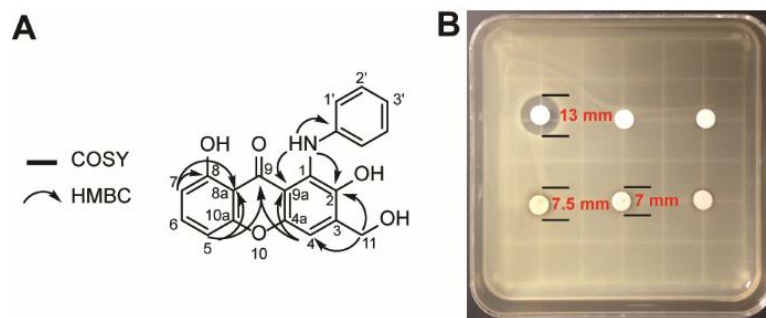
Figure 3.3. a) Selected 2D NMR correlations of **20**. b) Multidrug-resistant *S. aureus* diffusion disk assay with zones of inhibition. Top left to right: 25 µg vancomycin, 50 µg ampicillin, and methanol control. Bottom: 100 µg, 50 µg, and 25 µg **20** per disc.

Xanthone A (**3**) was identified from the vorinostat treatment based on its abundance in the relative expression analysis (508.1 *m/z* @ 14.5 min, Figure 3.1b). Multidimensional NMR experiments indicated the presence of a xanthone structure similar to compound **20** as well as an adenosine moiety (Figure 3.4a).[27] HMBC experiments optimized for long and

short-range coupling (4-10 Hz) were unsuccessful at establishing the connection between the two fragments. Comparison of the adenosine ^1H and ^{13}C chemical shifts with literature values indicated that the 1' and 2' positions varied significantly, and the chemical shift for the anomeric proton (δ_H 6.46 and δ_C 89.5) and the C-2' position on the ribose (δ_H 5.50 and δ_C 85.4) support the C1-C2' rather than the C1-C3' linkage. QM NMR calculations of the two regioisomers were performed and compared with DP4+ probability.[28] Overall, the NMR-based calculations support the connection of the xanthone to the ribose via a C1-C2' linkage (Appendix B, Figure B7).
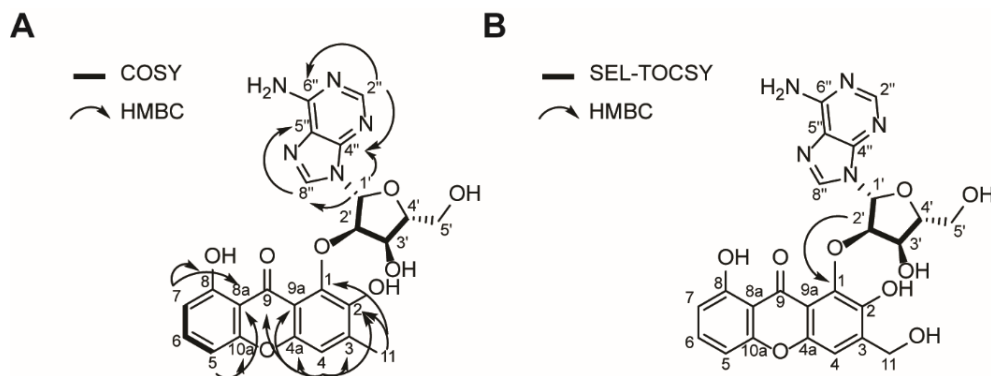
Figure 3.4. a) Selected COSY and HMBC correlations for **21**. b) Selective TOCSY confirms the presence of the ribose moiety while a single additional HMBC correlation establishes the 1-2' connectivity in **22**.

HR-ESI-MS analysis of xanthone B (**22**) provided a formula of $C_{24}H_{22}N_5O_9$ ([M+H]$^+$) based on an *m/z* of 524.1413 (calcd for $C_{24}H_{22}N_5O_9$, 524.1410; Δ ppm = 0.6), differing from **3** by one oxygen atom. The ^1H NMR spectra of **22** and **21** are almost identical with

the exception of a deshielded methylene singlet at 5.34 ppm in **22** instead of the methyl group in **21**. Based on an NMR correlation in the sidechain, we placed the hydroxy at carbon 11, which resembles the hydroxylation pattern already found in isofusidienols B and D (**24, 25**). This time, we were able to establish the connectivity between the xanthone backbone and the nucleoside with a clear HMBC correlation from H2' to C1 in d_5-pyridine (Figure 4b). Both compounds exhibit positive specific rotation values (+74 and +82, respectively) indicative of a similar chromophore connection. Comparison of the experimental ECD spectra of **21** and **22** with the TDDFT calculated theoretical ECD spectrum of **21** provides further evidence for the absolute configurations of the adenosine-coupled xanthones **21** and **22** (Appendix B, Figure B8).

Previously described natural products do not offer a clear biosynthetic hypothesis for chalaniline A or B.[29, 30] We suspected that *Chalara* sp. 6661 could utilize aniline from the catabolism of vorinostat and other aromatic nitrogen sources in its production of the otherwise PKS-based chalanilines as reported in one case previously.[31] Consistent with this hypothesis, we observed catabolic derivatives of vorinostat in the culture media in our metabolomics analysis, e.g. carboxylic acid derivative **29** and vorinostat amide (data not shown).[32] Furthermore, we confirmed that vorinostat does not undergo spontaneous degradation in YPD media without *Chalara* sp. during the time course of these studies (see Supporting Information page S6). Next, we treated cultures of *Chalara* sp. with aniline, acetanilide, and vorinostat and were able to detect the formation of **19** in extracted ion chromatograms in all cases (Figure 3.5a). To confirm that vorinostat was the source of aniline in **19** and **20**, d_5-vorinostat was synthesized according to published procedures[33]

and supplemented to *Chalara* sp. cultures. Catabolism of d_5-**23** resulted in the production of d_5-**19** as confirmed by both LCMS and ^{13}C NMR data (Figure 3.5b, Appendix B, Figure B9). Based on the proposed biosynthesis for the isofusidienol class of antibiotics from this fungus and the incorporation of d_5-**23** into chalaniline A, we propose a mixed, 'unnatural' biosynthetic origin. A proposed 5,6 arene-oxide intermediate (**30**), could rearrange and ring contract to create a five-membered ring similar to coniochaetone biosynthesis (Figure 3.5c).[34] Aniline catabolized from vorinostat might then intercept the aldehyde intermediate (**31**) to form the Schiff base (**32**), which could tautomerize to the conjugated and more stabilized structure of **19**. Nucleophilic attack on a xanthone 1,2 arene-oxide and subsequent aromatization could result in the formation of either **20**, **21**, or **22** depending on the intercepting nucleophile. While some biotransformations have been reported from fungi that acetylate anilines or glycosylate xenobiotics,[35,36] and many cases of precursor directed biosynthesis have been reported,[37, 38] examples of the popular epigenetic modifying drug vorinostat (**23**) being catabolized and incorporated into a unique, unnatural metabolite are exceedingly rare. Notably, Cichewicz and colleagues reported in 2011 on acetanilides utilized by *Aspergilli* and recently on chemoreactive natural products in *Tolypocladium* that can detoxify xenobiotics by coupling shikimate to compounds including vorinostat.[39]
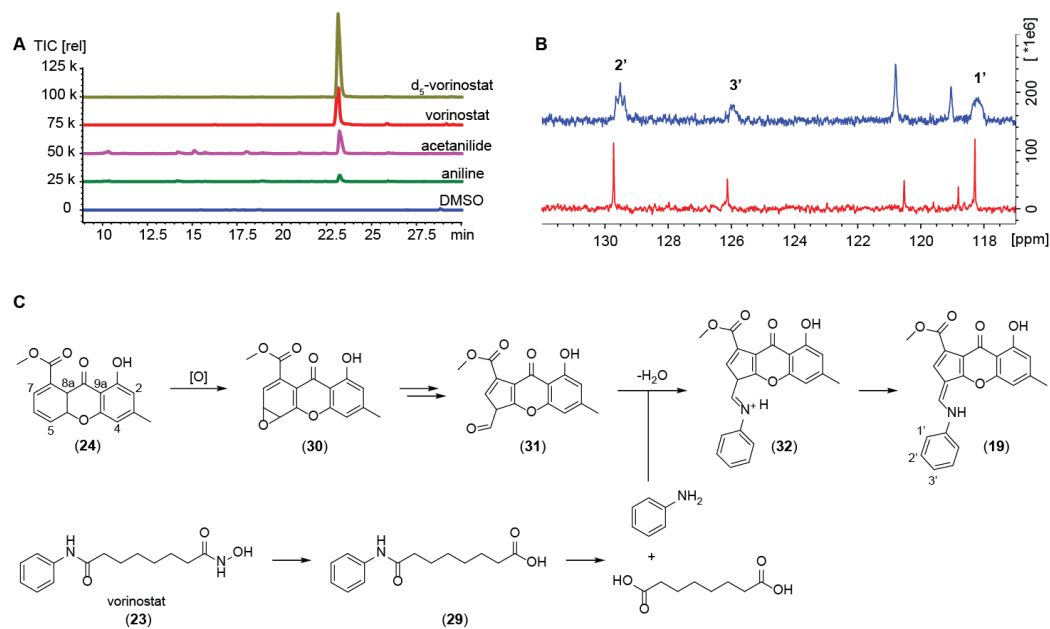
Figure 3.5. a) Extract ion chromatograms of *Chalara* sp. extracts showing chalaniline A (**19**) production when d_5-**23**, **23**, acetanilide, aniline (all at 1 mM), or DMSO (control) is supplemented. EIC detection of **19** is set to *m/z* 376 (or 381 for d_5-**23** treatment) b) ^{13}C NMR spectrum excerpt of the aromatic region of **19** (red) and d_5-**19** (blue) in d_6-DMSO. Deuterium-^{13}C coupling is observed in the ^{13}C NMR experiment for aromatic resonances. c) Biosynthetic hypothesis for the formation of **19** in *Chalara* sp. 6661 via an arene oxide intermediate (**30**), rearrangement into aldehyde **31** followed by interception of vorinostat-derived aniline from eukaryote catabolism.

In summary, a metabolomics and bioactivity-guided approach led to the isolation of four structurally new compounds from HDAC inhibitor vorinostat-treated cultures of an

ascomycete fungus. The structures of the xanthone metabolites **19**-**22** were verified by extensive spectroscopic analysis, and the compounds were tested for bioactivity. Compound **20** has modest antibacterial activity against multidrug-resistant pathogen *S. aureus* (ATCC BAA-44), but no potent cytotoxicity was observed. We uncovered that the aniline moiety in **19** and **20** is derived from vorinostat and verified incorporation of d_5-aniline from synthetic d_5-vorinostat into chalaniline A, demonstrating that this fungus is able to incorporate environmental aniline into biosynthetic products to produce 'unnatural' natural products. Discovery of new natural product scaffolds from the microbial world is needed to replenish the drying pipeline of compounds for pharmaceutical development. Here we present two rare aniline-containing 'unnatural' polyketides and two new adenosine-coupled xanthones for activity exploration. The study shows that utilization of epigenetic modifying reagents can access the chemical diversity of genetically encoded small molecules from filamentous fungi, and moreover allows insights into fungal metabolism that can be utilized to expand known chemical space.

3.4 Acknowledgements

3.5 Supporting information

The Supporting Information is available free of charge on the ACS Publications website at DOI: 10.1021/acschembio.7b00268 and in Appendix B of this dissertation.

3.6 References

1. Butler, M. S. *J. Nat. Prod.* **2004**, *67*, 2141.
2. Aly, A. H.; Debbab, A.; Proksch, P. *Fungal Diversity* **2011**, *50*, 3.
3. Rutledge, P. J.; Challis, G. L. *Nat. Rev. Microbiol.* **2015**, *13*, 509.
4. Chiang, Y. M.; Lee, K. H.; Sanchez, J. F.; Keller, N. P.; Wang, C. C. *Nat. Prod. Commun.* **2009**, *4*, 1505.
5. Lim, F. Y.; Sanchez, J. F.; Wang, C. C. C.; Keller, N. P. *Methods Enzymol.* **2012**, *517*, 303.
6. Wiemann, P.; Keller, N. P. *J Ind. Microbiol. Biotechnol.* **2014**, *41*, 301.
7. Brakhage, A. A.; Schroeckh, V. *Fungal Genet. Biol.* **2011**, *48*, 15.
8. Scherlach, K.; Hertweck, C. *Org. Biomol. Chem.* **2009**, *7*, 1753.
9. Connolly, L. R.; Smith, K. M.; Freitag, M. *PLoS Genet.* **2013**, *9*, e1003916.
10. Niehaus, E.-M.; Kleigrewe, K.; Wiemann, P.; Studt, L.; Sieber, Christian M. K.; Connolly, Lanelle R.; Freitag, M.; Güldener, U.; Tudzynski, B.; Humpf, H.-U. *Chem. Biol.* **2013**, *20*, 1055.
11. Bode, H. B.; Bethe, B.; Hofs, R.; Zeeck, A. *ChemBioChem* **2002**, *3*, 619.
12. Lösgen, S.; Magull, J.; Schulz, B.; Draeger, S.; Zeeck, A. *Eur. J. Org. Chem.* **2008**, *2008*, 698.
13. Asai, T.; Yamamoto, T.; Shirata, N.; Taniguchi, T.; Monde, K.; Fujii, I.; Gomi, K.; Oshima, Y. *Org. Lett.* **2013**, *15*, 3346.
14. Du, L.; King, J. B.; Cichewicz, R. H. *J. Nat. Prod.* **2014**, *77*, 2454.
15. Vervoort, H. C.; Draskovic, M.; Crews, P. *Org. Lett.* **2011**, *13*, 410.
16. Williams, R. B.; Henrikson, J. C.; Hoover, A. R.; Lee, A. E.; Cichewicz, R. H. *Org. Biomol. Chem.* **2008**, *6*, 1895.
17. Adpressa, D. A.; Loesgen, S. *Chem Biodivers* **2016**, *13*, 253.
18. Hou, Y.; Braun, D. R.; Michel, C. R.; Klassen, J. L.; Adnani, N.; Wyche, T. P.; Bugni, T. S. *Anal. Chem.* **2012**, *84*, 4277.
19. Kurita, K. L.; Glassey, E.; Linington, R. G. *Proc. Natl. Acad. Sci. U.S.A.* **2015**, *112*, 11999.
20. Crous, P. W.; Wingfield, M. J.; Richardson, D. M.; Le Roux, J. J.; Strasberg, D.; Edwards, J.; Roets, F.; Hubka, V.; Taylor, P. W.; Heykoop, M.; Martin, M. P.; Moreno, G.; Sutton, D. A.; Wiederhold, N. P.; Barnes, C. W.; Carlavilla, J. R.; Gene, J.; Giraldo, A.; Guarnaccia, V.; Guarro, J.; Hernandez-Restrepo, M.; Kolarik, M.; Manjon, J. L.; Pascoe, I. G.; Popov, E. S.; Sandoval-Denis, M.; Woudenberg, J. H.; Acharya, K.; Alexandrova, A. V.; Alvarado, P.; Barbosa, R. N.; Baseia, I. G.; Blanchette, R. A.; Boekhout, T.; Burgess, T. I.; Cano-Lira, J. F.; Cmokova, A.; Dimitrov, R. A.; Dyakov, M. Y.; Duenas, M.; Dutta, A. K.; Esteve-Raventos, F.; Fedosova, A. G.; Fournier, J.; Gamboa, P.; Gouliamova, D. E.; Grebenc, T.; Groenewald, M.; Hanse, B.; Hardy, G. E.; Held, B. W.; Jurjevic, Z.; Kaewgrajang, T.; Latha, K. P.; Lombard, L.; Luangsa-Ard, J. J.; Lyskova, P.; Mallatova, N.; Manimohan, P.; Miller, A. N.; Mirabolfathy, M.; Morozova, O. V.; Obodai, M.; Oliveira, N. T.; Ordonez, M. E.; Otto, E. C.; Paloi, S.; Peterson, S. W.; Phosri, C.; Roux, J.; Salazar, W. A.; Sanchez, A.; Sarria, G. A.; Shin,

H. D.; Silva, B. D.; Silva, G. A.; Smith, M. T.; Souza-Motta, C. M.; Stchigel, A. M.; Stoilova-Disheva, M. M.; Sulzbacher, M. A.; Telleria, M. T.; Toapanta, C.; Traba, J. M.; Valenzuela-Lopez, N.; Watling, R.; Groenewald, J. Z. *Persoonia* **2016**, *36*, 316.

21. Davis, R. A.; Pierens, G. K. *Magn. Reson. Chem.* **2006**, *44*, 966.
22. Shao, C.; Wang, C.; Wei, M.; Gu, Y.; Xia, X.; She, Z.; Lin, Y. *Magn. Reson. Chem.* **2008**, *46*, 1066.
23. Wang, Y.; Zheng, Z.; Liu, S.; Zhang, H.; Li, E.; Guo, L.; Che, Y. *J. Nat. Prod.* **2010**, *73*, 920.
24. Anderson, A. G.; Ko, R. P. *J. Org. Chem.* **1982**, *47*, 1971.
25. Häfner, K. H.; König, C.; Kreuder, M.; Ploss, G.; Schulz, G.; Sturm, E.; Vöpel, K. H. *Angew. Chem.* **1963**, *2*, 123.
26. Bally, T.; Rablen, P. R. *J. Org. Chem.* **2011**, *76*, 4818.
27. Ciuffreda, P.; Casati, S.; Manzocchi, A. *Magn. Reson. Chem.* **2007**, *45*, 781.
28. Grimblat, N.; Zanardi, M. M.; Sarotti, A. M. *J. Org. Chem.* **2015**, *80*, 12526.
29. Watanabe, K.; Hotta, K.; Praseuth, A. P.; Koketsu, K.; Migita, A.; Boddy, C. N.; Wang, C. C. C.; Oguri, H.; Oikawa, H. *Nat. Chem. Biol.* **2006**, *2*, 423.
30. Wang, Y.; Zheng, J.; Liu, P.; Wang, W.; Zhu, W. *Mar. Drugs* **2011**, *9*, 1368.
31. Henrikson, J. C.; Ellis, T. K.; King, J. B.; Cichewicz, R. H. *J. Nat. Prod.* **2011**, *74*, 1959.
32. Soli, E. D.; Braun, M. P. *J Labelled Compd. Radiopharm.* **2006**, *49*, 437.
33. Gediya, L. K.; Chopra, P.; Purushottamachar, P.; Maheshwari, N.; Njar, V. C. O. *J. Med. Chem.* **2005**, *48*, 5047.
34. Deng, L.; Niu, S.; Liu, X.; Che, Y.; Li, E. *Fitoterapia* **2013**, *89*, 8.
35. Tixier, C.; Sancelme, M.; Aït-Aïssa, S.; Widehem, P.; Bonnemoy, F.; Cuer, A.; Truffaut, N.; Veschambre, H. *Chemosphere* **2002**, *46*, 519.
36. Zhan, J.; Gunatilaka, A. A. L. *J. Nat. Prod.* **2005**, *68*, 1271.
37. Grüschow, S.; Rackham, E. J.; Elkins, B.; Newill, P. L. A.; Hill, L. M.; Goss, R. J. M. *ChemBioChem* **2009**, *10*, 355.
38. Korp, J.; König, S.; Schieferdecker, S.; Dahse, H.-M.; König, G. M.; Werz, O.; Nett, M. *ChemBioChem* **2015**, *16*, 2445.
39. Du, L.; You, J.; Nicholas, K. M.; Cichewicz, R. H. *Angew. Chem. Int. Ed.* **2016**, *55*, 4220.

Chapter 4 – adapted from the published article

"Bioprospecting chemical diversity and bioactivity in a marine derived *Aspergillus terreus*"

Donovon A. Adpressa and Sandra Loesgen

4.1 Abstract

A comparative metabolomic study of a marine derived fungus (*Aspergillus terreus*) grown under various culture conditions is presented. The fungus was grown in 11 different culture conditions using solid agar, broth cultures, or grain based media (OSMAC). Multivariate analysis of LC/MS data from the organic extracts revealed drastic differences in the metabolic profiles and guided our subsequent isolation efforts. The compound 7-desmethylcitreoviridin was isolated and identified, and is fully described for the first time. In addition, 16 known fungal metabolites were also isolated and identified. All compounds were elucidated by detailed spectroscopic analysis and tested for antibacterial activities against five human pathogens and tested for cytotoxicity. This study demonstrates that LC/MS based multivariate analysis provides a simple yet powerful tool to analyze the metabolome of a single fungal strain grown under various conditions. This approach allows environmentally-induced changes in metabolite expression to be rapidly visualized, and uses these differences to guide the discovery of new bioactive molecules.

4.2 Introduction

Natural products, or compounds isolated from biological sources, account for the vast majority of clinically approved drugs.[1,2] Approximately one-quarter of these natural product derived therapeutics were first isolated from fungi, one-quarter from bacteria, and one-half from plants.[3] Fungal metabolites have revolutionized how some major diseases are treated, including the antibiotic penicillin, the immune suppressant cyclosporin, and the cholesterol lowering agent lovastatin. The number of fungal species is estimated to be five

times greater than the number of plant species and fifty times greater than the number of

bacterial species.[4] Only 5-10% of this fungal diversity has been describes and far less has

been chemically analyzed.[5] In particular, many plants and algae host symbiotic fungi, also

called endophytic fungi, that can increase plant growth rates, improve their disease

resistance, and enhance their tolerance of abiotic stressors.[6] Recently, these fungi have been

recognized as prolific producers of bioactive compounds, yielding 20% more novel

compounds in chemical screens than typical fungal strains.[7]

As part of our ongoing research program to identify and isolate bioactive compounds

from marine derived fungi, we explored the chemical diversity and bioactivity of

compounds produced by a marine derived endophyte *Aspergillus terreus* G15 under

different culture conditions. The OSMAC approach (one strain-many compounds) is an

empirical method that alters culture conditions in order to elicit the production of

previously unknown secondary metabolites.[8,9] Recent studies have combined OSMAC

with bioinformatical analysis, which enabled the discovery of aspoquinolones A-D.[10] In

this study, we combine the OSMAC approach with principal component analysis (PCA) of

liquid-chromatography derived mass spectrometry data to examine the metabolome of

Aspergillus terreus G15. This comparative metabolomic analysis resulted in the isolation

of cytotoxic 7-desmethylcitreoviridin (**33**), which has not been spectroscopically

characterized previously, as well as 15 known fungal metabolites. In addition, using this

approach we identified the cytotoxic compound terrein (**34**), which was expressed at higher

concentration and produced potent cytotoxicity exclusively when G15 was grown in

potato-dextrose broth media. All compounds were identified using well-established NMR methodologies and tested for antibacterial and anti-cancer activity.

4.3 Results and discussion

4.3.1 Isolation of fungus G15 and molecular identification by DNA extraction, PCR and sequencing. Fungus G15 was isolated from the marine environment by BioViotica Naturstoffe GmbH (Germany) and given to us for chemical analysis. A preliminary morphological analysis indicated fungus G15 belongs to the genus *Aspergillus*. Phylogenetic identification using 18S-ITS rDNA sequencing via amplification with 5.8S/SR6R primers established a 99% sequences identity to *Aspergillus terreus*.[11]

4.3.2 Culture conditions and statistical analysis of fungal metabolites. We have previously demonstrated that there are very substantial changes in the compounds produced by fungi when grown under solid versus broth media conditions. For example, *Chalara sp.* produces two bioactive metabolites (isofusidienol A and B) when grown on malt agar, but produces an additional two novel antibiotics when static broth malt was used.[12] We chose five nutrient conditions (malt, glycerol, malt buffered at pH=6, oatmeal, potato-dextrose) to grow G15, and each was prepared as solid agar and broth cultures. Additionally, we grew *Aspergillus* G15 in barley-spelt medium. Organic extracts of all eleven culture conditions were prepared in biological replicates (n=2) and subjected to LC/MS analysis (3 individual runs). A principal component analysis (PCA) of the LC/MS data was performed with MZmine 2.14.2 and Multibase 2015.[13,14] Briefly, a principal component analysis identifies the metabolites that most effectively describe the differences in the

metabolome between growth conditions. Growth conditions that were separate from the other growth conditions in the PCA projection were interpreted as more chemically unique and were selected for further study. In addition, we compared the metabolome produced in each growth condition to the average metabolome produced across all growth conditions. A contour plot of the log-ratio shows substantial differences in the metabolites expressed for the liquid malt, barley spelt, and potato dextrose broth grows (Fig. 4.1-4.4).
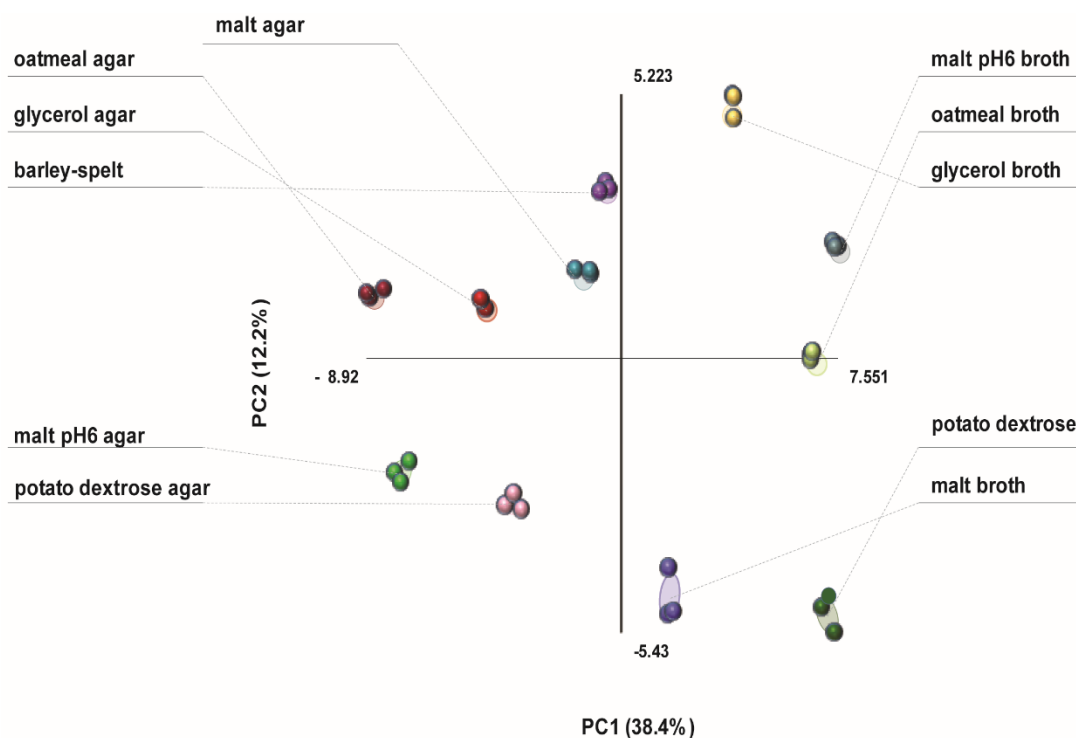
Figure 4.1: Principal component analysis of the LC/MS based data received from eleven culture conditions of *Aspergillus terreus* G15.

4.3.3 Antibiotic-activity guided isolation and identification of fungal metabolites.

All extracts were tested for antibiotic and anti-cancer activity in cell based assays following established protocols.[15,16] The antimicrobial activity was evaluated against the following human pathogens: *Escherichia coli* (Gram-negative bacteria implicated in food poisoning)*, Pseudomonas aeruginosa* (Gram-negative bacteria and model organism for biofilm formation), *Bacillus subtilis* (Gram-positive bacteria and model for endospore forming pathogens)*, Staphylococcus aureus* (Gram-positive bacteria responsible for most post-surgical infections)*, Enterococcus faecium* (Gram-positive bacteria that can cause skin lesions and meningitis), and *Candida albicans* (fungus that causes opportunistic skin and genital infections). Interestingly, we found that *Aspergillus* G15 grown on static agar dishes showed moderate antifungal activity independent of the nutrient source, while most broth cultures exhibited antibiotic activity. Bio-guided fractionation following the antimicrobial activity resulted in the isolation of lovastatin (**35**), and mevinolinic acid methyl ester (**36**) from malt agar plates. Both molecules were identified by comparing mass spectrometry and NMR data to literature values.[17,18] Mevinolinic acid methyl ester was most active in a plate diffusion assay against *Candida albicans* and showed an 11 mm zone of inhibition compared to the positive control amphotericin B, which showed a 16 mm zone of inhibition.

Next, we explored the antibiotic activity of G15 grown in broth cultures. The metabolome of G15 grown in malt pH6 buffered media was compared to the average metabolome across all other growth conditions (Fig. 4.2). Isolation of the unique metabolites resulted in the identification of several members of the butyrolactone class of

compounds: butyrolactone I (**37**), IV (**38**), V (**39**), VII (**40**), aspernolide A (**41**) as well as 4-hydroxy mellein (**42**).[19-22] All molecules were compared to previously published spectroscopic data. Butyrolactone I (**37**) was the most active compound against *Bacillus subtilis* in our agar diffusion assay with a zone of inhibition of 15 mm, while our positive control antibiotic chloramphenicol produced a 21 mm zone of inhibition.
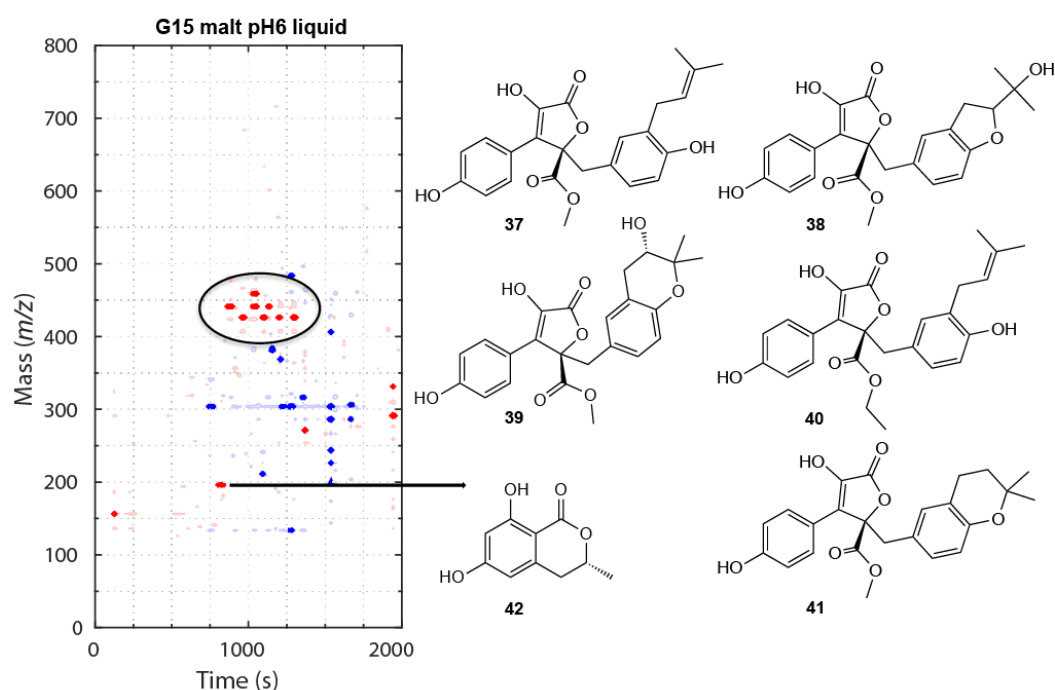
Figure 4.2: Multivariate analysis of metabolite production of G15 in malt pH6 buffered media compared to the other ten culture conditions. Two-dimensional heat map of LC/MS data shows metabolites produced at higher levels (red) versus lower levels (blue) in this media condition. Several known members of the butyrolactone class of compounds were isolated (**37-41**) as well as 4-hydroxy mellein (**42**).

4.3.4 Metabolic profiling guided discovery and structure elucidation of 7-desmethylcitreoviridin. An analysis of the metabolites that G15 produced at elevated levels when grown in barley-spelt media guided us to a pair of compounds with a previously unobserved retention time, *m/z* value, and UV chromophore (Fig. 4.3). We were ultimately able to identify these compounds as citreoviridin (**44**), an α-pyrone mycotoxin known from *Penicillium* and *Aspergillus*[23,24] as well as its congener 7-desmethylcitreoviridin (**33**), which is described here for the first time.[25] **33** was obtained as a yellow amorphous solid and the molecular formula of **1** was determined as $C_{22}H_{28}O_6$ by HR-ES-MS *m/z* [M+Na]$^+$ 411.1760, calc. 411.1778 with nine degrees of unsaturation. The carbon NMR of 7-desmethylcitreoviridin (**33**) showed clear similarities to the spectroscopic data found for citreoviridin (**44**)[24], exhibiting typical chemical shifts for the pyrone (δ_C 172.9, 164.3, 156.2, 109.0, 89.2), polyene (δ_C 141.6, 135.9, 134.8, 131.7, 129.0, 127.8, 119.6, 119.4), and tetrahydrofuran moieties (δ_C 86.3, 84.7, 79.7, 79.0), additionally, one methoxy (δ_C 56.3) and three methyl groups (δ_C 17.7, 13.4, 9.0) could be established. The proton spectra of **1** was almost identical to the proton NMR data for citreoviridin, however one methyl signal (δ_C 13.7) was missing. Analysis of COSY, HMBC, HSQC, TOCSY and NOE experiments established the relative configuration of 7-desmethylcitreoviridin (**33**) shown in Figure 4.3. NOE correlations within the tetrahydrofuran ring clearly indicate the same relative orientation of **33** as reported for (-) citreoviridin (**44**). Additionally, TOCSY experiments were done to support the loss of a methyl group at C7. Uninterrupted TOCSY correlations were found in the polyene chain for **1** while citreoviridin TOCSY correlations are only found between C8 to C14 indicating

a methylation at C7 that stops the TOCSY transfer.[26] Optical rotation and circular dichroism analysis were compared to commercially available citreoviridin as well as computationally derived ECD data (see experimental and supplemental data, Appendix C, Fig. C1), which allowed the assignment of the absolute configuration of citreoviridin (**44**) and 7-desmethylcitreoviridin (**33**) (Fig 4.3). Both metabolites were moderately cytotoxic in a single dose assay against human colon cancer cells and the IC50 was determined to be 4 μM for citreoviridin (**44**) and 8 μM for 7-desmethylcitreoviridin (**33**). It is worth noting that the polyene mycotoxins (**33, 44**) are sensitive to light and acidic conditions.[22]
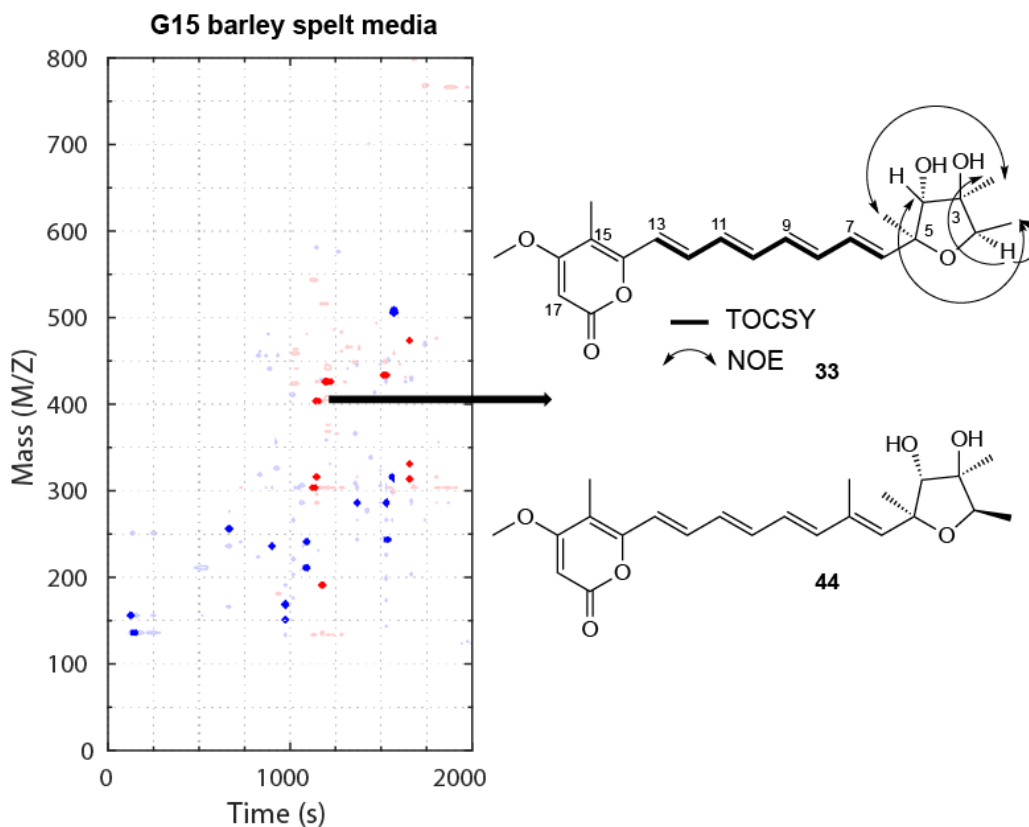
Figure 4.3: Multivariate analysis of metabolite production of G15 in barley media compared to the other ten culture conditions. Two-dimensional heat map of LC/MS data shows metabolites produced at higher levels (red) versus lower levels (blue) in this media condition. Citreoviridin (**44**) and 7-desmethylcitreoviridin (**33**) were isolated from the highlighted region. Key NOE and TOCSY correlations are shown in **1**.

Further exploration of the barley-spelt media resulted in the isolation of the known fungal metabolites 6-hydroxy kigelin (**43**), novobenzomalvin C (**45**), *cis* and *trans* 1-

phenylalanineamide (**46**, **47**), and methyl 3,4,5-trimethoxy-2-(2-(nicotinamido) benzamido) benzoate (**48**) (Figure 4.4).[27-30]
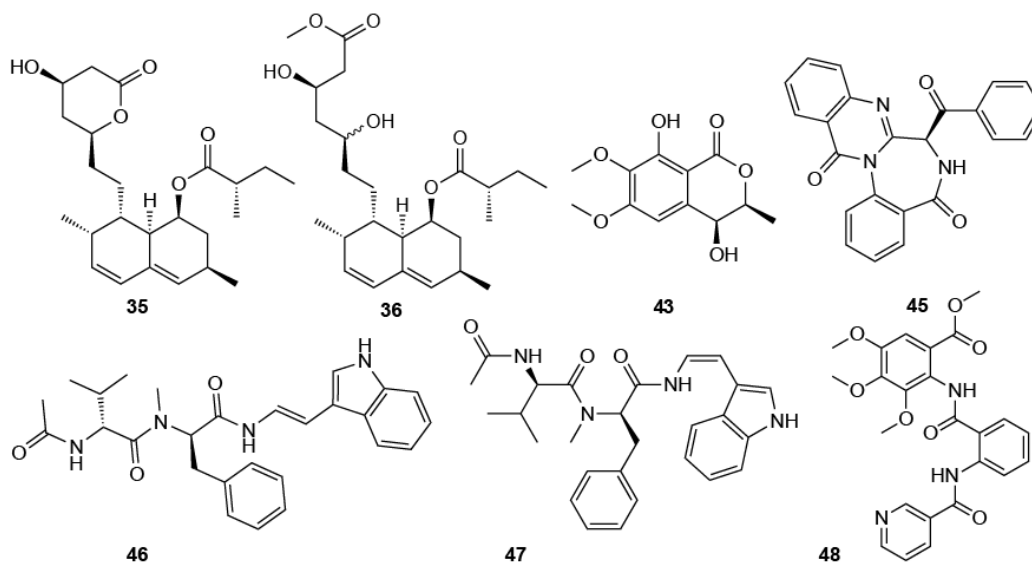
Figure 4.4: Metabolites isolated from *Aspergillus* G15 under various culture conditions using the OSMAC approach.

4.3.5 Anti-cancer activity guided isolation of terrein. All extracts of *Aspergillus* G15 were also tested in a cytotoxicity assay in a human colon cancer model (HCT-116) (Fig. 4.4). Surprisingly, only when G15 was grown in potato-dextrose broth was potent cytotoxicity observed, with a 20% cell survival in a single dose cell viability assay using 10 μg/ml of extract. The metabolites produced of *Aspergillus* G15 grown in potato-dextrose broth were compared to the other growth conditions, which showed a unique chemical entity in the polar region, eluted at 3 min with an *m/z* value of 155 (Fig. 4.5). Isolation of

this compound, terrein (**34**), and re-testing in the cell viability assay verified potent

cytotoxic activity comparable to a recently published study.[31]
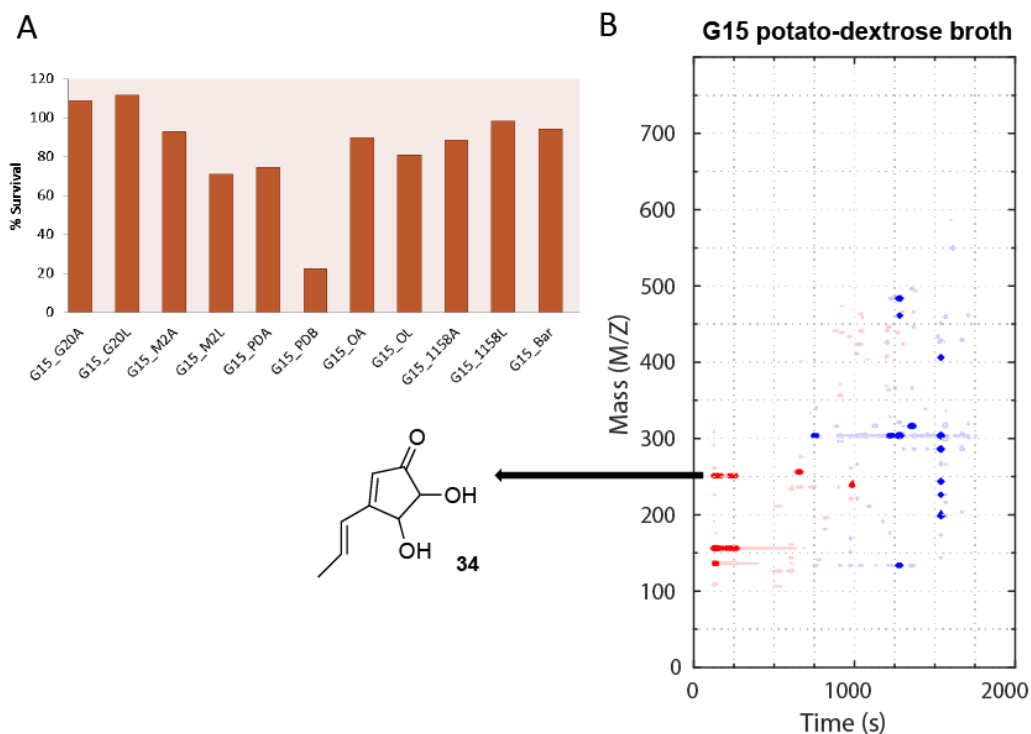
Figure 4.5: Fungus G15 grown in 11 culture conditions, crude extracts tested against HCT-116 human colon cancer cells (A). (B) Multivariate analysis of metabolite production of G15 in potato-dextrose broth (PDB) media compared to the other ten culture conditions. Two-dimensional heat map of LC/MS data shows metabolites produced at higher levels (red) versus lower levels (blue) in this media condition. Terrein (**34**, insert) was identified as the cytotoxic metabolite mainly produced in PDB.

4.4 Acknowledgement

4.5 Experimental

General experimental procedures. Optical rotations were measured on a JASCO P-1010 polarimeter. Circular dichroism and UV measurements were recorded using a JASCO J-815 spectropolarimeter. IR spectra were recorded on a Thermo Scientific Nicolet IR100 FTIR spectrometer. NMR spectra were acquired on a Bruker Avance III 500 MHz or Bruker Avance III 700 MHz spectrometer, equipped with a 5 mm TXI probe or ^{13}C cryoprobe respectively, with the residual solvent used as an internal standard. Low resolution ESI-MS and HRTOFMS (ESI$^+$) mass spectra were recorded on Agilent 1100 series LC with MSD 1946 and Agilent 1200 series LC with 6230 TOF MS, respectively. A Teledyne Isco CombiFlash Companion system was used for automated flash chromatography. Analytical HPLC was performed using an Agilent 1100 HPLC system equipped with a photodiode array detector. The mobile phase consisted of ultra-pure water (A) and acetonitrile (B) with 0.05% formic acid in each solvent. A gradient method from 10% B to 100% B in 35 min at a flow rate of 0.8 ml/min was used. The column (Phenomenx

kinetex C_{18}, 5 μm x 150 mm x 4.6 mm) was re-equilibrated before each injection and the column compartment was maintained at 30 ˚C throughout each run. Semi preparative HPLC (Phenomenx kinetex C_{18}, 5 μm x 150 mm x 10mm) was operated at room temperature, using isocratic elution condition or gradient system with a flow rate of 4 ml/min. All samples were filtered through a 0.45 μm nylon filter before LC/MS and HPLC analysis. Open column chromatography (CC) was performed on silica gel 60 (70-230 mesh, Silicycle). Analytical thin layer chromatography (TLC) was performed on pre-coated silica gel 60 F_{254} plates (Eppendorf). TLC plates were visualized by UV (254 and 360 nm), and by spraying with anisaldehyde solution followed by heating at 80 °C. General reagents were from Sigma-Aldrich Corp. and VWR International.

Identification of fungus G15. The fungal strain was grown in 50 ml of potato-dextrose broth for 5 days and 0.5 ml of mycelia cells were collected by centrifugation. The cell pellet was frozen in liquid N_2 then 0.5 ml of zirconium silicate beads were added and the mixture vortexed for 10 minutes. DNA extraction was done with a *Qiagen DNEasy Plant Mini Kit* (Qiagen, Valencia, CA) following the manufacturers instructions. 5.8S forward primer and SR6R reverse primer were used to amplify the ITS-1 sequence of the extracted DNA. The resultant 260 base-pair consensus sequence had a 99% sequence identity to that of *A. terreus* Gene bank # KR610363.1.g

Culture media. Malt: malt extract (10 g/l), yeast extract (4 g/l), glucose (4 g/l), pH = 7.0 prior to sterilisation. Malt pH 6 buffered: malt extract (20 g/l), glucose (10 g/l), yeast extract (2 g/l), $(NH_4)_2HPO_4$ (0.5 mg/l), pH = 6.0 prior to sterilization. Glycerol: glycerol (20 g/l), malt extract (10 g/l), yeast extract (4 g/l). Oatmeal: oatmeal powder (20 g/l), 2.5 ml/L trace

element solution, pH = 7.0 prior to sterilisation. Trace element solution: $CaCl_2 \cdot 2\ H_2O$ (3 g/l), Fe^{III}-citrate (1 g/l), $MnSO_4$ (0.2 g/l), $ZnCl_2$ (0.1 g/l), $CuSO_4 \cdot 5\ H_2O$ (25 mg/l), $Na_2B_4O_7 \cdot 10\ H_2O$ (20 mg/l), $CoCl_2$ (4 mg/l), $Na_2MoO_4 \cdot 2\ H_2O$ (10 mg/l). Barley-spelt solid media: 200 g barley (Bob's Red Mill), 200 g spelt whole grain flakes (Arrowhead Mills), 2 g soy peptone, 2 mg $MnCl_2$, 250 ml distilled water. Potato dextrose broth was prepared according to manufacturer directions as received (HiMedia). For agar plates 17 g/l nutrient agar was added to the culture media before sterilization.

Fermentation. Aspergillus terreus sp. G15 was cultivated at 28 ˚C on an orbital shaker at 200 rpm (broths, each 250 ml) or at room temperature, static (10 agar dishes each or 400 g of grains) for 20 days for the OSMAC experiment. Agar cultures were inoculated with mycelia tissue from 5 day old malt agar cultures. Broth cultures were inoculated with a 1 cm^2 piece of a 5 day old malt agar dish. Each nutrient media condition was grown with replicates (n=2) . Subsequent larger growths of conditions of interest to isolate pure compounds are described below.

Preparation of organic extracts. Each fungal culture was blended in the presence of an equivalent volume of DI H_2O for 5 min, followed by extraction with a volume of ethyl acetate equivalent to the growth media volume. The organic layer was collected, dried over anhydrous $MgSO_4$, and concentrated under vacuum.

Isolation of compounds. Similar procedures were applied for all compounds. For compounds **37-43**, 18 l of malt pH6 broth was inoculated with 1 cm^2/L of mycelial tissue from 7 day old potato-dextrose agar dishes. The culture was allowed to grow 28 days. The pH of the culture was adjusted to 5, the mycelia filtered off through cheesecloth, and the

supernatant passed over XAD-7 resin for 1 hour before rinsing with 12 l of water. The extract was eluted with a combined 2 L MeOH and 2 l acetone, respectively. The combined organic fractions were evaporated to dryness to yield 8.5 g of extract. This was fractionated via vacuum liquid column chromatography to give 7 fractions using a gradient of 99:1 to 100:0 DCM to MeOH. CC was used to further separate fractions 4 and 5 with an isocratic mixture of cyclohexane/ EtOAc/MeOH/AcOH, 5:10:2:0.1). Compounds were further purified by preparative HPLC to yield 15.1, 1.8, 2.7, 1.1, 0.9, 6.9, 5.4 mg of **37-43** respectively.

Lovastatin (**35**) and mevinolinic acid methyl ester (**36**) were isolated from organic extract (529 mg) derived from 40 malt agar plates (each 25 ml medium). The extract was subjected to VLC as described above and further purified by preparative HPLC to yield 1.9 and 2.2 mg respectively.

7-Desmethylcitreoviridin (**33**), citreoviridin (**44**), novobenzomalvin C (**45**), *trans* l-phenylalanineamide (**47**), and methyl 3,4,5-trimethoxy-2-(2-(nicotinamido) benzamido) benzoate (**48**) were isolated from barley-spelt medium. Eight grams of organic extract was dry loaded on 25 g of silica gel and subjected to automated flash chromatograph with a 40 g preloaded NP silica column (Grace) using a gradient from 100% n-hexane to 100% ethyl acetate over 34 min then to 100% MeOH over 34 min with a flow rate of 40 ml/min to yield 10 fractions. Semi-preparative HPLC of fraction 5 contained gave 3.1 mg of **45**, compound **33**, **44**, **47**, **48** were isolated from fractions 7-8 (1.2, 5.4, 1.7, and 2.1 mg respectively). Compounds **34** (6.1 mg) and **46** (0.9 mg) were isolated by preparative HPLC

directly from small culture extracts from potato-dextrose broth and oatmeal agar, respectively.

Multivariate analysis. 10 µL extract (5 mg/ml) from each media condition was analyzed in triplicate on an Agilent 1100 series LC/MS platform. Positive mode ionization was found to detect most metabolites, similar results have been previously observed by other groups.[31,32] Positive mode was used for all further analyses. Data sets were exported from Agilent's Chemstation software as .netCDF files and imported into MZmine 2.14.2.[32] MZmine peak picking was performed with established protocols[33] with the following changes: Noise level: 5E2 for mass detection, *m/z* tolerance 0.05 throughout, absolute minimum height 1.0E4 for chromatogram deconvolution, retention time tolerance 0.1 min for gap filling and alignment. Multivariate analysis was performed utilizing Multibase 2015.[14] The relative expression of metabolites in each growth condition was examined by calculating the log-ratio as:

$$\varphi = \log\left(\frac{X + X_0}{\bar{X} + X_0}\right)$$

where X is the LC/MS count at a given mass and retention time for a given growth condition, $\bar{X}$ is the median of X across all growth conditions, and X_0 is an arbitrary value that prevents indeterminate values for mass/retention time values with no or very few counts (set to 1×10^4). The count X was taken as the median count across all injections of the same sample, but since the mass of the sample injected was held constant for all LC/MS experiments no other normalization of X was performed. To aid in visualization, the resulting values were boxcar filtered and downsampled to an *m/z* resolution of 2.5 and a

retention time resolution of 5s. Contour lines of φ are plotted at the 0.25% (dark blue), 2.5% (light blue), 97.5% (light red), and 99.75% (dark red) percentiles. All calculations were performed using custom-written MATLAB scripts (MATLAB R2015a, Mathworks).

Antimicrobial assays. Organic extracts and isolated compounds were tested for inhibitory activity against *Bacillus subtilis, Staphylococcus aureus, Escherichia coli, Pseudomonas aeruginosa, and Candida albicans* in agar diffusion disk assays. Agar plates were inoculated with pathogen according to literature[15] and tested at 250 µg/disk for extracts and fractions, and 50 µg/disk for isolated compounds.

Cytotoxicity assay. Cytotoxic activities of extracts and pure compounds were evaluated against a human colorectal carcinoma model (HCT-116, ATCC CCL-247). Cytotoxicity assays were carried out using an MTT (3-(4,5-dimethylthiazol-2-yl)-2,5-diphenyl-2H-tetrazolium bromide) cell proliferation assay kit (American Type Culture Collection) according to the instructions provided.[16] Briefly, HCT-116 cells were seeded in 96-well tissue culture plates at a density of 2×10^4 cells/well in 150 µl of growth media and allowed to adhere for 24 h. Organic extracts, dissolved in DMSO, were added to each well to a final concentration of 10 µg/ml for single dose evaluation. IC50 values for pure compounds were determined using a 12-point dilution. Control wells received an equivalent portion of DMSO and etoposide was used as a positive control. At the end of 72 h of incubation, 100 µl of PBS containing 10% MTT was added to the cultures and incubated for 2 h. The media was then replaced with DMSO and cell viability was assessed with a Bioteck Synergy 96-well absorbance plate reader at 550 nm.

*7-Desmethylcitreoviridin **33** (=6-((1E,3E,5E,7E)-8-((2S,3R,4R,5R)-3,4-dihydroxy-2,4,5-trimethyltetrahydrofuran-2-yl)octa-1,3,5,7-tetraen-1-yl)-4-methoxy-5-methyl-2H-pyran-2-one*. Yellow solid. $[\alpha]_D^{20}$-62 (MeOH, c=0.1); UV (MeOH) λ_{max} 396 (4.86), 383 (3.85), 295 (2.82), 237 (2.89); ECD (MeOH) 203.3 (+11.4), 238.1 (-4.8), 271.5 (0.7), 380.7 (1.2), 387.2 (-8.0), 391.7 (3.0), 407.7 (-2.9); IR (KBr) 3374, 2918, 2850, 1689, 1632, 1537, 1454, 1405, 1248, 1148, 1093; ^{1}H-NMR (700 MHz, methanol d_4): 7.14-7.19 (1H, m), 6.58-6.68 (2H, m,), 6.49-6.53 (1H, m), 6.41-6.47 (2H, m), 6.09-6.13 (1H, m), 5.51 (1H, s) 3.88 (3H, s, OMe), 3.85 (1H, q, J= 6.34), 3.76 (1H, s), 1.97 (3H, s), 1.28 (3H, s), 1.20 (3H, d, J=6.34), 1.19 (3H, s) ^{13}C-NMR/HSQC (700 MHz, CDCl3) 172.9, 164.3, 152.2, 141.6, 135.9, 134.8, 131.8, 129.1, 128.7, 127.8, 119.6, 119.4, 109.0, 89.0, 86.3, 84.7, 79.7, 79.0, 56.3, 17.7, 13.4, 9.0 HR-ESI-MS (*m/z*). 411.1760 ([M+Na]$^+$ $C_{22}H_{28}O_6Na^+$; calc. 411.1778).

4.6 Supplementary material

The supplementary material for this publication can be found in appendix C of this dissertation.

4.7 References

1. E. Patridge, P. Gareiss, M. S. Kinch, D. Hoyer, *Drug Discov. Today* **2015** doi:10. 1016/j.drudis.2015.01.00

2. D. J. Newman, G. M. Cragg, *J. Nat. Prod.* **2012**, *75*, 311-335.

3. J. Bérdy, *J. Antibiot.* **2012**, *65*, 385-395.

4. A. L. Demain, *Med. Res. Rev*. **2009**, *29*, 821-842.

5. D. L. Hawksworth, *Stud. Mycol*. **2004**, *50*, 9–18.

6. K. Saikkonen, J. Ahlholm, M. Helander, S. Lehtimäki, O. Niemeläinen, *Annu. Rev. Ecol. Syst.* **1998**, *29*, 319-343. J. A. Rudgers, A. L. Swafford *Basic Appl. Ecol.* **2009**, 1043-51.

7. B. Schulz, S. Draeger, T. E. dela Cruz, J. Rheinheimer, K. Siems, S. Loesgen, J. Bitzer, S. Schloerke, A. Zeeck, I. Kock, H. Hussein, J. Dai, K. Krohn, *Bot. Mar.* **2008**, *51*, 219-234.

8. H. B. Bode, B. Bethe, R. Hofs, A. Zeeck. *Chem. Bio. Chem*. **2002**, *3*, 619–627.

9. Y.-M. Chiang, K.-H. Lee, J. F. Sanchez, N. P. Keller, C. C. C. Wang, *Nat. Prod. Commun.* **2009**, *11*, 1505–1510.

10. K. Scherlach, C. Hertweck C. *Org. Biomol. Chem.* **2006**; 4:3517–3520.

11. T. J. White, T. D. Bruns, S. Lee, J. W. Taylor, 'Amplification and direct sequencing of fungal ribosomal RNA genes for phylogenetics', in: 'PCR Protocols: A Guide to Methods and Applications', eds. M. A. Innis, D. H. Gelfand, J. J. Sninsky, T. J. White, Academic Press, Inc., New York, 1990, p. 315-322.

12. S. Lösgen, J. Magull, B. Schulz, S. Draeger, A. Zeeck, *Eur. J. Org. Chem.* **2008**, 698-703.

13. T. Pluskal, S. Catsillo, A. Villar-Briones, M. Oresic, *BMC Bioinform.* **2010***, 11*, 395.

14. Cluster analysis (or PCA, PLS analysis) was performed using the Excel add-in Multibase package (Numerical Dynamics, Japan) free of charge download.

15. Agar diffusion assays were performed as described in the Clinical and Laboratory Standards Institute (CLSI) guidelines: National Committee for Clinical Laboratory Standards. Approved Standard M02-A11 and M100-S25. NCCLS, Wayne, PA, USA, 2002.

16. ATCC MTT assay kit, accessed Sept. 21, 2015:
https://www.atcc.org/~/media/DA5285A1F52C414E864C966FD78C9A79.ash

17. L. Qiao, D. Xie, Q. Liu, J. Zou, Z. Shen, J. Dai, *Acta Pharm. Sin. B* **2012**, *2*, 300-305.

18. J. K. Chan, R. N. Moore, T. T. Nakashima, J. C. Vederas, *J. Am. Chem. Soc.* **1983**, *105*, 3334.

19. K. V. Rao, A. K. Sadhukhan, M. Veerender, V. Ravikumar, E. V. Mohan, S. D. Dhanvantri, M. Sitaramkumar, J. M. Babu, K. Vyas, G. O. Reddy, *Chem. Pharm. Bull.* **2000**, *48*, 559.

20. R. Haritakun, P. Rachtawee, R. Chanthaket, N. Boonyuen, M. Isaka, *Chem. Pharm. Bull.* **2010**, *58,* 1545-1548.

21. R. R. Parvatkar, C. D'Souza, A. Tripathi, C. G. Naik, *Phytochemistry* **2009**, *70*, 128.

22. R. J. Cole, J. H. Moore, N. D. Davis, J. W. Kirksey, U. L. Diener, *J. Agric. Food. Chem.* **1971**, *19*, 909.
23. M. W. da Rocha, I. S. Resck, E. D. Caldas, *Food Addit. Contam., Part A.* **2014**, *32*, 584.
24. B. Franck, H.-P. Gehrken, *Angew. Chem., Int. Ed. Engl.* **1980**, *19*, 461.
25. Scifinder, version 2007.1; Chemical Abstracts Service: Columbus, OH, 2007; CAS RN 117558-71-0 (accessed Sept. 21, 2015). Offered by AnalytiCon Discovery as NP-001638. However spectroscopic data was not available upon request.
26. G. Englert, *ChemInform* **1991**, *22*, no.
27. A. Shimada, T. Inokuchi, M. Kusano, S. Takeuchi, R. Inoue, M. Tanita, S. Z. Fujioka, *Naturforsch., C: J. Biosci.* **2004**, *59*, 218
28. K. Ishikawa, T. Hosoe, T. Itabashi, F. Sato, H. Wachi, H. Nagase, T. Yaguchi, K.-I. Kawai, *Sci. Pharm.* **2011**, *79*, 937.
29. S. G. Toske, P. R. Jensen, C. A. Kauffman, W. Fenical, *Tetrahedron* **1998**, *54*, 13459.
30. K. Arai, S. Shimizu, Y. Yamamoto. *Chem. Pharm. Bull.* **1980**, 29, 1005-1012.
31. W. Y. Liao, C. N. Shen, L. H. Lin, Y. L. Yang, H. Y. Han, J. W. Chen, S. C. Kuo, S. H. Wu, C. C. Liaw, *J. Nat. Prod.* **2012**, *75*, 630.
32. Y. Hou, D. R. Braun, C. R. Michel, J. L. Klassen, N. Adnani, T. P. Wyche, T. S. Bugni. *Anal. Chem.* **2012**, 84, 4277-4283
33. U. R. Abdelmohsen, C. Cheng, C. Viegelmann, T. Zhang, T. Grkovic, S. Ahmed, R. J. Quinn, U. Hentschel, R. Edrada-Ebel. *Mar. Drugs*. **2014**, 12, 1220-1244.

Chapter 5 – adapted from the published article

"Co-Culture of two Developmental Stages of a Marine-derived *Aspergillus alliaceus* Results in the Production of the Cytotoxic Bianthrone Allianthrone A"

Paige E. Mandelare, Donovon. A. Adpressa, Elizabeth N. Kaweesa, Lev. N. Zakharov, Sandra Loesgen

5.1 Introduction

The genetically encoded, small-molecule chemical diversity of filamentous fungi is still largely unexplored and represents an attractive source for the discovery of new compounds. Here we report the production of new chlorinated bianthrones from co-culture of two different developmental stages, or morphs, of a marine alga-derived *Aspergillus alliaceus* (teleomorph: *Petromyces alliaceus*) strain. The vegetative stage (asexual morph) can be separated from the morph that switched to sexual development (sclerotial morph); both produce distinct secondary metabolite patterns. Ochratoxin (**49**) was mainly found in the monoculture of the sclerotial morph, while the anthraquinone pigment nalgiovensin (**50**) was produced by the asexual morph. Surprisingly, combining cultures from both developmental stages in a co-culture experiment, changed the metabolite profile drastically. The chlorinated congener nalgiolaxin (**51**) was abundant and newly produced bianthrones were found**.** Allianthrone A (**52**) and its two diastereomers [allianthrones B (**53**) and C (**54**)] were isolated and the new structures were determined by extensive NMR spectroscopic analysis, supported by optical properties and X-ray crystallography. All metabolites were tested in antibiotic and cytotoxicity assays, and allianthrone A (**52**) showed weak cytotoxic activity against the HCT-116 colon cancer and SK-Mel-5 melanoma cell line.

Natural products, or compounds isolated from biological sources, have inspired the vast majority of clinically approved drugs.[1,2] Fungal metabolites including the antibiotic penicillin, the immunosuppressant cyclosporine, and the cholesterol-lowering agent lovastatin, have revolutionized how some major diseases are treated. Even more promising,

there is a tremendous diversity of bioactive natural products yet to be discovered. First, only a small percentage of the currently ~100,000 described fungal species have been screened for bioactive compounds.[3,4] Indeed, endophytic fungi, which are symbiotic fungi living within plants and algae hosts, have been shown to enhance plant growth, improve disease resistance and increase tolerance of abiotic stressors. Endophytic fungi are recognized as prolific producers of bioactive compounds,[5-8] and many of them grow sustainably in laboratory cultures to produced diverse chemistry,[9-11] yielding 20% more novel compounds in chemical screens than typical fungal strains.[12] Second, genomic studies indicate that in most fungal strains the number of gene clusters for secondary metabolites far exceed the number of compounds identified in chemical studies.[13] This suggests that under standard laboratory conditions many of these gene clusters are transcriptionally suppressed. In addition to these silent gene clusters, most sequenced fungi exhibit a large number of cryptic gene clusters for which no gene product is known. Several approaches have been employed to drive expression of inactive genes. Chromatin manipulation with epigenetic modifiers has been successfully used to elicit production of small molecules.[14-16] Another approach exposes a single strain to multiple growth conditions, e.g., varied nutrients or temperature, or utilizes co-cultivation of microorganisms in order to induce production of metabolites.[17] Some successful examples of molecules derived from co-cultivation include berkeleylactones,[18] chaunopyran A,[19] citrifelins,[20] libertellenones[21] and emericellamides[22] from fungal co-cultures, as well as pestalone[23] and pestalotiolactones A and B,[24] among other polyketides, from mixed bacterium-fungus co-cultures.

In a continuation of our research on bioactive metabolites from endophytic fungi, we investigated the alga-derived, endophytic *A. alliaceus.* We were able to culture two distinct developmental forms, a rapidly growing vegetative form that generates typical conidiophores and asexual spores (conidia) found in aspergilli, and a sexual form, which shows almost no conidiation but clear onset of sclerotium formation. What exactly determines this developmental switch in *A. alliaceus* is not clear, but both morphs can be chemically analyzed separately. Interestingly, the metabolic profile and bioactivity changed drastically when the morphs were co-cultured.

5.2 Results and discussion

What turned out to be a new strain of *Aspergillus alliaceus* (internal designation G4) was isolated from a marine alga by BioViotica Naturstoffe GmbH (Germany) and given to us for chemical analysis. We observed two developmental, morphologically distinct forms, the asexual morph and the sclerotial morph, which we separately grew for further chemical analyses (Figure D1, Appendix D). The species was tentatively identified by Sanger sequencing of PCR fragments amplified from the rDNA ITS, beta-tubulin, and calmodulin loci. DNA sequences from both morphs showed 99% sequence identity to *Petromyces alliaceus* NRRL 315 (Appendix D, Figures D2-D4); no other known species gave a better match.[29] Historically, the asexual stage was first described as *A. alliaceus*[25] and the sexual (teleomorph) stage was later named *Petromyces alliaceus*; both stages are known producers of the mycotoxin ochratoxin.[26,28] While many fungi reproduce sexually, no sexual state is known for the majority of aspergilli (64%). Many fungi need compatible partners to mate (heterothallic), while a minority of species are self-fertile (homothallic). It is likely that *P.*

alliaceus is the only known sexually reproducing fungus classified in *Aspergillus* section *Flavi*, which is homothallic and does not require a mate of different genotype to undergo sexual development.[27] The sclerotial morph in our hands generates sparse conidia and early darkly pigmented sclerotia, but so far has never fully developed to generate ascospores within stromata, as previously observed.[26] Thus, the sclerotial morph initiated all events of early sexual development but arrested well before meiosis. In previous studies, type strains of *A. alliaceus* were tested for the formation of stromata and ascocarps but not all strains matured; sometimes completion of the sexual cycle took years, depending on the specific nutrient conditions.[30,31] As expected, subcultures generated from the sclerotial morph returned to the asexual, conidial form, a process accelerated by incubation at higher temperatures (37 °C instead of 25 °C) on Czapek-Dox agar (Appendix D, Figures D5-D6). Curiously, we have not been able to find culture conditions to initiate sexual development from the conidial morph by a change of nutrients. Taken together, DNA sequence-based identification, initial chemotyping and morphological and developmental pattern strongly suggest that our strain belongs in *A. alliaceus*.

When grown on malt-based, buffered liquid media, the sclerotial morph of *Aspergillus alliaceus* produced ochratoxin A (**49**), a known mycotoxin originally isolated from *Aspergillus ochraceus*.[32-34] HRMS data, the UV spectrum and 1D and 2D NMR data matched previous published spectroscopic data for **49**.[34-37] The asexual morph of *Aspergillus alliaceus* produces the known anthraquinone nalgiovensin (**50**) in malt-based media, along with traces of nalgiolaxin, its chlorinated congener (**51**). These anthraquinone pigments were first isolated from *Penicillium nalgiovense* [38-40] and their full spectroscopic

characterization was recently reported.[41] The UV, IR, HRMS, 1D and 2D NMR data for **50** and **51** in $CDCl_3$, and a crystal structure of **50** (Appendix D, Figure D7) assuredly match the recently reported data.

Once both morphs have been grown in co-culture together for at least three weeks, each newly inoculated culture had its metabolic profile drastically changed. An LCMS-based analysis of the metabolites produced in co-culture showed elevated levels of nalgiolaxin (**51**) approximately seven times over nalgiovensin (**50**) and a set of compounds with previously unobserved retention times, *m/z* value, and UV chromophore. We were ultimately able to identify allianthrone A (**52**), a new bianthrone dimer of nalgiolaxin (Figure 5.1). Compound **53** was obtained as a dark yellow amorphous solid and the molecular formula of **52** was determined as $C_{36}H_{32}Cl_2O_{10}$ by HRESIMS with 20 degrees of unsaturation. The IR spectrum showed absorptions at 1620 cm^{-1} (chelated C=O), 1610 and 1580 cm^{-1} (aromatic rings). The UV spectrum exhibited maxima at 270, 336, and 369 nm consistent with the UV spectra of bianthrones.[42-44] The carbon NMR spectrum of **52** showed clear similarities to the spectroscopic data found for neobulgarone,[45,46] exhibiting typical chemical shifts for the bianthrone ring system, and the same sidechain found in nalgiovensin and nalgiolaxin (δ_C 68.5, 46.4, 23.8, 23.5). Additionally, a methoxy group (δ_C 57.4) and hydroxy-bearing carbons could be established (δ_C 162.3, 162.2, 159.37, 159.36). The ^{1}H NMR spectrum showed signals arising from the 2-hydroxypropyl side chain (δ_H 4.68, 2.65, 2.59, 1.16, 1.13), two methoxy groups, two sp^3 methine protons at the bridge positions (δ_H 4.67), six aromatic protons (δ_H 6.76, 6.74, 6.40, 6.39, 6.32, 6.28), and four chelated hydroxy protons (δ_H 12.422, 12.419, 11.434, 11.432). Notably, we observed

chemically distinct proton NMR signals for the anthronyl protons which indicates asymmetry in this bianthrone which supports a recent report that symmetric (H-10/10') bianthrones prefer energy-minimized gauche forms with a face-stacked conformation.[47] 2D NMR experiments, including COSY, HSQC, and HMBC (Figure 5.2A), further support the relative structure of the 10 (sp^3)-10'(sp^3)-bianthrone (Figure 5.1).
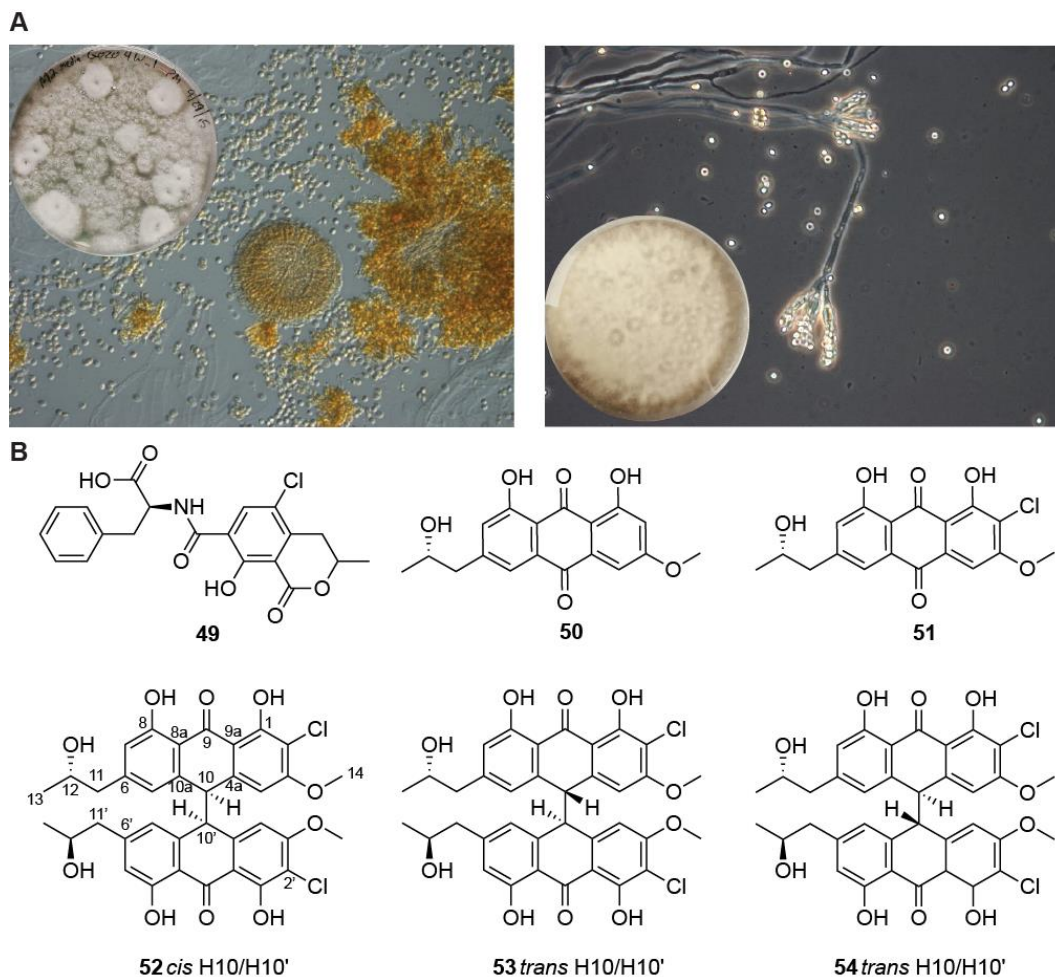
Figure 5.1 A) Phenotypic differences of *Aspergillus alliaceus* cultures, sclerotial morph (left), asexual (conidia forming, right). B) Isolated compounds from sclerotial morph *A. alliaceus* (**49**), asexual *A. alliaceus* (**50,51**), and from co-culture (**52-54**).

Computation of the lowest-energy conformation additionally predict the overall *gauche* conformation for H-10/10' in allianthrone A in solution. Chiral substituted bianthrones can exist as two pairs of racemates with cis and trans H-10/10' axial connectivity. The four diastereomers are often described as either meso (cis) or racemic (trans) with regards to

their optical properties. Interestingly, compound **52** does not exhibit an optical rotation or an ECD spectrum, as is known for these meso compounds, which confirms its cis conformation.[47]

Allianthrone A formed X-ray diffraction suitable crystals after being dissolved in acetone and then placed in a 90% hexanes-10% $CHCl_3$ atmosphere (Figure 5.2B). The Flack parameter of 0.029(6) conveys strong confidence in the absolute configuration of **52** as 10*R*, 10'*S*, 12*S*, 12'*S*. Additionally, we employed ultra-high resolution ^{13}C NMR spectroscopy to identify signals in **52** that arise from Cl-substitution by exploiting the $^{35}Cl/^{37}Cl$ isotope shift and confirmed carbons C-2 and C-2' being bound to chlorine (Appendix D, Figure D8).[48] Fungal bianthrones were first found in *Penicillium*[46] and *Aspergillus*,[42,49-51] and structurally related metabolites are the neobulgarones,[45,46] flavoobscurins A, B$_1$, and B$_2$[52] and the fungal derived[42,50,53] and plant derived[54] physcion bianthrone.
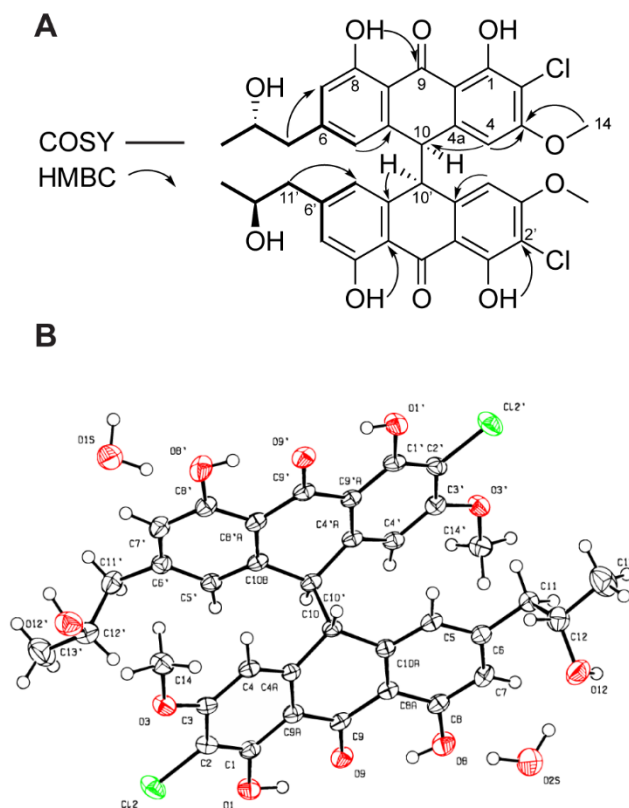
Figure 5.2 A) Selected HMBC and COSY correlations and B) ORTEP plot of compound **52.**

Allianthrone A was first observed at day 15 of co-cultivation (Appendix D, Figure D9-D10), along with two congeners with similar UV profile and mass. The three allianthrones were found in a 2:1:1 ratio (**52**:**53**:**54**) and their production peaks around day 20 of co-culture. Allianthrone B (**53**) and allianthrone C (**54**) eluted earlier in reversed-phase chromatography compared to allianthrone A, (R_t 24.7, 24.9, 25.3 min respectively). The isomers were separated by liquid chromatography but can interconvert under acidic,

oxidative, and high UV conditions. While the UV absorption and HRMS data were identical, **53** and **54** are easily distinguished by specific rotations, ECD spectra, and NMR data (Table 5.1). In contrast to the cis bianthrone **52**, the trans H-10/10' allianthrones B and C exhibit pseudo-enantiomeric properties with well-defined specific rotation and ECD spectra, as well as chemically equivalent and indistinguishable NMR signals for the two anthronyl rings (Table 5.1).[55] To determine the absolute configurations, ECD spectra were recorded and calculated for bianthrones **53** and **54**. Conformational searches of **53** and **54** were performed with Spartan '14 using the MMFF94 force field and geometries were further optimized at the gas-phase B3LYP/6-31G(d) level in Gaussian 09 to give 30 (10*S*,10'*S*, 12*S*, 12'*S*), and 30 (10*R*,10'*R*, 12*S*, 12'*S*) energy-minimized conformers within a 5 kcal/mol energy threshold from the global minimum. The optimized conformers were then subjected to a more rigorous QM optimization at the CAM-B3LYP/TZVP level of theory with IEFPCM in MeCN. Finally, ECD spectra were computed for all conformers comprising greater than one percent of the conformational space using the Time Dependent Density Functional Theory method (TDDFT) at the ωB97XD/TZVP level utilizing IEFPCM in MeCN for 40 states. Spectra were then Boltzmann averaged and wavelength corrected using SpecDisc[56] software and an in-house script. Comparison of the experimental and calculated ECD spectra for **53** and **54** showed excellent agreement (Figure 5.3) with absolute configuration 10*R*,10'*R*, 12*R*, 12'*S* for allianthrone B (**53**), and 10*S*,10'*S*, 12*S*, 12'*S* for allianthrone C (**54**).

Table 5.1 NMR tabulations of allianthrones A-C in d3-acenitrile.

	52		53		54	
position	δ_C ,type	δ_H (J in Hz)	δ_C ,type	δ_H (J in Hz)	δ_C ,type	δ_H (J in Hz)
1	159.36, C		159.6, C		159.5, C	
1-OH		12.419, s		12.40, s		12.38 br, s
2	108.61, C		108.7, C		108.7, C	
3	161.1, C		161.1, C		161.0, C	
4	105.7, CH	6.28 br,s	105.7, CH	6.23 br, s	105.6, CH	6.17 br, s
4a	141.4, C		141.6, C		141.5, C	
5	122.6, CH	6.391, d (4.2)	122.8, CH	6.54 br, s	123.0, CH	6.51 br, s
6	150.2, C		150.5, C		150.8, C	
7	117.9, CH	6.74, d (1.1)	118.2, CH	6.75 s	118.2, CH	6.77, s
8	162.2, C		162.1, C		162.1, C	
8-OH		11.432, s		11.47, s		11.45 br, s
8a	115.33, C		115.6, C		115.6, C	
9	191.3, C		191.4, C		191.4, C	
9a	112.6, C		112.5, C		112.5, C	
10	56.2, CH	4.647, m	56.3 CH	4.71, s	56.3, CH	4.66, s
10a	142.3, C		142.3, C		142.2, C	
11	46.40, CH2	2.65 (a), 2.587 (b), m	46.3, CH2	2.67 (a), dd (13.4, 7.7, 7.4)/ 2.62 (b), dd (13.4, 5.9, 5.4)	46.4, CH2	2.67 (a), dd (13.2, 4.9,4.7)/ 2.59 (b), dd (13.4, 8.8, 8.5)
12	68.5, CH	3.91, m	68.4, CH	3.91, m (17.9, 11.4, 7.4, 5.9, 6.1)	68.5, CH	3.95 br,s
12-OH		2.83, br		2.78, d (4.9)		2.76, s br
13	23.5, CH3	1.13, d (6.2)	23.7, CH3	1.15 d (6.1)	23.9, CH3	1.17, d (6.1)
14-OCH3	57.4, CH3	3.87, s	57.4, CH3	3.86, s	57.4, CH3	3.84, s
1'	159.37, C		159.6, C		159.5, C	
1'-OH		12.422, s		12.40, s		12.38 br, s
2'	108.64, C		108.7, C		108.7, C	
3'	161.2, C		161.1, C		161.0, C	
4'	105.7, CH	6.32 br,s	105.7, CH	6.23 br, s	105.6, CH	6.17 br, s
4a'	141.4, C		141.6, C		141.5, C	
5'	122.9, CH	6.404, d (4.2)	122.8, CH	6.54 br, s	123.0, CH	6.51 br, s
6'	150.4, C		150.5, C		150.8, C	
7'	118.2, CH	6.76, d (1.3)	118.2, CH	6.75 s	118.2, CH	6.77, s
8'	162.3, C		162.1, C		162.1, C	
8'-OH		11.434 s		11.47, s		11.45 br, s
8a'	115.35, C		115.6, C		115.6, C	
9'	191.3, C		191.4, C		191.4, C	
9a'	112.7, C		112.5, C		112.5, C	
10'	56.3, CH	4.651, m	56.3 CH	4.71, s	56.3, CH	4.66, s
10a'	142.4, C		142.3, C		142.2, C	
11'	46.41, CH2	2.67 (a), 2.592 (b), m	46.3, CH2	2.67, dd (13.4, 7.7, 7.4)/ 2.62, dd (13.4, 5.9, 5.4)	46.4, CH2	2.67, dd (13.2, 4.9,4.7) / 2.59, dd (13.4, 8.8, 8.5)
12'	68.5, CH	3.95, m	68.4, CH	3.91, m (17.9, 11.4, 7.4, 5.9, 6.1)	68.5, CH	3.95 br,s
12'-OH		2.86, br		2.78, d (4.9)		2.76, s br
13'	23.8, CH3	1.16, d (6.3)	23.7, CH3	1.15 d (6.1)	23.9, CH3	1.17, d (6.1)
14'-OCH3	57.4, CH3	3.88, s	57.4, CH3	3.86, s	57.4, CH3	3.84, s
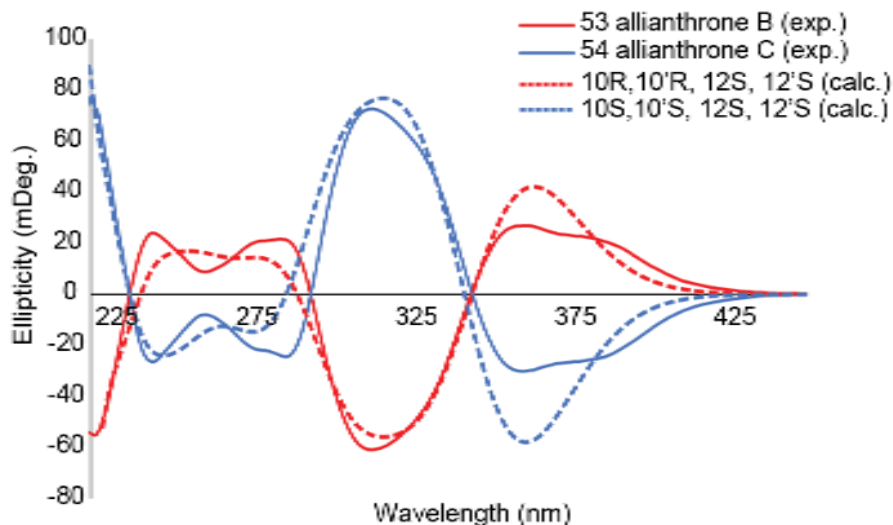
Figure 5.3 Calculated (dashed lines) and experimental (solid lines) electronic circular dichroism (ECD) spectra of allianthrone B and C.

To further explore the chiral properties of **52**, **53**, and **54**, we used chiral-phase column chromatography with various packing materials and column dimensions, each of which showed single peaks for each of the three diastereomers **52-54**. While four diastereomers are possible for chiral bianthrones[47] only three allianthrones were identified from co-culture in this study, similar to the recent discovery of three rhamnepalins from *Rhamnus nepalensis*[43] and three bianthrones from *Senna longiracemosa*.[44] Similar to known plant-derived bianthrones, the carbon-carbon bond formation may be assisted by a dirigent-like protein that facilitates a site-specific radical bond formation to yield a single, diastereomeric bianthrone (**52**) (Appendix D, Figure D11).[60-62] Due to the known instability of bianthrones in low pH conditions, and the slightly acidic pH of ~5 after the fermentation period, allianthrone A may be the sole biosynthetic product and allianthrones B and C are possibly artifacts formed during the cultivation and extraction process.

Bianthrones are known to be easily oxidized under normal atmospheric conditions,[57,58] and we observed polymerization if **52** is kept in DMSO. Similar sensitivity has been observed previously in the formation of hypericin from emodin bianthrone[57,58] and penicilliopsin[59] in oxidative, high pH, and high UV conditions. The structure and properties of the derived polymer are currently being investigated.

Recent developments in gene activation and manipulation have played a crucial role in reinvigorating microbial natural products based drug discovery.[66] This study presents the first case of elicitation of new fungal chemistry by a co-culture approach of two different developmental stages of one, homothallic *Aspergillus* species. For some Aspergilli, including *A. alliaceus,* sexual and asexual developmental stages are known, however rarely do they co-exist at the same time as shown in this report.[26, 28-30] Even more surprising is the production of new bianthrones when the asexual and sclerotial morph of the same species are co-cultured. There are only a few case studies that show differences in the metabolite production in fungi depending on their developmental stage,[67,68] or distinct chemical profiles for the two mating types of heterothallic fungi.[69,70]

The newly disclosed bianthrones were identified via extensive NMR and MS analyses and in the case of **52**, by X-ray diffraction analysis. The main metabolite allianthone A exists as a pseudo-meso compound as seen in the crystal structure, ECD, and NMR spectra. Two minor bianthrones, allianthrone B (**53**) and C (**54**), were isolated most likely as artifacts. **52-54** were reliably produced at high yields when the asexual and sclerotial morphs of *A. alliaceus* were combined in liquid cultures for at least two weeks and then propagated into new media (Appendix D, Figure D1). Variation of the culture media for

each morph did not yield the production of allianthrones, at least in all culture conditions tested thus far. Allianthrone A (**52**) showed weak cytotoxic activity when tested against the HCT-116 colon cancer and SK-Mel-5 melanoma cell lines. Additionally, we tested allianthrone A in an agar diffusion assay against the conidial and the sclerotial morph of *A. alliaceus*, respectively, and found no statistically significant effects.

In summary, new bianthrones are produced if the asexual and sclerotial morph of *A. alliaceus* are co-cultured, a rare example of co-existing and persisting developmental stages of one endophytic, marine-derived *Aspergillus* species, and the first example of self-induced metabolomic changes resulting in the production of allianthrones.

5.3 Experimental

5.3.1 General Experimental Procedures. Optical rotations were measured on a JASCO P-1010 polarimeter. UV and ECD spectra were recorded using a JASCO J-815 spectropolarimeter. Infrared (IR) spectra were recorded on a Thermo Scientific Nicolet IR100 FTIR spectrometer. NMR spectra were acquired on a Bruker Avance III 500 MHz or Bruker Avance III 700 MHz spectrometer, equipped with a 5 mm TXI probe or ^{13}C cryoprobe respectively, solvent peaks were used as an internal standards: acetonitrile-d_3 (δ_H 1.94; δ_C 1.32), acetone-d_6 (δ_H 2.05; δ_C 29.82), and CDCl$_3$ (δ_H 7.26; δ_C 77.06).[71] Low resolution ESI-MS were recorded on Agilent 1100 series LC with MSD 1946 and high resolution ESI-MS-TOF spectra on an Agilent 6230 MSD spectrometer. Agilent 1100 and 1260 Infinity HPLC systems were used for analytical, semi-preparative, and preparative separations, all equipped with photodiode array detectors. For analytical LCMS, a standard

gradient method was employed with ultra-pure H_2O (A) and MeCN (B) with 0.05% formic acid (FA) in each solvent (10% B to 100% B in 35 min) at a flow rate of 0.8 mL/min. For normal phase chromatography, hexanes (A) and 2-propanol (B) were used. All columns (Phenomenex Kinetex C_{18}, 5 μm x 150 mm x 4.6/21.5 mm; Phenomenex Luna C_{18}, 5 μm x 150 mm x 4.6 mm; Chiracel OD and OD-R, 10 μm x 250 mm x 4.6/10 mm) were re-equilibrated before each injection. All samples were filtered through a 0.45 μm nylon filter before LC/MS and HPLC analyses. Size exclusion chromatography (CC) was performed with Sephadex LH20 in acetone. Thin layer chromatography (TLC) was performed on pre-coated silica gel 60 F_{254} plates (Merck). TLC plates were visualized by UV (254 and 360 nm), and by spraying with anisaldehyde solution followed by heating at 80 °C. Solvents, media ingredients, and general reagents were from Sigma-Aldrich Corp., Fisher Scientific, and VWR International.

5.3.2 Culture Conditions Sclerotial Morph. Malt pH 6 agar plates (40 x 25 mL) were inoculated with a 1 cm^2 piece of agar/hyphae from a single culture and allowed to grow at ambient light and temperature for 4 weeks. The agar plates were frozen, then the agar cultures were blended with an equivalent portion of EtOAc (1 L). The organic layer was separated and washed with 1 L of d-H_2O and dried *in vacuo*. The resultant extract was separated by flash chromatography on an ISCO CombiFlash with an adaptive gradient from 100% hexane to 100% EtOAc to 100% MeOH monitored at 254 nm with the gradient paused for collection of peaks to yield seven fractions. Fraction 3 was estimated by LCMS to be greater than 80% pure and was analyzed by 1D and 2D NMR spectroscopy. The major component was identified as ochratoxin A (**49**) by UV, HRMS, and NMR data.

5.3.3 Co-Culture Experiments. Both developmental stages of *A. alliaceus* were grown on separate agar plates and used to inoculate each 50 mL of malt liquid media. After 2 weeks, the two cultures were combined into 1 L malt-based buffered media and cultivated at 28 ˚C on an orbital shaker at 110 rpm for 30 days. Prior to extraction, the co-culture cells were inoculated onto malt-based agar to monitor phenotypic changes. The culture medium was extracted using equal parts EtOAc to media for 24 h with stirring. The solution was filtered through cheesecloth and the culture broth subjected to two more extractions using EtOAc. The combined organic layers were dried over anhydrous $MgSO_4$, and concentrated under vacuum. The extract (458 mg) was subjected to a defatting bilayer method using 2:1:1 hexane:MeOH:MeCN to yield 398 mg.[41] The defatted extract was subjected to preparative HPLC using an isocratic gradient of 65% MeCN with 0.05% FA to yield compounds **50** (4.7 mg/L, orange solid), **51** (3.2 mg/L, yellow solid, and **52** (36.5 mg/L, reddish-brown solid), respectively. Compound **52** was not stable in DMSO and formed insoluble black specks after initial NMR characterization. To re-isolate more **52,** we used Sephadex LH-20 size exclusion chromatography in acetone for the remaining extract (115 mg). In a second step, preparative HPLC (isocratic 55% MeCN with 0.05% FA) afforded compounds **53** (1.1 mg/L), **54** (2.4 mg/L), and **52** (3.4 mg/L), respectively.

5.3.4 Characterization of secondary metabolites.

Nalgiovensin (50): orange, needle-like solid; $[\alpha]_D^{19}$+38 (*c* 0.1, $CHCl_3$); Lit. Value: $[\alpha]_{5790}^{20}$+39.7(*c* 0.1786, $CHCl_3$).[39,40,79]

Nalgiolaxin (51)*:* yellow, needle like solid; $[\alpha]_D^{22.5}$+30 (*c* 0.1, $CHCl_3$); Lit. Value: $[\alpha]_{5790}^{22}$+40.3 (*c* 0.1072, $CHCl_3$). [38,40,79]

Allianthrone A (52) (9*R*,9'*S*)-3,3'-dichloro-4,4',5,5'-tetrahydroxy-7,7'-bis((S)-2-hydroxypropyl)-2,2'-dimethoxy-[9,9'-bianthracene]-10,10'(9H,9'H)-dione): orange-yellow solid; $[\alpha]_D^{21.9}$+0.3 (*c* 0.1, MeCN); UV (*c* 0.1, MeCN) λ_{max} (log ε) 282 (1.30), 360 (1.31), 606 (1.09) nm; IR (ATIR, CH$_2$Cl$_2$) 3359, 2924, 2853, 1612, 1560, 1484, 1410, 1370, 1261, 1196, 1104 cm^{-1}; ^{1}H and ^{13}C NMR data, Table 5.1; HRESIMS: *m/z* 693.1308 [M-H]$^-$ (calcd for C$_{36}$H$_{31}$Cl$_2$O$_{10}$, 693.1300; Δppm = 1.2).

Allianthrone B (53) (9R,9'R)-3,3'-dichloro-4,4',5,5'-tetrahydroxy-7,7'-bis((S)-2-hydroxypropyl)-2,2'-dimethoxy-[9,9'-bianthracene]-10,10'(9H,9'H)-dione): pale yellow solid; $[\alpha]_D^{21.9}$+69 (*c* 0.1, MeCN); UV (*c* 0.1, MeCN) λ_{max} (log ε) 281 (1.14), 358 (1.19), 604 (1.09) nm; IR (ATIR, EtOAC) 2980, 2881, 2336, 1613, 1385, 1252, 1155 cm^{-1}; ECD (*c* 0.1, MeCN), λ_{max} ($\Delta\varepsilon$) 378 (+5.0), 363 (+5.6), 314 (-7.3), 285 (+4.8), 264 (+3.1), 245 (+5.2), 226 (-6.4) nm; ^{1}H and ^{13}C NMR data, Table 5.1; HRESIMS: *m/z* 693.1283 [M-H]$^-$ (calcd for C$_{36}$H$_{31}$Cl$_2$O$_{10}$, 693.1300; Δppm = 2.4)

Allianthrone C (54) ((9S,9'S)-3,3'-dichloro-4,4',5,5'-tetrahydroxy-7,7'-bis((S)-2-hydroxypropyl)-2,2'-dimethoxy-[9,9'-bianthracene]-10,10'(9H,9'H)-dione): yellow solid; $[\alpha]_D^{21.9}$-40 (*c* 0.1, MeCN); UV (MeCN) λ_{max} (log ε) 279 (1.22), 358 (1.22), 605 (1.09) nm; IR (ATIR, EtOAC) 2981, 2360, 2341, 1616, 1372, 1241, 1106 cm^{-1}; ECD (*c* 0.1, MeCN), λ_{max} ($\Delta\varepsilon$) 382 (-3.7) 362 (-4.4), 314 (+10.6), 287 (-3.6), 263 (-1.2), 245 (-3.9), 226 (+11.4)nm; ^{1}H and ^{13}C NMR data, Table 5.1; HRESIMS: *m/z* 693.1295 [M-H]$^-$ (calcd for C$_{36}$H$_{31}$Cl$_2$O$_{10}$ 693.1300; Δppm = 0.7)

5.3.5 Computational Details. Initial conformational analyses for allianthrones A-C (**52-54**) were performed in Spartan '14 (Wavefunction) using MMFF94 with 100000

maximum conformers for each candidate structure (three total). All conformers with a relative energy lower than 5 kcal/mol were carried forward for QM analysis and optimization. The conformers were saved as an .SDF file and a Python script was used to generate Gaussian 09[82] input files for each conformer for gas and solvated geometry optimization and frequency calculations as well as TDDFT computations. Gas phase geometry optimization and frequency calculations were performed at the B3LYP/6-31G level and were analyzed for duplicate conformers and imaginary frequencies using a Python script.[83] Conformers with a relative energy lower than 5 kcal/mol were once again carried forward for more rigorous QM geometry optimization with integral equation formalism variant polarizable continuum model (IEFPCM) in MeCN at the CAM-B3LYP/TZVP level. The Gaussian outfiles were analyzed as above, and conformers contributing to greater than 1% were carried forward in TDDFT calculations. The ECD spectra were calculated by the TDDFT methodology at the ωB97XD/TZVP level utilizing IEFPCM with 40 states in MeCN. UV and ECD spectra were generated and Boltzmann averaged utilizing a Python script developed by the authors which is available upon request. The script relies significantly on the computational chemistry parsing utility cclib.[84] The resultant spectra were compared in MS Excel. Based on these computations we were able to assign compound **53** as 10-*R*, 10'-*R* and compound **54** and 10-*S*, 10'-*S*.

5.4 Acknowledgements

5.5 Supporting information

The Supporting Information is available free of charge on the ACS Publications website at DOI: 10.1021/acs.jnatprod.8b00024 and in Appendix D of this dissertation.

5.6 References

1. Newman, D. J.; Cragg, G. M. *J. Nat. Prod.* **2016**, *79*, 629-261.
2. Patridge, E.; Gareiss, P.; Kinch, M.; Hoyer, D. *Drug Discov. Today* **2016**, *21*, 204-207.
3. Schueffler, A.; Anke, T. *Nat. Prod. Rep.* **2014**, *31*, 1425-1448.
4. Bills, G.; Gloer, J. *Microbiol. Spectrum* **2016**, *4*, 1087-1119.
5. Strobel, G.; Daisy, B. *Microbiol. Mol. Biol. Rev.* **2003**, *67*, 491-502.
6. Strobel, G. A. *Microb. Infect.* **2003**, *5*, 535-544.
7. Aly, A. H.; Debbab, A.; Proksch, P. *Appl. Microbiol. Biotechnol.* **2011**, *90*, 1829-1845.
8. Nisa, H.; Kamili, A. N.; Nawchoo, I. A.; Shafi, S.; Shameem, N.; Bandh, S. A. *Microb. Pathog.* **2015**, *82*, 50-59.
9. Loesgen, S.; Bruhn, T.; Meindl, K.; Dix, I.; Schulz, B.; Zeeck, A.; Bringmann, G. *Eur. J. Org. Chem.* **2011**, *2011*, 5156-5162.
10. Lösgen, S.; Schlörke, O.; Meindl, K.; Herbst-Imer, R.; Zeeck, A. *Eur. J. Org. Chem.* **2007**, *2007*, 2191-2196.
11. Lösgen, S.; Magull, J.; Schulz, B.; Draeger, S.; Zeeck, A. *Eur. J. Org. Chem.* **2008**, *2008*, 698-703.
12. Schulz, B.; Draeger, S.; dela Cruz, T.; Rheinheimer, J.; Siems, K.; Loesgen, S.; Bitzer, J.; Schloerke, O.; Zeeck, A.; Kock, I.; Hussain, H.; Dai, J.; Krohn, K. *Bot. Mar.* **2008**, *51*, 219-234.
13. Grigoriev, I.; Nikitin, R.; Haridas, S.; Kuo, A.; Ohm, R.; Otillar,R.;Riley, R.; Salamov,A.; Zhao, X.; Korzeniewski, F.; Smirnova, T.; Nordberg, H.; Dubchak, I.; Shabalov, I. *Nucleic Acids Res.* **2014**, *42*, D699-D704.
14. Brakhage, A. A.; Schroeckh, V. *Fungal Genet. Biol.* **2011**, *48*, 15-22.
15. Scherlach, K.; Hertweck, C. *Org. Biomol. Chem.* **2009**, *7*, 1753-1760.
16. Adpressa, D. A.; Stalheim, K. J.; Proteau, P. J.; Loesgen, S. *ACS Chem. Biol.* **2017**, *12*, 1842-1847
17. Bode, H. B.; Bethe, B.; Hofs, R.; Zeeck, A. *Chembiochem* **2002**, *3*, 619-627.
18. Stierle, A.; Stierle, D.; Decato, D.; Priestley, N.; Alverson, J.; Hoody, J.; McGrath, K.; Klepacki, D. *J. Nat. Prod.* **2017**, *80*, 1150-1160.
19. Shang, Z.; Salim, A.; Capon, R. *J. Nat. Prod.* **2017**, *80*, 1167-1172.
20. Meng, L.; Liu, Y.; Li, X.; Xu, G.; Ji, N.; Wang, B. *J. Nat. Prod.* **2015**, *78*, 2301-2305.
21. Oh, D.; Jensen, P.; Kauffman, C.; Fenical, W. *Biorg. Med. Chem.* **2005**, *13*, 5267-5273.
22. Oh, D.; Kauffman, C.; Jensen, P.; Fenical, W. *J. Nat. Prod.* **2007**, *70*, 515-520.
23. Cueto, M.; Jensen, P.; Kauffman, C.; Fenical, W.; Lobkovsky, E.; Clardy, J. *J. Nat. Prod.* **2001**, *64*, 1444-1446.
24. Liu, S.; Dai, H.; Heering, C.; Janiak, C.; Lin, W.; Liu, Z.; Proksch, P.; *Tetrahedron Lett.* **2017**, *58*, 257-261.
25. Thom, C.; Raper, K.B. Chapter XXI, The Aspergillus wentii group. *Manual of the Aspergilli.* Williams and Wilkins, Baltimore, Maryland. 1945; p 241-249.
26. Malloch, D.; Cain, R.F. *Can. J. Bot.* **1972**, *50*, 2613–2628.
27. Dyer, P.; O'Gorman, C. *FEMS Microbiol. Rev.* **2012**, *36*, 165-192.
28. Fennell, D.; Warcup, J. *Mycologia* **1959**, *51*, 409-415.

29. McAlpin, C.; Wicklow, D. *Can. J. Microbiol.* **2005**, *51*, 1039-1044.

30. McAlpin, C.; Wicklow, D. *Can. J. Microbiol.* **2005**, *51*, 765-771.

31. Frisvad, J.; Peterson, L.; Kirstine Lyhne, E.; Larsen, T. *PLoS One* **2014**, *9*, 1-11.

32. Bayman, P.; Baker, J. *Mycopathologia* **2006**, *162*, 215-223.

33. Bayman, P.; Baker, J.; Doster, M.; Michailides, T.; Mahoney, N. *Appl. Environ. Microbiol.* **2002**, *68*, 2326-2329.

34. van der Merwe, K.; Steyn, P.; Fourie, L.; Scott, D.; Theron, J. *Nature* **1965**, *205*, 1112-1113.

35. Dais, P.; Stefanaki, I.; Fragaki, G.; Mikros, E.; *J. Phys. Chem. B* **2005**, *109*, 16926.

36. Bredenkamp, M.; Dillen, J.; van Rooyen, P.; Steyn, P.; *J. Chem. Soc*. **1989**, *2*, 1835-1839.

37. Pohland, A.; Schüller, P.; Steyn, P.; van Egmond, H. *Pure Appl. Chem.* **1982**, *54*, 2219-2284.

38. Birch, A.; Stapleford, K. *J. Chem.Soc*. **1967**, *0*, 2570-2571.

39. Birch, A.; Massy-Westropp, R. *J. Chem. Soc.* **1957**, *0*, 2215-2217.

40. Raistrick, H.; Ziffer, J. *Biochem. J*. **1951**, *49*, 563-575.

41. Figueroa, M.; Jarmusch, A.; Raja, H.; El-Elimat, T.; Kavanaugh, J.; Horswill, A.; Cooks, R.; Cech, N.; Oberlies, N. *J. Nat. Prod.* **2014**, *77*, 1351-1358.

42. Du, L.; Zhu, T.; Liu, H.; Fang, Y.; Zhu, W.; Gu, Q. *J. Nat. Prod.* **2008**, *71*, 1837-1842.

43. Mai, L.; Gueritte, F.; Dumontet, V.; van Tri, M.; Hill, B.; Thoison, O.; Guénard, D.; Sévenet, T. *J. Nat. Prod.* **2001**, *64*, 1162-1168.

44. Alemayehu, G.; Abegaz, B.; Snatzkea, G.; Duddeck, D. *Phytochemistry*. **1993**, *32*, 1273-1277.

45. Eilbert, F.; Anke, H.; Sterner, O. *J. Antibiot.* **2000**, *53*, 1123-1129.

46. Aly, A.; Debbab, A.; Clements, C.; Edrada-Ebel, R.; Orlikova, B.; Diederich, M.; Wray, V.; Lin, W.; Proksch, P. *Biorg. Med. Chem.* **2011**, *19*, 414-421.

47. Ji, N.; Liang, X.; Sun, R.; Miao, F. *RSC Adv.* **2014**, *4*, 7710-7715.

48. Wang, X.; Duggan, B.; Molinski, T. *J. Am. Chem. Soc.* **2015**, *137*, 12343-12351.

49. Sun, H.; Li, X.; Meng, L.; Cui, C.; Gao, S.; Li, C.; Wang, B. *Helv. Chim. Acta* **2013**, *96*, 458-462.

50. Bachmann M.; Blaser, P.; Lüthy J.; Schlatter, C. *J. Environ. Pathol. Toxicol. Oncol.* **1992**, *11*, 113-116.

51. Assante, G.; Camarda, L.; Nasini, G. *Gazz. Chim. Ital.* **1980**, *110*, 629-631.

52. Yosioka, I.; Yamauchi, H.; Norimoto, E.; Eitagawa, I. *Tetrahedron Lett.* **1968**, *34*, 3749-3752.

53. Miyake, Y.; Ito, C.; Kimura, T.; Suzuki, A.; Nishuda, Y.; Itoigama, M. *Food Sci. Technol. Res.* **2014**, *20*, 139-146.

54. Monache, G. D.; Rosa, M. C.; Scurria, R.; Monacelli, B.; Pasqua, G.; Olio, G. D.; Botta, B. *Phytochemistry* **1991**, *30*, 1849–1854.

55. Cameron, D.; Edmonds, J.; Raverty, W. *Aust. J. Chem.* **1976**, *29*, 1535-1548.

56. Bruhn, T.; Schaumloffel, A.; Hemberger, Y.; Bringmann, G. *Chirality* **2013**, *25*, 243-249.

57. Labadie, R. *Pharm. Weekbl.* **1969**, *104*, 257-261.

58. Falk, H.; Schoppel, G. *Monatsh. Chem.* **1992**, *123*, 931-938.

59. Brockmann, H.; Eggers, H. *Eur. J. Inorg. Chem.* **1958**, *91*, 81-100.

60. Pickel, B.; Schaller, A. *Appl. Microbiol. Biotechnol.* **2013**, *97*, 8427-8438.

61. Dewick, P. *Medicinal Natural Products: A Biosynthetic Approach*; John Wiley and Sons: New York, 2009; p 106-107.

62. Keseru G.; Norgradi, M. In *Stud. Nat. Prod. Chem.*; Elsevier Science: 1998; Vol. 20 p 263.

63. Standards, N. C. f. C. L. *Approved Standard M02-A11 and M100-S25. NCCLS, Wayne, PA, USA* **2002**.

64. Assay, A.-K. M. C. P. *American Type Culture Collection, 2011* **Accessed September 21, 2015**.

65. Mosmann, T. *J. Immunol. Methods*. **1983**, *65*, 55-63.

66. Pye, C.; Bertin, M.; Scott Lokey, R.; Gerwick, W.; Linington, R. *Proc. Natl. Acad. Sci. U. S. A.* **2017**, *114*, 5601-5606.

67. Calvo, A. M.; Wilson, R. A.; Bok, J. W.; Keller, N. P. *Microbiol. Mol. Biol. Rev.* **2002**, *66*, 447-459.

68. Bayram, Ö.; Braus, G. H. *FEMS Microbiol. Rev.* **2012**, *36*, 1-24.

69. Bidard, F.; Clave, C.; Saupe, S. J. *G3 Bethesda, Md..* **2013**, *3*, 1015-1020.

70. Schachtschabel, D.; David, A.; Menzel, K. D.; Schimek, C.; Wostemeyer, J.; Boland, W. *ChemBioChem*. **2008**, *9*, 3004-3012.

71. Babij, N. R.; Whiteker, G.T.; Canturk, B.; Choy, N.; Creemer, L.; De Amicis, C. V.; Hewlett, N.; Johnson, P.L.; Knobelsdorf, J.A.; Li, F.; Lorsbach, B.A.; Nugent, B.; Ryan, S.J.; Smith, M.R.; Yang, Q. *Org. Process Res. Dev.* **2016**, *20*, 661-667.

72. White, T. J.; Bruns, T.D.; Lee, S.B.; Taylor, J.W. In *PCR - Protocols and Applications - A Laboratory Manual*; Academic Press: 1990, p 315-322.

73. Balajee, S.A.; Lindsley, M.D.; Iqbal, N.; Ito, J.; Pappa, P.G.; Brandt, M.E. *J. Clin. Microbiol.* **2007**, *45*, 2701-2703.

74. Larena, I.; Salazar, O.; Gonzalez, V.; Julian, M.C.; Rubio, V. *J. Biotechnol.* **1999**, *75*, 187-194.

75. Glass, N.L.; Donaldson, G.C. *Appl. Environ. Microbiol.* **1995**, *61*, 1323-1330.

76. Orbach, M.J.; Porro, E.B.; Yanofsky, C. *Mol. Cell. Biol.* **1986**, *6*, 2452-2461.

77. Serra, R.; Peterson, S.W. *Mycologia* **2007**, *99*, 78-87.

78. Peterson, S.W. *Mycologia* **2008**, *100*, 205-226.

79. Thomson, R. In *Naturally Occurring Quinones* Academic Press, 2012, p 445-447.

80. Sheldrick, G.M. Bruker/Siemens Area Detector Absorption Correction Program, Bruker AXS, Madison, WI, 1998

81. Sheldrick, G. M. *Acta Cryst. C*, **2015**, *71*, 3-8.

82. Frisch, M. J.; Trucks, G. W.; Schlegel, H. B.; Scuseria, G. E.; Robb, M. A.; Cheeseman, J. R.; Scalmani, G.; Barone, V.; Mennucci, B.; Petersson, G. A.; Nakatsuji, H.; Caricato, M.; Li, X.; Hratchian, H. P.; Izmaylov, A. F.; Bloino, J.; Zheng, G.; Sonnenberg, J. L.; Hada, M.; Ehara, M.; Toyota, K.; Fukuda, R.; Hasegawa, J.; Ishida, M.; Nakajima, T.; Honda, Y.; Kitao, O.; Nakai, H.; Vreven, T.; Montgomery Jr., J. A.; Peralta, J. E.; Ogliaro, F.; Bearpark, M. J.; Heyd, J.; Brothers, E. N.; Kudin, K. N.; Staroverov, V. N.; Kobayashi, R.; Normand, J.; Raghavachari, K.; Rendell, A. P.; Burant, J. C.; Iyengar, S. S.; Tomasi, J.; Cossi, M.; Rega, N.; Millam, N. J.; Klene, M.;

Knox, J. E.; Cross, J. B.; Bakken, V.; Adamo, C.; Jaramillo, J.; Gomperts, R.; Stratmann, R. E.; Yazyev, O.; Austin, A. J.; Cammi, R.; Pomelli, C.; Ochterski, J. W.; Martin, R. L.; Morokuma, K.; Zakrzewski, V. G.; Voth, G. A.; Salvador, P.; Dannenberg, J. J.; Dapprich, S.; Daniels, A. D.; Farkas, Ö.; Foresman, J. B.; Ortiz, J. V.; Cioslowski, J.; Fox, D. J.; Gaussian, Inc.: Wallingford, CT, USA, 2009.

83. Willoughby, P. H.; Jansma, M. J.; Hoye, T. R. *Nat. Protocols* **2014**, *9*, 643-660.

84. O'Boyle, N. M.; Tenderholt, A. L.; Langner, K. M. *J. Comput. Chem.* **2008**, *29*, 839-845b.

Chapter 6 – General Conclusion

Donovon A. Adpressa

6.1 General Conclusion

Advances in genome sequencing recently enabled an unprecedented look into the chemical potential of microorganisms.[1,2] With the advent of the genomic era came the understanding that microbes harbored a far greater set of secondary metabolite gene clusters than previously expected or observed in the laboratory. The genome of *Streptomyces coelicolor* sequenced in 2002 revealed genes encoding for more than 20 natural products, where only half as many were known or expected.[3] Exploration of fungal genomes in the decades following have demonstrated that fungi possess at least as much genetic potential as bacteria, if not more (Chapter 1, Figure 1.2).[4] Recent reviews have indicated that the prospective for the future of natural products research remains strong, with the number of unique compound motifs disclosed in the literature remaining steady over the last few decades.[5] Furthermore, the recent successes of companies focused on the discovery of natural product drugs, such as Warp Drive Bio, Lodo Theraputics, Mycosynthetics, LifeMine, and Hexagon Bio, indicate a renewed interest in the development of natural products for treatment of disease.

A component of the continued success in natural products discovery has been the persistent focus on activation strategies for the production of silent metabolites.[6-8] This area has been the dominant focus of all of the research presented within this dissertation. Approaches such as subjecting microbes to oxidative stress or nutrient challenges, as was the case with *Aspergillus terreus*, remain a valuable method to elicit the production of genetcially encoded small molecules. However, a growing understanding of the various mechanisms by which fungi control the production of their secondary metabolites, as well

as an understaning of the function of these molecules within the biological context of fungal development, will enable a more comprehensive view on the fungal metabolome. Techniques focused on activation of specific pathways, such as the epigenetic manipulation, have yielded dozens of novel, and often bioactive, secondary metabolites from fungi. The activation of approximately two thirds of the secondary metabolome of *Fusarium graminearum* by deletion of the histone lysine methyltransferase kmt6, paired with isolation of previously cryptic tricinterpenes, exemplifies this approach.[9] Furthermore, the application of genetic analysis and transcriptomic techniques alongside biosynthetic dogma allowed for the de-orphanization of two biosynthetic gene clusters in Chapter Two. The connection of gene products to their biogenic origins not only inform a deeper understanding of the chemical mechanisms responsible for the formation of these complex products, but enable future studies on their biological and ecological function.

The work in *Chalara* sp. further illustrates the success of targeting regulatory pathways for the discovery of novel scaffolds. The adenosine-coupled xanthones described in Chapter Three were produced under HDAC inhibition by both vorinostat and sodium butyrate. The use of small molecule inhibitors to effect the production of otherwise silent secondary metabolites have and continue to be a broadly accessible tool for natural productdiscovery.[10,11] Furthermore, the intriguing biotransformation of vorinostat into chalanilines A and B represent one of many examples of the diversification of natural product scaffolds into 'unnatural' natural products with unforeseen bioactive motifs.[12,13]

In addition to techniques focused on the activation of silent biosynthetic pathways, the continued pace of novel discovery in the field of natural products can be attributed to the

development of techniques focused on the rapid detection of novel or differentially produced metabolites.[14] Combination of metabolomics approaches with techniques such as heterologous expression of gene clusters, gene activation strategies, or bioassay activity data have yielded new chemical diversity from natural sources, particularly in the area of fungal natural products discovery.[15-19] To this end, much of the work presented in this dissertation, particularly Chapters Two, Three, and Four, focused on the application of LCMS metabolomics for the rapid prioritization of isolation efforts. The isolation of novel xanthones from *Chalara* sp. in Chapter Three, as well as novel terpenes from *F. graminearum* in Chapter Two*,* was enabled by the use of relative expression analyses which rapidly highlighted the difference in production of these metabolites between treatment conditions. Furthermore, LCMS metabolomics coupled with bioassay data holds significant promise in the rapid isolation of not just newly produced, but bioactive compounds as well.[20,21] Such was the case with the rapid identification of know fungal metabolite terrein as the cytotoxic component produced in potato dextrose broth media described in Chapter Four.

The further development of techniques such as those presented here will continue to push the discovery of new chemical diversity from fungi in the future. Continued discovery of novel structural motifs from fungi will serve to inform our understanding of the ecological purpose these chemical messengers serve in nature, as well as provide humanity with new tools to combat antimicrobial resistance, the growing threat of cancer, agriculture pestilence, and more.

6.2 References

1. Grigoriev, I. V.; Nikitin, R.; Haridas, S.; Kuo, A.; Ohm, R.; Otillar, R.; Riley, R.; Salamov, A.; Zhao, X.; Korzeniewski, F. *Nucleic Acids Res.* **2013**, gkt1183.

2. Land, M.; Hauser, L.; Jun, S.-R.; Nookaew, I.; Leuze, M. R.; Ahn, T.-H.; Karpinets, T.; Lund, O.; Kora, G.; Wassenaar, T.; Poudel, S.; Ussery, D. W. *Funct. Ingr. Genomics* **2015**, *15*, 141.

3. Bentley, S. D.; Chater, K. F.; Cerdeno-Tarraga, A. M.; Challis, G. L.; Thomson, N. R.; James, K. D.; Harris, D. E.; Quail, M. A.; Kieser, H.; Harper, D.; Bateman, A.; Brown, S.; Chandra, G.; Chen, C. W.; Collins, M.; Cronin, A.; Fraser, A.; Goble, A.; Hidalgo, J.; Hornsby, T.; Howarth, S.; Huang, C. H.; Kieser, T.; Larke, L.; Murphy, L.; Oliver, K.; O'Neil, S.; Rabbinowitsch, E.; Rajandream, M. A.; Rutherford, K.; Rutter, S.; Seeger, K.; Saunders, D.; Sharp, S.; Squares, R.; Squares, S.; Taylor, K.; Warren, T.; Wietzorrek, A.; Woodward, J.; Barrell, B. G.; Parkhill, J.; Hopwood, D. A. *Nature* **2002**, *417*, 141.

4. Alberti, F.; Foster, G. D.; Bailey, A. M. *Appl. Microbiol. Biotechnol.* **2017**, *101*, 493.

5. Pye, C. R.; Bertin, M. J.; Lokey, R. S.; Gerwick, W. H.; Linington, R. G. *Proc. Natl. Acad. Sci. U. S. A.* **2017**, *114*, 5601.

6. Ochi, K.; Hosaka, T. *Appl. Microbiol. Biotechnol.* **2013**, *97*, 87.

7. Lim, F. Y.; Sanchez, J. F.; Wang, C. C. C.; Keller, N. P. *Methods Enzymol.* **2012**, *517*, 303.

8. Brakhage, A. A.; Schroeckh, V. *Fungal Genet. Biol.* **2011**, *48*, 15.

9. Connolly, L. R.; Smith, K. M.; Freitag, M. *PLoS Genet.* **2013**, *9*, e1003916.

10. Pettit, R. K. *Microb. Biotechnol.* **2011**, *4*, 471.

11. Rutledge, P. J.; Challis, G. L. *Nat. Rev. Microbiol.* **2015**, *13*, 509.

12. Boecker, S.; Zobel, S.; Meyer, V.; Süssmuth, R. D. *Fungal Genet. Biol.* **2016**, *89*, 89.

13. Leitão, A. L.; Enguita, F. J. *Microbiol. Res.* **2014**, *169*, 652.

14. Kurita, K. L.; Glassey, E.; Linington, R. G. *Proc. Natl. Acad. Sci. U.S.A.* **2015**, *112*, 11999.

15. Hautbergue, T.; Jamin, E. L.; Debrauwer, L.; Puel, O.; Oswald, I. P. *Nat. Prod. Rep.* **2018**, *35*, 147.

16. Covington, B. C.; McLean, J. A.; Bachmann, B. O. *Nat. Prod. Rep.* **2017**, *34*, 6.

17. Barkal, L. J.; Theberge, A. B.; Guo, C. J.; Spraker, J.; Rappert, L.; Berthier, J.; Brakke, K. A.; Wang, C. C.; Beebe, D. J.; Keller, N. P.; Berthier, E. *Nat. Commun.* **2016**, *7*, 10610.

18. Albright, J. C.; Henke, M. T.; Soukup, A. A.; McClure, R. A.; Thomson, R. J.; Keller, N. P.; Kelleher, N. L. *ACS Chem. Biol.* **2015**, *10*, 1535.

19. Hoffmann, T.; Krug, D.; Hüttel, S.; Müller, R. *Anal. Chem.* **2014**, *86*, 10780.

20. Tawfike, A. F.; Tate, R.; Abbott, G.; Young, L.; Viegelmann, C.; Schumacher, M.; Diederich, M.; Edrada‑Ebel, R. *Chem. Biodivers.* **2017**, *14*, e1700040.

21. Kellogg, J. J.; Todd, D. A.; Egan, J. M.; Raja, H. A.; Oberlies, N. H.; Kvalheim, O. M.; Cech, N. B. *J. Nat. Prod.* **2016**, *79*, 376.

Appendix A – Supplementary Material for Chapter 2
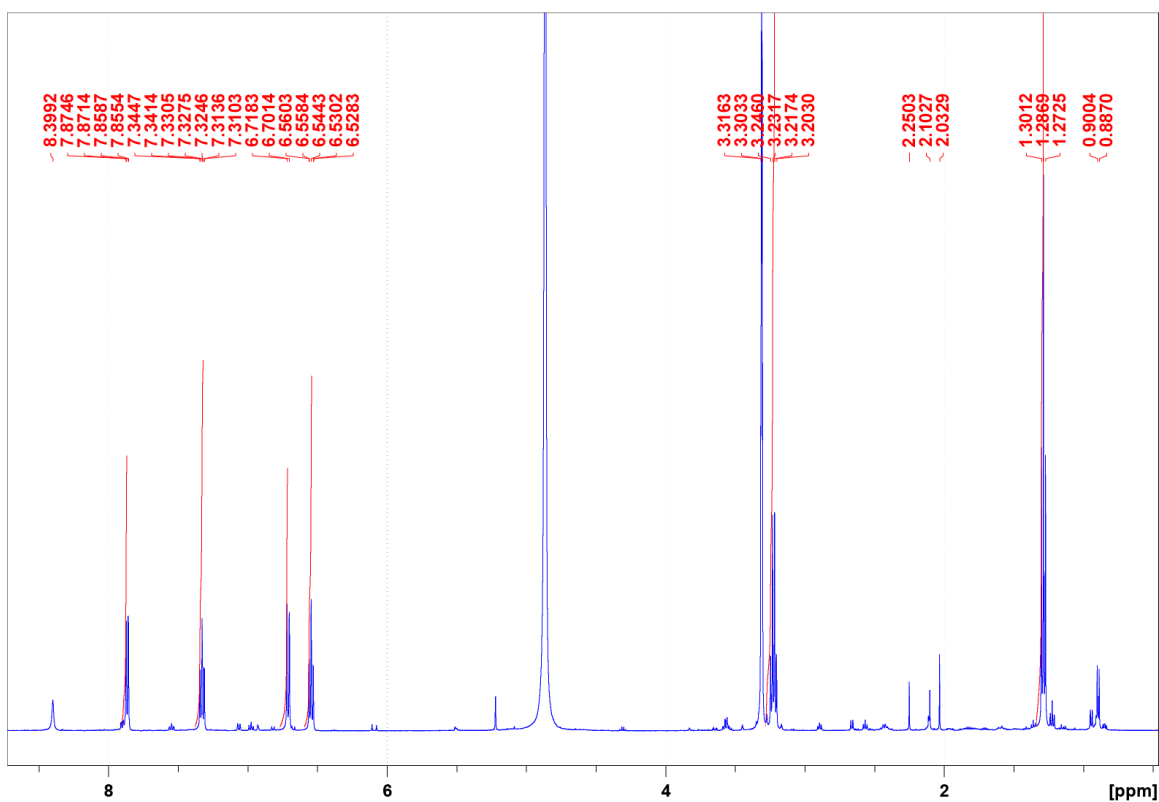
Figure A1. ^{1}H NMR spectrum of *N*-ethylanthranilic acid from *F. graminearum Δkmt6* aqcuired at 500 MHz in d$_4$-methanol.
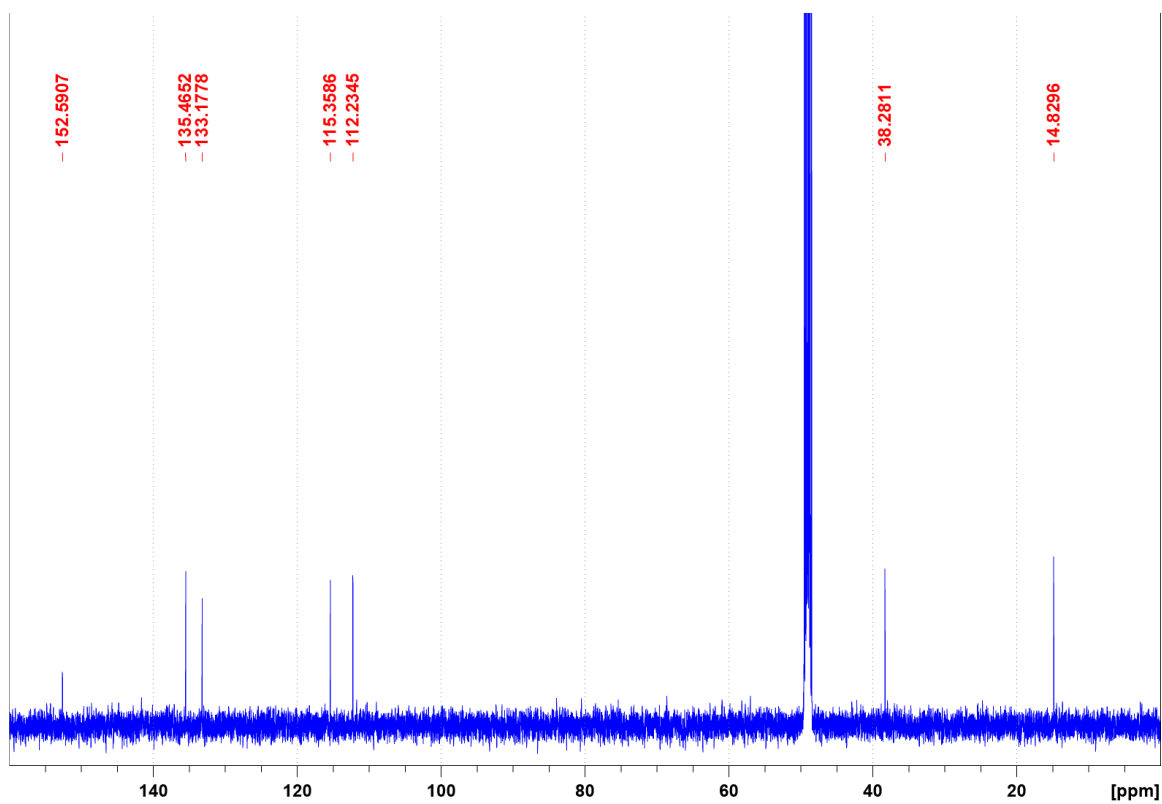
Figure A2. ^{13}C NMR spectrum of *N*-ethylanthranilic acid at 125 MHz in d$_4$-methanol.
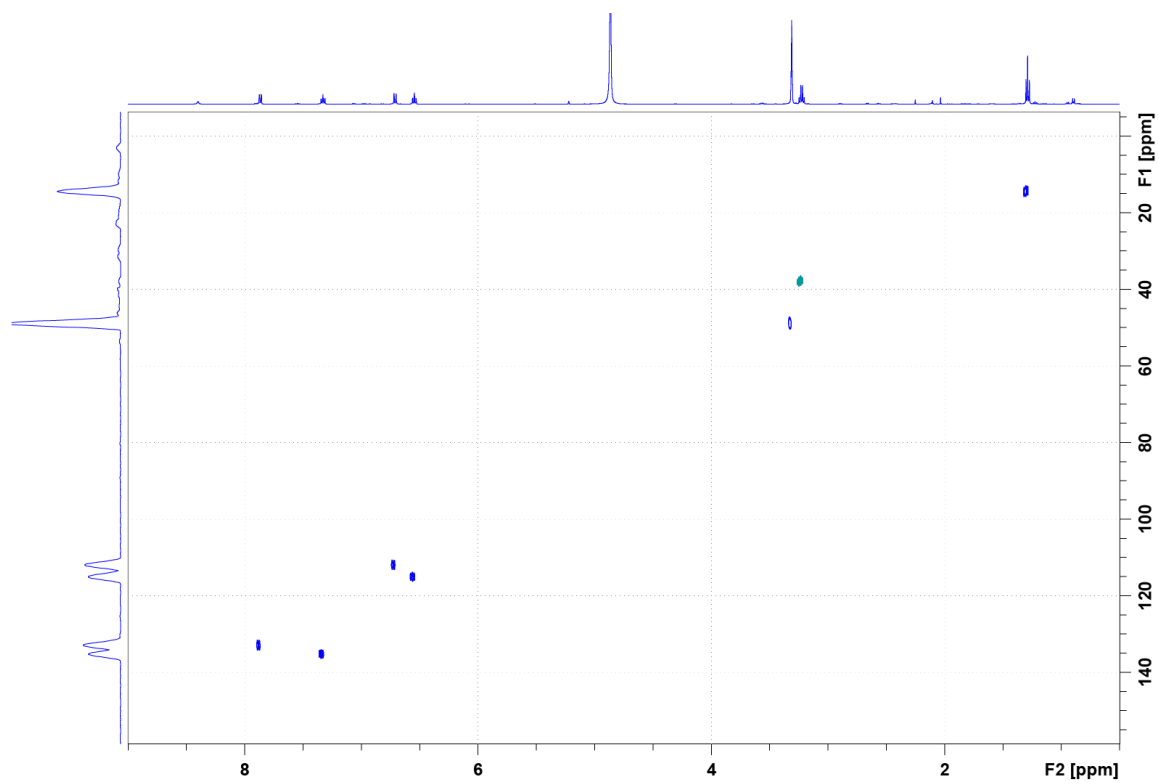
Figure A3. HSQC spectrum of *N*-ethylanthranilic acid in d₄-methanol.
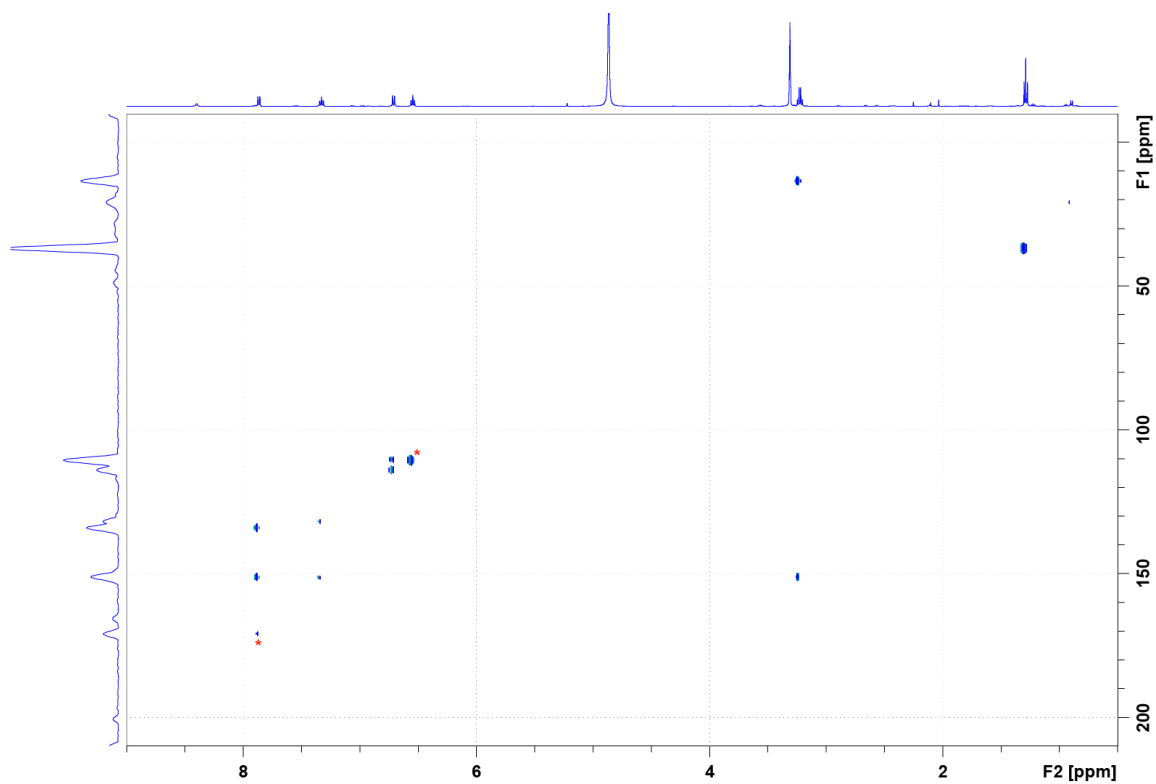
Figure A4. HMBC spectrum of *N*-ethylanthranilic acid in d₄-methanol. * indicate carbon signals assigned from HMBC correlations no apparent in the ¹³C spectrum.
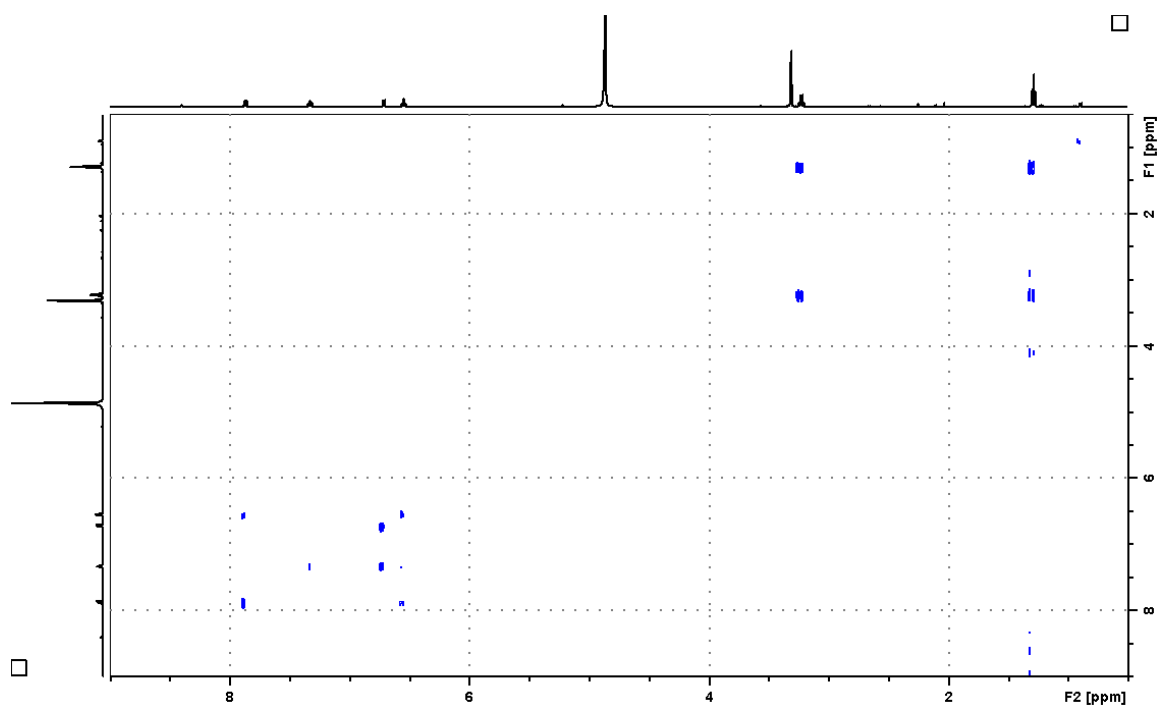
Figure A5. COSY spectrum of *N*-ethylanthranilic acid in d₄-methanol.
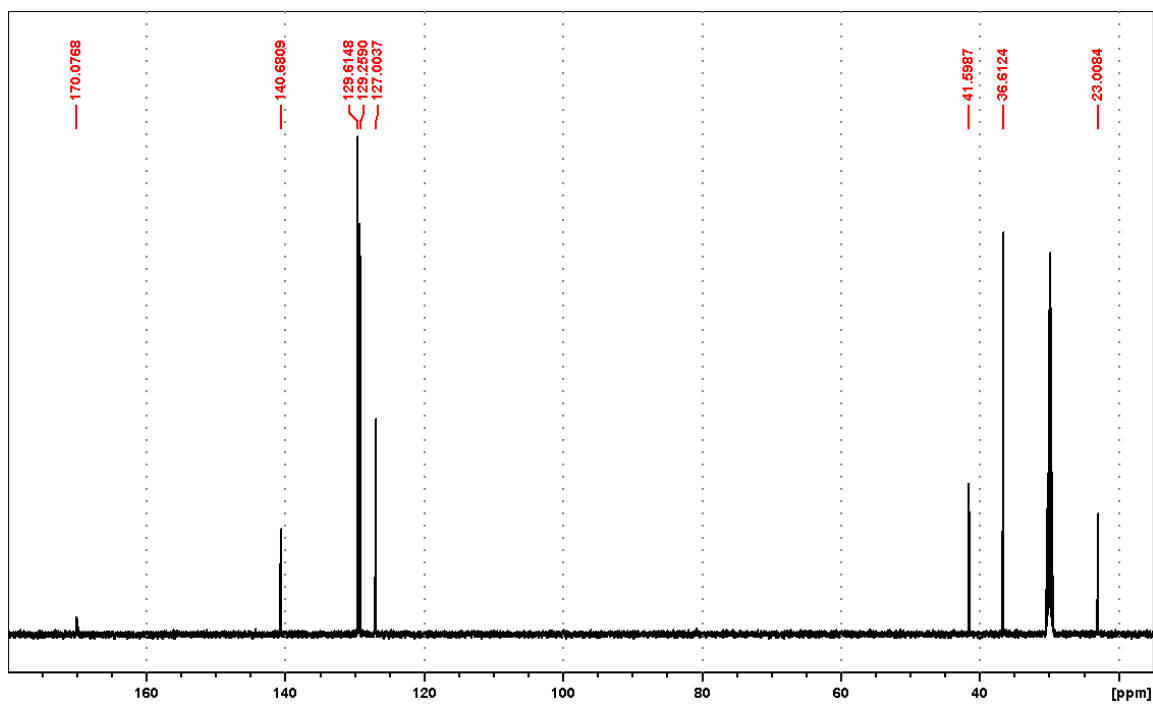
Figure A6. ^{1}H spectrum of phenethylacetamide in d$_6$-acetone at 500 MHz.
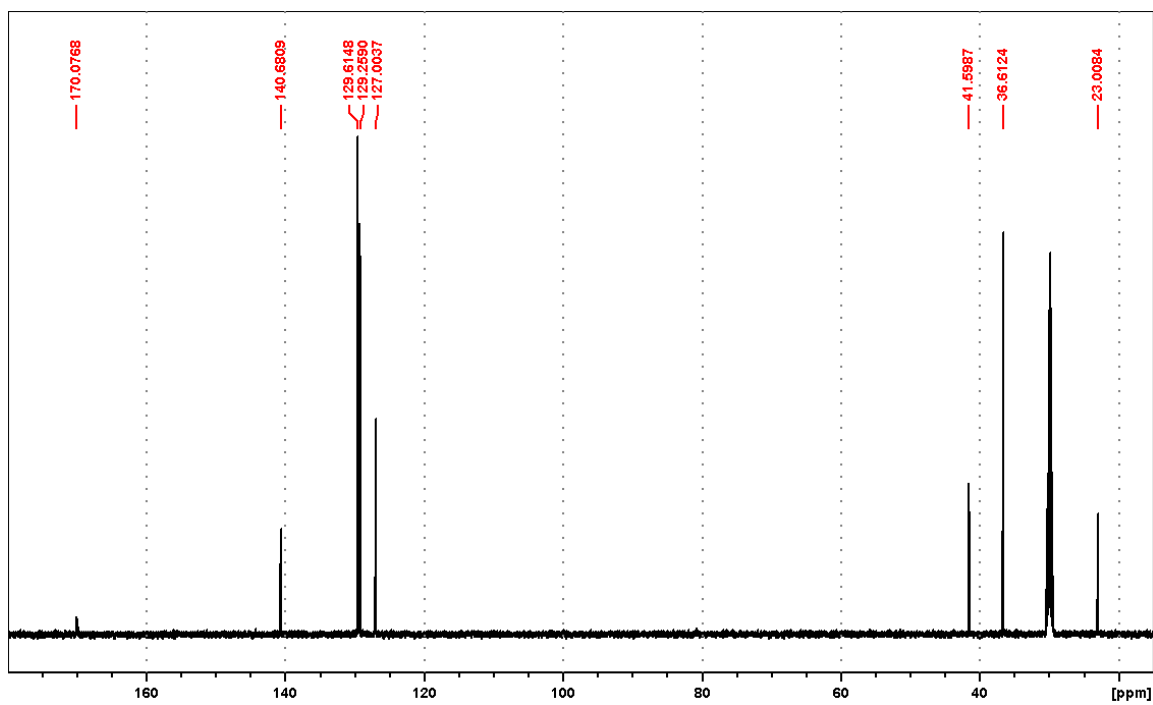
Figure A7. ^{13}C spectrum of phenethylacetamide at 125 MHz in d$_6$-acetone.
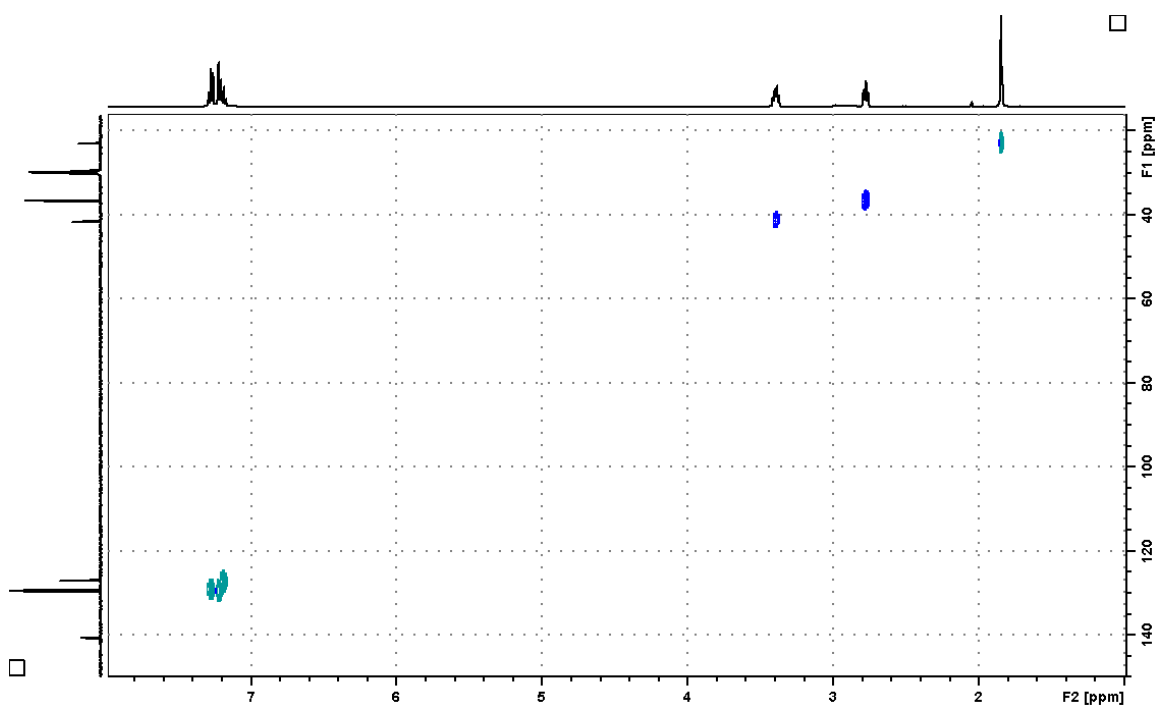
Figure A8. Multiplicity-edited HSQC of phenethylacetamide in d$_6$-acetone.
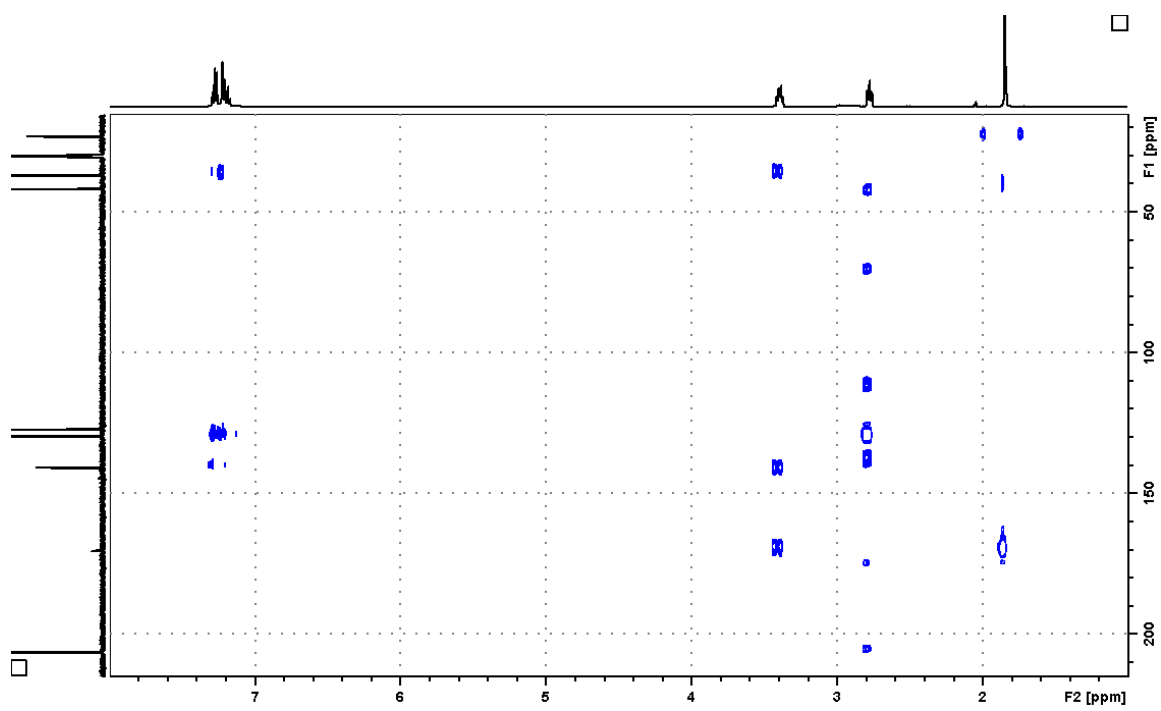
Figure A9. HMBC of phenethylacetamide in d$_6$-acetone.
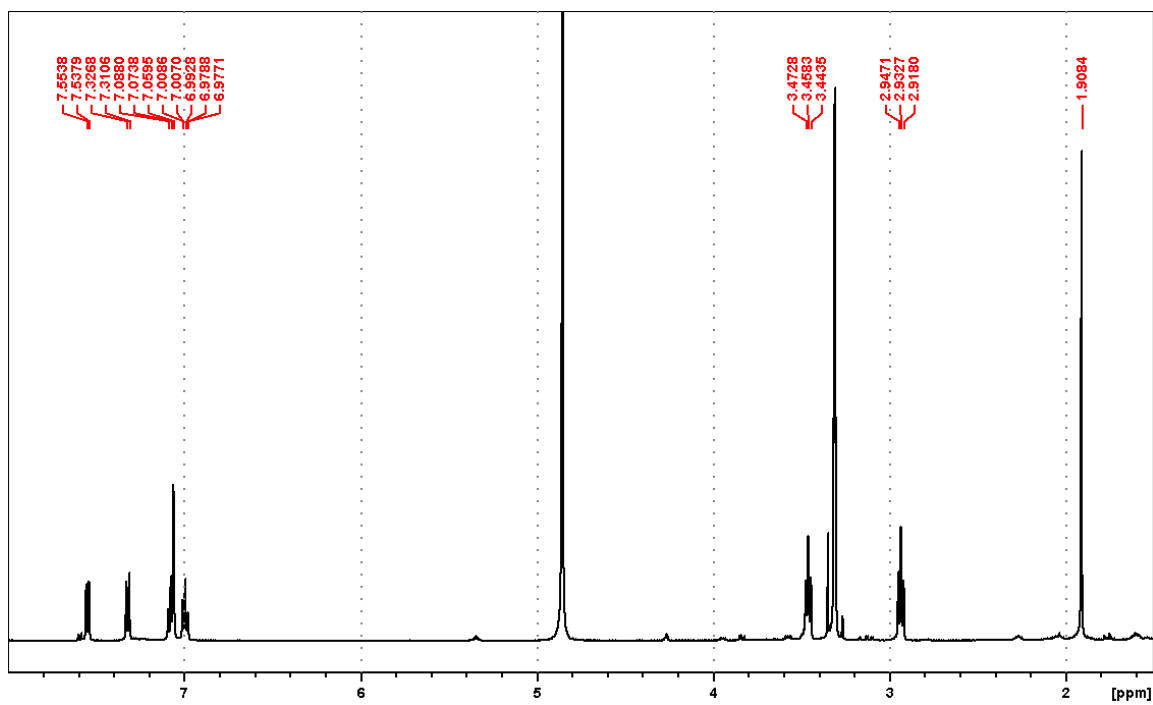
Figure A10. ^{1}H spectrum of *N*-acetyltryptamine in d$_4$-methanol at 500 MHz.
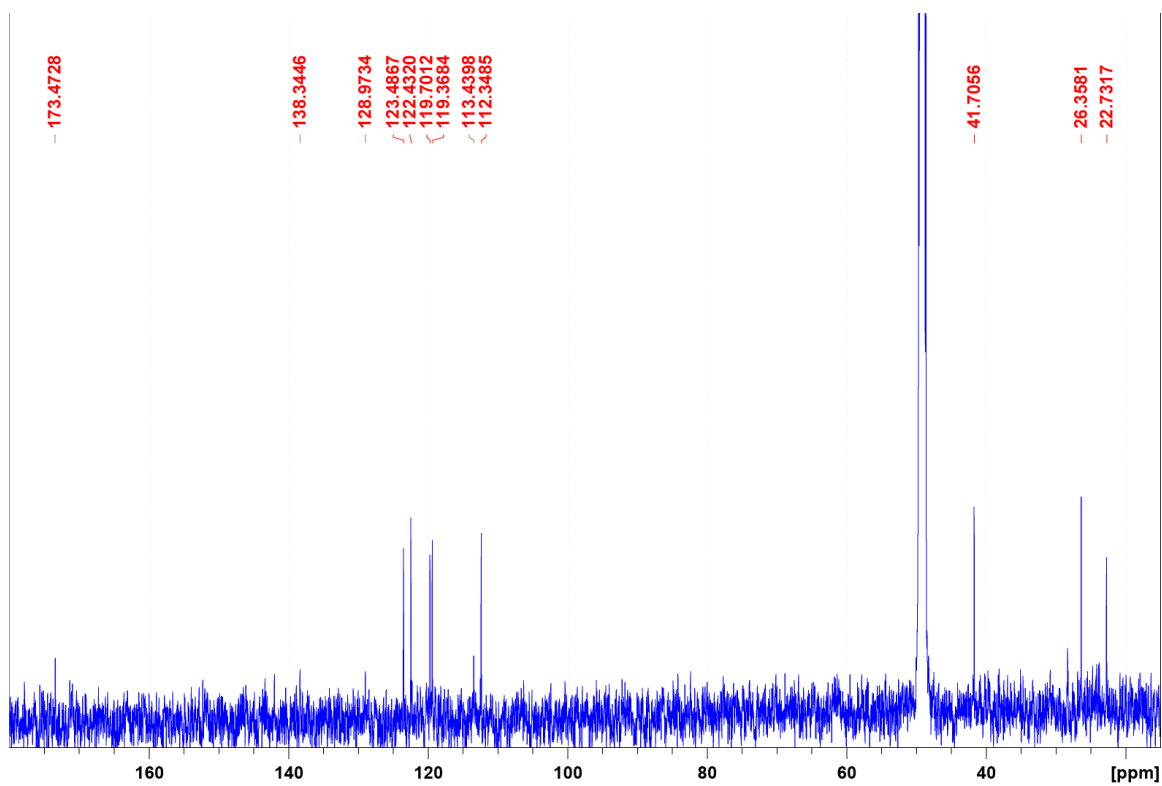
Figure A11. ^{13}C spectrum of *N*-acetyltryptamine at 125 MHz in d$_4$-methanol.
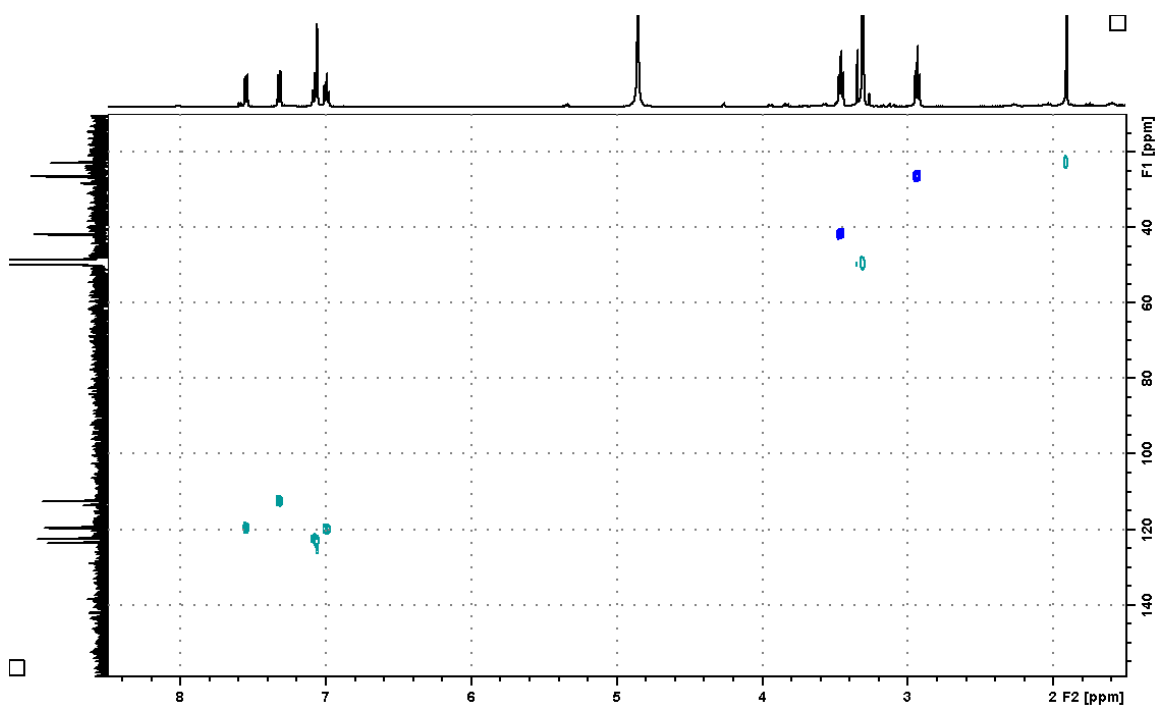
Figure A12. Multiplicity-edited HSQC spectrum of *N*-acetyltryptamine in d₄-methanol.
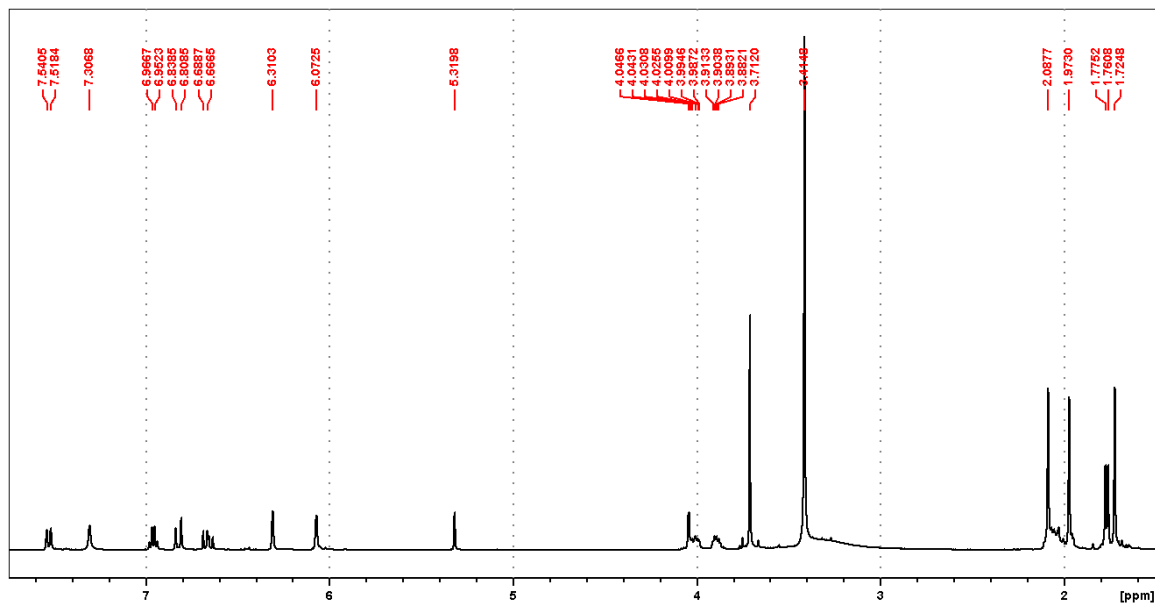
Figure A13. ^{1}H spectrum of fusarin C in CD$_2$Cl$_2$ at 500 MHz.
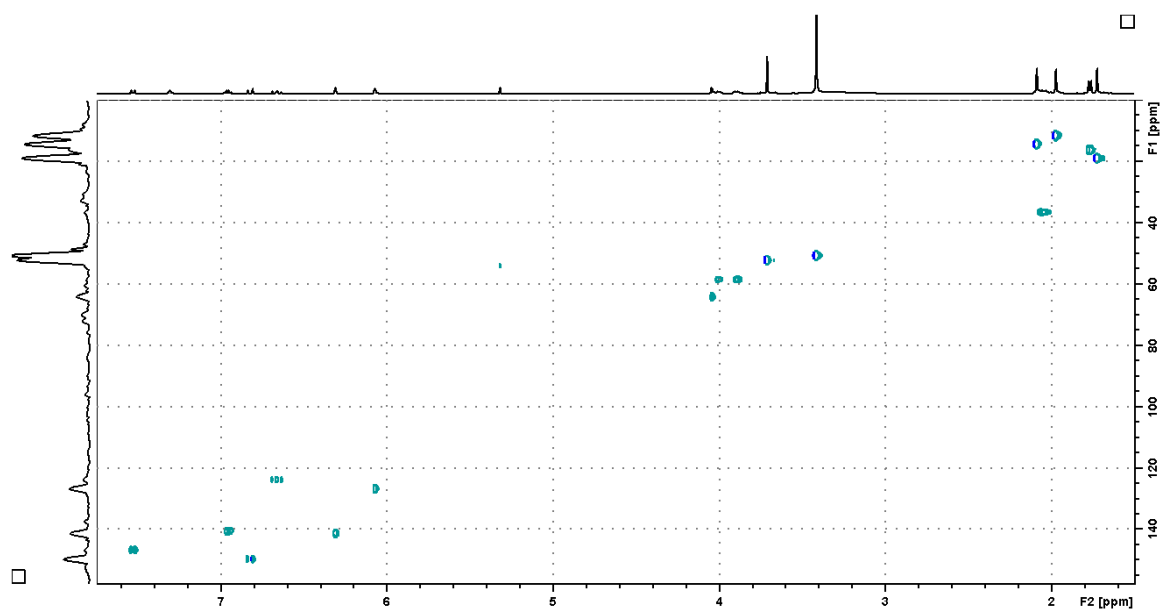
Figure A14. HSQC spectrum of fusarin C in CD_2Cl_2 at 500 MHz.
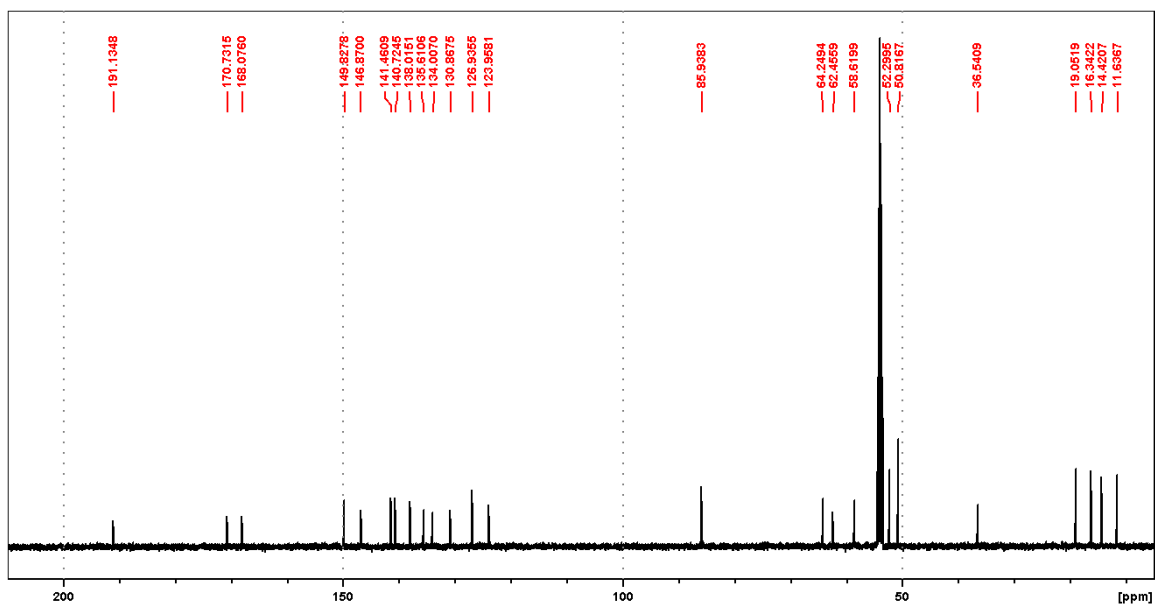
Figure A15. ^{13}C NMR spectrum of fusarin C in CD$_2$Cl$_2$ at 125 MHz.
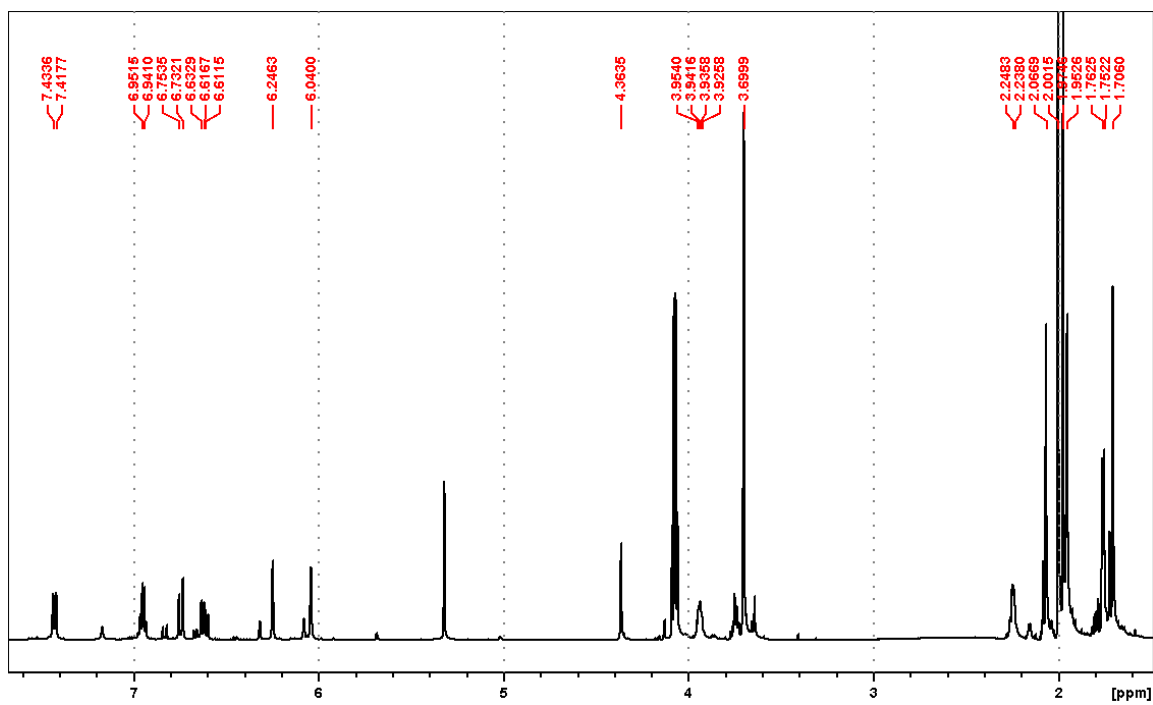
Figure A16. ^{1}H NMR of fusarin D in CD_2Cl_2 at 700 MHz.
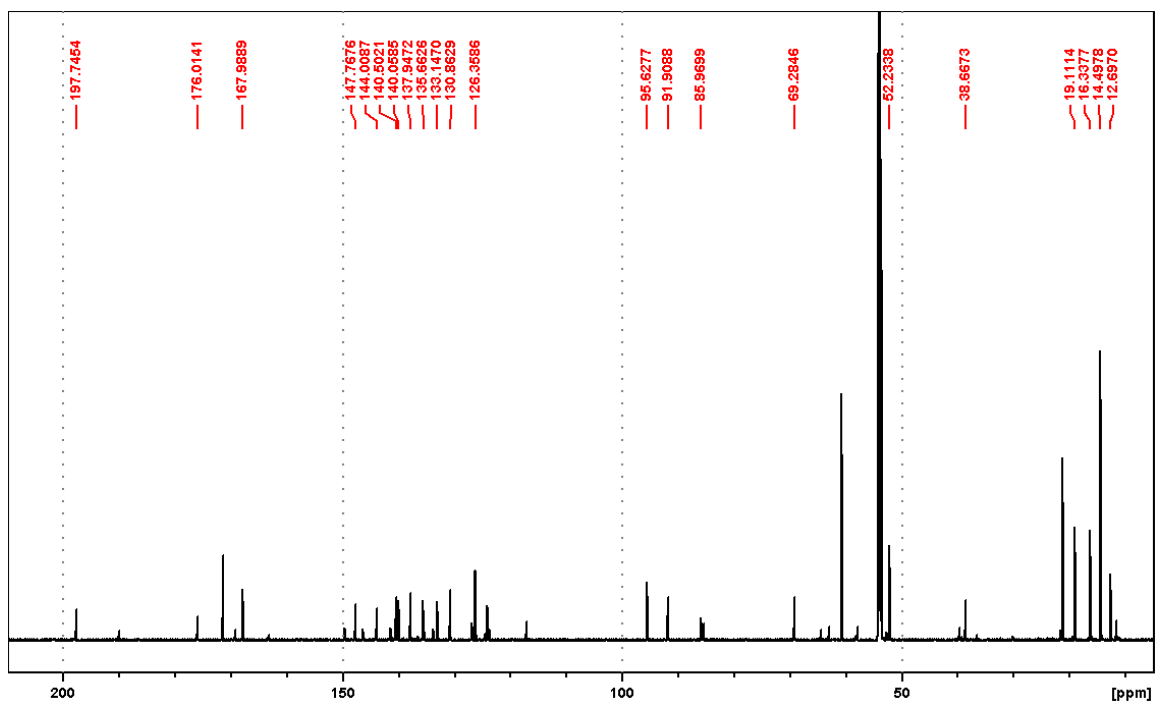
Figure A17. ^{13}C NMR of fusarin D in CD$_2$Cl$_2$ at 176 MHz.
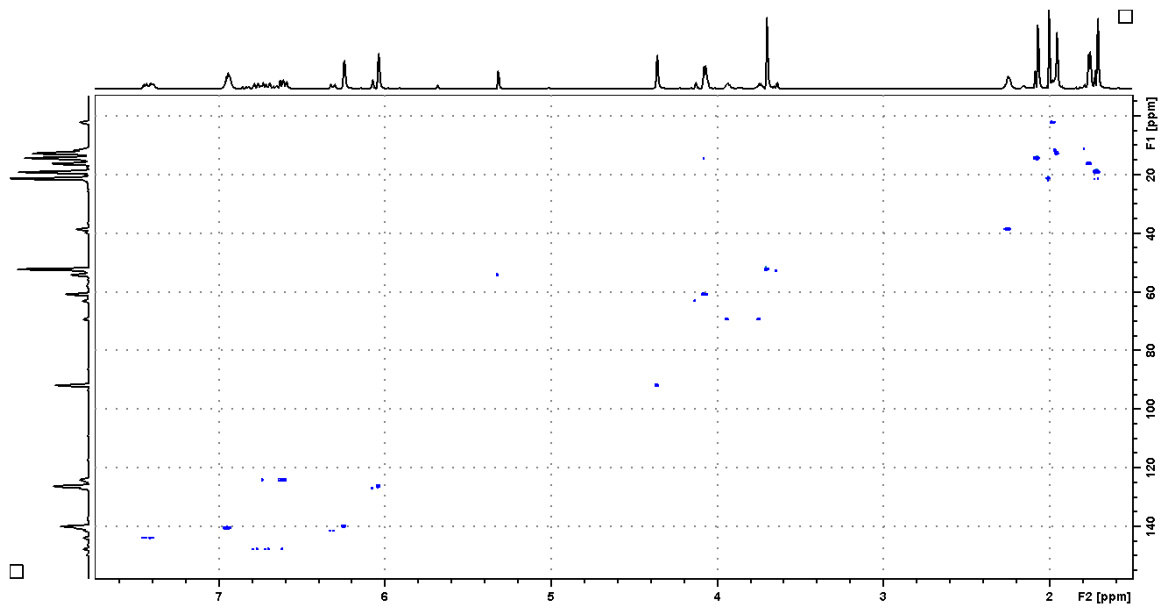
Figure A18. HSQC of fusarin D in CD$_2$Cl$_2$.
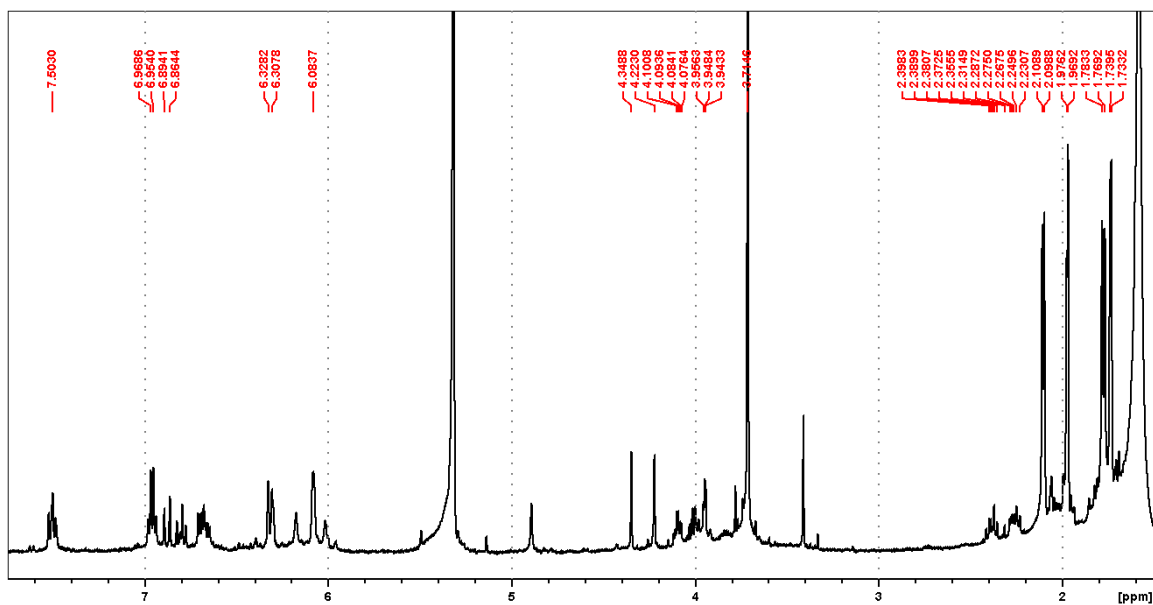
Figure A19. ^{1}H NMR of fusarin A at 500 MHz in CD_2Cl_2.

Figure A20. HSQC of fusarin A in CDCl$_2$.
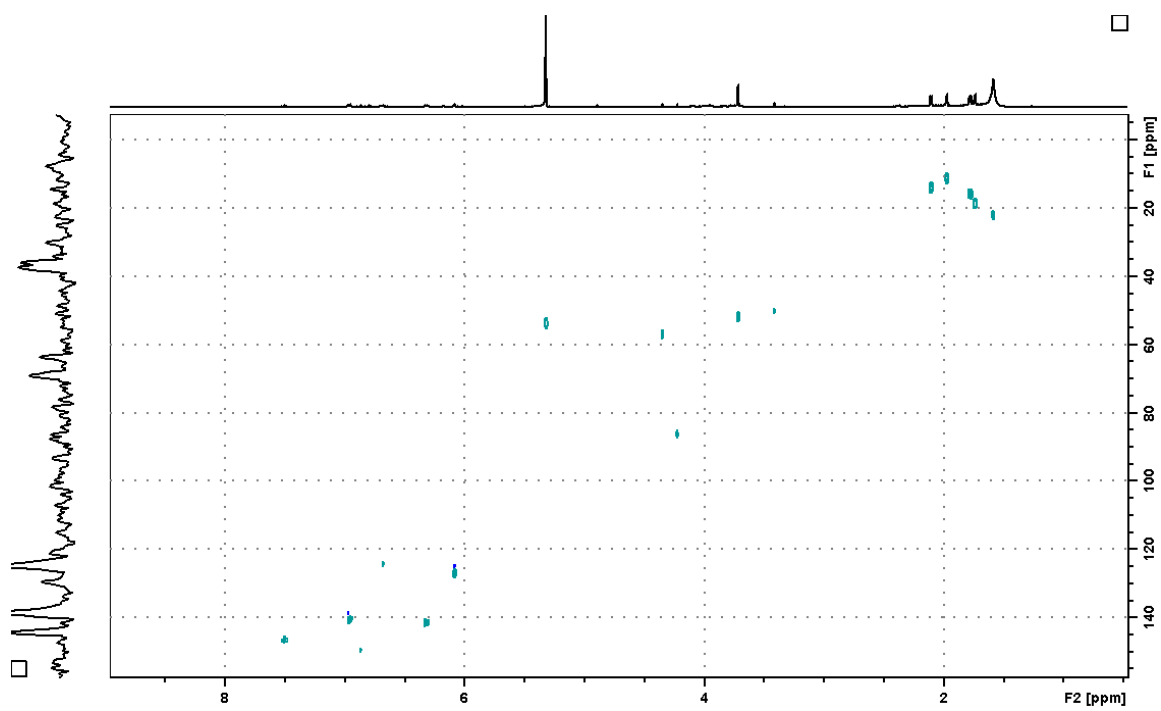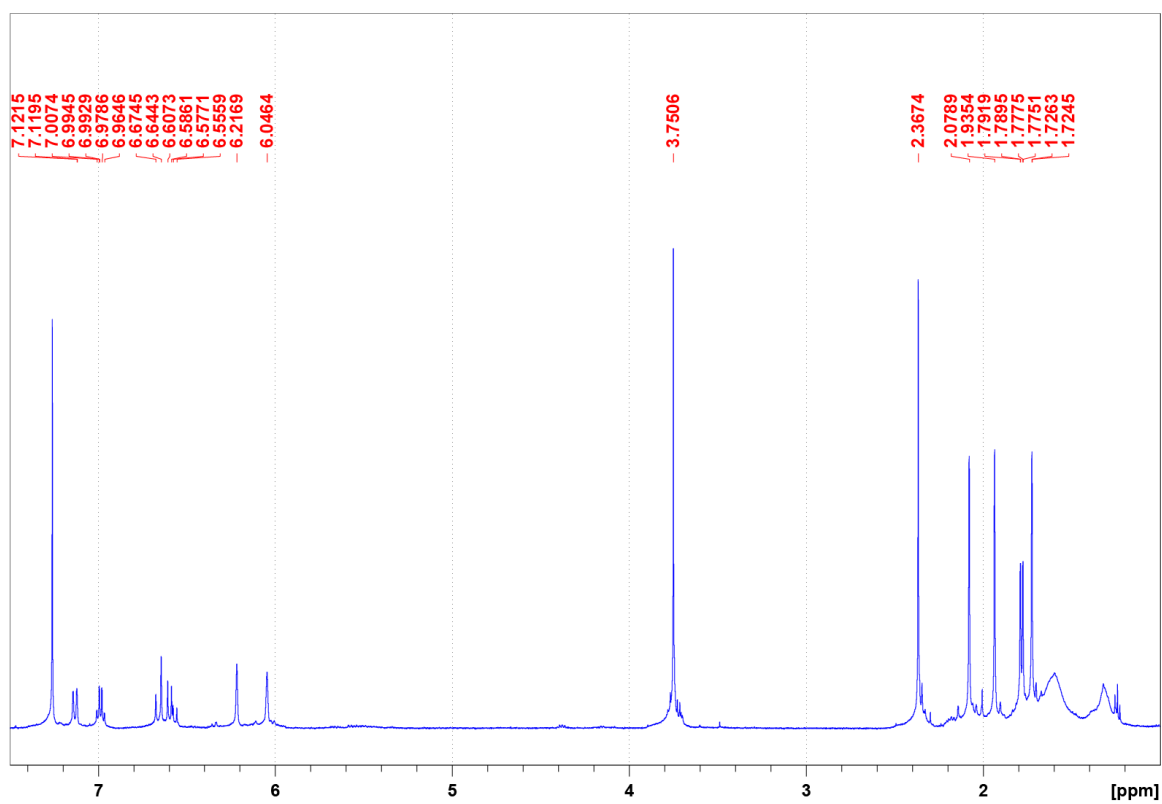
Figure A21. ^{1}H NMR spectrum of protofusarin at 500 MHz in CDCl$_3$.
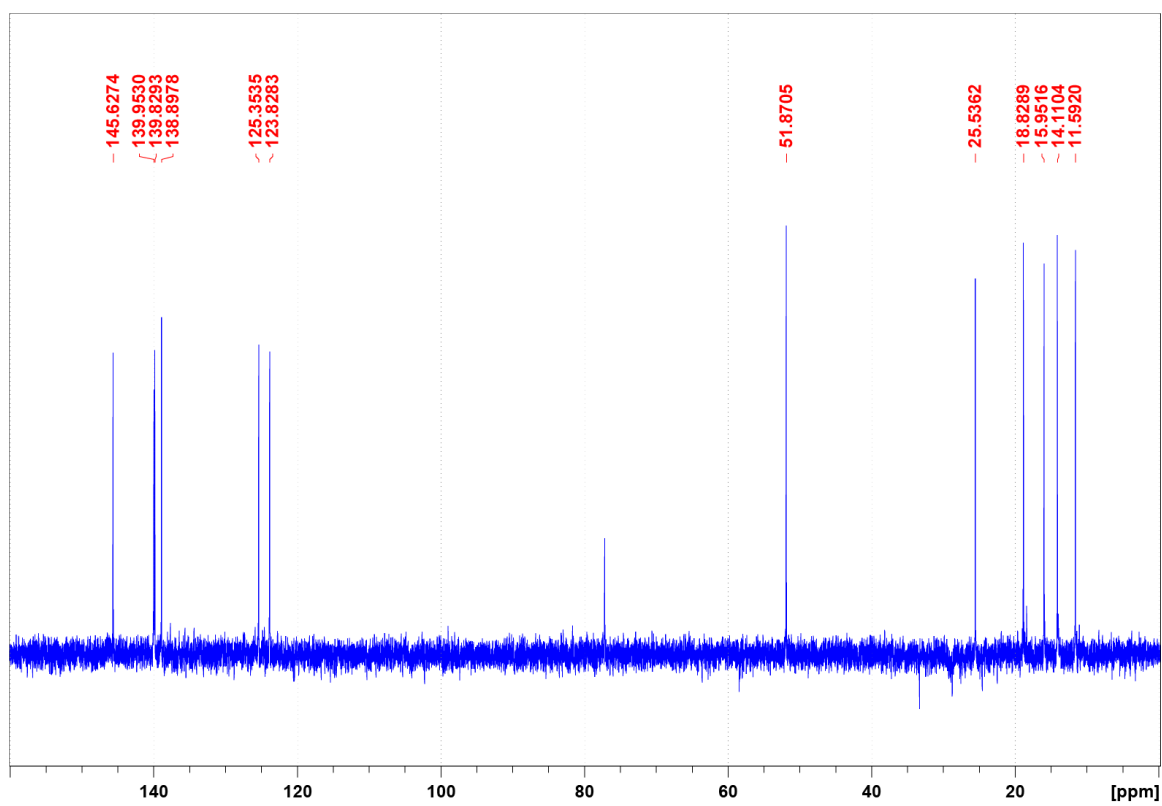
Figure A22. DEPT135 ^{13}C NMR spectrum of protofusarin at 125 MHz in CDCl$_3$.
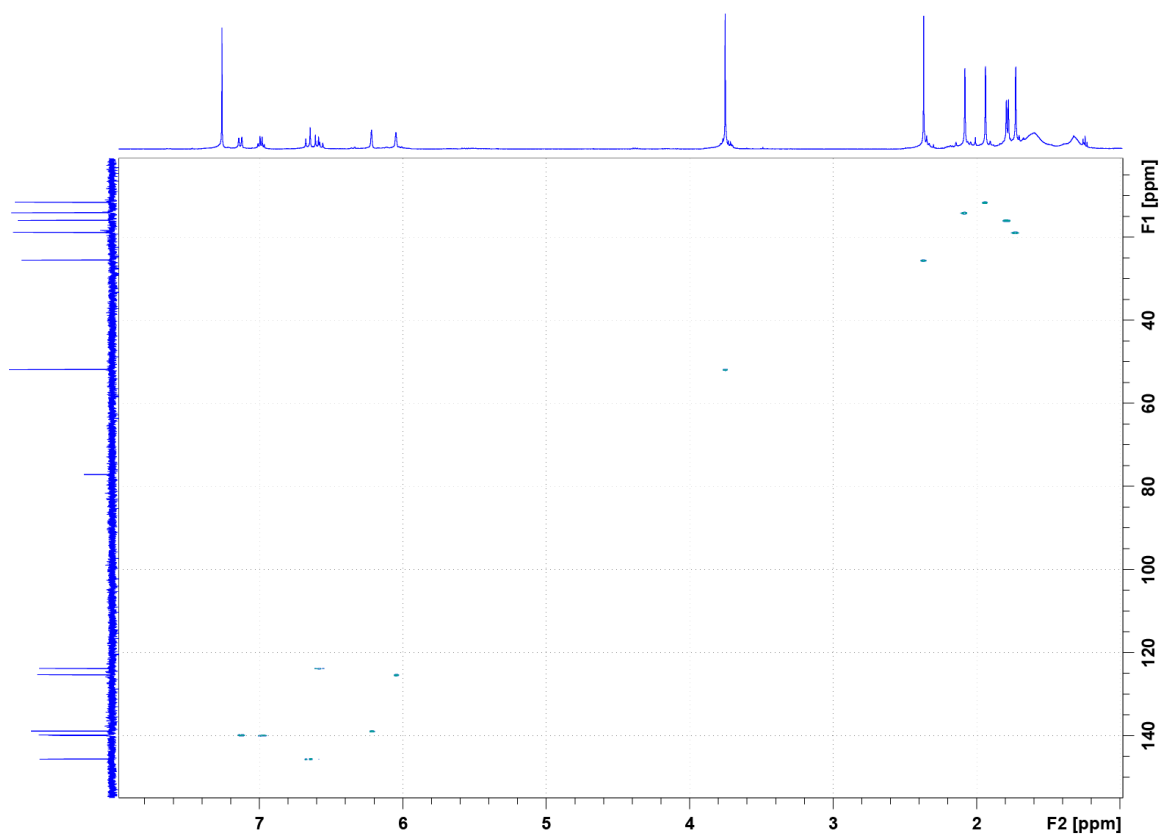
Figure A23. HSQC spectrum of protofusarin in CDCl$_3$.
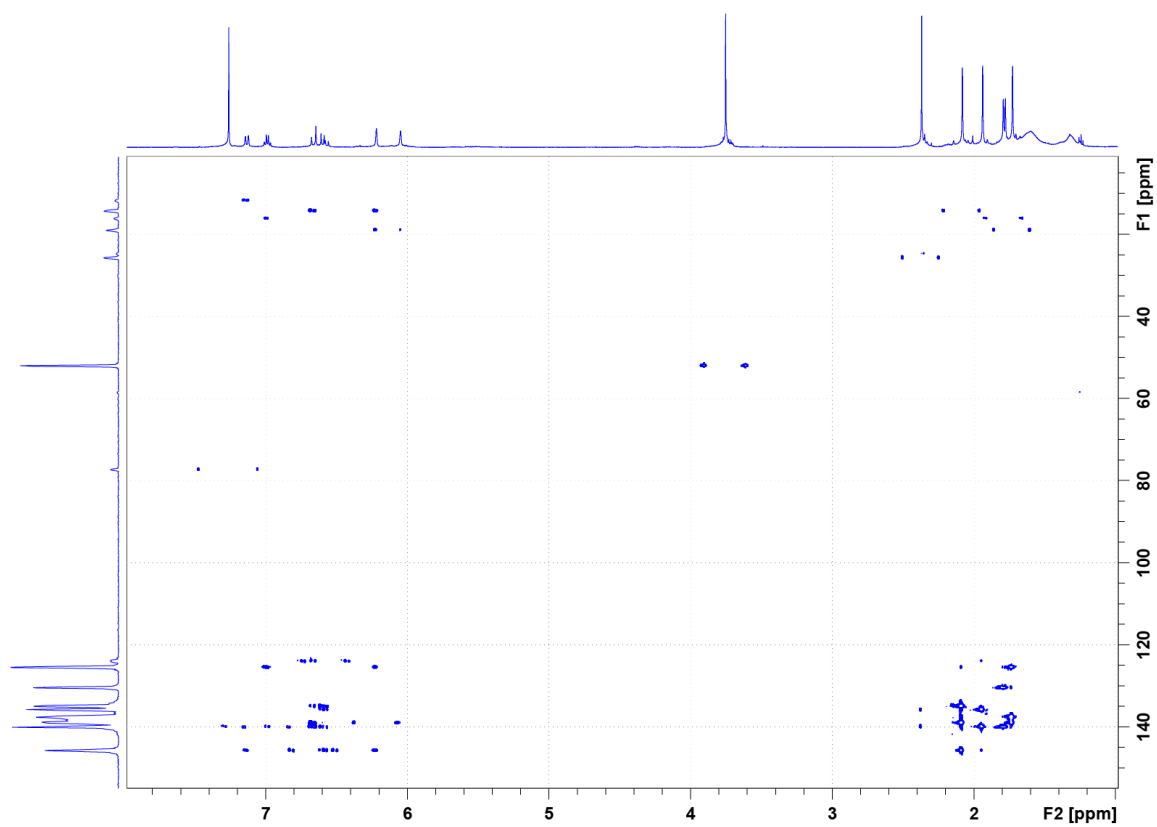
Figure A24. HMBC of protofusarin in CDCl$_3$.
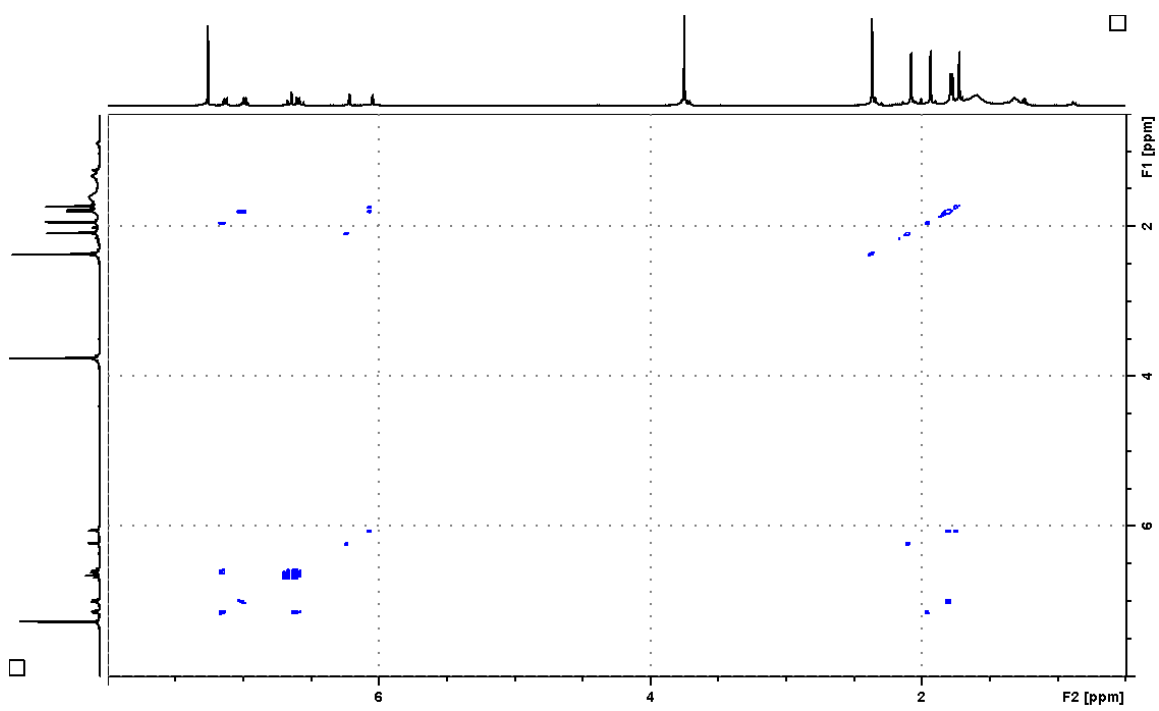
Figure A25. COSY spectrum of protofusarin in CDCl₃.
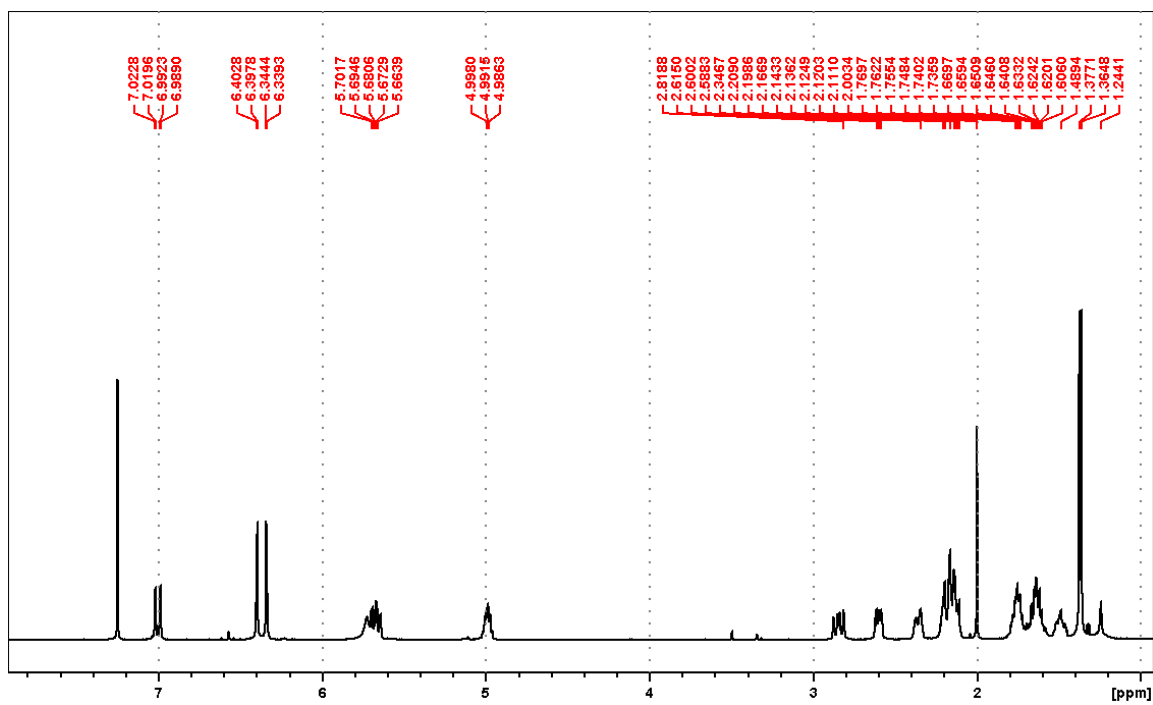
Figure A26. ^{1}H spectrum of zearalenone in CDCl$_3$ at 500 MHz.
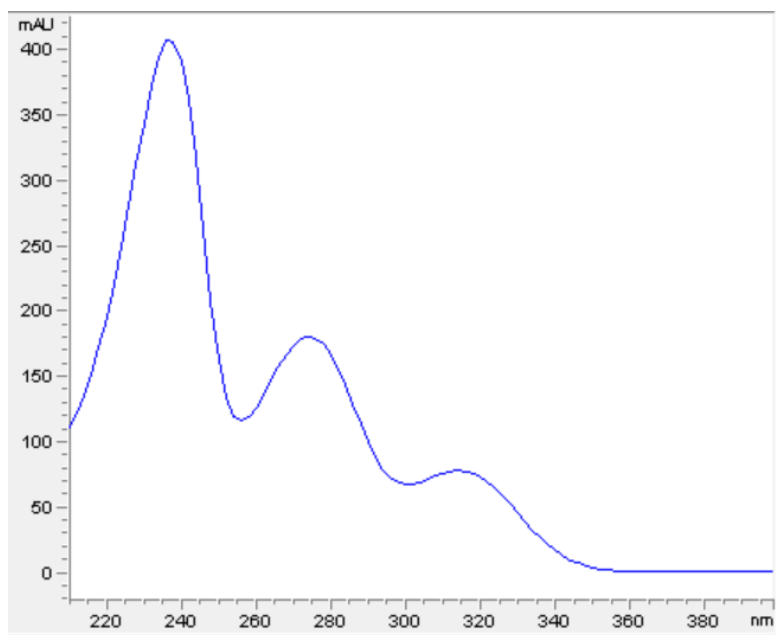
Figure A27. UV Spectrum of zearalenone
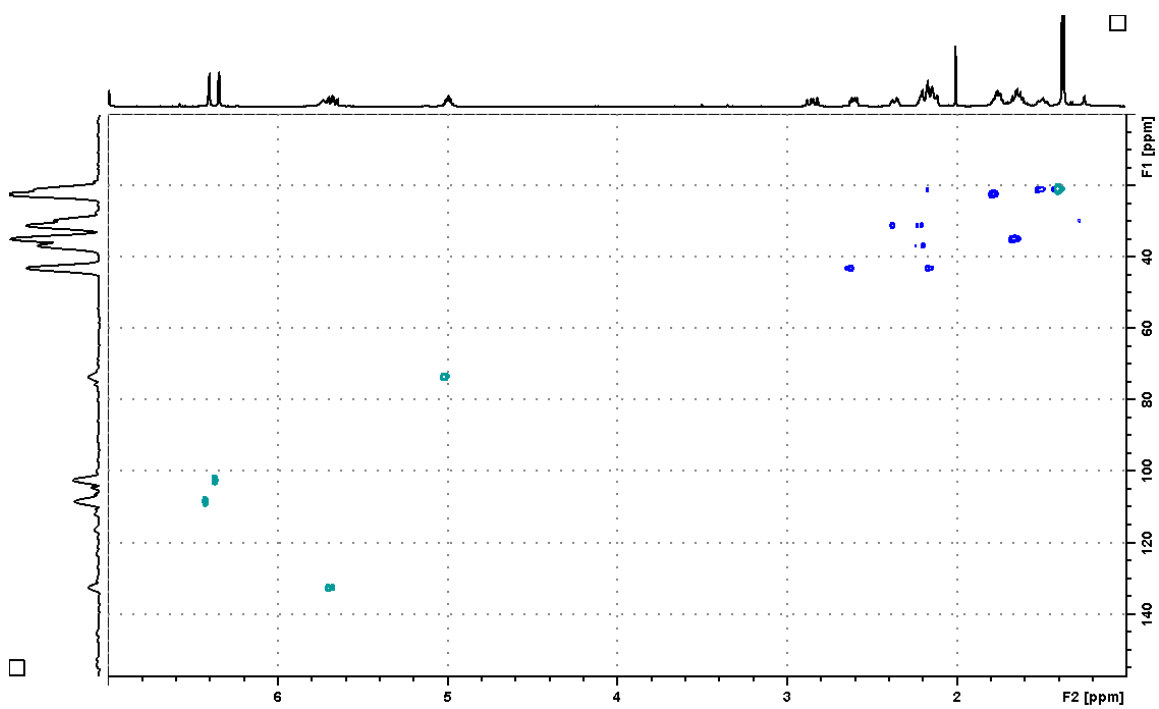
Figure A28. HSQC of zearalenone from *F. graminearum Δkmt6* in CDCl₃ at 500 MHz.
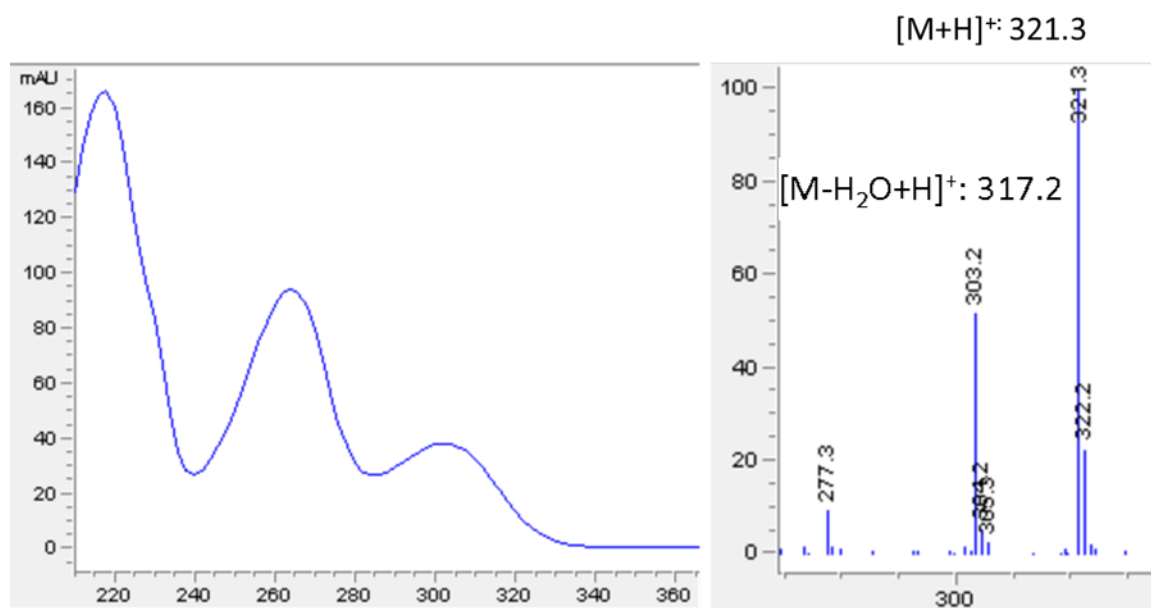
Figure A29. UV spectrum and LRMS of zearalenol.
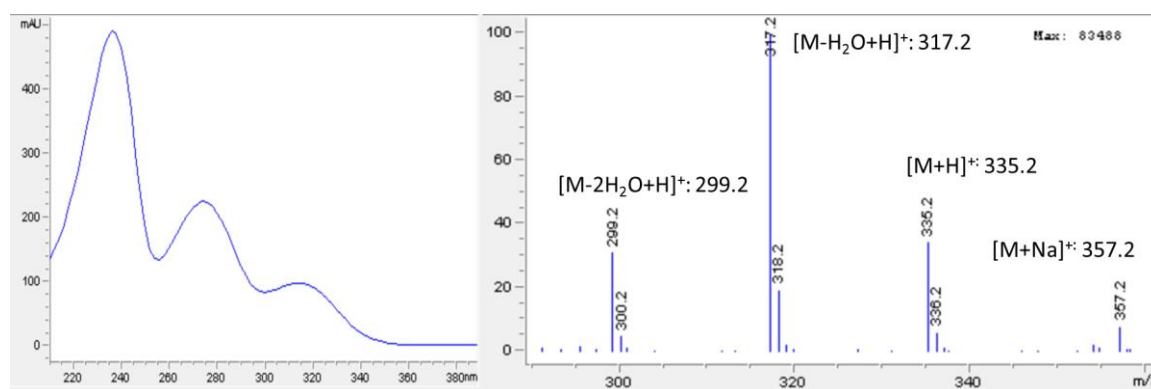
Figure A30. UV spectrum and LRMS of 8'hydroxyzearalenone
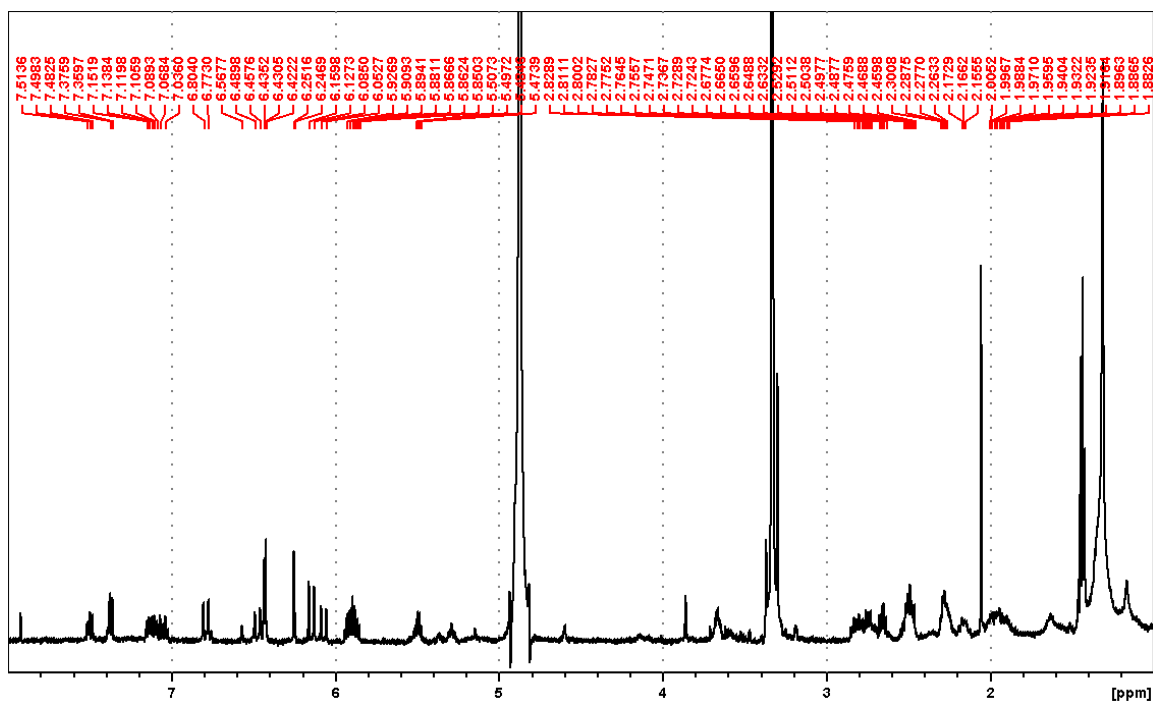
Figure A31. ^{1}H spectrum of 3'-hydroxyzearalenone with solvent suppression in d$_4$-methanol at 500 MHz.
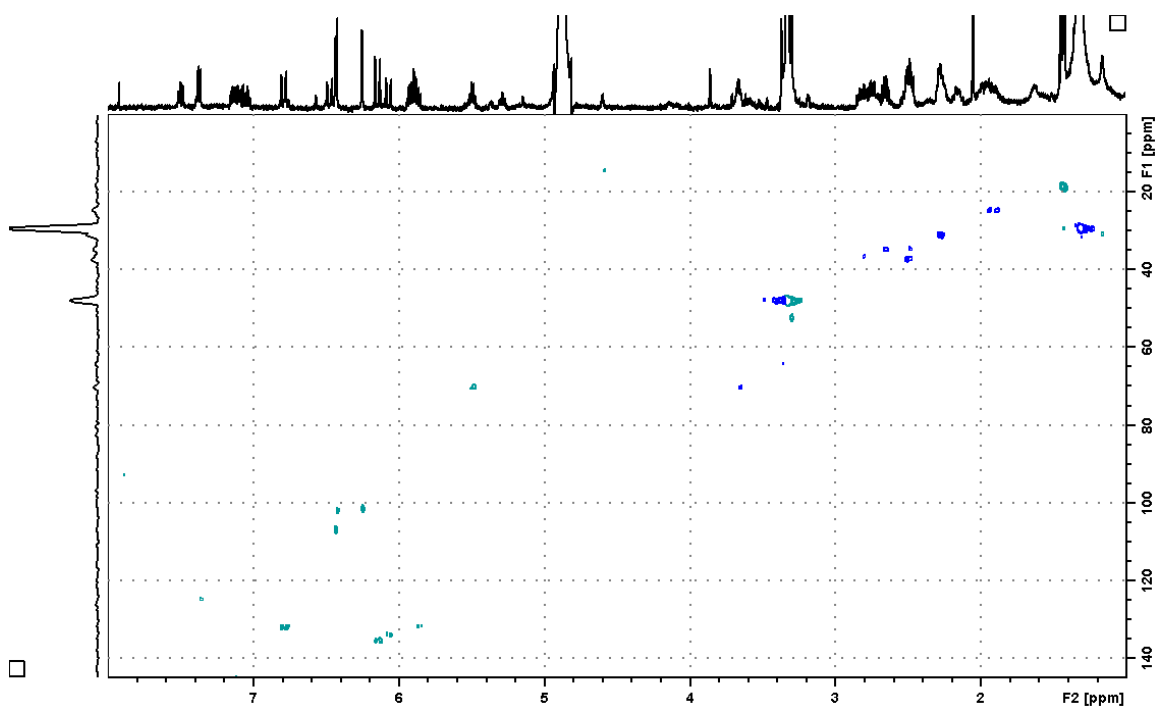
Figure A32. HSQC of 3'-hydroxyzearalenone in d$_4$-methanol.
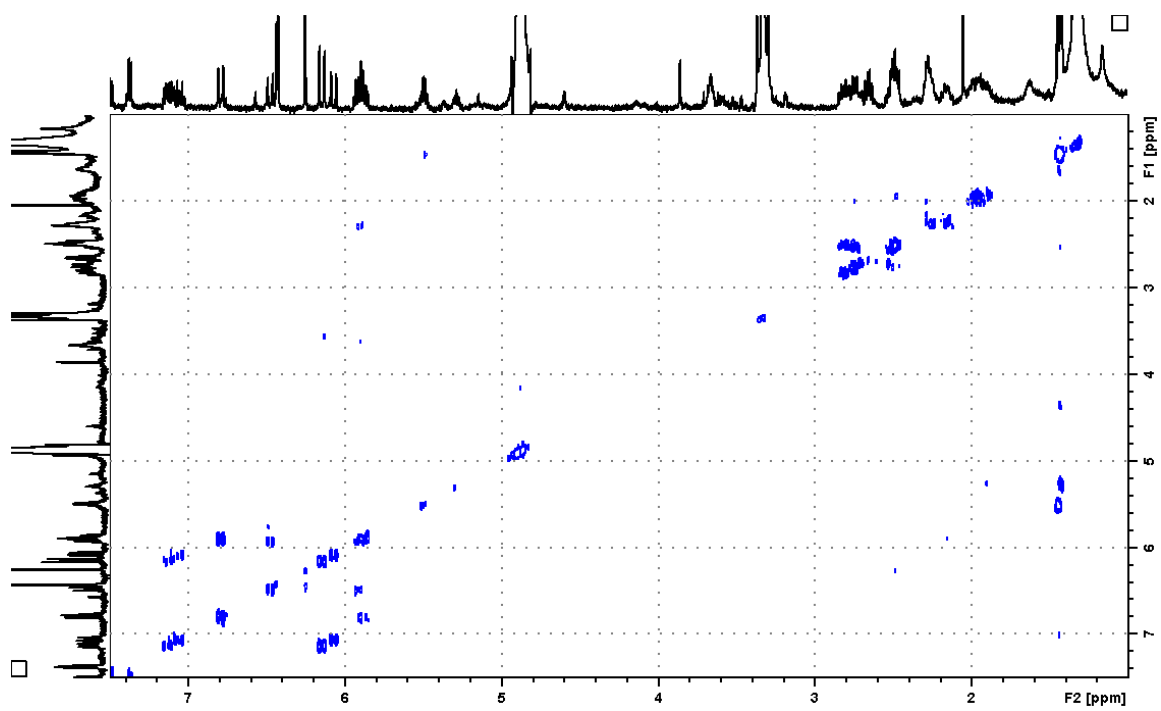
Figure A33. COSY spectrum of 3'-hydroxyzearalenone in d₄-methanol.

Figure A34. ^{1}H spectrum of 6',8'-dihydroxyzearalene in d$_4$-methanol at 125 MHz.
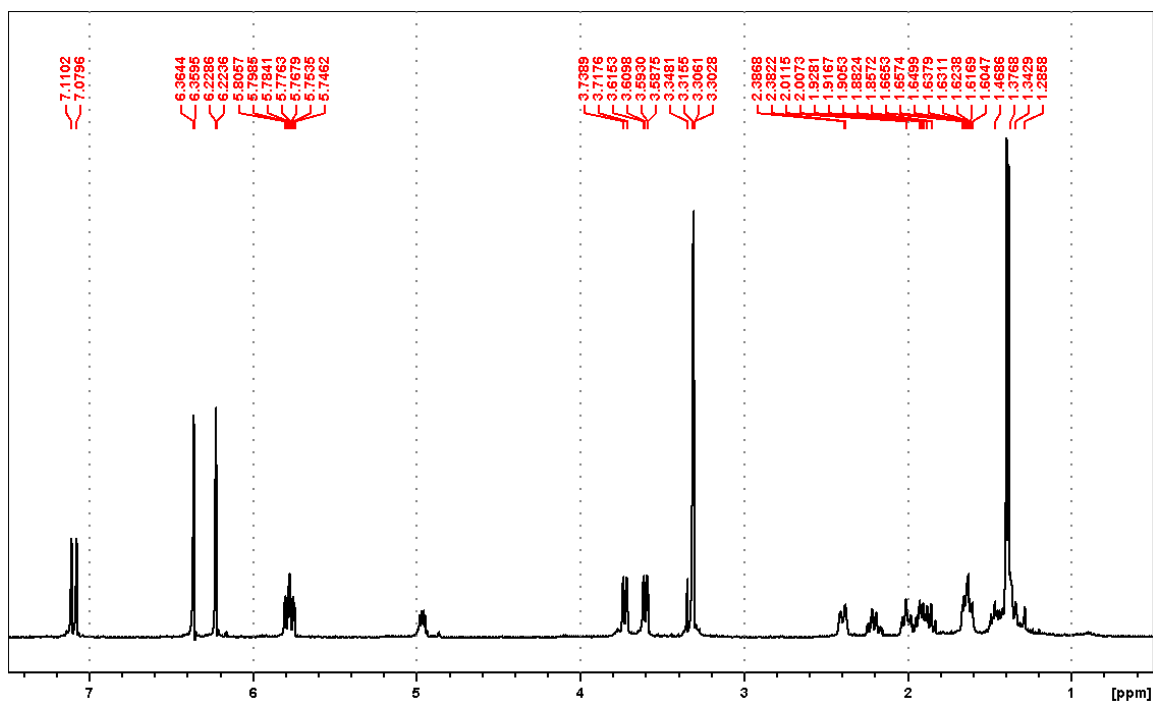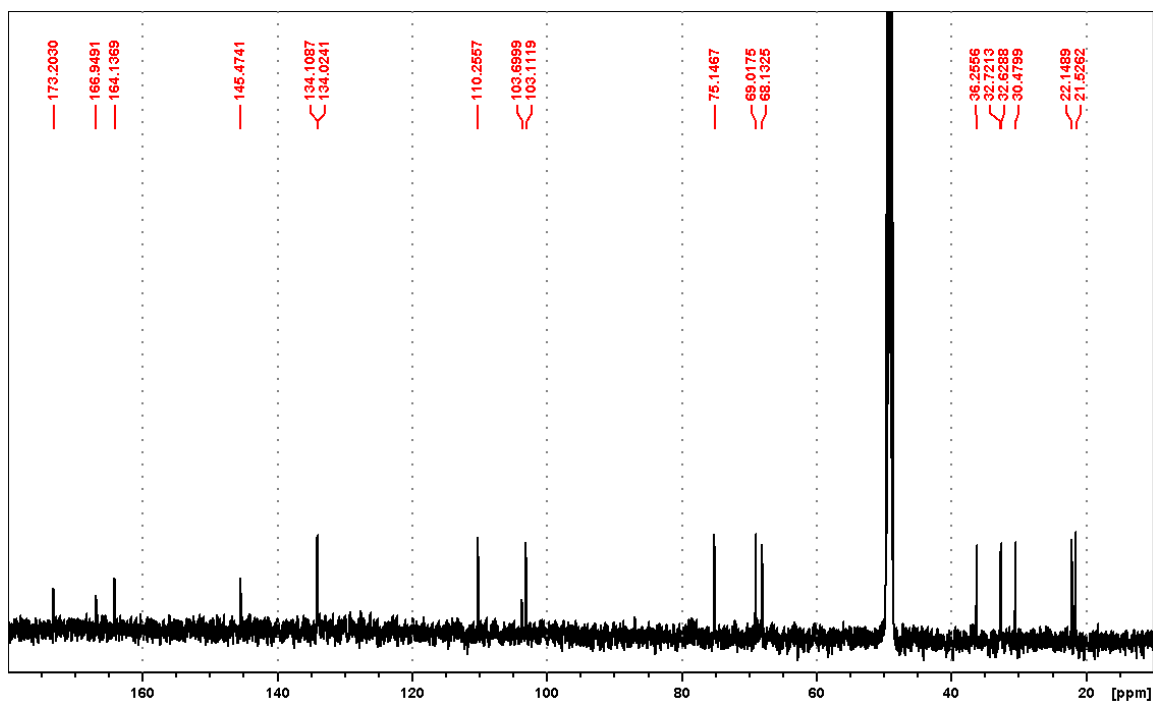
Figure A35. ^{13}C spectrum of 6',8'-dihydroyzearalene in d$_4$-methanol at 125 MHz.
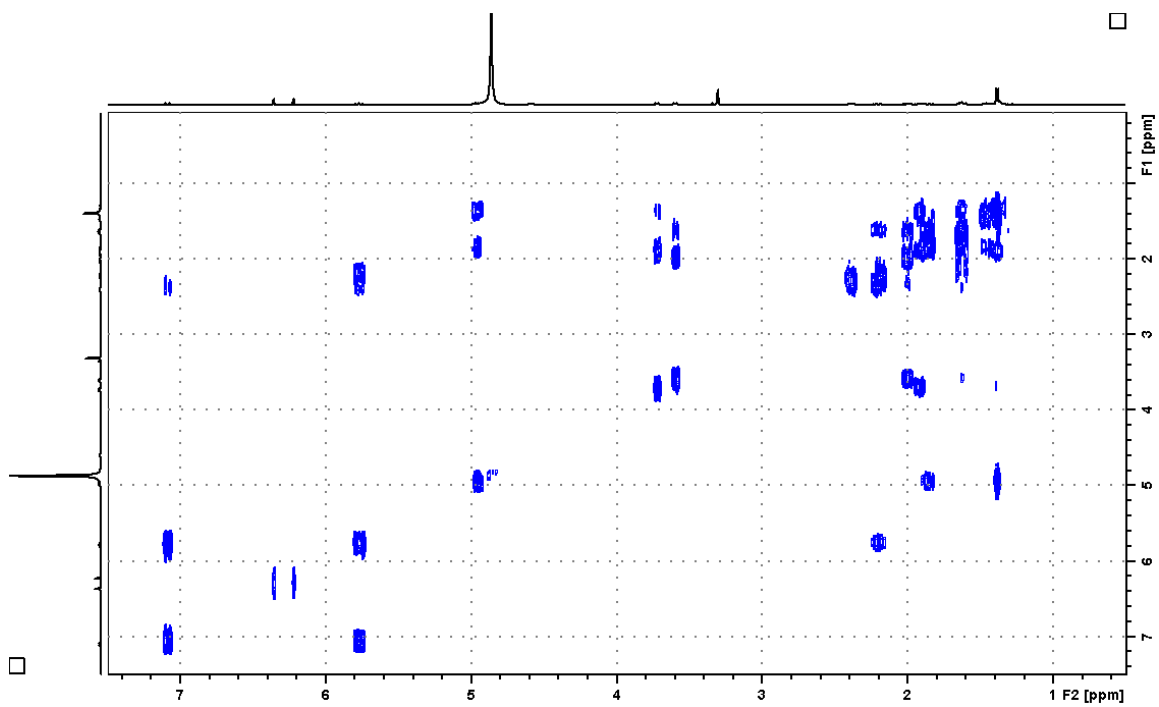
Figure A36. COSY spectrum of 6',8'-dihydroxyzearalene in d_4-methanol.
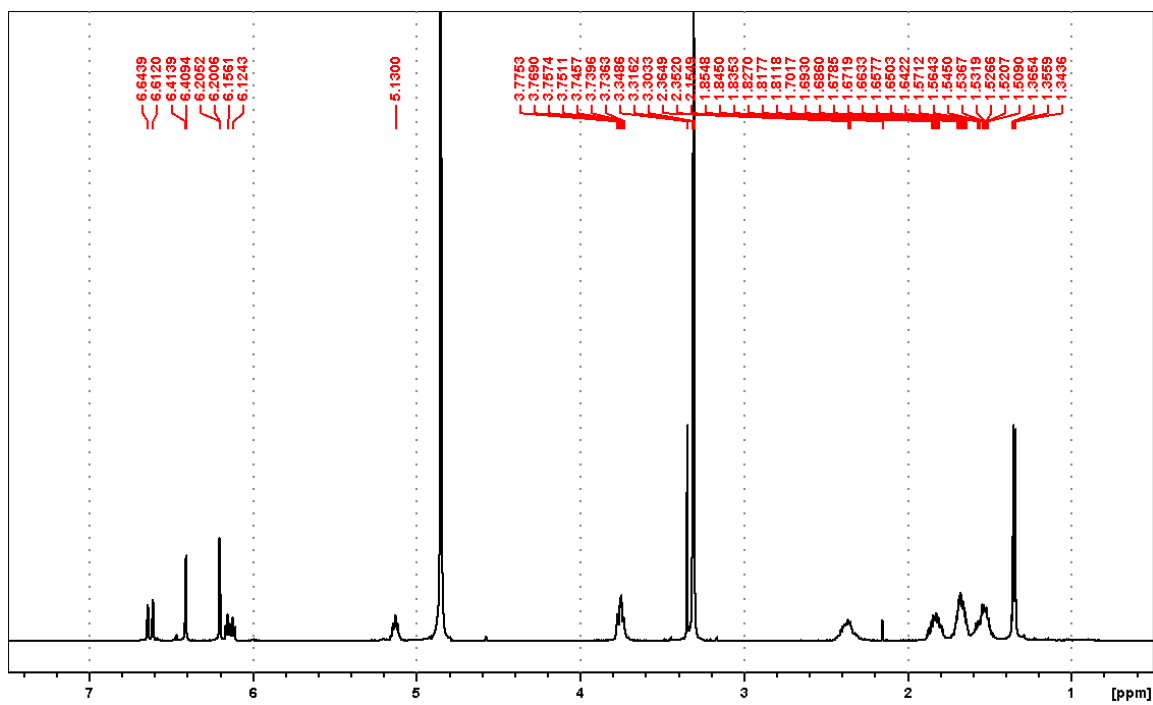
Figure A37. ^{1}H spectrum of 5'-hydroyzearalenol at 500 MHz in d$_4$-methanol
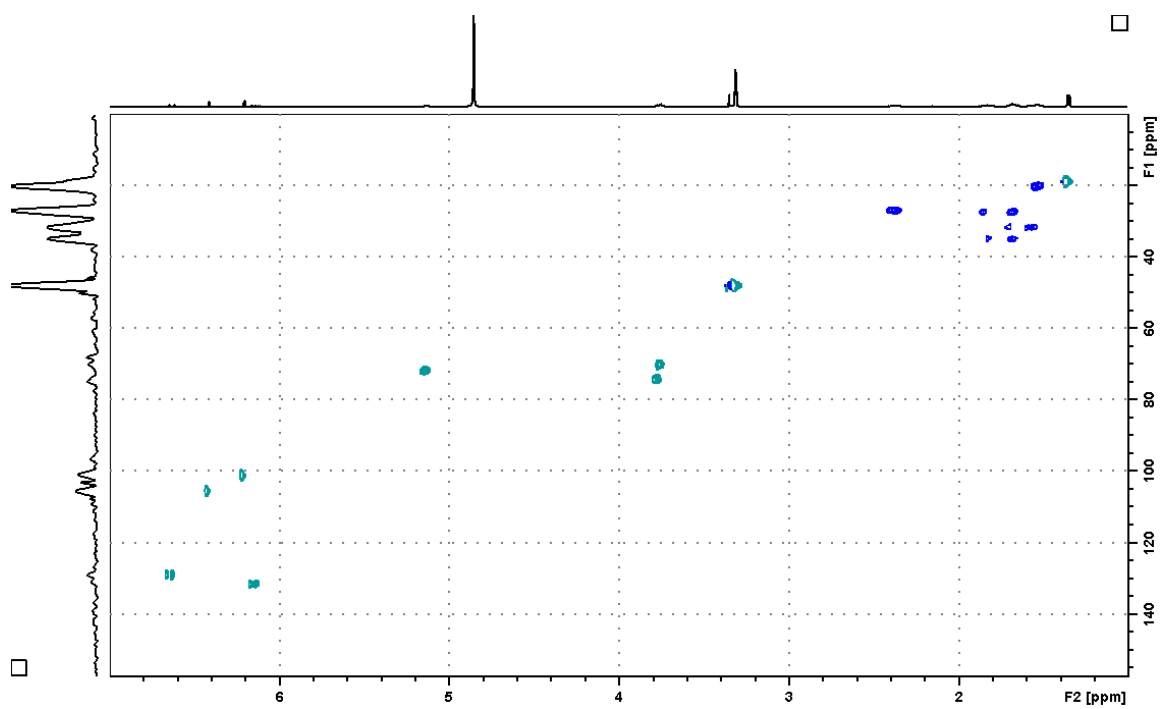
Figure A38. Multiplicity-edited HSQC spectrum of 5'-hydroxyzearalenol in d₄-methanol.
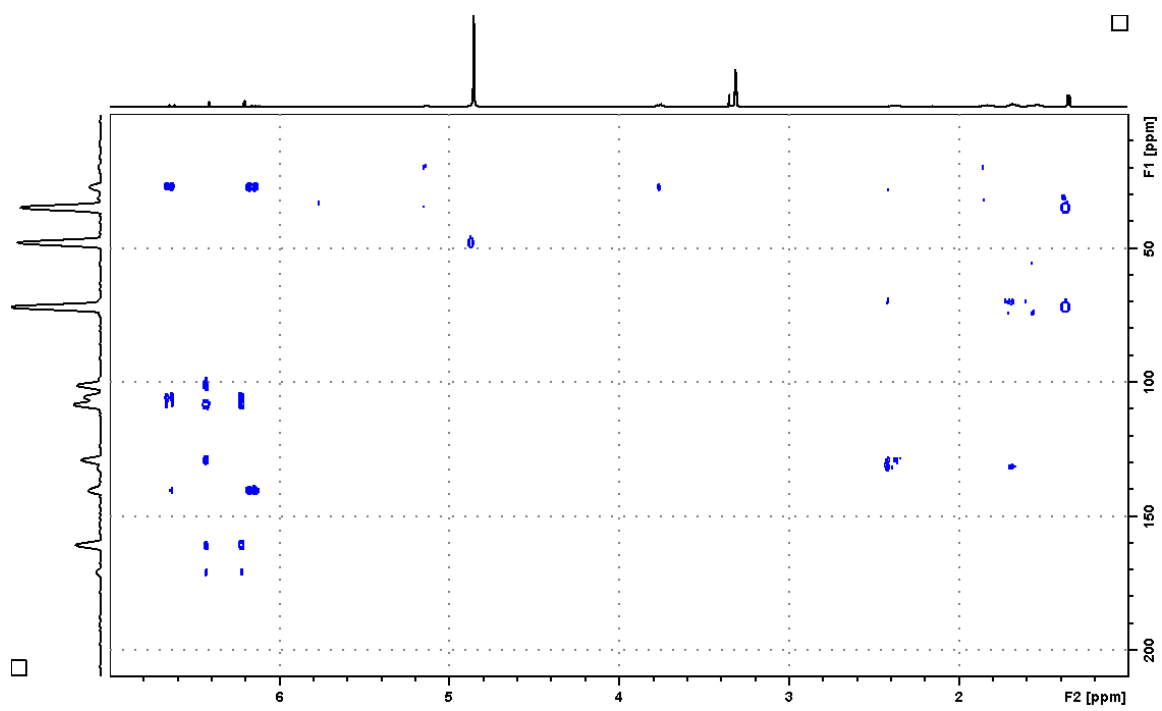
Figure A39. HMBC of 5'-hydroxyzearalenol.
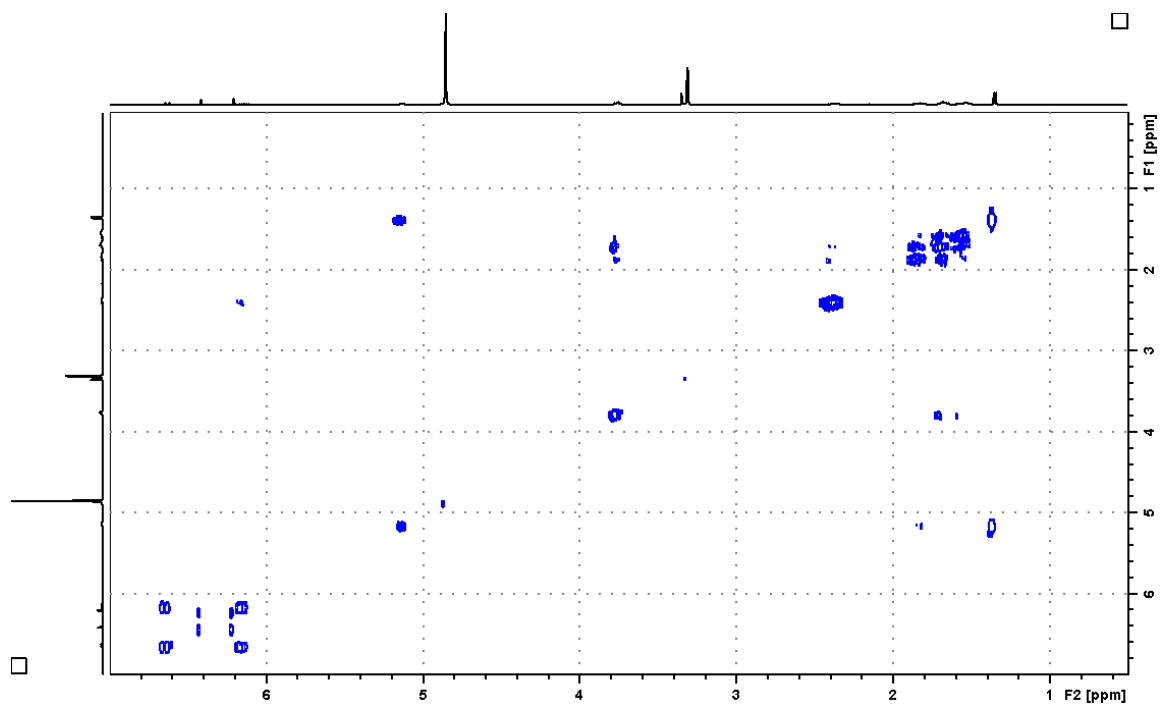
Figure A40. COSY spectrum of 5'-hydroxyzearalenol.
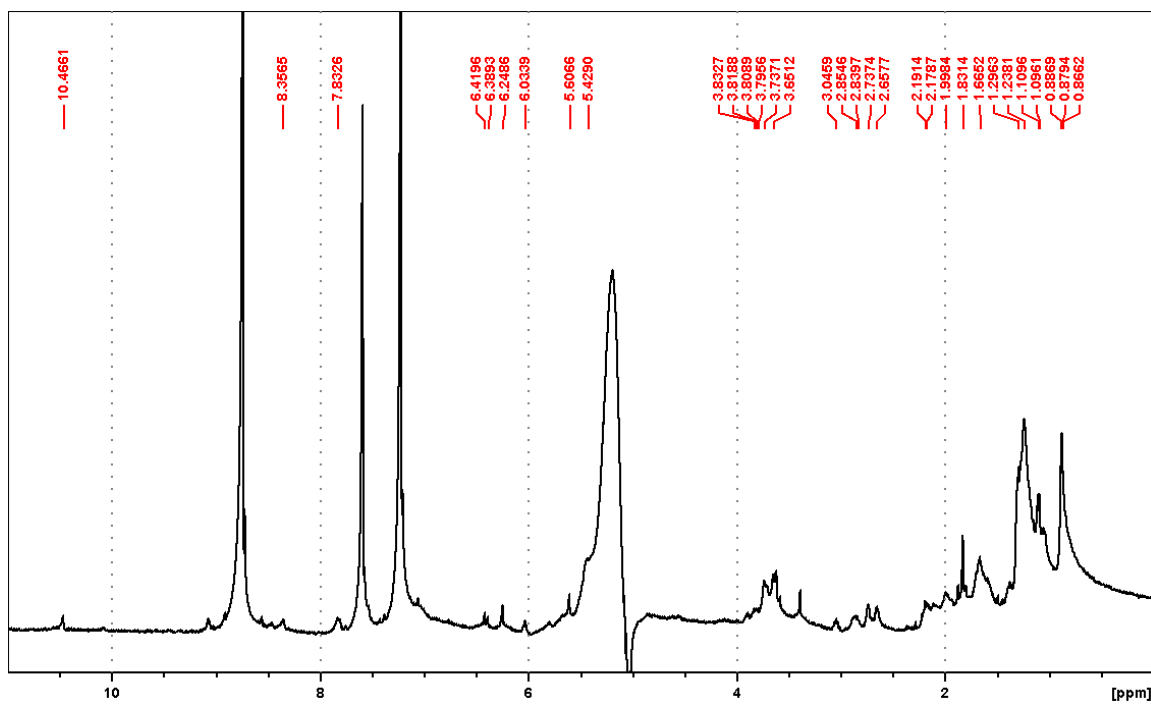
Figure A41. ^{1}H NOESY-presaturated solvent suppression spectrum of fusaristatin A in d$_5$-pyridine.
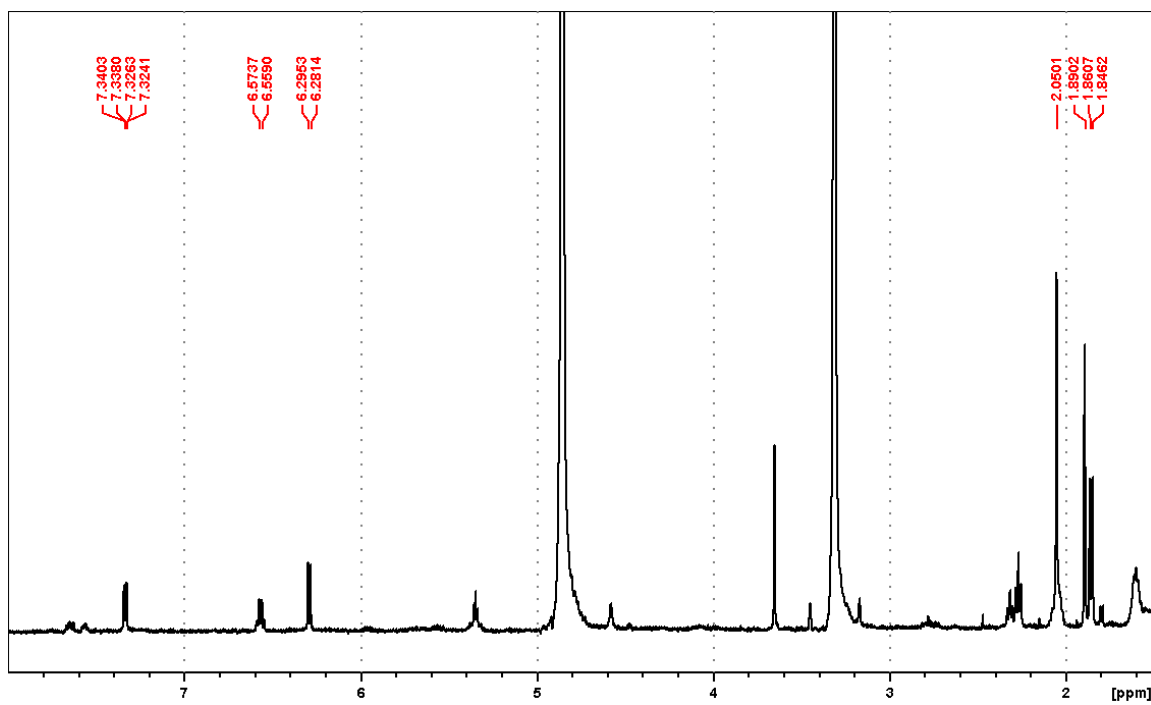
Figure A42. ^{1}H spectrum of gibepyrone A in d_4-methanol at 500 MHz.
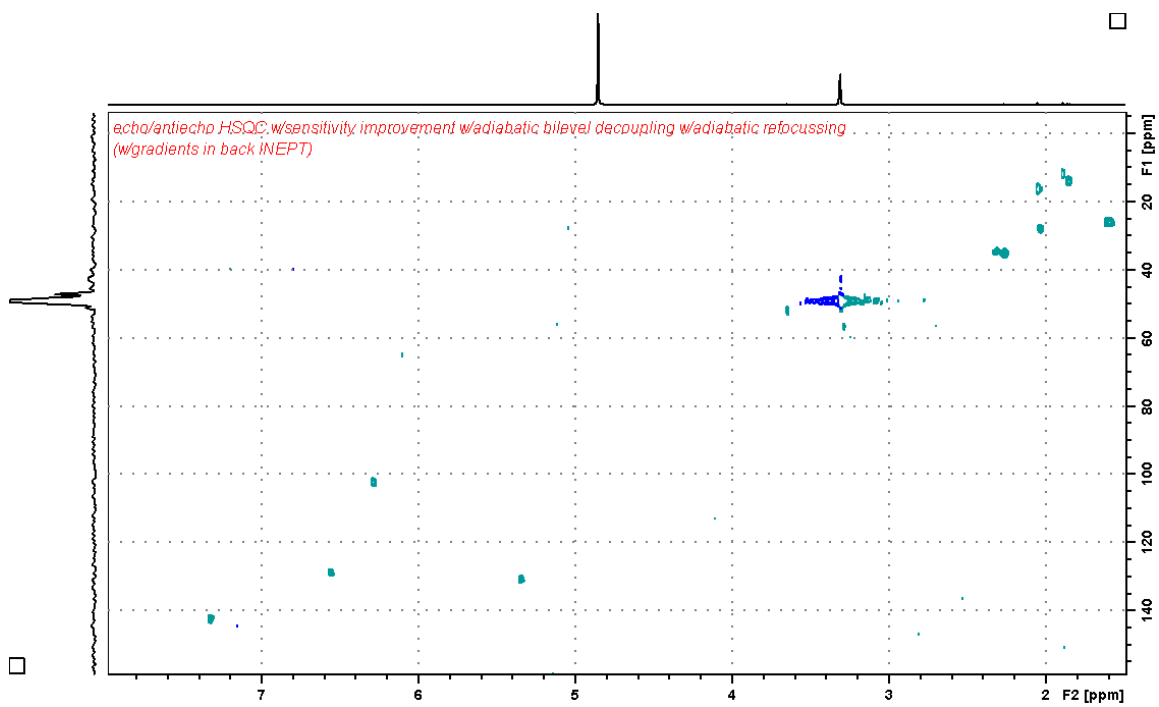
Figure A43. HSQC spectrum of gibepyrone A at 500 MHz.
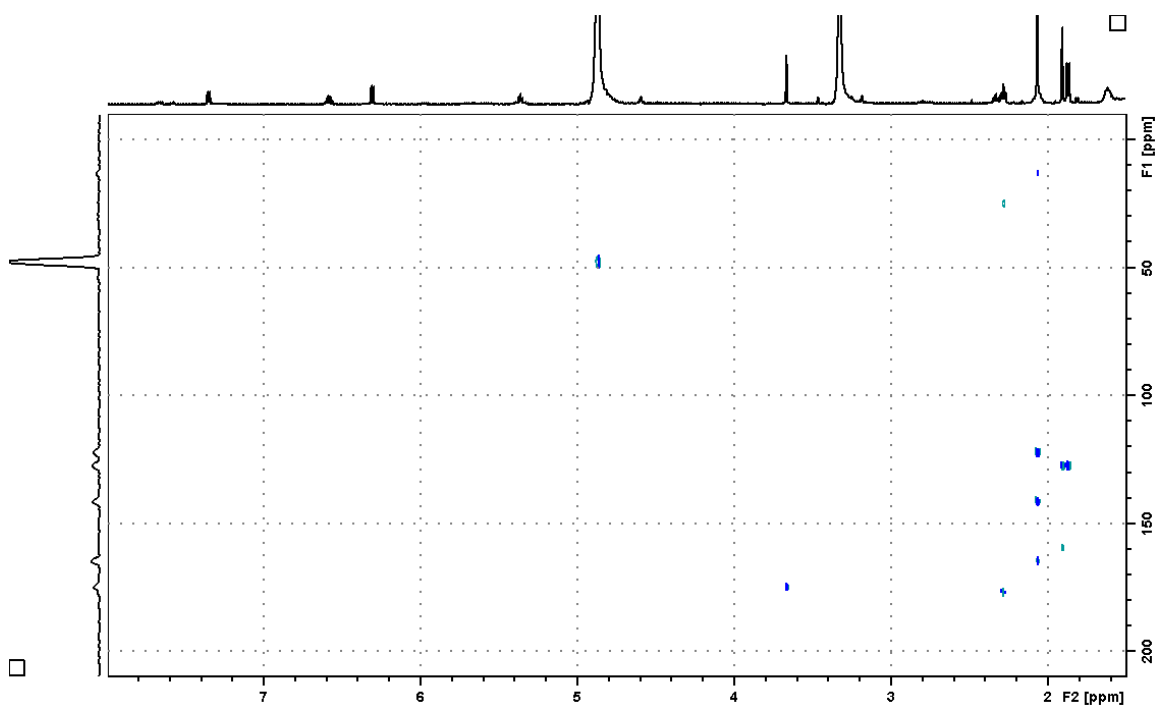
Figure A44. HMBC of gibepyrone A in d$_4$-methanol.
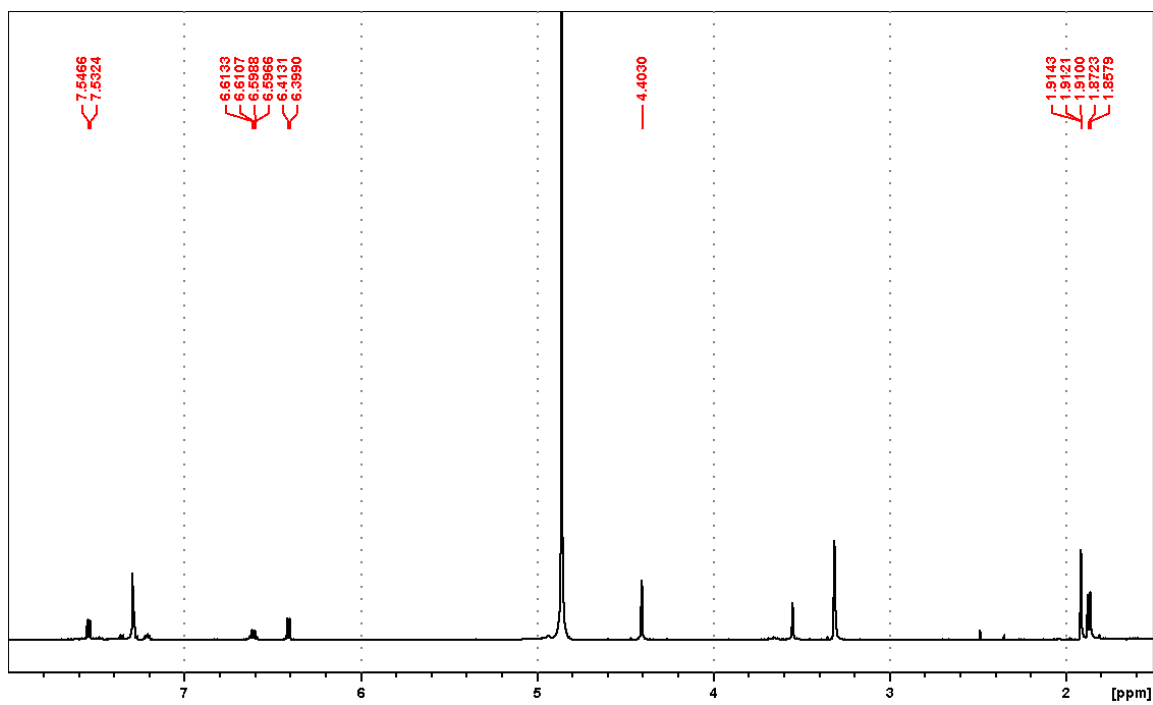
Figure A45. ^{1}H spectrum of fusarpyrone A in d$_4$-methanol at 500 MHz.
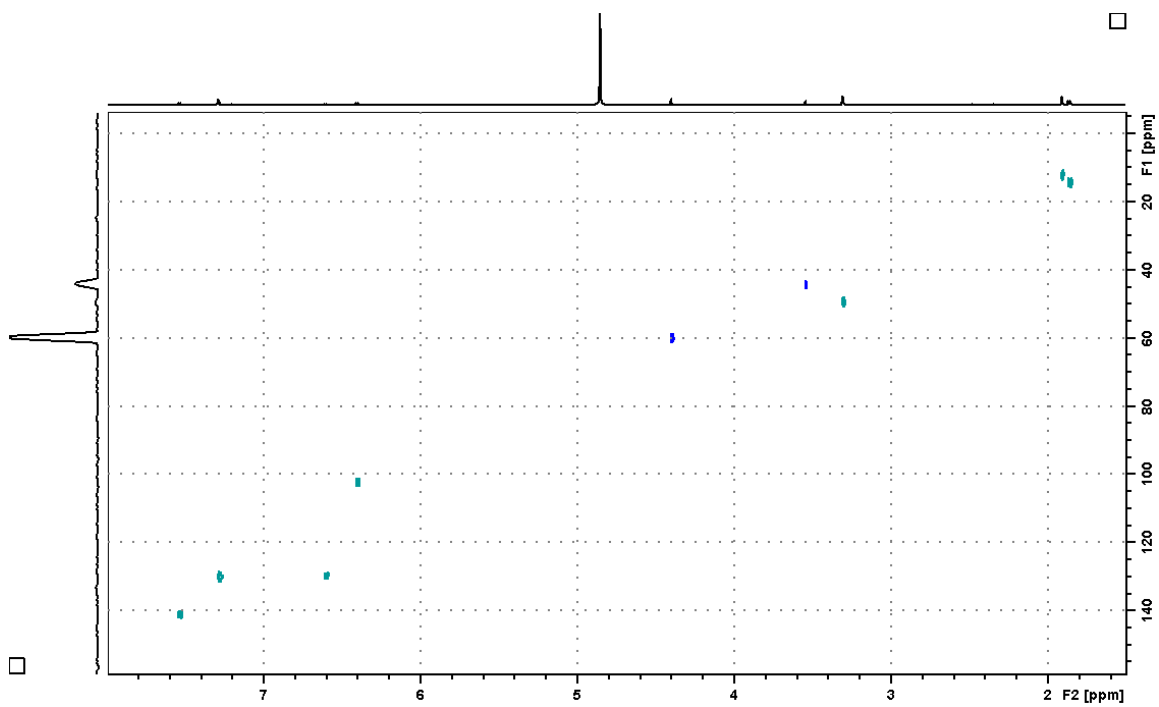
Figure A46. Multiplicity-edited HSQC spectrum of fusarpyrone A in d$_4$-methanol.
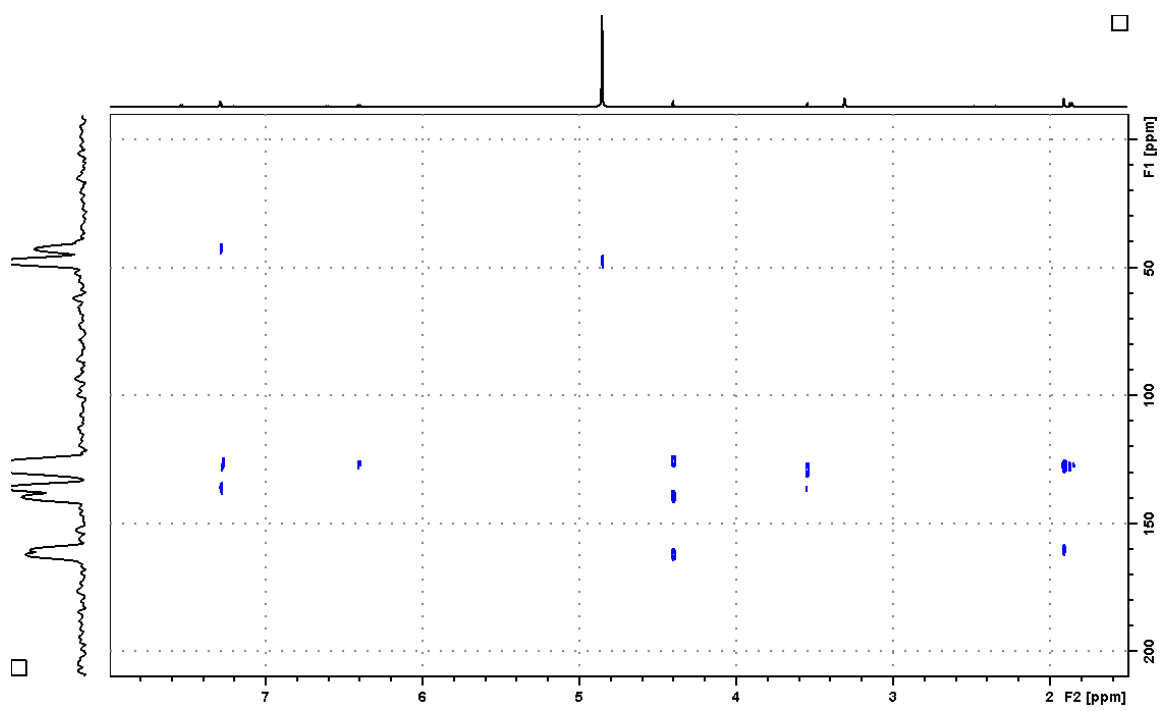
Figure A47. HMBC spectrum of fusarpyrone A in d$_4$-methanol.
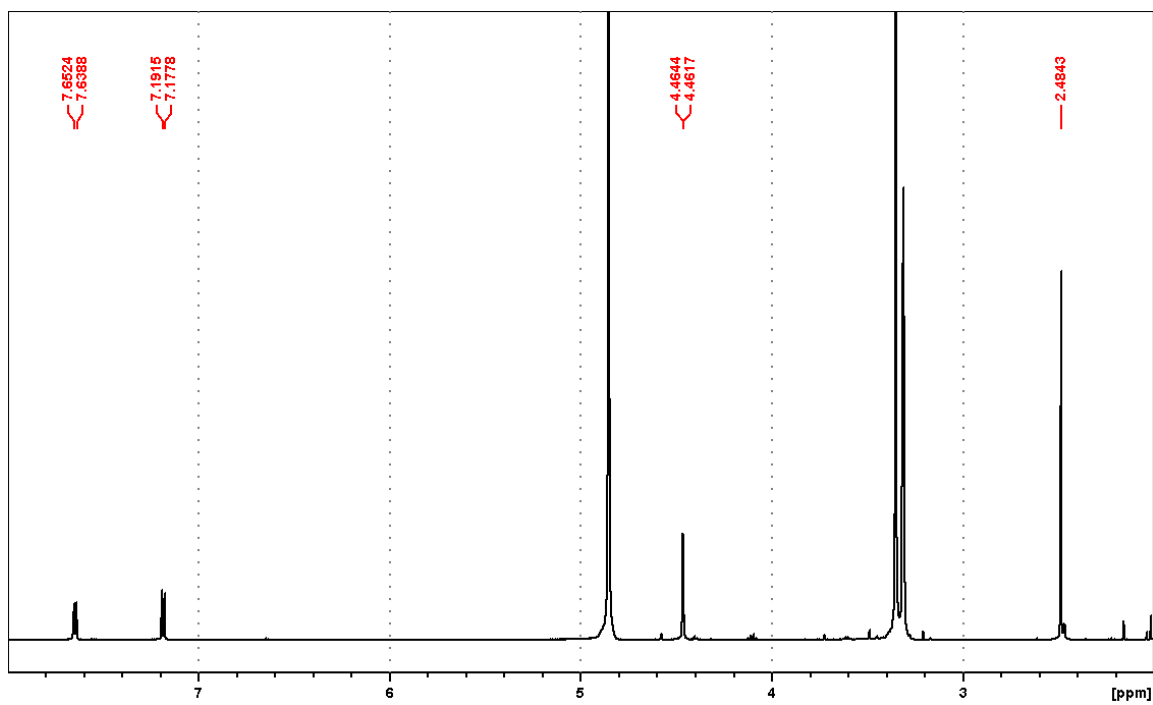
Figure A48. ^{1}H NMR spectrum of fusarpyrone B in d$_4$-methanol at 500 MHz.
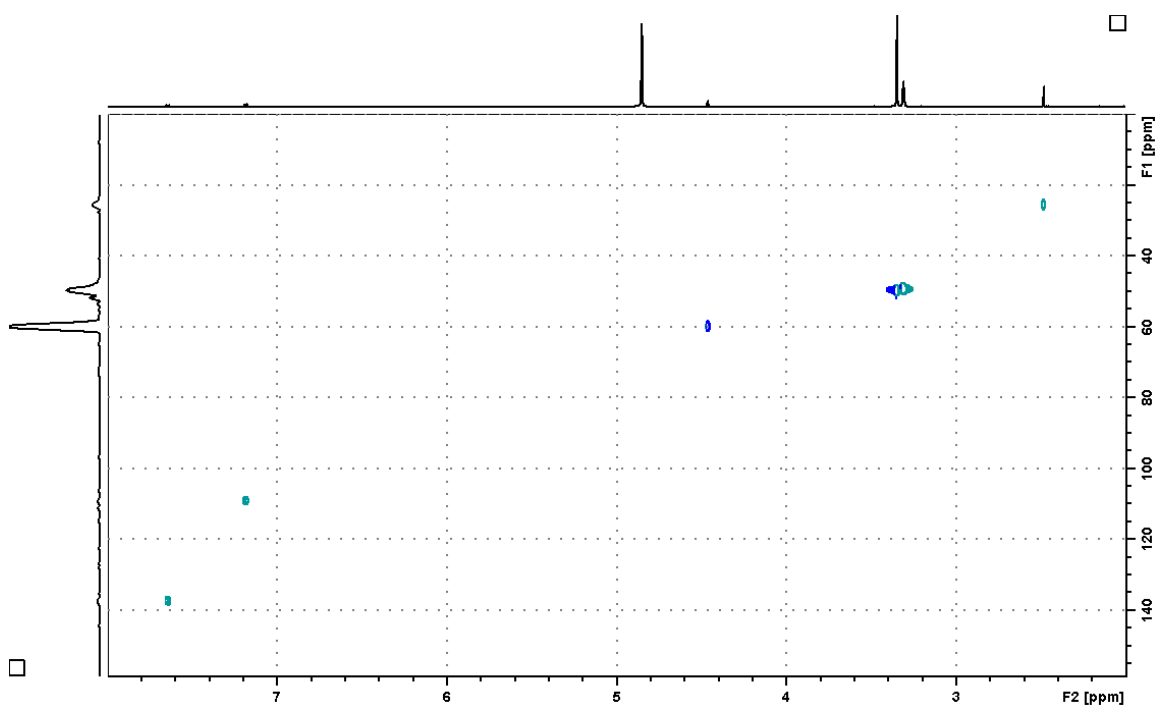
Figure A49. HSQC spectrum of fusarpyrone B in d$_4$-methanol.
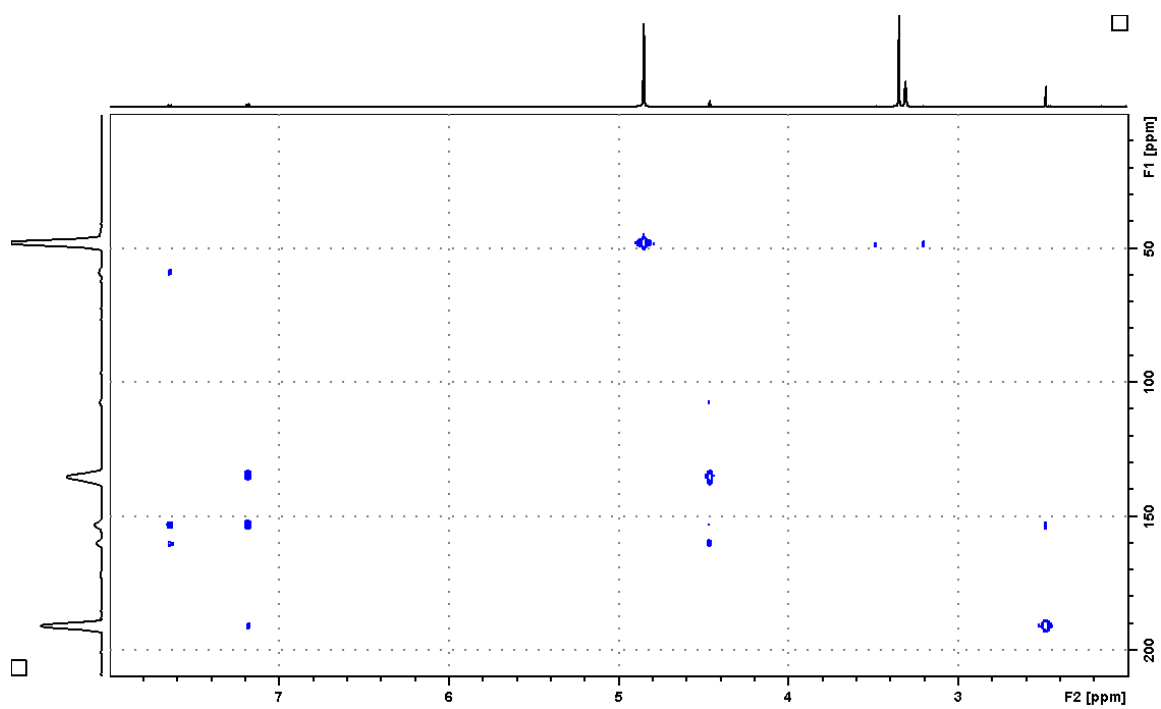
Figure A50. HMBC of fusarpyrone B in d$_4$-methanol.
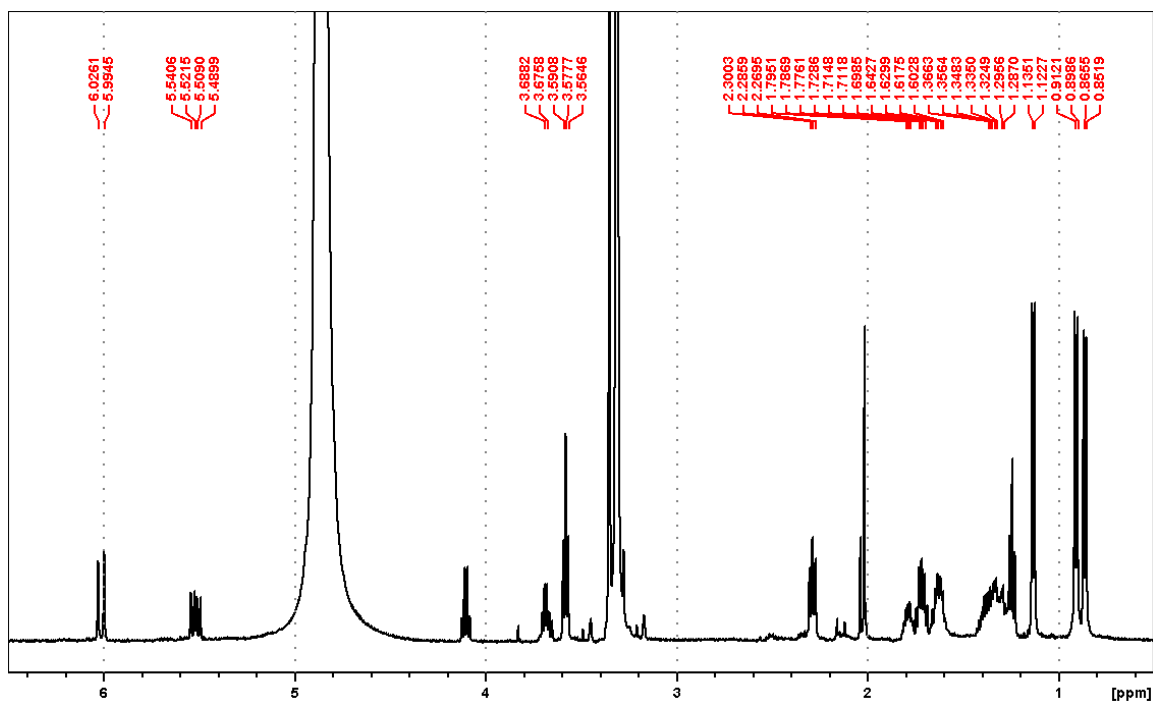
Figure A51. ^{1}H spectrum of tricindiol in d$_4$-methanol at 700 MHz.
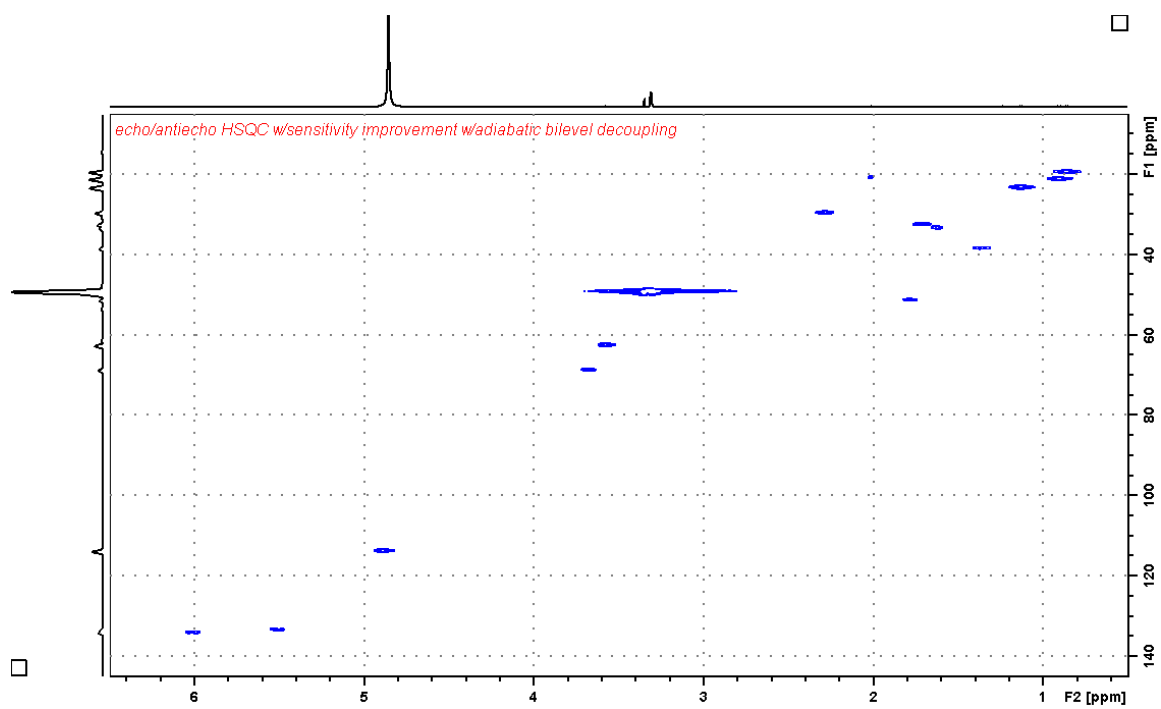
Figure A52. HSQC spectrum of tricindiol in d_4-methanol.
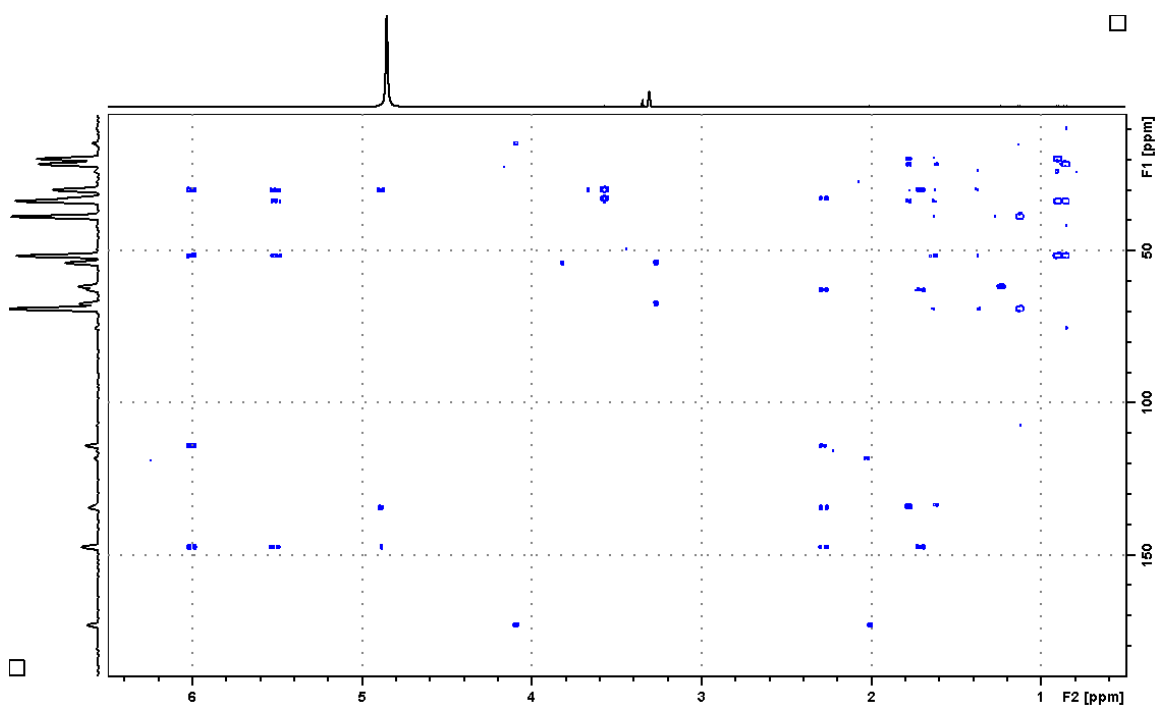
Figure A53. HMBC spectrum of tricindiol in d$_4$-methanol.
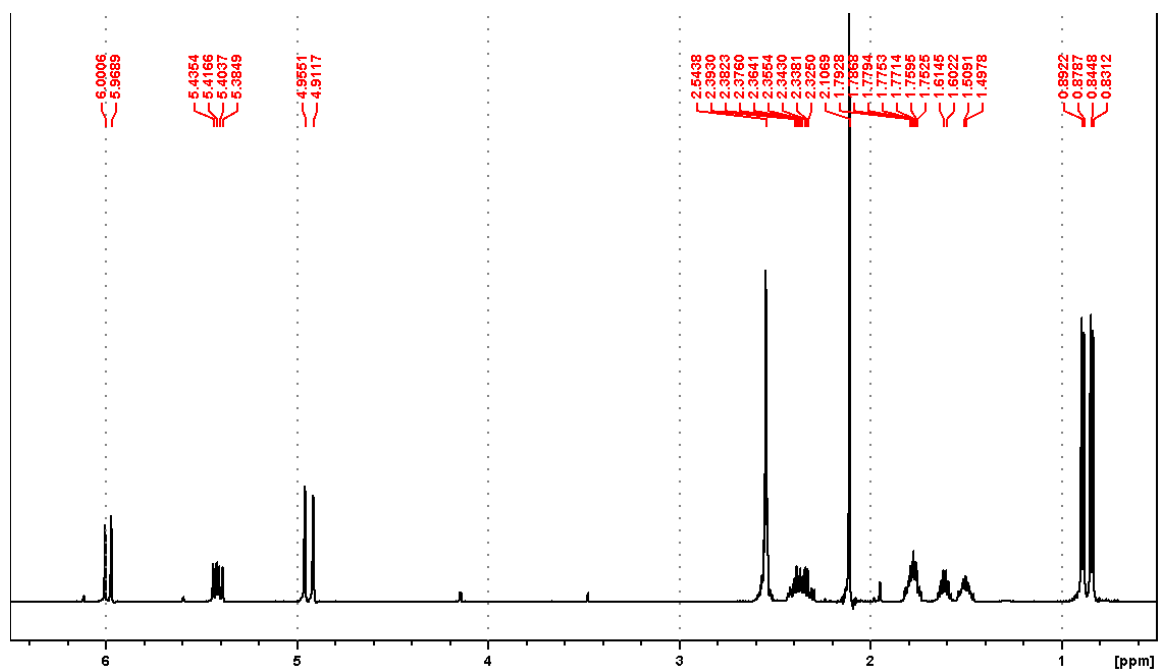
Figure A54. ^{1}H NMR spectrum of tricinonoic acid in CDCl$_3$ at 500 MHz.
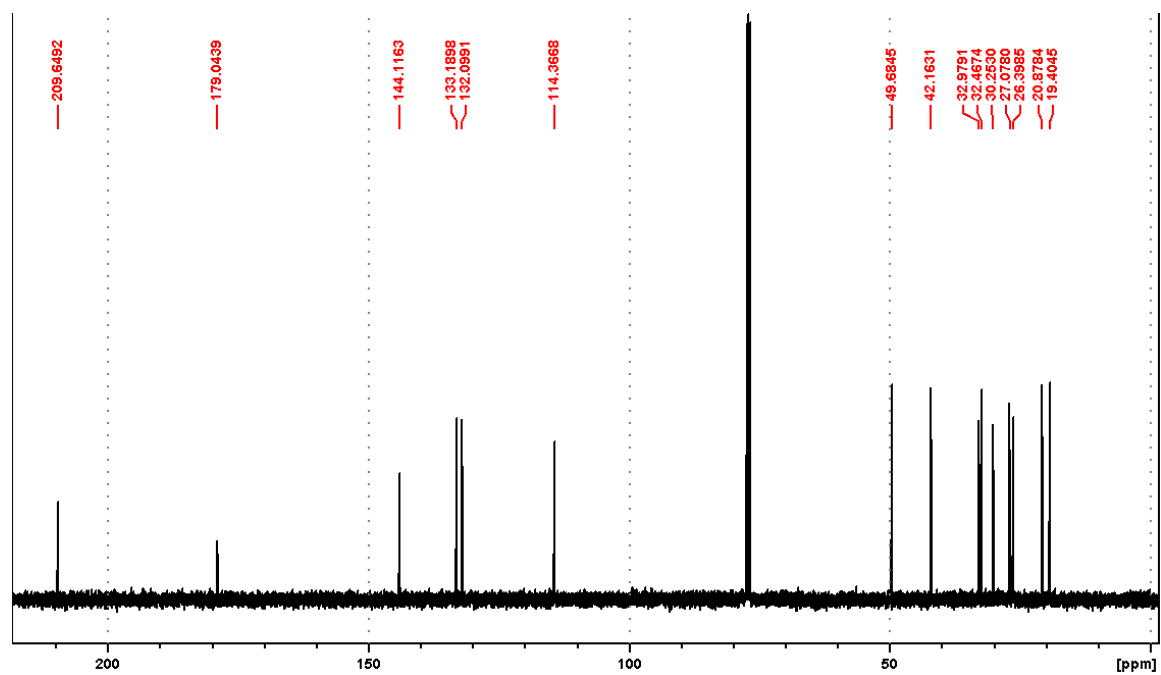
Figure A55. ^{13}C NMR spectrum of tricinonoic acid in CDCl$_3$ at 125 MHz.
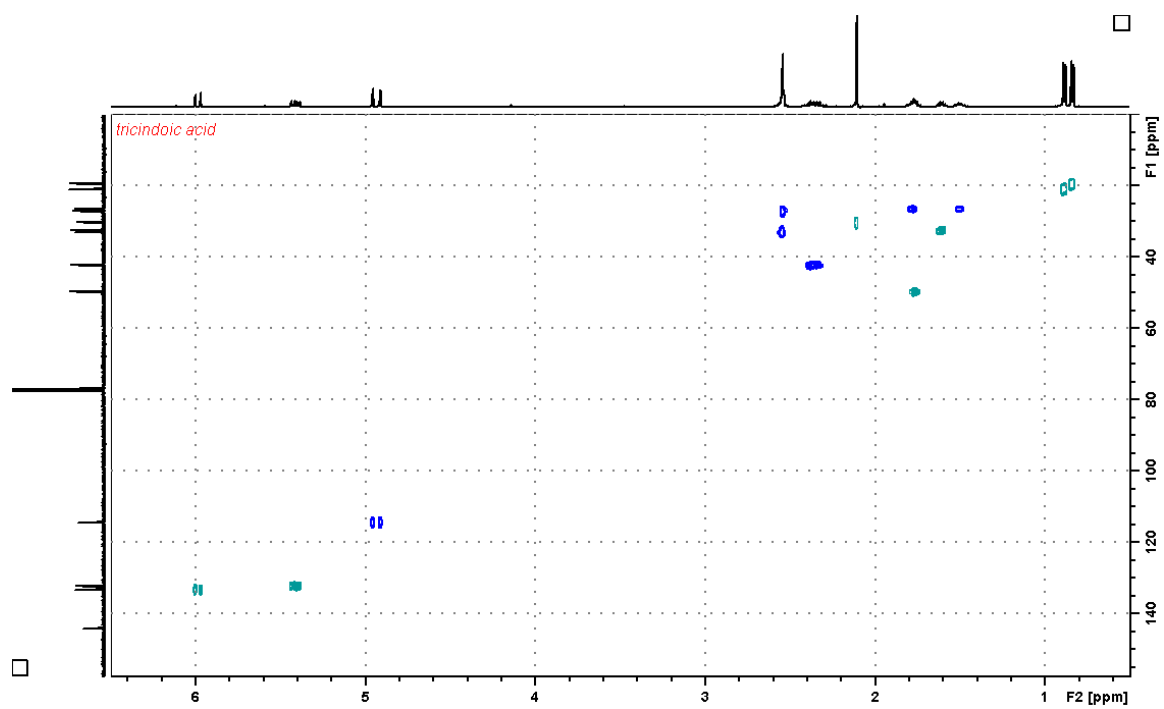
Figure A56. Multiplicity-edited HSQC spectrum of tricinonoic acid in CDCl₃.
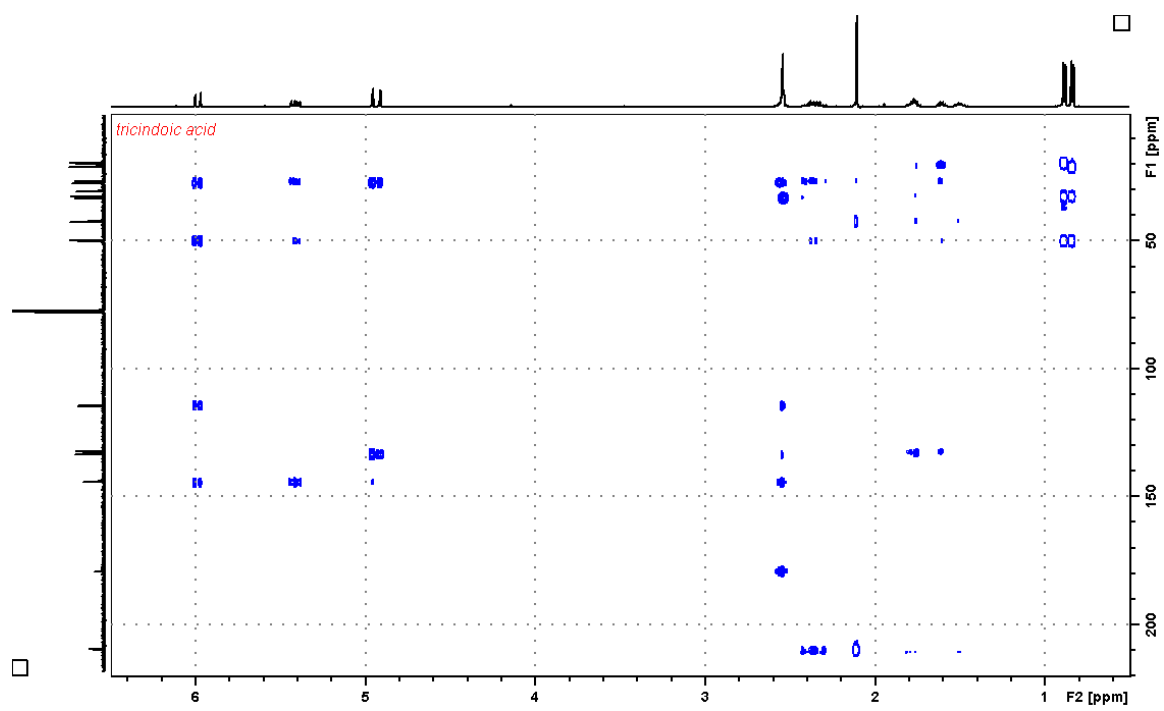
Figure A57. HMBC spectrum of tricinonoic acid in CDCl$_3$
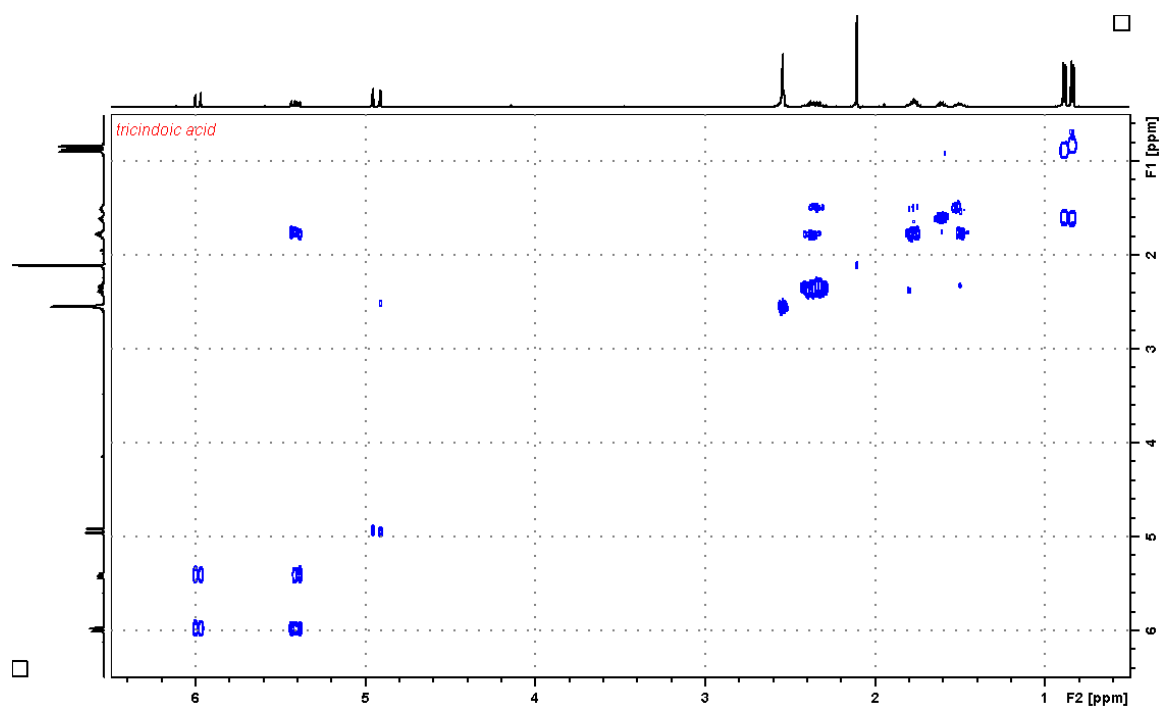
Figure A58. COSY spectrum of tricinonoic acid in CDCl₃ at 500 MHz.
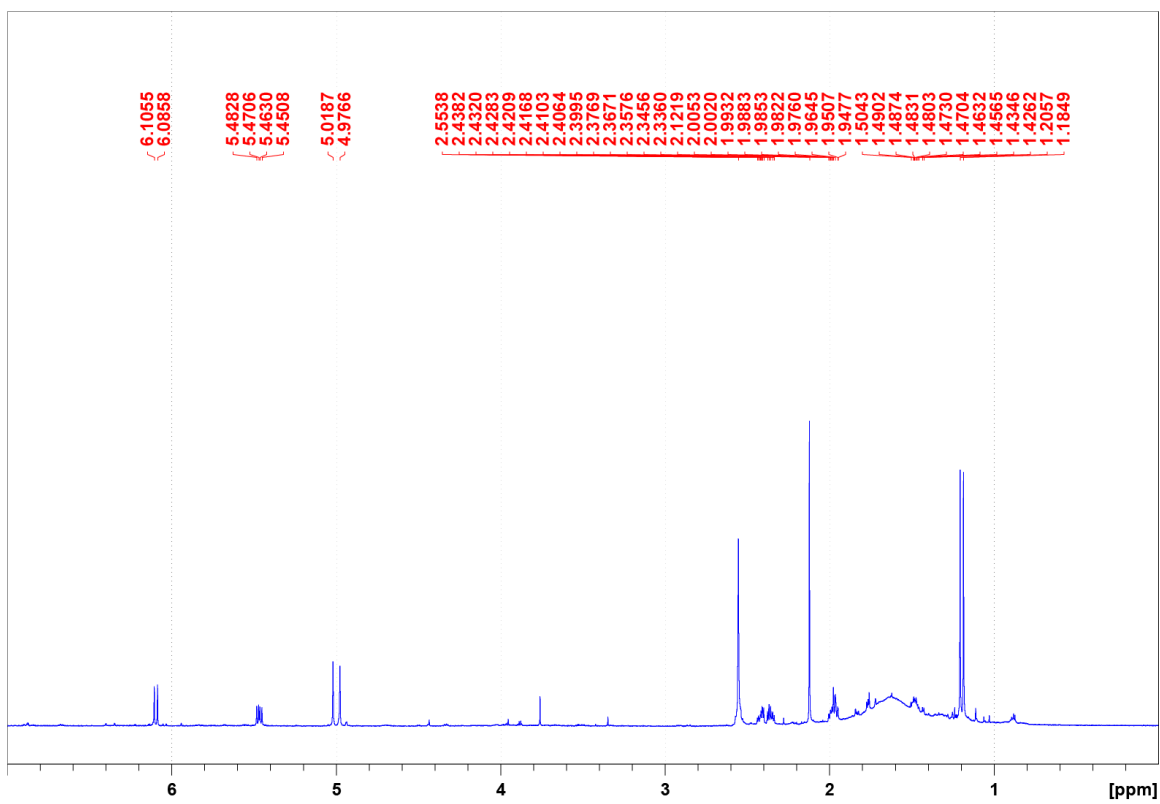
Figure A59. ^{1}H spectrum of tricinolonoic acid in CDCl$_3$ at 800 Mhz.
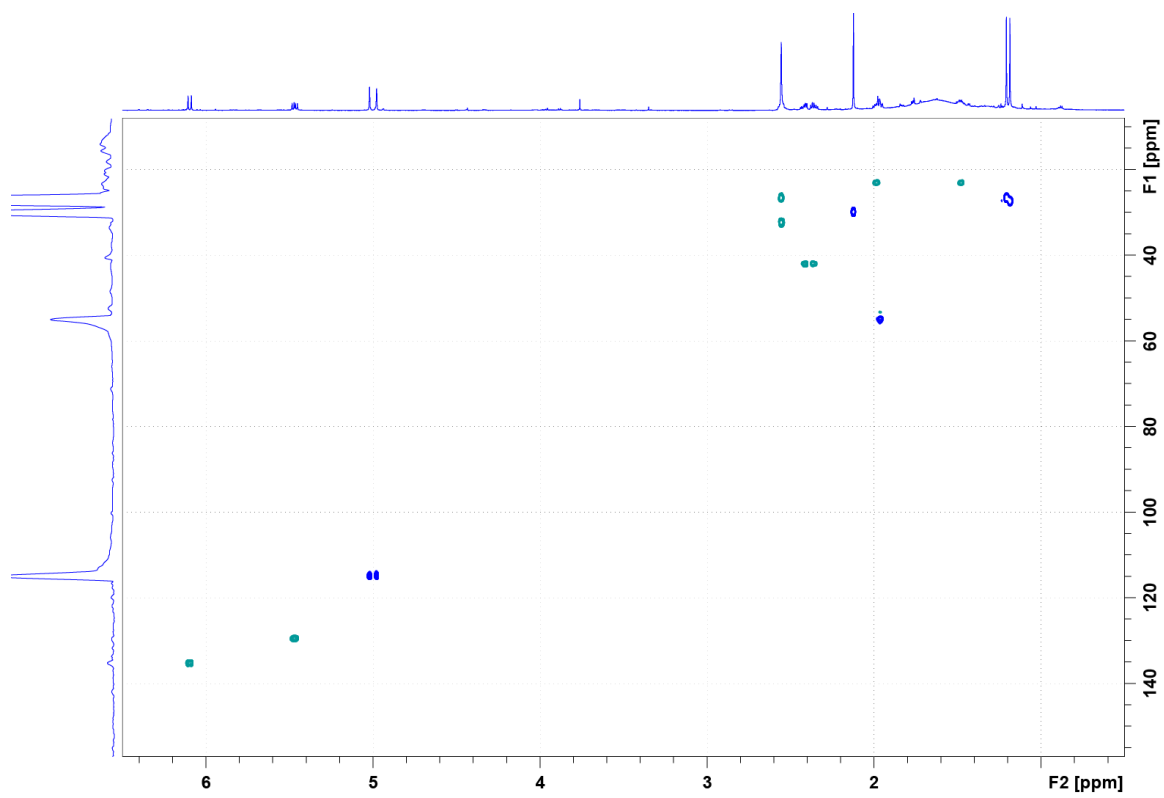
Figure A60. Multiplicity-edited HSQC of tricinolonoic acid in CDCl$_3$.
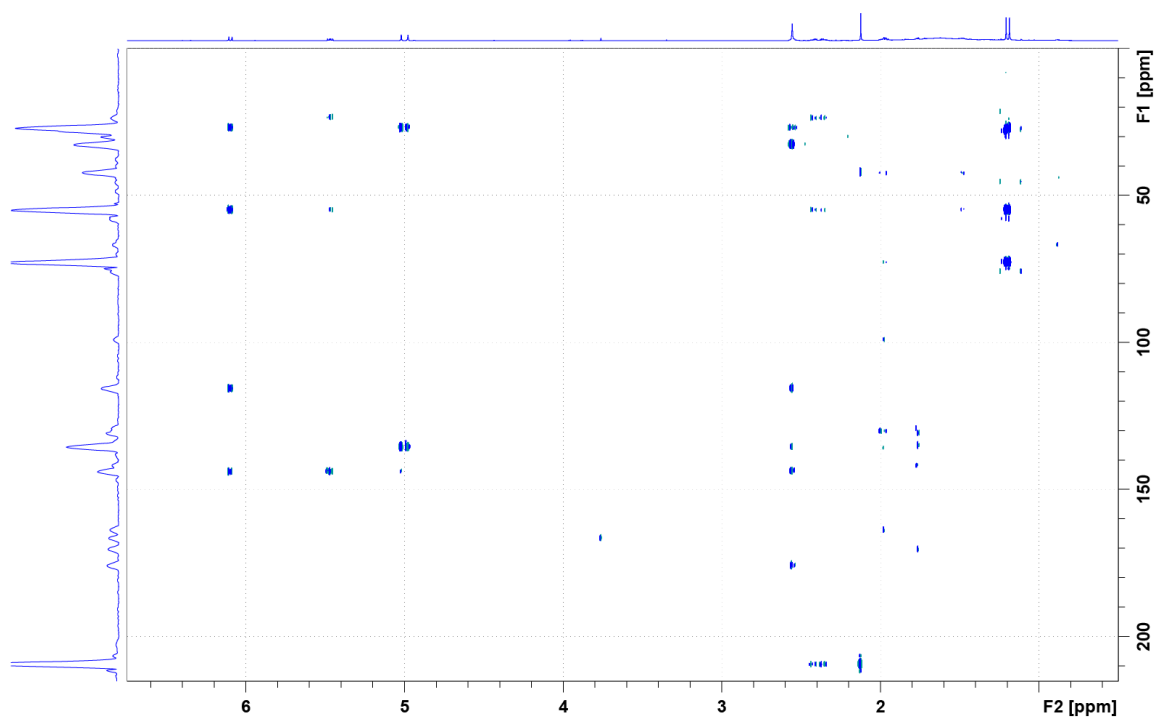
Figure A61. HMBC of tricinolonoic acid in CDCl₃.
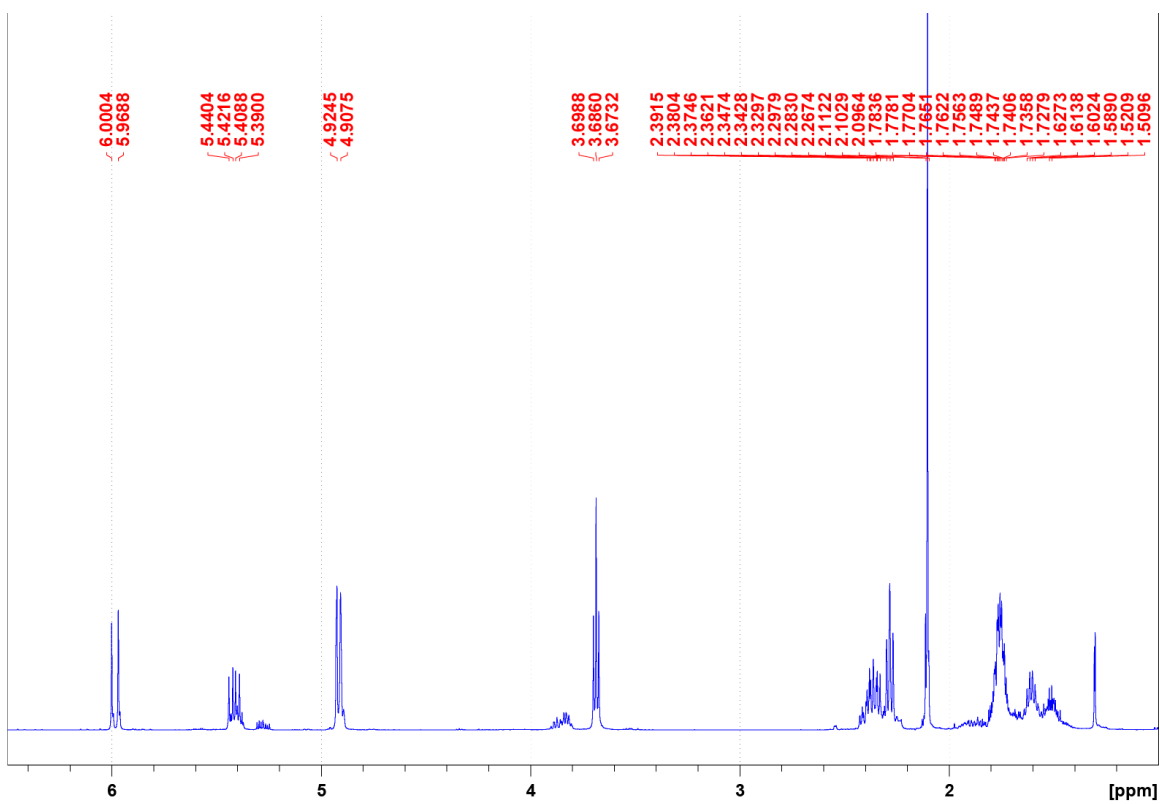
Figure A62. ^{1}H spectrum of tricinolone in CDCl$_3$ at 500 MHz.
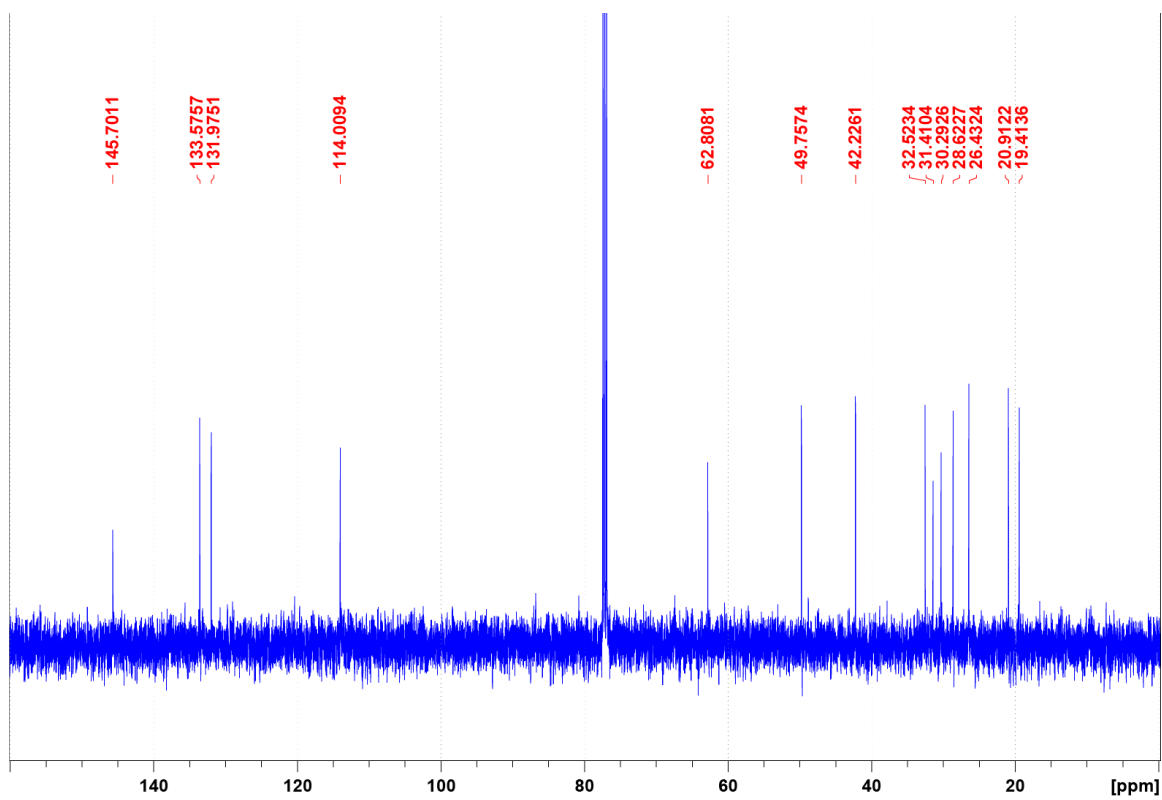
Figure A63. ^{13}C spectrum of tricinolone in CDCl$_3$ at 125 MHz.
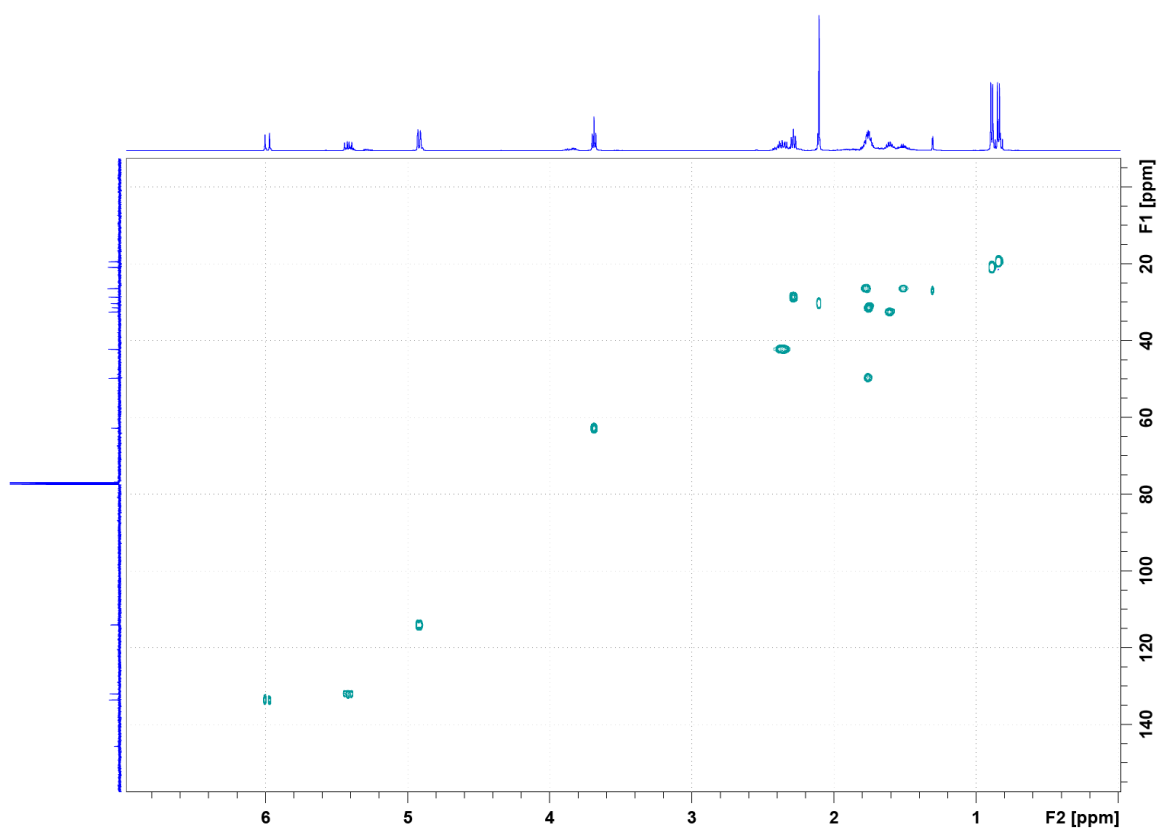
Figure A64. HSQC of tricinolone in CDCl$_3$.
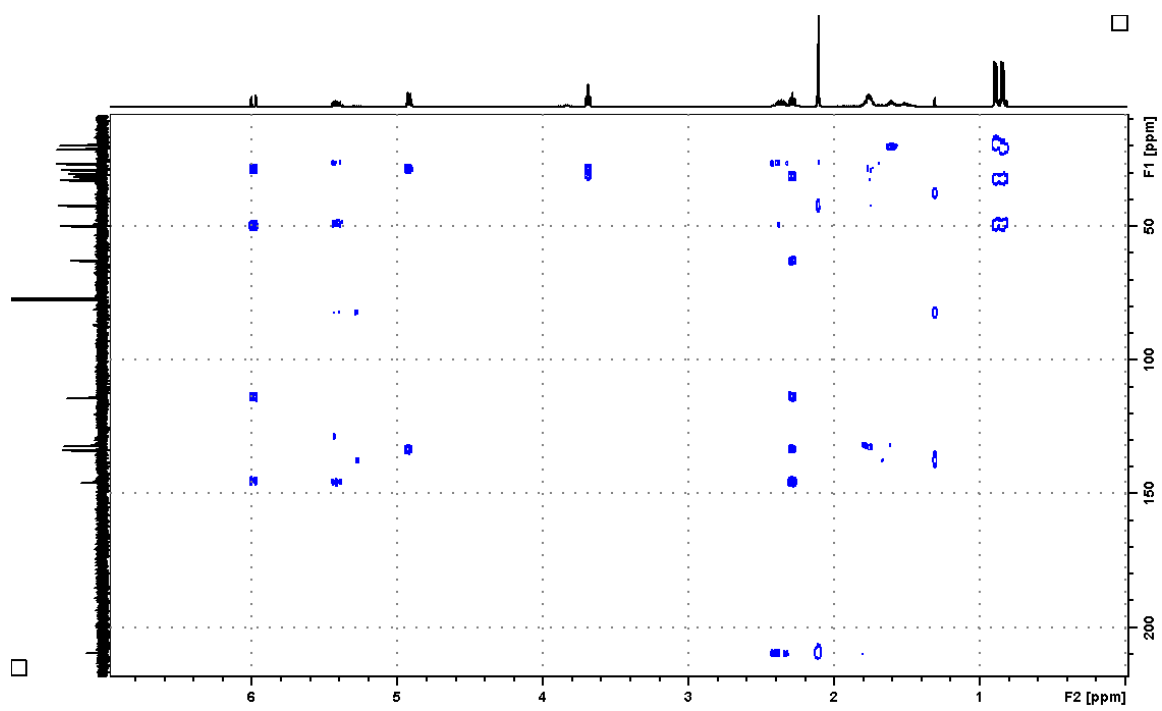
Figure A65. HMBC spectrum of tricinolone in CDCl$_3$.
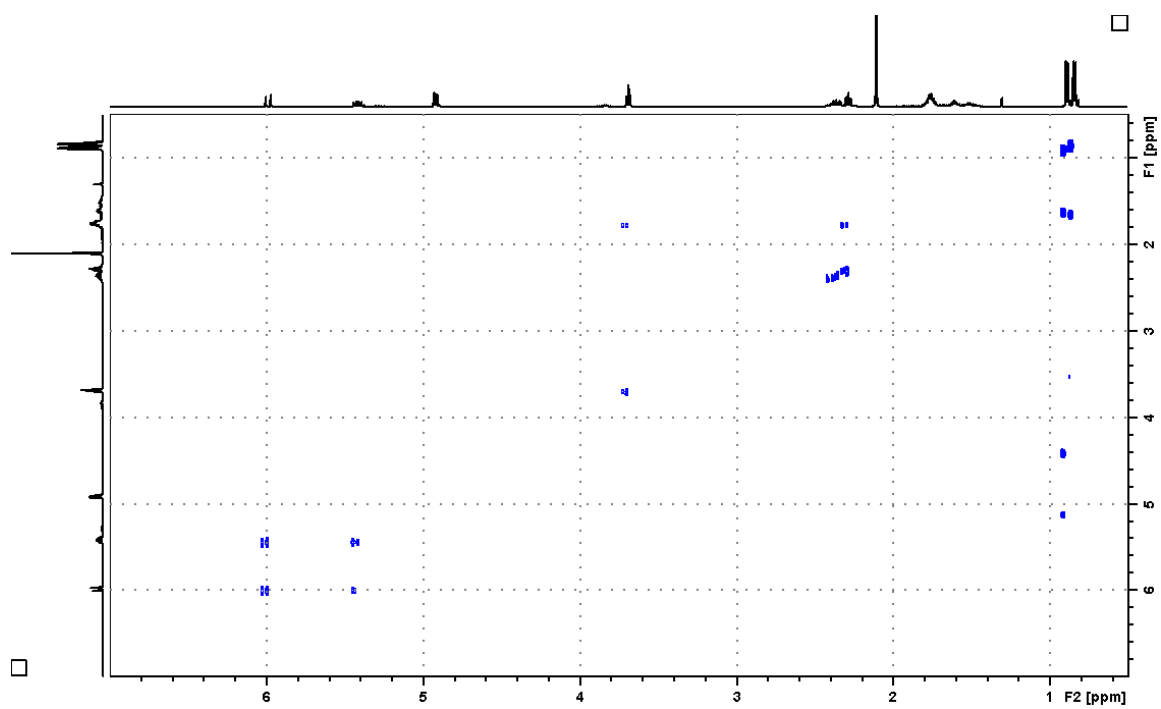
Figure A66. COSY spectrum of tricinolone in CDCl$_3$.
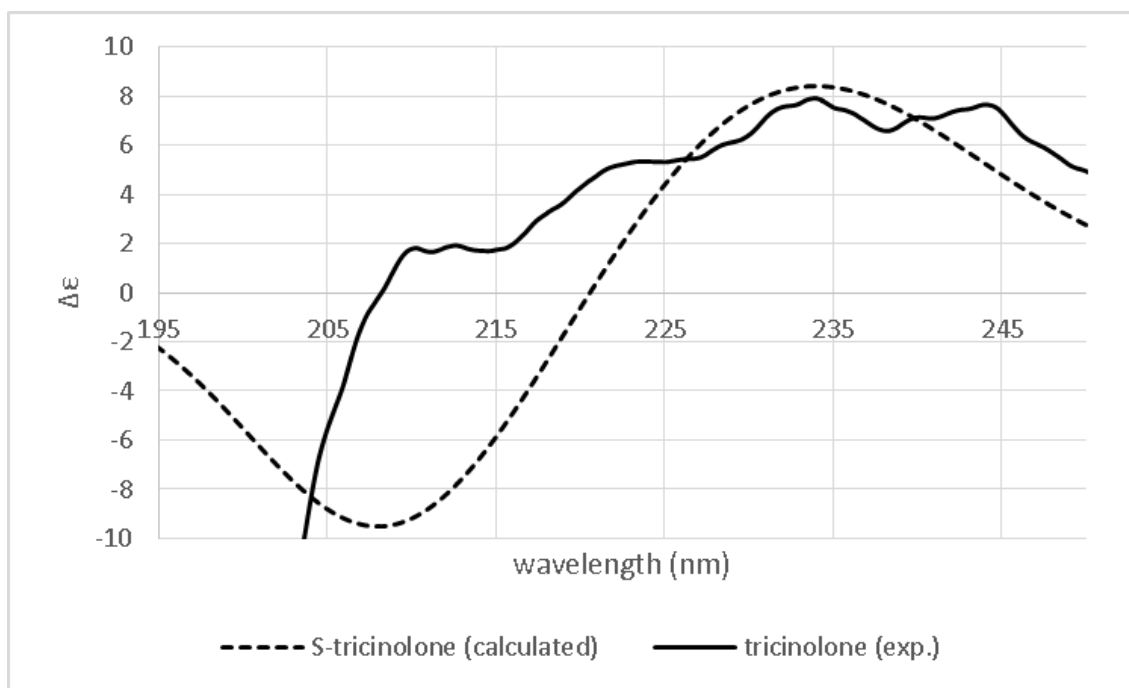
Figure A67. Experimental ECD spectrum of tricinolone overlaid with calculated spectrum for *S*-tricinolone in acetonitrile indicating an *S* configuration.
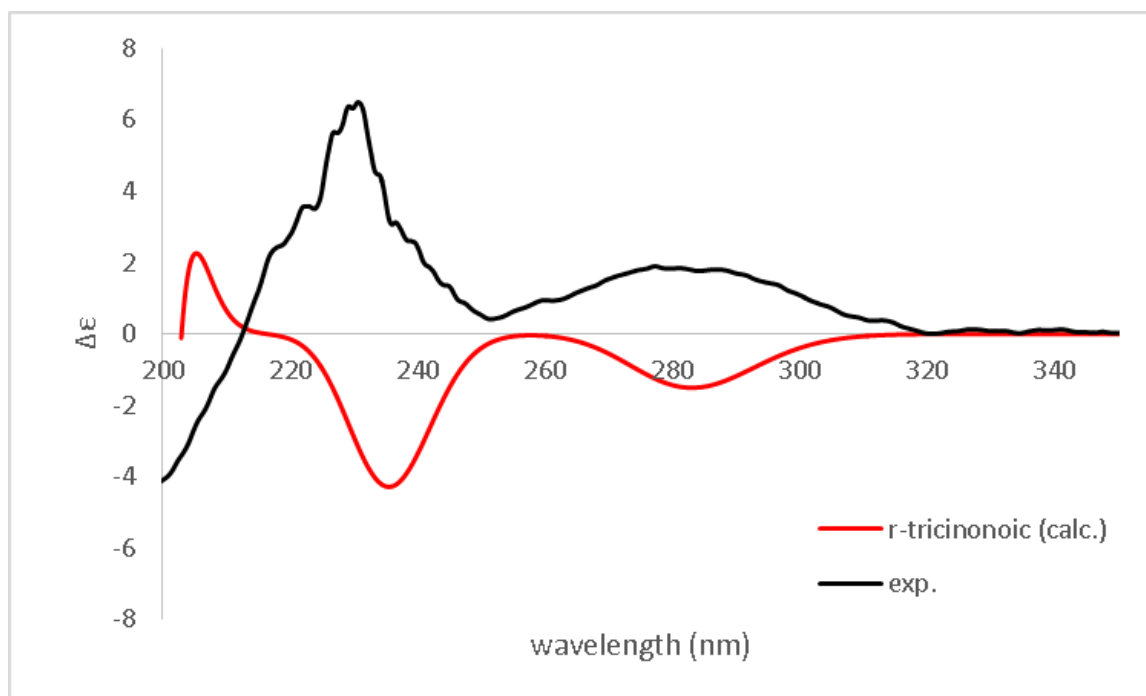
Figure A68. Experimental ECD spectrum of tricinonoic acid overlaid with calculated spectrum for *R*-tricinonoic acid in acetonitrile indicating an *S* configuration.
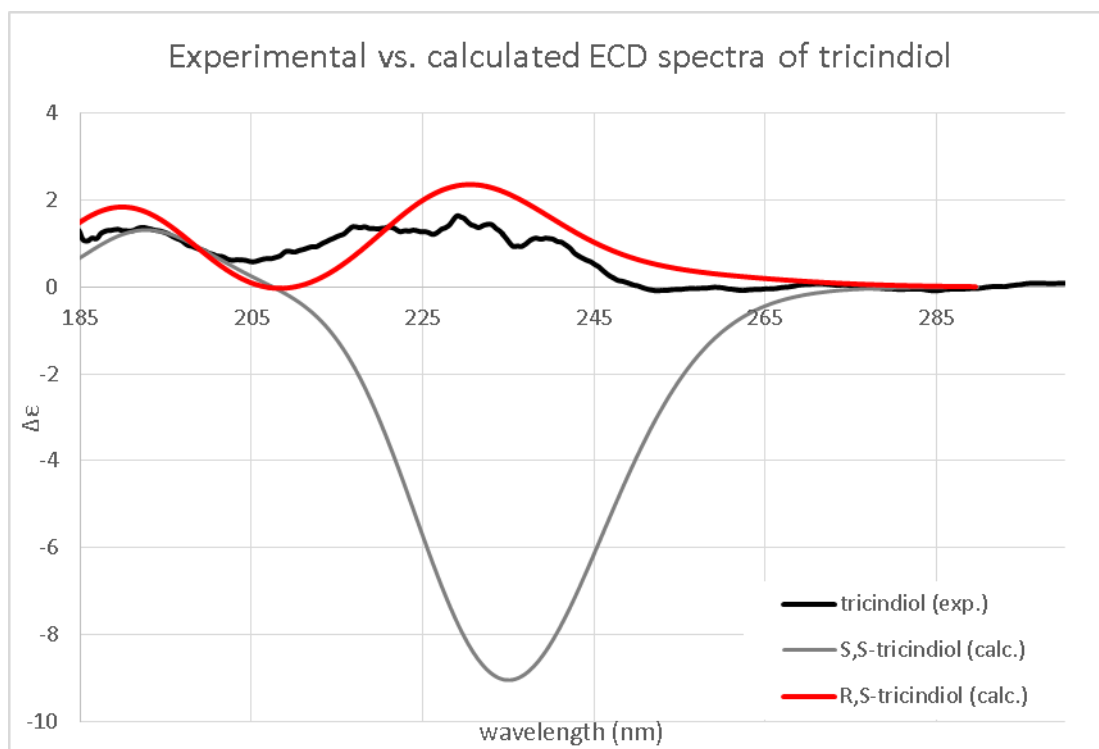
Figure A69. Calculated and experimental ECD spectra for tricindiol indicating an *R,S*-configuration for tricindiol.

	^{13}C		
position	exp.	R,S	S,S
1	62.80	63.30	63.53
2	32.30	34.26	31.55
3	28.60	30.69	31.11
4	147.00	148.26	148.36
5	134.20	131.04	130.99
6	133.60	136.14	136.40
7	51.40	51.49	51.77
8	29.40	29.60	30.96
9	38.60	36.31	35.91
10	68.70	69.01	69.50
11	23.30	22.91	22.73
12	114.00	112.23	111.55
13	33.30	36.29	37.00
14	21.20	19.32	19.88
15	19.40	16.94	16.57
CMAD:		1.88	1.56
sDP4+:		94.70%	5.30%
uDP4+		90.90%	9.10%
DP4+		100.00%	0.00%

	^{1}H		
position	exp.	R,S	S,S
1	3.69	3.44	3.42
2	1.72	1.69	1.67
3	2.29	2.27	2.29
5	6.01	5.96	5.95
6	5.52	5.74	5.89
7	1.62	1.93	1.92
8a	1.79	1.62	1.52
8b	1.26	1.46	1.68
9	1.37	1.28	1.28
10	3.68	3.73	3.67
11	1.31	1.10	1.08
12a	4.91	4.88	4.87
12b	4.89	4.87	4.79
13	1.63	1.67	1.68
14	0.91	0.91	0.88
15	0.86	0.91	0.89
CMAD:		0.05	0.07
uDP4+:		99.29%	0.71%
sDP4+		93.16%	6.84%
DP4+		100.00%	0.00%

Figure A70. DP4+ computed NMR chemical shift results for 7*R*,10*S* and 7*S*, 10*S* diastereomers. With high confidence, tricindiol's absolute configuration is 7*R*, 10*S*.

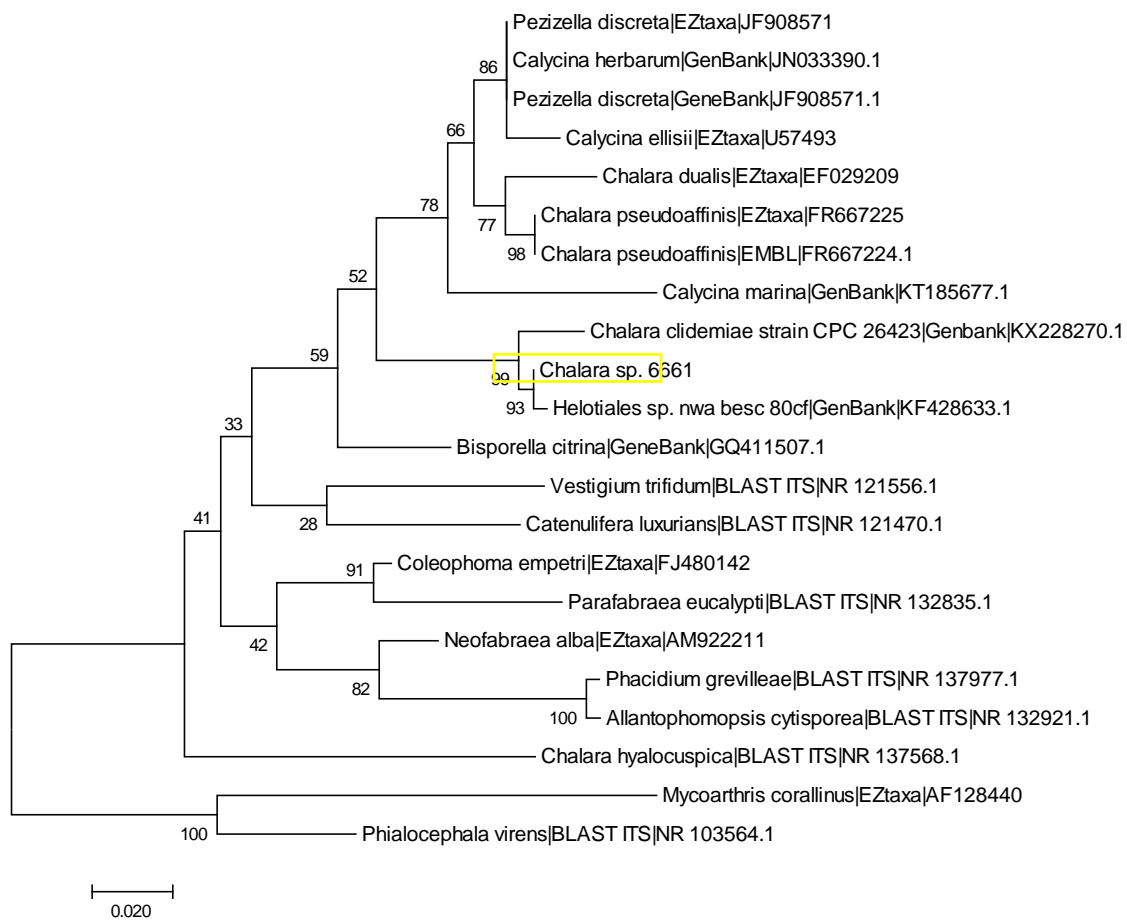# Appendix B – Supplementary Material for Chapter 3

Figure B1. Phylogenetic analysis of *Chalara* sp. 6661 ITS region

TCCGTAGGTGAACCTGCGGAAGGATCATTACAGAGTTCGTGCCCTTCGGG

GTAGACCTCCCACCCTTTGTATACCTACCTTTGTTGCTTTGGCGGGCCGTCGC

AAGACCGGCGGCTTCGGCTGTCGTGTGCCCGCCAGAGGACCCCAAACTCTGA

ATACAGTGTCGTCTGAGTACTATATAATAGTTAAAACTTTCAACAACGGATCT

CTTGGTTCTGGCATCGATGAAGAACGCAGCGAAATGCGATAAGTAATGTGAA

TTGCAGAATTCAGTGAATCATCGAATCTTTGAACGCACATTGCGCCCCTTGGT

ATTCCGGGGGGCATGCCTCTTCCAGCGTCATTTCACCCCTCAAGCTCTGCTTG

GTTTTGGGCCGCGCCGGCAACGGCGGGCCTCGAAAATAGTGGCGACGCCATC

GTGCTCTCAGCGTAGTAATTCTTCTCGCTGTTGGGTCCCGGTGGTCGTCCGCC

AGCAACCCCCAACTTTCTTAAGTTTGACCTGGGATGAGGTAGGGATACCCGC

TGAACTTAAGCATATCAATAAGCGGAG

Figure B2. Consensus sequence of *Chalara* sp. 6661 ITS region from primers ITS1 and ITS4.
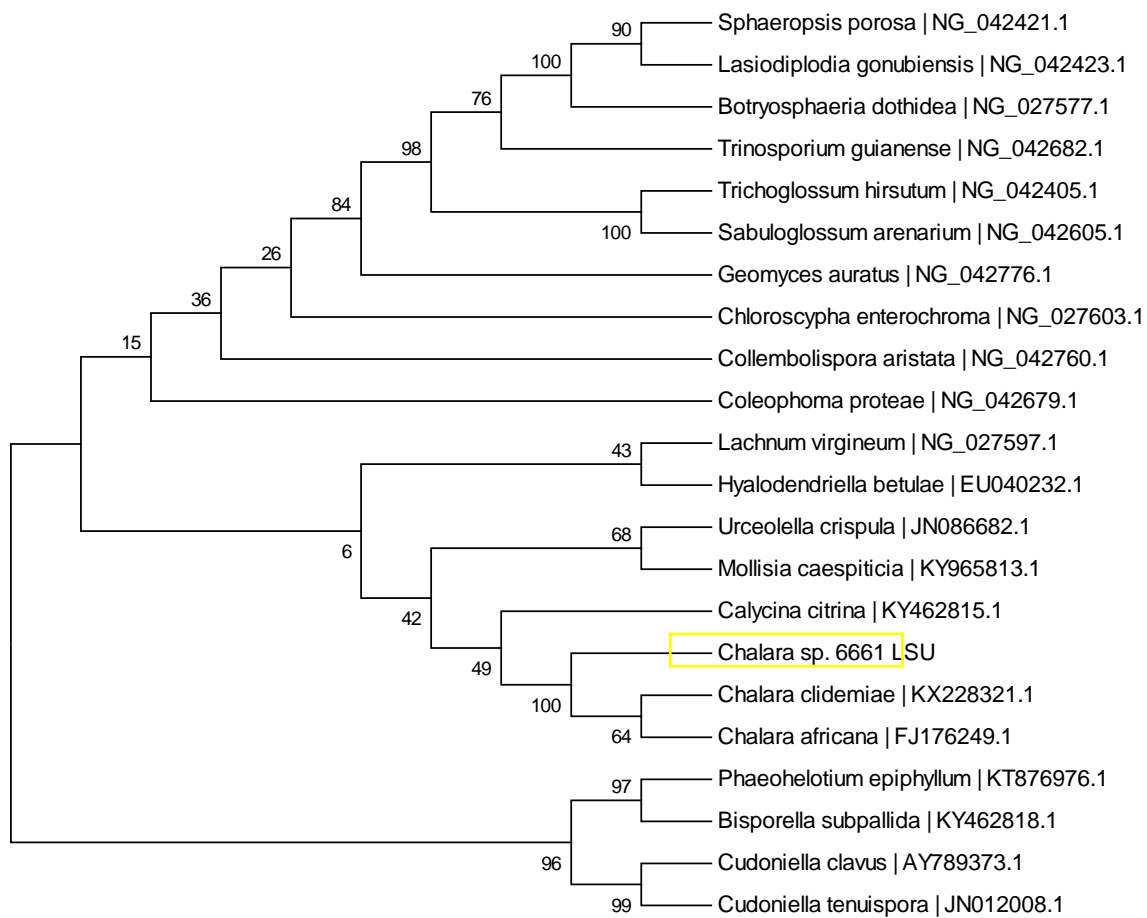
Figure B3. 28S rRNA phylogenetic analysis

Figure B4. 28S rRNA sequence from primers LR0R, LR16 and LR5

CCGCTGAACTTAAGCATATCAATAAGCGGAGGAAAAGAAACCAACAGGG
ATTGCCTCAGTAACGGCGAGTGAAGCGGCAACAGCTCAAATTTGAAATCTGG
TCCTTTCAGGTCCCGAGTTGTAATTTGTAGAAGATGCTTCGAGCGTGGCTCCG
GTCTAAGTCCCTTGGAACAGGGCGTCATAGAGGGTGAGAATCCCGTATGTGA
CTGGCTGCCTTCGCTTATCGTGAAGCTCTTTCGACGAGTCGAGTTGTTTGGGA
ATGCAGCTCAAAATGGGTGGTAAATTTCATCTAAAGCTAAATATTGGCCAGA
GACCGATAGCGCACAAGTAGAGTGATCGAAAGATGAAAGCACTTTGGAAA
GAGAGTTAAACAGTACGTGAAATTGTTGAAAGGGAAGCGCTTGCAATCAGAC
TTGCGCGCCGTTGATCATCCTCGGTTCTCCGGGGTGCACTCGGCGGCGCTCAG
GCCAGCATCGGTTTCGGTGGTCGGATAAAGGCCTTGGGAATGTGGCTCCTTTC
GGGGAGTGTTATAGCCCTCGGTGCAATGCGGCCTACCGGGACCGAGGACCGC
GCTTCGGCTAGGATGCTGGCGTAATGGTTGTAAGCGACCCGTCTTGAAACAC
GGACCAAGGAGTCTAACACTTATGCGAGTGTTTGGGTGTTAAACCCATACGC
GTAATGAAAGTGAACGGAGGTGAGAACCCTTAAGGGTGCATCATCGACCGGT
CCTGAAGTTTACGGACGGATCTGAGTAAGAGCATAATTGTTGGGACCCGAAA
GATGGTGAACTACGCCCGAATAGGGTGAAGCCAGAGGAAACTCTGGTGGAG
GCTCCCACCGGTTCTGACGTGCAAATCGATCGT
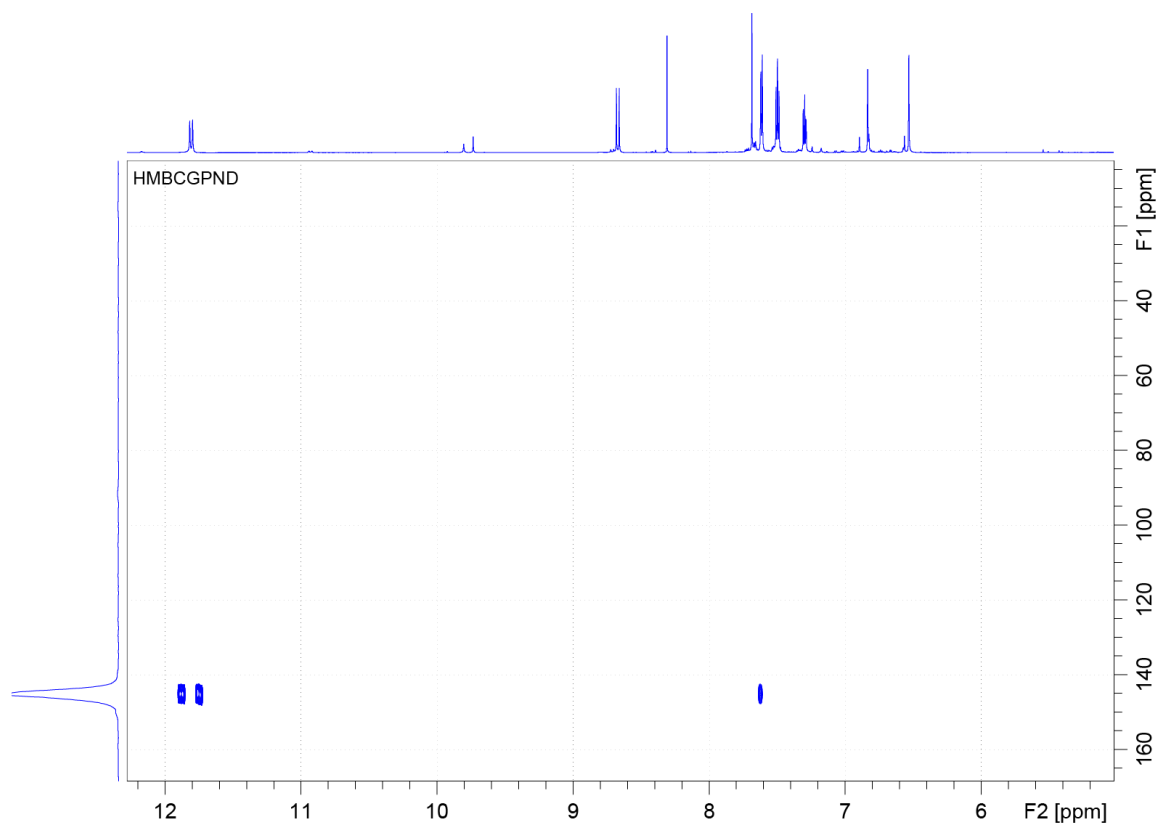
Figure B5. ^{1}H-^{15}N HMBC of **chalaniline A**

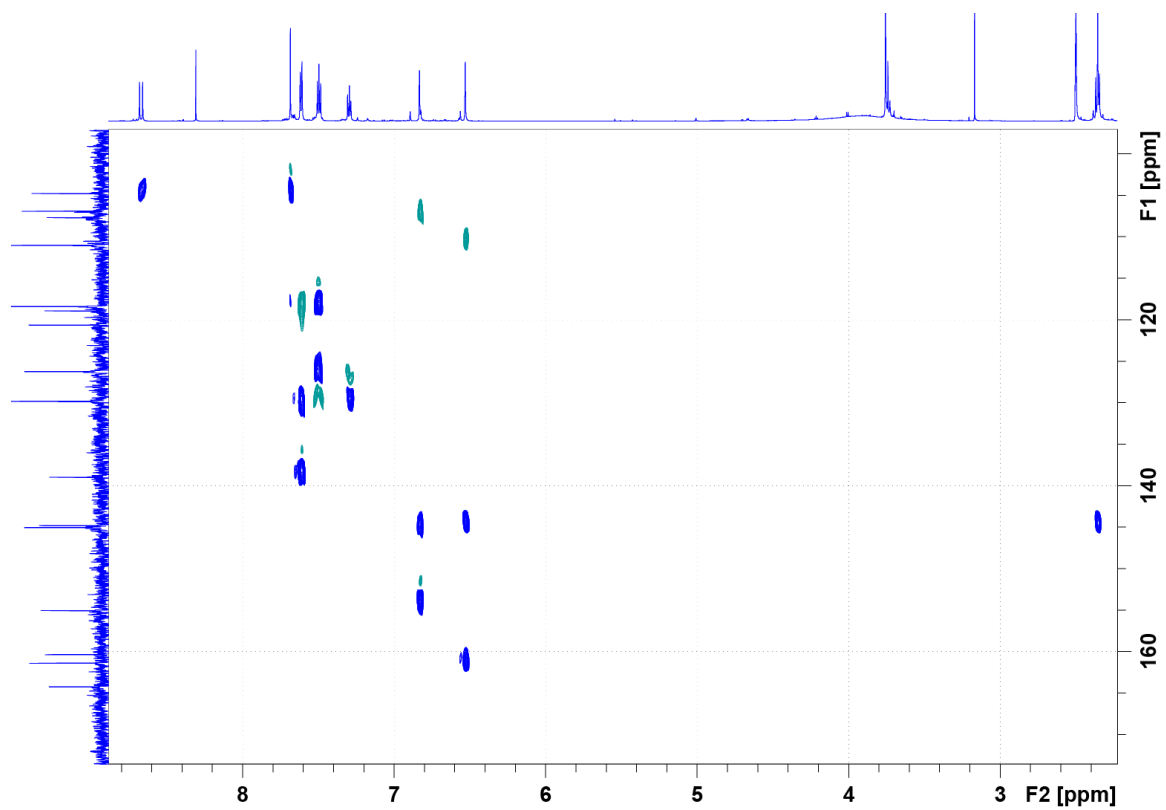Figure B6. 1,1 Homodecoupled ADEQUATE of **chalaniline A**

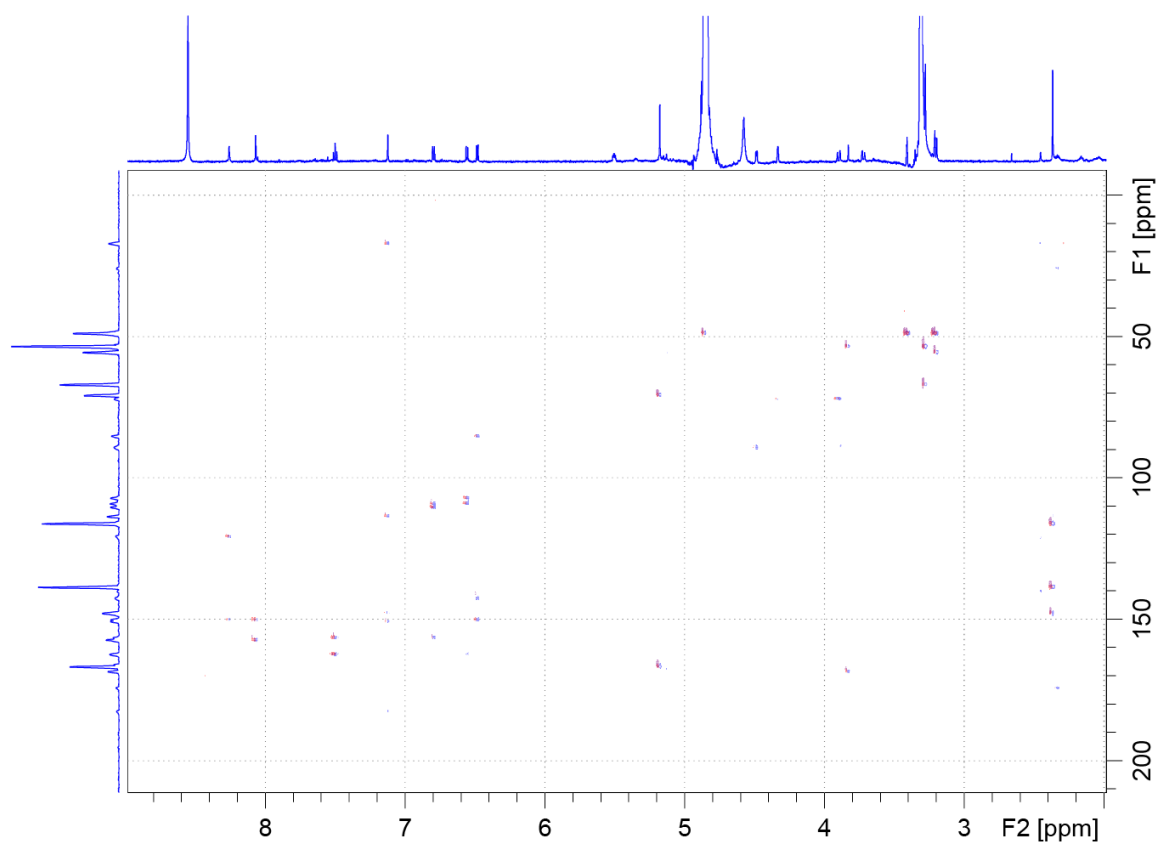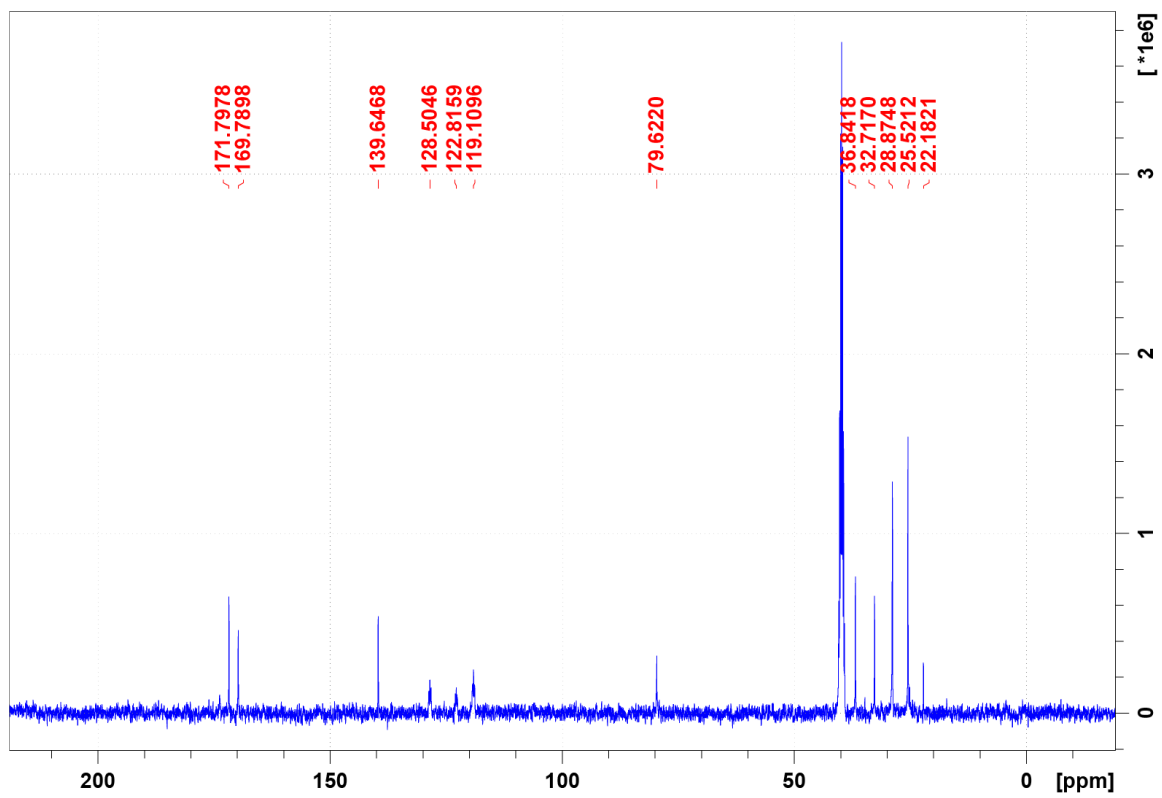Figure B7. ^{1}H-^{13}C HMBC of **xanthone A** in d$_4$-methanol at 4, 8, and 10Hz evolutions.

Figure B8. ^{13}C of d$_5$-vorinostat
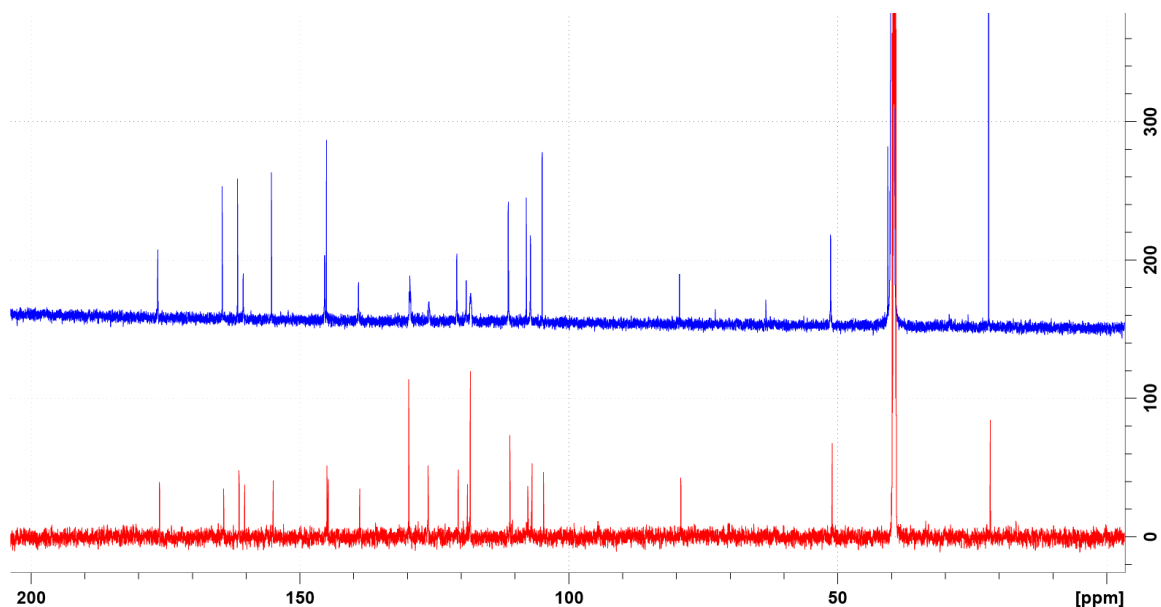
Figure B9. ^{13}C NMR of chalaniline A (red) and d$_5$-chalanline A (blue) in d$_6$-DMSO

Table B1. Chemical shifts for **chalaniline A** in d$_6$-DMSO

| position	δ_C, type	δ_H, (J in Hz)	HMBC	1,1 ADEQUATE
		Chalaniline A		
1	161.3, C			
2	111.0, CH	6.53, s	1, 4, 10	1, 3
3	144.7, C			
4	106.8, CH	6.83, s	2, 4a, 8, 10	3, 4a
4a	155.0, C			
5	104.7, C			
6	120.6, CH	7.69, s	5, 7, 7a, 8, 9a, 11, 12	5
7	118.9, C			
7a	110.5, C			
8	176.1, C			
8a	107.6, C			
9a	160.3, C			
10	21.7, CH$_3$	2.36, s	2, 3, 4	3
11	145.0, CH	8.70, d, J = 14.7	5, 7, 9a, 1'a	5
12	164.2, C			
13	51.0, CH$_3$	3.76, s	12	
1'	118.3, CH	7.61, d, J = 7.8	1', 1'a, 2', 3'	1'a, 2'
1a'	138.9, C			
2'	129.8, CH	7.50, t, J = 7.8	1', 1'a, 2', 3'	1', 3'
3'	126.2, CH	7.30, t, J = 7.8	1', 1'a, 2'	2'
OH		13.9, brd		
NH		11.81, d, J = 14.7	1', 1'a, 5	

Appendix C – Supplementary Material for Chapter 4
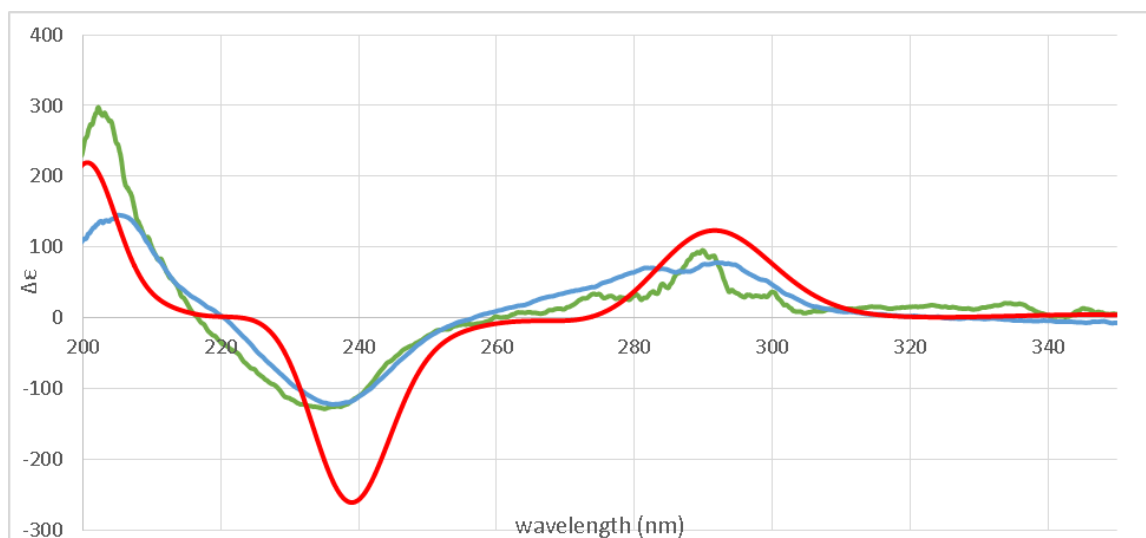
Figure C1. Experimental ECD spectra of purchased citreoviridin (from *Penicillium citreviride*) in green, isolated citreoviridin in blue, and calculated ECD spectra of citreoviridin in red show overall agreement. Initial conformational analysis was performed in Avogadro using the MMFF94 molecular mechanics force field and weighted rotor conformational search with 1000 conformers. Density functional theory (DFT) calculations were performed using the Gaussian 09 package at the B3LYP/6-31G(d) level. The ECD spectrum was calculated by the TDDFT methodology at the B3LYP/6-311G(2d,2p) level utilizing integral equation formalism variant polarizable continuum model (IEFPCM) with 40 states in methanol. ECD spectra were simulated using SpecDis 1.62

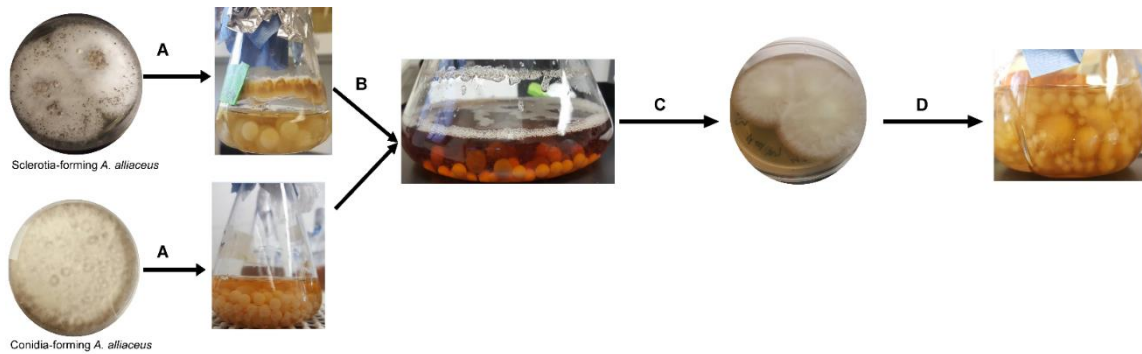# Appendix D – Supplementary Material for Chapter 5

Figure D1. A) Sclerotia-forming and conidia-forming phenotype of *A. alliaceus* on agar plates were propagated into malt-based broth media and grown for 14 days in separate flasks. B) After 14 days of growth, the mycelia from each flask were combined into a single flask containing buffered-malt broth and placed on a 200 rpm shaker at ambient light and temperature for 15-20 days. C) Before extraction, the flask of combined mycelia was streaked out and a phenotypic change was observed, different compared to either starting phenotypes. D) The metabolically activated *A. alliaceus* was propagated into another flask containing buffered-malt broth and grown for 15-20 days.
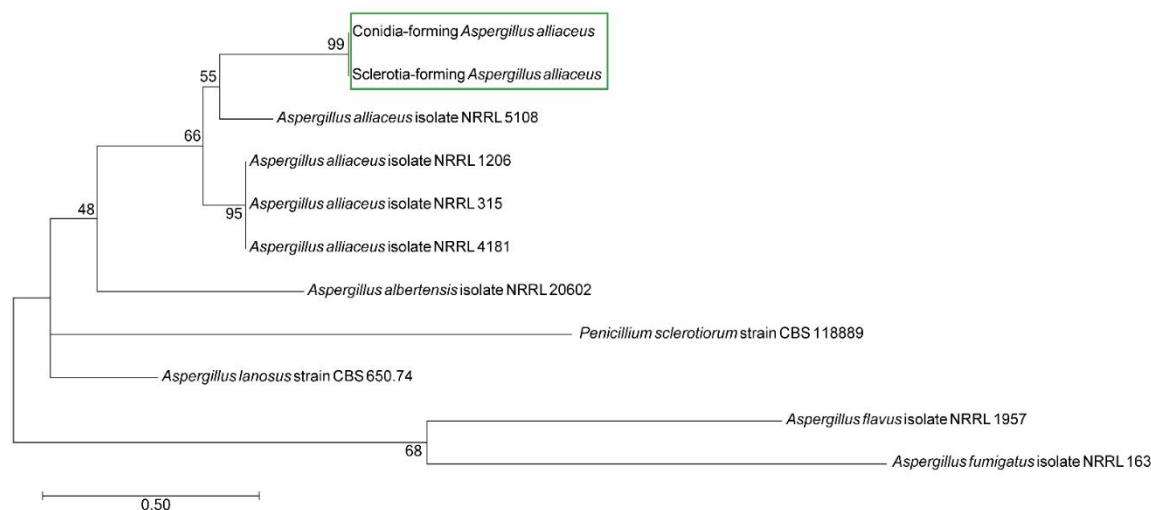
Figure D2. Molecular phylogenetic analysis of the total loci (Beta-Tubulin Bt2a/Bt2b, Calmodulin CF1M/ CF4, and Internal Transcribed Spacer ITS5/4 and ITS1/4) of the *Aspergillus alliaceus* phenotypes by Maximum Likelihood method. The evolutionary history was inferred by using the Maximum Likelihood method based on the Tamura-Nei model.[1] The tree with the highest log likelihood (-11779.1611) is shown. The percentage of trees in which the associated taxa clustered together is shown next to the branches. Initial tree(s) for the heuristic search were obtained automatically by applying Neighbor-Join and BioNJ algorithms to a matrix of pairwise distances estimated using the Maximum Composite Likelihood (MCL) approach, and then selecting the topology with superior log likelihood value. The tree is drawn to scale, with branch lengths measured in the number of substitutions per site. The analysis involved 11 nucleotide sequences. All positions with less than 95% site coverage were eliminated. That is, fewer than 5% alignment gaps, missing data, and ambiguous bases were allowed at any position. There were a total of 1243 positions in the final dataset. Evolutionary analyses were conducted in MEGA7.[2] *A. alliaceus* strains NRRL 315, 5108, and 4181 are referred to as the *Petromyces alliaceus*[3] and *A. alliaceus* strain NRRL 1206 is referred to as *Aspergillus alliaceus*[4].

GATCCCTACCGA-
TGCATGGGATCTAATGCGTCCCATTACTTCTGCCACGTGTTTGCTAACGGTTTTACAG
GCAGACCATTTCTGGCGAGCACGGCCTTGACGGCTCCGGTGTGTAAGTACAACCCGT
GTACA--TCTCGAACGAAGGACAATCCGTTGG-CGATGGAAGGGTCTGAAAGGG-
TCTGACGGGAAGGATAGTTACAATGGCTCCTCCGACCTCCAGCTGGAGCGCATGAAC
GTCTACTTCAACGAGGTGCGTACCTCAGATTTTGCAGCCTCCCTAGAAACGCCGTGC
AGGCCCTGACC—
ACTTCTCCAGGCTAGTGGAAACAAGTATGTTCCTCGTGCCGTCCTCGTCGATCTTGAG
CCCGGTACCATGGACGCCGTCCGCGCAGGTCCCTTANGTCAGCTTTTCCGTCCCGAC
AACTTCGTTGATGGTCTTGGTGGAATGCATACTGACTTGAGTTTTCTTGGGCTCCTAA
TAGGACAAGGATGGTGATGGTTAGTACATCATGTTCCATAAAACCCCCCTTCTAGTG
CGACCGACAGTTTTCAGCCGCTATAATCGTCTCCATATTTTTTATTGTTCGATCGGCT
GAAGTCTTGGCGTTGATAAATTGACTCGATATGCAGGCCAGATCACCACCAAGGAGT
TGGGCACTGTGATGCGCTCTCTGGGCCAGAACCCTTCTGAGTCGGAACTCCAGGATA
TGATCAACGAGGTTGATGCCGATAACAATGGCACCATCGACTTCCCTGGTACGCGAG
GGCTTTCCTACGGCTCACAGACAAAGAAATTCTATTAACGTTCGATTAGAGTTCCTTA
CGATGATGGCCAGAAAGATGAAGGATACCGACTCTGAGGAGGAGATCCGGGAGGCT
TTCAAGGTTTTCGACCGTGATAACAACGGCTTTATCTCCGCCGCGGAGCTGCGCCAC
GTCATGACCTCCATCGGTGAGAAACTTACCGATGATGAAGTTGATGAGATGATCCGC
GAGGCGGATCAGGACGGTGATGGCCGGATCGATTGTACGTTGAGAACAACTCCCCAT
TTCTTTTACCCGCTGAGGATGAATGTGGATGTGAACCAACCTCCCACCCGTGTATACT
GTACCTTCGTTGCTTCGGCGGGCCCGCCGTCATGGCCGCCGGGGGGCTTCTGCCCC-
CGGGCCCGCGCCCGCCGGAGACACATGAACTCTGTCTG-
ATGTAGTGAAGTCTGAGTTG-ATTGTCACACAATCAGTTAAAACTTTCA----
ACAATGGATCTCTTGGTTCCGGCATCGATGAAGAACGCAGCGAAATGCGATAACTAA
TGTGAATTGCAGAATTCCGTGAATCATCGAGTCTTTGAACGCACATTGCGCCCCCTG
GTATTCCGGGGGGCATGCCTGTCCGAGCGTCATTGCTGCCCATCAAGCACGGCTTGT
GTGTTGGGTCCTCGTCCCCCCGGGGG-
ACGTGCCCGAAAGGCAGCGGCGGCACCGCGTCCG-
GTCCTCGAGCGTATGGGGCTTTGTCACCCGCTCTGCAGGCCCGGCCGGCGCTGGCCG
ACGCGAAAG

Figure D3. Conidia-forming *Aspergillus alliaceus* consensus sequence (1545 bp) of Beta-

tubulins (black letters), Calmodulin (blue letters), and ITS region (green letters)

GATCCCTACCGA-
TGCATGGGATCTAATGCGTCCCATTACTTCTGCCACGTGTTTGCTAACGGTTTTACAG
GCAGACCATTTCTGGCGAGCACGGCCTTGACGGCTCCGGTGTGTAAGTACAACCCGT
GTACA--TCTCGAACGAAGGACAATCCGTTGG-CGATGGAAGGGTCTGAAAGGG-
TCTGACGGGAAGGATAGTTACAATGGCTCCTCCGACCTCCAGCTGGAGCGCATGAAC
GTCTACTTCAACGAGGTGCGTACCTCAGATTTTGCAGCCTCCCTAGAAACGCCGTGC
AGGCCCTGACC—
ACTTCTCCAGGCTAGTGGAAACAAGTATGTTCCTCGTGCCGTCCTCGTCGATCTTGAG
CCCGGTACCATGGACGCCGTCCGCGCAGGTCCCTTCGGTCAGCTTTTCCGTCCCGACA
ACTTCGTTGATGGTCTTGGTGGAATGCATACTGACTTGAGTTTTCTTGGGCTCCTAAT
AGGACAAGGATGGTGATGGTTAGTACATCATGTTCCATAAAACCCCCCTTCTAGTGC
GACCGACAGTTTTCAGCCGCTATAATCGTCTCCATATTTTTTATTGTTCGATCGGCTG
AAGTCTTGGCGTTGATAAATTGACTCGATATGCAGGCCAGATCACCACCAAGGAGTT
GGGCACTGTGATGCGCTCTCTGGGCCAGAACCCTTCTGAGTCGGAACTCCAGGATAT
GATCAACGAGGTTGATGCCGATAACAATGGCACCATCGACTTCCCTGGTACGCGAGG
GCTTTCCTACGGCTCACAGACAAAGAAATTCTATTAACGTTCGATTAGAGTTCCTTAC
GATGATGGCCAGAAAGATGAAGGATACCGACTCTGAGGAGGAGATCCGGGAGGCTT
TCAAGGTTTTCGACCGTGATAACAACGGCTTTATCTCCGCCGCGGAGCTGCGCCACG
TCATGACCTCCATCGGTGAGAAACTTACCGATGATGAAGTTGATGAGATGATCCGCG
AGGCGGATCAGGACGGTGATGGCCGGATCGATTGTACGTTGAGAACAACTCCCCATT
TCTTTTACCCGCTGAGGATGAATGTGGATGTGAACCAACCTCCCACCCGTGTATACTG
TACCTTCGTTGCTTCGGCGGGCCCGCCGTCATGGCCGCCGGGGGGCTTCTGCCCC-
CGGGCCCGCGCCCGCCGGAGACACATGAACTCTGTCTG-
ATGTAGTGAAGTCTGAGTTG-ATTGTCACACAATCAGTTAAAACTTTCA----
ACAATGGATCTCTTGGTTCCGGCATCGATGAAGAACGCAGCGAAATGCGATAACTAA
TGTGAATTGCAGAATTCCGTGAATCATCGAGTCTTTGAACGCACATTGCGCCCCCTG
GTATTCCGGGGGGCATGCCTGTCCGAGCGTCATTGCTGCCCATCAAGCACGGCTTGT
GTGTTGGGTCCTCGTCCCCCCGGGGG-
ACGTGCCCGAAAGGCAGCGGCGGCACCGCGTCCG-
GTCCTCGAGCGTATGGGGCTTTGTCACCCGCTCTGCAGGCCCGGCCGGCGCTGGCCG
ACGCGAAAG

Figure D4. Sclerotia-forming *Aspergillus alliaceus* consensus sequence (1545 bp) of Beta-tubulins (black letters), Calmodulin (blue letters), and ITS region (green letters)
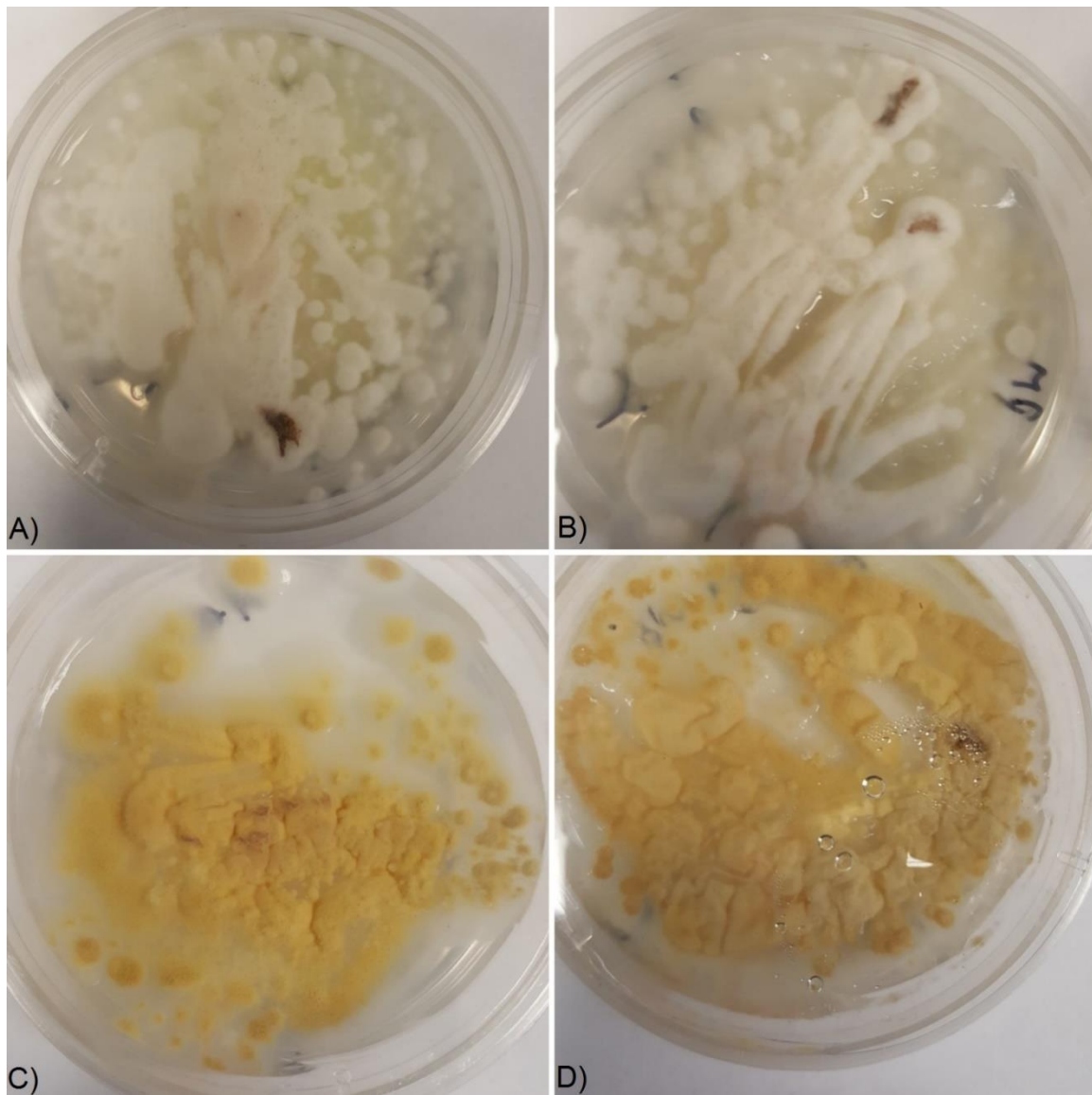
Figure D5. Conidia-forming *A. alliaceus* phenotype study on Czapek-Dox agar under A) no light, 25°C, B) light, 25°C, C) no light, 37°C and D) light, 37°C with photos taken between five and seven days of growth.
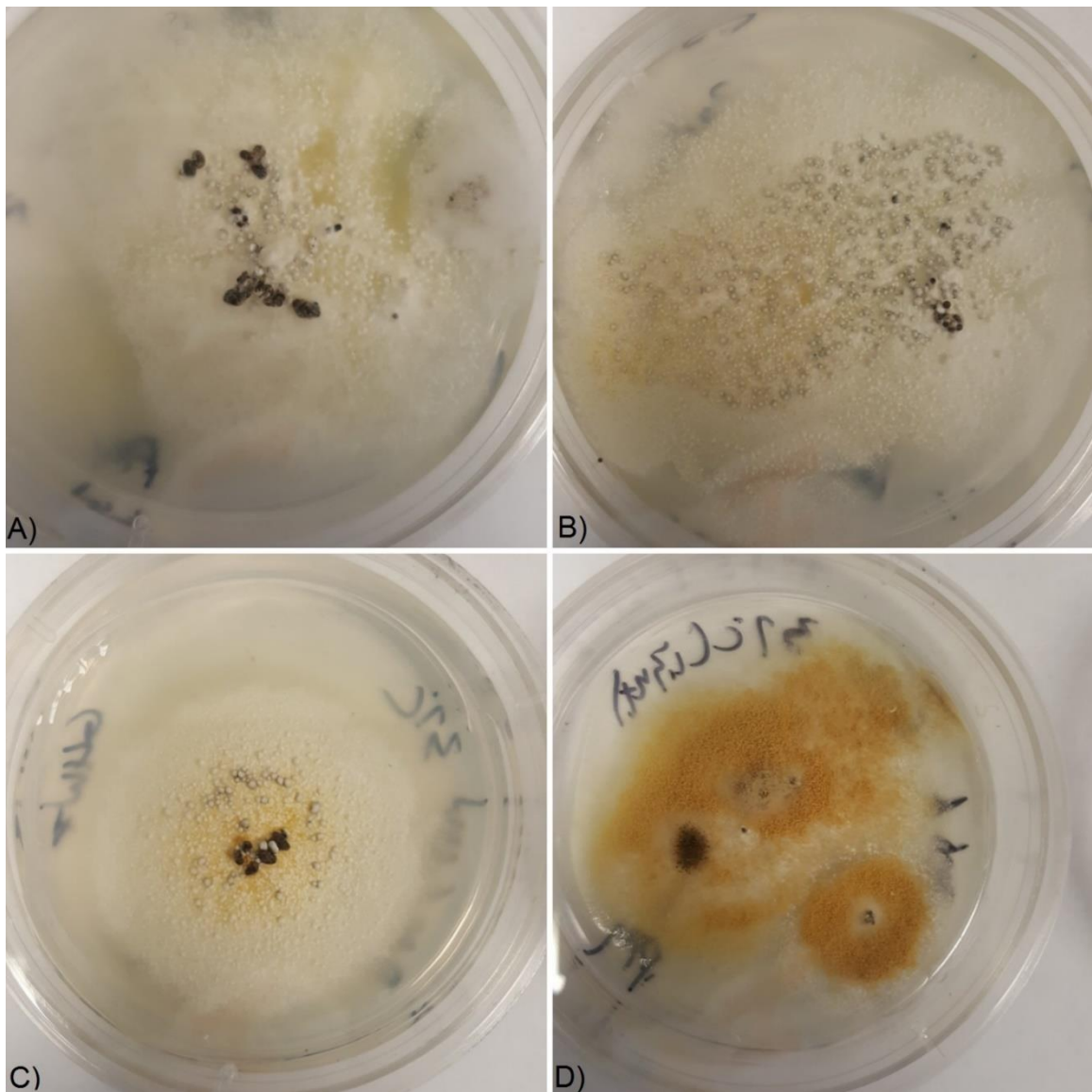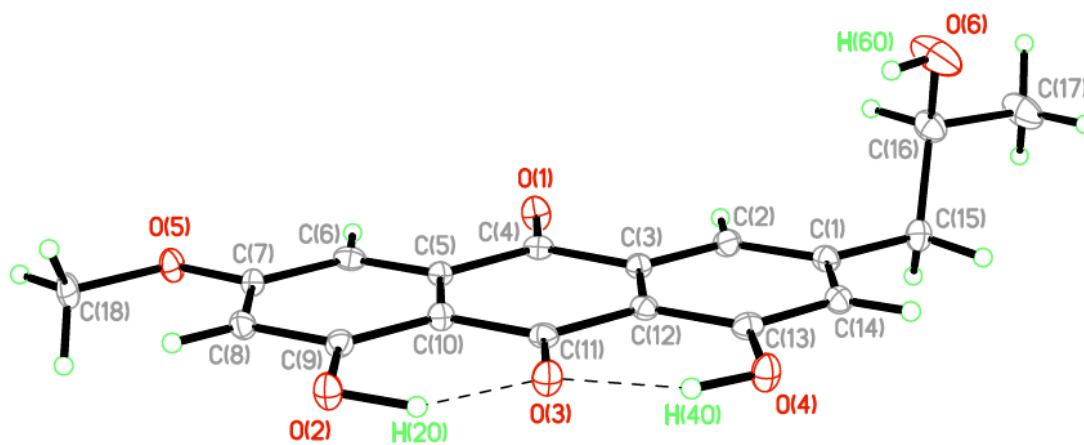
Figure D6. Sclerotia-forming *A. alliaceus* phenotype study on Czapek-Dox agar under A) no light, 25°C, B) light, 25°C, C) no light, 37°C and D) light, 37°C with pictures taken between five and seven days of growth.

Figure D7. X-ray diffraction derived ORTEP plot of compound nalgiovensin. Compound nalgiovensin was dissolved in chloroform and placed in a vial with 50:50 methanol:water to create a crystal via solvent diffusion
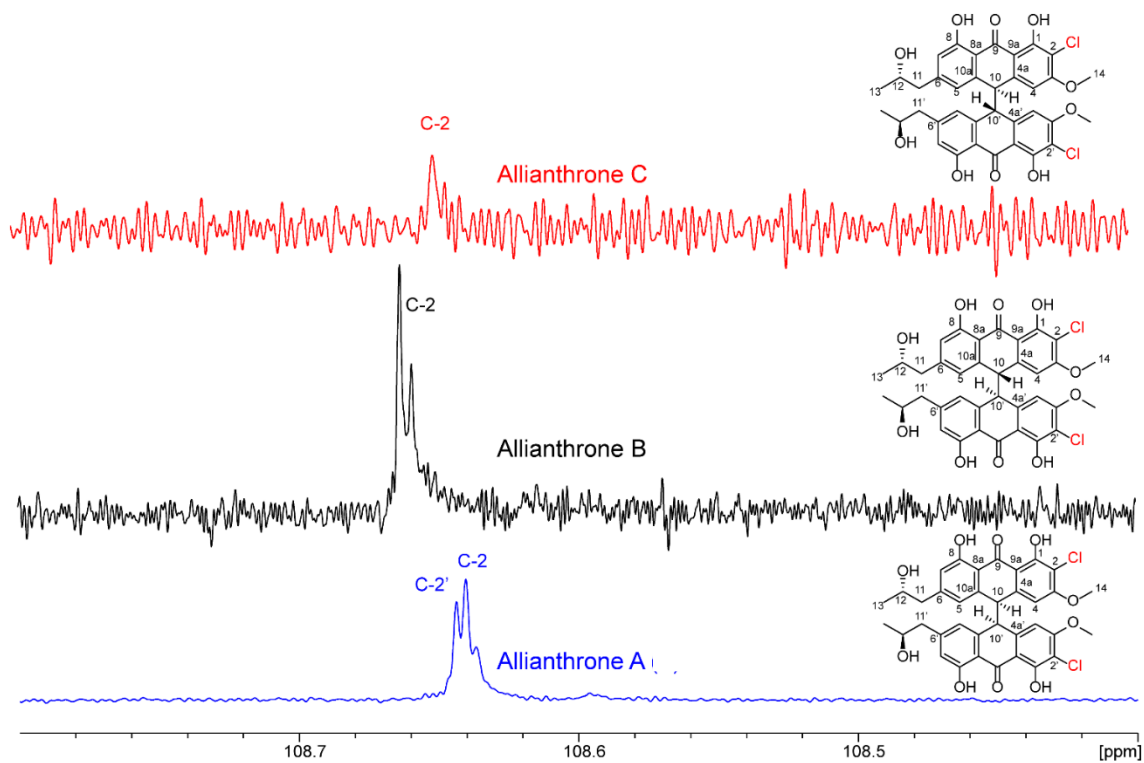
Figure D8. Ultra-high resolution ^{13}C NMR of compounds allianthrones A-C in acetonitrile-d_3 with ^{37}Cl/^{35}Cl isotope shifts evident in the C-2 carbon signal. Allianthrone A exhibits non-chemical equivalence between the anthronyl rings, and thus exhibits two chlorine isotope effects for C-2 and C-2', while B and C are have chemically equivalent anthronyl rings and exhibit a single C-2 singlet with a Cl isotope shift.
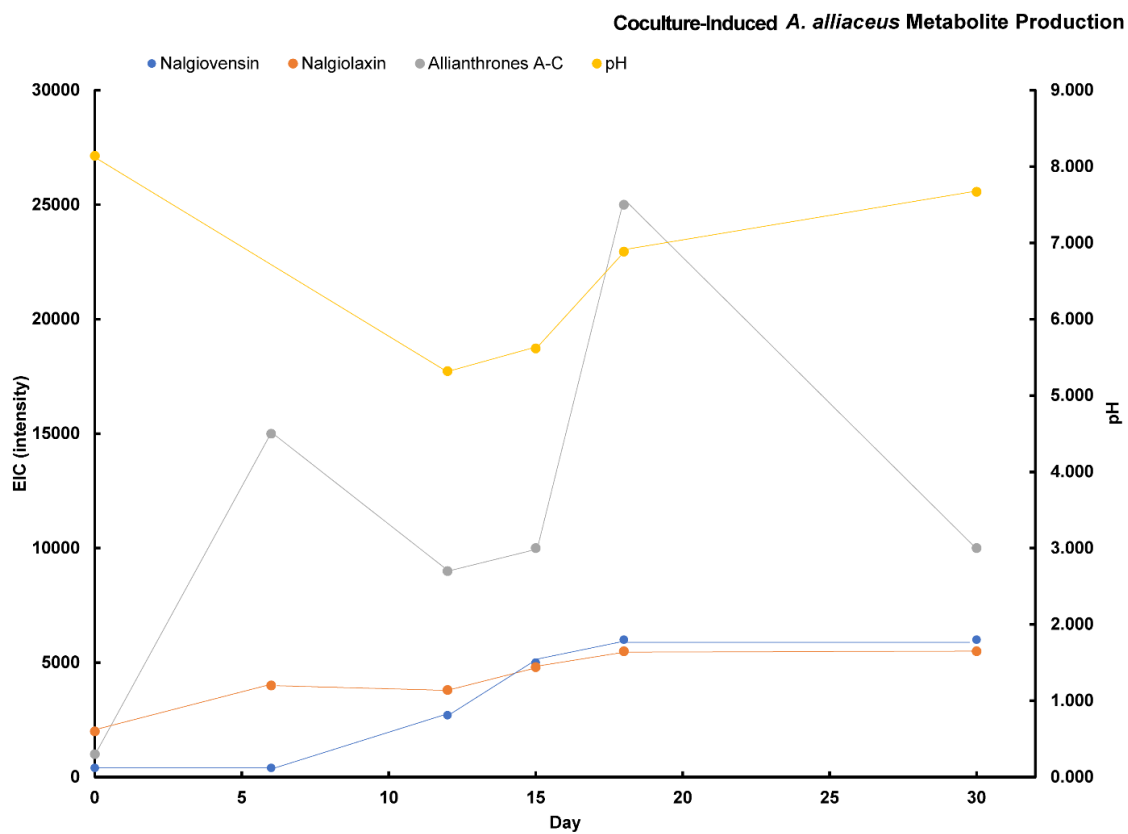
Figure D9. Production of **50-54** from phenotype coculture induced *Aspergillus alliaceus* monitored by extracted ion chromatography LCMS. Bianthrone production (gray) peaks around day 20, pH of the culture is also presented in yellow.
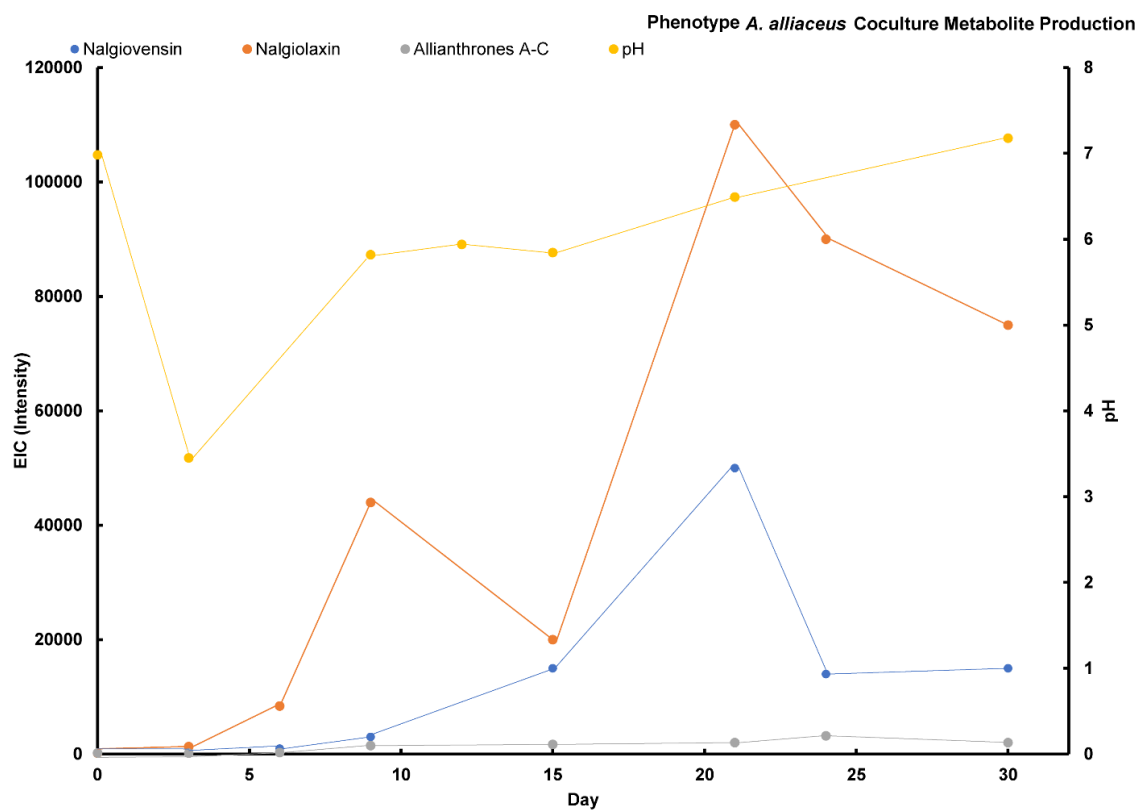
Figure D10. Production of **50-56** in a fresh initiated mixed culture of sclerotia-forming and conidia-forming *Aspergillus alliaceus* monitored by extracted ion chromatography LCMS. Bianthrone production (gray) is not observed in freshly combined fungal cultures. pH of the culture is presented in yellow.
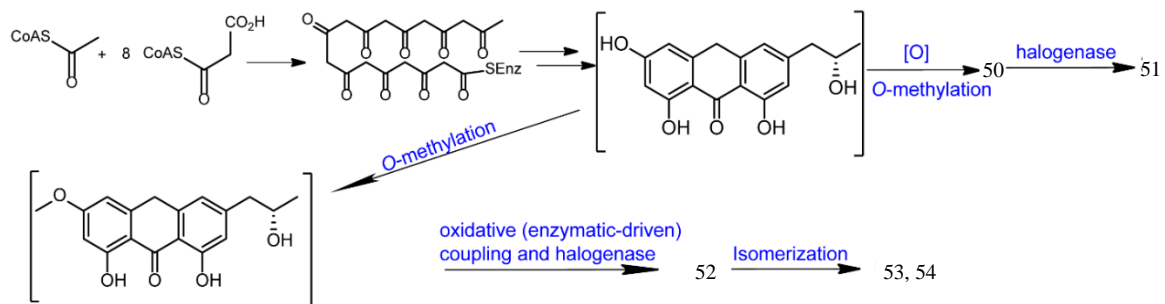
Figure D11. Abbreviated biosynthetic proposal of compounds **50-54**.